

Investigation of the genetic cause and related phenotypes of rare early onset retinal dystrophies

Sarah Hull

Institute of Ophthalmology, University College London

Submitted to the University College London for the degree of Doctor of Philosophy

Supervisors: Prof Andrew R Webster

Prof Anthony T Moore

March 2016

Declaration

I, Sarah Hull, confirm that the work presented in this thesis is my own. Where information has been derived from other sources, I confirm that this has been indicated in the thesis

Abstract

Early onset retinal dystrophies (EORD) are a group of disorders presenting in childhood with degenerative abnormalities in photoreceptor cells. They are one of the leading causes of sight impairment in the United Kingdom. Since the initial discovery of *Rho* causing dominant retinitis pigmentosa in 1990, more than 160 genes have been associated with retinal dystrophy. Many, including *CRB1*, *CRX*, and *RPE65* exhibit phenotypic heterogeneity and have been associated with more than one retinal disorder. Increasingly, with the advent of next generation sequencing, the association of non-syndromic retinal dystrophy with mutations in syndromic genes has been reported including *CEP290*, *CLN3*, and *BBS1*.

In this thesis, a large cohort of patients with EORD underwent both detailed phenotyping to characterise their condition and molecular genetic investigations to identify and investigate the underlying causative variants. Many areas of the presented research were driven by novel findings on whole-exome sequencing such as the association of *IFT140* with non-syndromic retinal dystrophy or *CRX* with macular dystrophy. Other areas were driven by unusual groups of patients with limited published data on their condition such as *COL18A1* and Knobloch syndrome, with novel phenotypic features of cone-rod dysfunction and pigmentary glaucoma. Sanger sequencing was performed for confirmation and segregation of identified variants but in addition, for investigation of phenotypically similar patient panels for unusual gene associations. This included systemically mild Hermansky-Pudlak syndrome due to *HPS6*, juvenile macular dystrophy and *CDH3*, macular dystrophy and *CRX* and microcephaly with familial exudative vitreoretinopathy due to *LRP5*. Functional investigation of missense variants in *IFT140* related retinal dystrophy was performed with transient cell transfection. This thesis highlights the vast heterogeneity of rare forms of EORD, presents novel clinical and molecular data and describes the key features of conditions to aid diagnosis and opportunities for future research.

Acknowledgments

I have been very fortunate to study within such a supportive, motivated and dynamic department. I am most grateful to my supervisors, Prof Tony Moore and Prof Andrew Webster, whose experience, expertise and enthusiasm have taught me so much. Within the laboratory, Dr Gavin Arno has been a great teacher of all molecular techniques and a great collaborator on papers. I am very grateful to Dr Nick Owen for his instruction and advice on cell studies. I would also like to thank Samantha Malka, research coordinator in the department for her essential administrative assistance and support as well as the genetic counsellor team.

I am grateful for the invaluable help and advice from many different experts in particular Prof Graham Holder and Dr Anthony Robson in the electrophysiology department as well as Prof Mike Cheetham and Prof Mike Michaelides.

This research would not be possible without the generous support of funding bodies specifically the National Institute for Health Research Biomedical Research Centre at Moorfields Eye Hospital, Special Trustees of Moorfields Eye Hospital, and the Foundation Fighting Blindness, USA.

To my incredible husband and family, thank you for your constant support and encouragement.

Finally, it has been a privilege to be able to investigate and care for a large number of families affected by early onset retinal dystrophies; their willingness to help with research and their optimism despite such challenges is an inspiration.

Table of contents

DECLARATION.....	2
ABSTRACT.....	3
ACKNOWLEDGMENTS.....	4
TABLE OF CONTENTS	5
LIST OF FIGURES.....	8
LIST OF TABLES.....	8
ABBREVIATIONS	10
1 INTRODUCTION	11
1.1 The neurosensory retina.....	12
1.1.1 Retinal development.....	14
1.1.2 Phototransduction and the visual cycle.....	14
1.2 Clinical assessment	16
1.2.1 Visual function	16
1.2.2 Ophthalmoscopy and retinal imaging.....	18
1.3 Molecular genetics	19
1.3.1 Mendelian inheritance	20
1.4 Types of retinal dystrophy.....	22
1.4.1 Leber congenital amaurosis.....	22
1.4.2 Rod cone dystrophy.....	25
1.4.3 Cone rod dystrophy	26
1.4.4 Macular dystrophy	26
1.4.5 Abnormal retinal vasculogenesis	26
1.4.6 Syndromic retinal dystrophies.....	27
1.5 Thesis aims.....	27
2 METHODS.....	28
2.1 Clinical methods.....	28
2.1.1 History and examination	28
2.1.2 Retinal imaging.....	29
2.1.3 Electrophysiology	32
2.2 Molecular genetic methods	35
2.2.1 DNA isolation and quantification	35
2.2.2 Polymerase chain reaction	35
2.2.3 Sanger sequencing.....	38
2.2.4 Next generation sequencing	39
2.2.4.1 Massively parallel sequencing.....	39
2.2.4.2 Variant call alignment and analysis	40
2.2.4.3 Whole genome sequencing	41
2.2.5 Other molecular investigations.....	41
2.2.6 Variant analysis and functional predictive tools.....	43
2.2.6.1 Determining novelty	43
2.2.6.2 Predicting pathogenicity.....	43
2.2.6.3 Protein modelling	44
2.3 Cell studies	44
2.3.1.1 Plasmid transformation of cells.....	44
2.3.1.2 Culture of single colonies.....	45
2.3.1.3 Sequencing of plasmid open reading frame	46
2.3.1.4 Site directed mutagenesis	46
2.3.1.5 Culture of hTERT-RPE1 cells.....	49
2.3.1.6 Transient transfection of hTERT-RPE1 cells.....	50
2.4 Zebrafish studies.....	54
2.4.1.1 Retinal immunohistochemistry.....	54
2.4.1.2 Tunel assay	55

2.4.1.3	Rescue experiments	55
3	RETINAL DYSTROPHY DUE TO MUTATIONS IN THE CONE-ROD HOMEBOX GENE	56
3.1	Introduction	56
3.2	Methods	56
3.2.1	Ascertainment of patients	56
3.2.2	Clinical assessment.....	57
3.2.3	Molecular investigations	57
3.3	Results	58
3.4	Discussion	68
4	ENHANCED S-CONE SYNDROME IN CHILDREN.....	72
4.1	Introduction	72
4.2	Methods	72
4.2.1	Patient ascertainment.....	72
4.2.2	Clinical assessment.....	72
4.2.3	Molecular investigations	73
4.3	Results	73
4.4	Discussion	80
5	NON-SYNDROMIC RETINAL DYSTROPHY DUE TO BI-ALLELIC MUTATIONS IN <i>IFT140</i>	83
5.1	Introduction	83
5.2	Methods	84
5.2.1	Patient ascertainment.....	84
5.2.2	Clinical investigations	84
5.2.3	Molecular investigations	84
5.2.4	Cell studies.....	85
5.2.5	Zebrafish studies	85
5.3	Results	85
5.4	Discussion	96
6	KNOBLOCH SYNDROME.....	100
6.1	Introduction	100
6.2	Methods	100
6.2.1	Ascertainment of patients	100
6.2.2	Clinical assessment.....	101
6.2.3	Molecular investigations	101
6.3	Results	101
6.4	Discussion	108
7	PRESERVED VISUAL FUNCTION IN RETINAL DYSTROPHY DUE TO HYPOMORPHIC <i>RPE65</i> MUTATIONS	112
7.1	Introduction	112
7.2	Methods	112
7.2.1	Ascertainment of patients	112
7.2.2	Clinical assessment.....	113
7.2.3	Molecular investigations	113
7.3	Results	114
7.4	Discussion	121
8	FAMILIAL EXUDATIVE VITREORETINOPATHY AND MICROCEPHALY	125
8.1	Introduction	125
8.2	Methods	125
8.2.1	Ascertainment of patients	125
8.2.2	Clinical assessment.....	125
8.2.3	Molecular investigations	126
8.3	Results	127
8.4	Discussion	132

9	HERMANSKY-PUDLAK SYNDROME 6	135
9.1	Introduction	135
9.2	Methods	135
9.2.1	Ascertainment of patients	135
9.2.2	Clinical assessment.....	136
9.2.3	Systemic investigations	136
9.2.4	Molecular investigations	136
9.3	Results	137
9.4	Discussion	140
10	CDH3 RELATED CONGENITAL HYPOTRICHOSIS WITH JUVENILE MACULAR DYSTROPHY	143
10.1	Introduction	143
10.2	Methods	143
10.2.1	Ascertainment of patients	143
10.2.2	Clinical assessment.....	144
10.2.3	Molecular investigations	144
10.3	Results	145
10.4	Discussion	151
11	MACULOPATHY DUE TO MUTATIONS IN CRB1	155
11.1	Introduction	155
11.2	Methods	155
11.2.1	Patient ascertainment	155
11.2.2	Clinical assessment.....	155
11.2.3	Molecular methods	156
11.3	Results	156
11.4	Discussion	159
12	CONE-ROD DYSTROPHY DUE TO MUTATIONS IN ADAM9	161
12.1	Introduction	161
12.2	Methods	161
12.2.1	Patient ascertainment	161
12.2.2	Clinical assessment.....	161
12.2.3	Molecular investigations	161
12.3	Results	162
12.4	Discussion	164
13	SOMATIC MOSAIC MUTATION OF IKBKG IN A MALE PATIENT WITH INCONTINENTIA PIGMENTI	165
13.1	Introduction	165
13.2	Methods	165
13.2.1	Patient ascertainment	165
13.2.2	Clinical investigations	166
13.2.3	Molecular investigations	166
13.2.3.1	DNA extraction from multiple tissue sources.....	166
13.2.3.2	Sequencing methods.....	166
13.3	Results	167
13.4	Discussion	169
14	CONCLUSIONS	171
14.1	Future directions	172
15	REFERENCES	174
16	APPENDIX: PUBLICATIONS RELATED TO THIS RESEARCH	206

List of figures

Figure 1-1: Retinal layers.....	12
Figure 1-2: Schematic representation of transduction and the visual cycle	16
Figure 1-3: Examples of visual acuity tests	17
Figure 1-4: Pedigree examples	21
Figure 2-1: Example colour fundus imaging	30
Figure 2-2: Examples of FAF imaging.....	30
Figure 2-3: Example of OCT imaging with layer segmentation.....	31
Figure 2-4: Examples of fundus fluorescein angiograms.....	32
Figure 2-5: Electroretinogram and pattern electroretinogram examples	34
Figure 2-6: Polymerase chain reaction.....	36
Figure 2-7: Temperature gradient optimisation example	38
Figure 2-8: Agarose gel of PCR site directed mutagenesis	48
Figure 2-9: Overnight LB agar plate culture of XL1-blue supercompetent cells	48
Figure 2-10: hTERT-RPE1 ciliated cells.....	53
Figure 3-1: Pedigrees	60
Figure 3-2: Retinal imaging in <i>CRX</i> related retinal dystrophy	61
Figure 3-3: Electroretinography features	62
Figure 3-4: Mutation codon position against age of onset	65
Figure 3-5: Schematic diagram of <i>CRX</i> structure and mutations.....	67
Figure 3-6: Conservation of missense variants across species	68
Figure 3-7: Conservation of missense variants across human paralogues.....	68
Figure 4-1: Fundal abnormalities in paediatric enhanced S-cone syndrome	75
Figure 4-2: Optical coherence tomography scans	76
Figure 4-3: Electrophysiology in enhanced S-cone syndrome.....	77
Figure 4-4: Pedigrees and mutation distribution for the 5 affected families	79
Figure 4-5: Conservation of missense mutations	80
Figure 5-1: Pedigrees of 5 families with mutation segregation	86
Figure 5-2: Retinal imaging in <i>IFT140</i> related rod-cone dystrophy	89
Figure 5-3: Skeletal imaging in <i>IFT140</i>	90
Figure 5-4: Conservation of missense variants	91
Figure 5-5: Aberrant localisation of <i>IFT140</i> with basal bodies in transiently transfected hTERT-RPE1 cells.....	92
Figure 5-6: Control experiments.....	93
Figure 5-7: Characterisation of an <i>ift140</i> zebrafish morphant.....	94
Figure 5-8: mRNA rescue experiments of morphant phenotype	95
Figure 6-1: Pedigrees and mutation segregation	102
Figure 6-2: Anterior segment and retinal imaging in Knobloch Syndrome	104
Figure 6-3: Cone-rod dysfunction in Knobloch syndrome.....	106
Figure 6-4: Neuroradiological findings in Knobloch syndrome.....	107
Figure 7-1: Pedigrees and segregation of <i>RPE65</i> variants.....	114
Figure 7-2: Retinal imaging in hypomorphic <i>RPE65</i> related dystrophy.....	116
Figure 7-3: Visual fields for patients 1, 2 and 4	117
Figure 7-4: Electrophysiology for patients 1 and 2.	118
Figure 7-5: Electrophysiology for patient 4.....	119
Figure 7-6: Comparison of VA age 18 years for 3 hypomorphes and 5 controls.....	120
Figure 7-7: Conservation of <i>RPE65</i> homologues throughout the species.	120
Figure 7-8: Crystalline structure of <i>RPE65</i> labelled with mutations	121
Figure 8-1: Pedigrees and mutations segregation for 10 FEVR families	129
Figure 8-2: Retinal imaging in FEVR with microcephaly.....	131
Figure 9-1: Anterior segment and retinal imaging in HPS-6	138
Figure 9-2: Pedigree of family 1 (patients 1 and 2) and <i>HPS6</i> chromatograms	139
Figure 9-3: Pedigree of family 2 (patient 3) and <i>HPS6</i> chromatograms.....	140
Figure 10-1: Pedigrees and chromatograms for patients with <i>CDH3</i> mutations	146
Figure 10-2: Retinal imaging in patients with HJMD	147
Figure 10-3: Serial imaging findings in <i>CDH3</i> related HJMD	148
Figure 10-4: Electroretinography in <i>CDH3</i> related HJMD	149

Figure 10-5: External photographs of patients 1, 6 and 7.....	150
Figure 10-6: Conservation of <i>CDH3</i> missense codons.....	150
Figure 10-7: Schematic diagram of <i>CDH3</i> with mutation codon location.....	152
Figure 11-1: Retinal imaging in <i>CRB1</i> related maculopathy.....	157
Figure 11-2: Hyperpigmented macular lesions.....	158
Figure 11-3: Preserved islands of RPE and photoreceptors.....	158
Figure 11-4: Conservation of novel missense residue in <i>CRB1</i>	159
Figure 12-1: Retinal imaging in a patient with <i>ADAM9</i> related CORD.....	162
Figure 12-2: Electrophysiology in <i>ADAM9</i> related CORD.....	163
Figure 12-3: Pedigree and sequencing results.....	163
Figure 13-1: Clinical features of incontinentia pigmenti.....	167
Figure 13-2: DNA chromatograms from Sanger sequencing of different tissue types.....	168

List of tables

Table 1-1: Conversion between Snellen and logMAR visual acuity.....	18
Table 1-2: Reported LCA genes, protein function and key features.....	23
Table 2-1: PCR protocol.....	36
Table 2-2: BIOTAQ and Mytaq protocols for PCR.....	37
Table 2-3: BigDye reaction.....	39
Table 2-4: List of 105 retinal genes in Manchester panel.....	42
Table 2-5: List of additional retinal genes in 176 gene panel.....	42
Table 2-6: Primer pairs for sequencing plasmid open reading frame.....	46
Table 2-7: Primer pairs for site directed mutagenesis.....	47
Table 2-8: Reaction mix for SDM.....	47
Table 2-9: Reaction steps for SDM.....	47
Table 2-10: Freezing medium components.....	50
Table 2-11: Optimisation of anti-FLAG antibody.....	52
Table 2-12: Optimisation of wild-type <i>IFT140</i> plasmid quantity.....	52
Table 3-1: Primer pairs for sequencing of <i>CRX</i>	57
Table 3-2: Key phenotypic features of patients.....	59
Table 3-3: Mutations in <i>CRX</i> found in this patient series.....	63
Table 3-4: Identified <i>CRX</i> variants of uncertain pathogenicity.....	64
Table 3-5: Previously reported mutations in <i>CRX</i>	66
Table 4-1: Primer pairs for sequencing of <i>NR2E3</i>	73
Table 4-2: Key clinical features.....	74
Table 4-3: Identified mutations in <i>NR2E3</i>	78
Table 5-1: Primer pairs for Sanger sequencing of <i>IFT140</i> in families 1 and 2.....	85
Table 5-2: Clinical summary of patients with <i>IFT140</i> related retinal dystrophy.....	87
Table 5-3: Previously reported mutations in <i>IFT140</i>	98
Table 6-1: Primer pair for sequencing <i>RPGRIP1</i>	101
Table 6-2: Key ophthalmic features in Knobloch syndrome.....	103
Table 6-3: Neuroradiological and systemic features.....	106
Table 6-4: Previously reported mutations in <i>COL18A1</i>	111
Table 7-1: Summary of clinical data.....	115
Table 8-1: Primer pairs for sequencing <i>LRP5</i> and <i>FZD4</i>	127
Table 8-2: Clinical summary for patients with FEVR and microcephaly.....	128
Table 8-3: Visual acuity based on retinal phenotype.....	129
Table 9-1: Primer pairs for sequencing of <i>HPS6</i> and <i>SLC38A8</i>	136
Table 9-2: Nine HPS genes and loci.....	137
Table 10-1: Primer pairs for <i>CDH3</i>	144
Table 10-2: Summary of clinical features in <i>CDH3</i> related macular dystrophy.....	145
Table 10-3: All reported mutations in <i>CDH3</i>	153
Table 11-1: Primer pairs for sequencing of <i>CRB1</i>	156
Table 11-2: Macula thickness in each eye compared with normative data.....	158
Table 12-1: Primer pair for sequencing of <i>ADAM9</i>	161
Table 13-1: Primer pairs for sequencing exon 8 of <i>IKBKG</i>	166

Abbreviations

AD	autosomal dominant	NGS	next generation sequencing
APEX	arrayed primer extension	NMD	nonsense mediated decay
ar	autosomal recessive	NPL	no perception of light
BLOC	biogenesis of lysosomal-related organelles	OCA	oculocutaneous albinism
bp	base pair	OCT	optical coherence tomography
CF	counting fingers	OFC	occipito-frontal circumference
CORD	cone-rod dystrophy	ONL	outer nuclear layer
CT	computed tomography	OPL	outer plexiform layer
cGMP	cyclic guanosine monophosphate	ORF	open reading frame
cPR	cone photoreceptor	ORTs	outer retinal tubulations
D	diopetre	OS	outer segment
DEXA	dual X-ray absorptiometry	PCR	polymerase chain reaction
DPF	days post fertilisation	PERG	pattern electroretinogram
DS	diopetre sphere	PL	perception of light
EDTs	electrodiagnostic tests	PTC	premature termination codon
EEMS	ectodermal dysplasia, ectrodactyly and macular dystrophy syndrome	RCD	rod-cone dystrophy
EORD	early-onset retinal dystrophy	RPE	retinal pigment epithelium
ERG	electroretinogram	SD	standard deviation
ESCS	enhanced S-cone syndrome	SNP	single nucleotide polymorphism
ETDRS	Early Treatment Diabetic Retinopathy Study	VA	visual acuity
FAF	fundus autofluorescence	VEP	visual evoked potential
FEVR	familial exudative vitreoretinopathy	WES	whole-exome sequencing
FFA	fundus fluorescein angiogram	WGS	whole-genome sequencing
GCL	ganglion cell layer	WT	wild type
HJMD	congenital hypotrichosis with juvenile macular dystrophy		
HM	hand movements		
HPS	Hermansky-Pudlak syndrome		
HRR	Hardy-Rand-Rittler		
IFT	intraflagellar transport		
ILM	inner limiting membrane		
INL	inner nuclear layer		
IP	incontinentia pigmenti		
IPL	inner plexiform layer		
ISe	inner segment ellipsoid		
LCA	Leber congenital amaurosis		
logMAR	logarithm of the Minimum Angle of Resolution		
MAF	minor allele frequency		
µm	micrometre		
MD	macular dystrophy		
MgCl₂	magnesium chloride		
MRI	magnetic resonance imaging		

1 Introduction

Early-onset retinal dystrophies (EORD) are inherited disorders presenting in childhood with visual impairment due to degenerative abnormalities of photoreceptors. EORD is an important cause of visual impairment registration in the United Kingdom.¹ The reported prevalence of both isolated and syndromic retinal dystrophy in children from a Danish population study was 13 in 100,000 with the majority of affected patients having Leber congenital amaurosis (LCA) or rod-cone dystrophy (RCD).² Approximately 57% of cases are non-syndromic with the most common syndromic cause being Usher syndrome in which RCD and sensorineural hearing impairment coincide.² Prevalence and genetic aetiology vary geographically with more isolated or consanguineous communities demonstrating a greater burden of disease.³

Since the initial discovery of *Rho* causing dominant RCD in 1990, more than 160 genes have been associated with retinal dystrophy.^{4,5} Many, including *CRB1*, *CRX*, *GUCY2D* and *RPE65* exhibit phenotypic heterogeneity and have been associated with more than one retinal disorder.⁶⁻⁹ Increasingly, with the advent of next generation sequencing (NGS), the association of non-syndromic retinal dystrophy with mutations in syndromic genes has been reported including *CEP290*, *CLN3*, and *BBS1*.¹⁰⁻¹² This clinical and molecular heterogeneity presents a diagnostic challenge.

NGS techniques including whole-exome screening (WES), allow parallel screening of multiple genes. Approximately 55% of non-syndromic retinal dystrophies and 80% of syndromic retinal dystrophies can achieve molecular diagnosis by WES.¹³⁻¹⁵ The remaining unsolved cases can be explained by missed variants on exome due to poor coverage, for instance the ORF15 region of *RPGR*, variants assumed to be non-pathogenic but in fact important for splicing, novel genes, copy number variants and non-coding region variants.¹⁰ These non-coding region variants can arise within promoters such as the locus control region of opsin genes and within introns creating alternate splice sites such as the common intronic variant in *CEP290* related disease, c.2991+1655A>G.^{12, 16, 17} Whole genome sequencing (WGS), has better coverage of regions that may not be covered well in WES.¹⁵ In addition, WGS will help identify copy number variants and non-coding region variants that may be responsible for disease.¹⁸ Ultimately, combined approaches with WGS and RNA analysis may be needed to solve undiagnosed cases.

1.1 The neurosensory retina

The neuroretina is the light sensitive structure within the eye responsible for transducing photons of incident light into electrical signals to be interpreted by the brain as images. Light enters the eye through the cornea, aqueous humour, pupillary aperture of the iris, lens and vitreous humour, with the cornea and lens the refractive structures that focus the light on to the retina. The laminated neuroretina comprises multiple different cell types to interpret and perform initial processing of these signals supported by the underlying retinal pigment epithelium (RPE, figure 1-1).

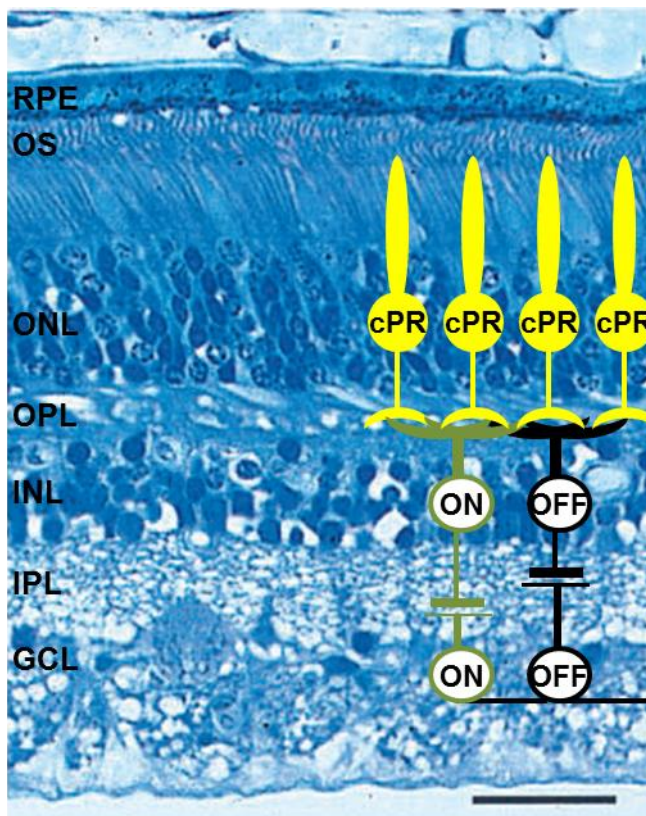


Figure 1-1: Retinal layers

Layers of the retina with superimposed basic cone photoreceptor cell circuitry (adapted from Fariss 2000¹⁹ and Busskamp 2010²⁰). RPE, retinal pigment epithelium; OS, outer segment; ONL, outer nuclear layer; OPL, outer plexiform layer; INL, inner nuclear layer; IPL, inner plexiform layer; GCL, ganglion cell layer; cPR, cone photoreceptor; ON and OFF bipolar cells in the INL and GCL layers. Scale bar 20 μ m.

The neurosensory retina comprises 6 broad types of neural cells, rod and cone photoreceptors, bipolar, horizontal, amacrine and ganglion cells as well as one main type of glial cell, the Müller glial cell. There are actually more than 60 diverse sub-types of neural cells reflecting the complex processing of the retina.²¹ Rod and cone photoreceptors comprise an inner segment containing the cell body, a connecting cilium and an outer segment. The outer segments are highly modified, photosensitive cilia, containing the membranous discs for phototransduction. They lack any capability

for protein production and rely on the intraflagellar transport (IFT) system, which comprises large protein complexes for transport from the cell body to cilium tip and back.^{22, 23} There are an estimated one thousand stacked discs in the rod outer segment which are discrete from the plasma membrane and extracellular space, whereas in the cone outer segment there are a series of membrane evaginations exposed to the extracellular space.²⁴ Ten percent of the discs in rods undergo distal shedding and phagocytosis by the RPE at daily onset of light, whilst new discs are formed at the base of the outer segment with an analogous process occurring in the cone outer segment.^{24, 25} There are approximately 4.6 million cones which comprise 3 types, long-wavelength sensitive (L), medium-wavelength sensitive (M) and short-wavelength sensitive (S).²⁶ Colour vision arises from two cone-opponent systems, the red-green system from compared responses between L- and M-cones and the blue-yellow system in which S-cone responses are compared to a combined L- and M-cone response.²⁷ There are 92 million rod photoreceptors with the highest density in a ring at the eccentricity of the optic disc and an absence of rods from the central fovea which is populated exclusively by cones.²⁶ Photoreceptor outer segments interdigitate with the underlying RPE, their cell bodies are located in the outer nuclear layer and their axonal processes form synapses in the outer plexiform layer with bipolar and horizontal cells.

There are approximately 12 types of bipolar cell, 11 of which are cone specific and each connect to multiple cone photoreceptors.²¹ Responses can be broadly classified in to ON and OFF channels which respond differently to light input and synapse with ganglion ON and OFF bipolar cells directly or via amacrine cells.²¹ Rod photoreceptors synapse with rod bipolar cells and then to amacrine cells. Amacrine cells, of which there are approximately 30 types, act as modifiers of bipolar and ganglion cell responses. The axonal processes of ganglion cells radiate across the retina, become the optic nerve, and then decussate in the optic chiasm before synapsing predominantly in the lateral geniculate nucleus. An additional photosensitive pigment, melanopsin also known as opsin 4, is found within a small subset of intrinsically photosensitive retinal ganglion cells with non-visual roles in circadian rhythm and the pupillary light reflex.²⁸ The major target of intrinsically photosensitive retinal ganglion cells is the suprachiasmatic nuclei, in which the main circadian clock in mammals is found.²⁹

The main non-neuronal cell of the retina, the Müller glia extend from the photoreceptors to the inner limiting membrane and have roles in retinal development, the visual cycle of cones and retinal neuron cell metabolism.^{30, 31} There are outer and inner plexi of retinal vessels throughout the retina except for a central foveal avascular zone of approximate diameter 450µm, essential for clear vision by reducing light

scatter due to blood vessels.³² The RPE comprises a single pigmented layer of cells essential in retinal metabolism and retinal structure. Underneath the RPE lies the choroid comprising Bruch's membrane, a capillary network, the choriocapillaris and the large choroidal vessels.

1.1.1 Retinal development

Multi-potential retinal progenitor cells can form any of the 6 retinal neurons or 1 retinal glial cell dependent on the temporal and spatial expression of transcription factors including PAX6, SOX2 and VSX2.^{33, 34} Ganglion cells are the initial cell type to appear. In humans, differentiation arises first in the fovea with the peripheral retina laminated by week 30 of gestation.³⁵ The foveal pit is created by displacement of inner retinal layers out of the centre. Photoreceptor maturation, in particular the lengthening of outer segments, continues after birth, is initially most developed in non-foveal regions and continues up until the age of approximately 13 years.³⁶ In addition, the ONL thickens in the fovea from approximately 3 weeks of age onwards due to central cone packing. This developmental process has implications on visual function, with infants having poor central vision.

Retinal vasculogenesis begins in the inner retina at the optic nerve head and radiates outwards, reaching the peripheral retina just before birth.³² The deeper retinal capillary networks arise by angiogenic sprouting from the inner retinal vessels. The process is regulated by pro and inhibitory angiogenic factors such as vascular endothelial growth factor (VEGF). Components of the Wnt signalling pathway, including FZD4, Norrin and LRP5 are central regulators of vascular endothelial cell development and are essential for normal retinal vascular growth and organisation.³⁷

1.1.2 Phototransduction and the visual cycle

Phototransduction is the process by which a photon of light is absorbed by light sensitive pigment in rods (rhodopsin) and cones (cone opsins) and converted in to an electrical signal (figure 1-2). Rhodopsin and the cone opsins comprise an opsin protein covalently bound to a light sensitive chromophore, 11-*cis*-retinaldehyde.³⁸ Upon light stimulation, this is isomerised to all-*trans*-retinaldehyde which induces conformational changes within the protein to an activated state.³⁸ The activated opsin binds to a G-protein, transducin, with subsequent activation of cGMP phosphodiesterase (PDE) resulting in decreased cGMP concentration and a consequent decrease of intra-discal calcium concentration by closure of cation gated channels. Reduced calcium leads to hyperpolarisation of the membrane forming the basis of generation of an electrical signal from a photon of light. Opsins are inactivated by phosphorylation and arrestin

binding. Restoration to the dark-adapted state relies on the function of guanylate cyclase to restore cGMP levels and re-open the cGMP gated cation channels.

Recycling of chromophores to regenerate 11-*cis*-retinaldehyde is an enzymatic process known as the visual cycle and arises in the RPE (figure 1-2).³⁸ All-*trans*-retinal diffuses from the disc membrane in to the cytoplasm or is transported via the transmembrane ATP-binding cassette, subfamily A, member 4 (ABCA4) in to the cytoplasm where it is reduced to all-*trans*-retinol by retinal dehydrogenases (RDH) including RDH12.³⁹ It then diffuses bound to binding proteins including interstitial retinol-binding protein (IRBP) in to the RPE where lecithin retinol acyltransferase (LRAT) esterification forms fatty acid retinal esters. The esters undergo isomerisation by retinal pigment epithelium-specific protein, 65kDa (RPE65) to form 11-*cis*-retinol which is oxidised to the 11-*cis*-retinal form by 11-*cis*-RDHs including RDH5.⁴⁰⁻⁴² The 11-*cis*-retinal diffuses back in to the outer segment again bound to IRBP to reform the stable opsin (or rhodopsin) pigment.

Mutations in genes encoding the key proteins involved in phototransduction and the visual cycle are associated with a range of inherited retinal dystrophies. This includes *GUCY2D* related LCA, *RPE65* related LCA and RCD, *LRAT* related LCA, *RDH5* related fundus albipunctatus, *RBP3* (encoding IRBP) related retinal dystrophy, *RDH12* related LCA, *ABCA4* related cone-rod dystrophy (CORD) and macular dystrophy (MD) and achromatopsia due to mutations in cone specific phototransduction genes *GNAT2*, *PDE6C*, *CNGA3*, *CNGB3* and *PDE6H*.⁴³⁻⁵⁰

There is an alternative cone-specific second pathway present in Müller cells in which 11-*cis*-retinol is generated which cones but not rods can use to regenerate their chromophores.³¹ The enzyme that catalyses the production of 11-*cis*-retinol is thought to be multifunctional *O*-acyltransferase (MFAT).³¹

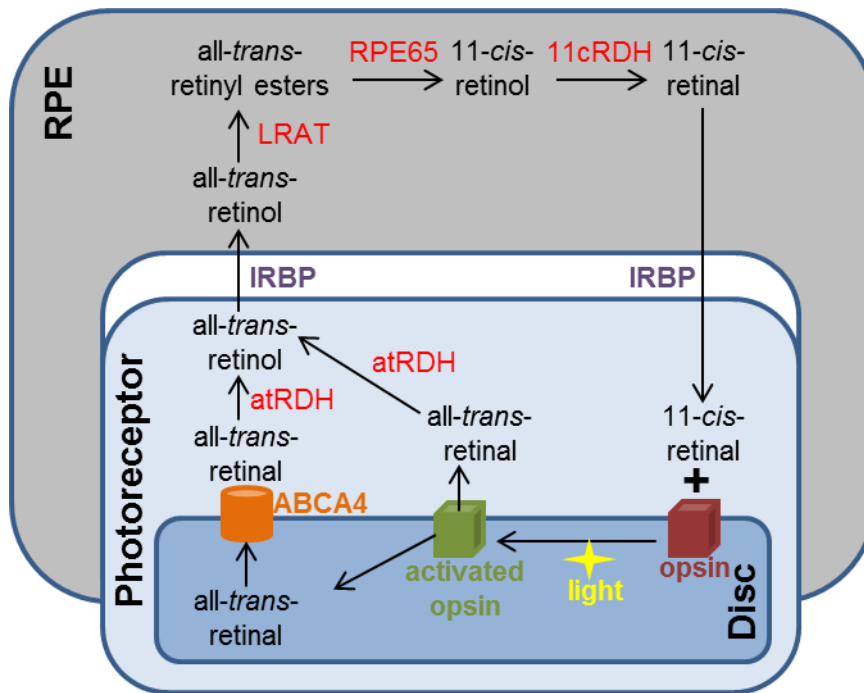


Figure 1-2: Schematic representation of transduction and the visual cycle

Image based on Palczewski 2014.³⁸ Opsin in the outer segment disc membrane is activated by a photon of light. All-*trans*-retinal is converted in the photoreceptor cytoplasm to all-*trans*-retinol by all-*trans* retinal dehydrogenase (atRDH). This is transported by IRBP in to the RPE where LRAT converts it to all-*trans*-retinyl esters. RPE65 isomerises this to 11-*cis*-retinol, RDH5 dehydrogenases this to 11-*cis*-retinal which IRBP transports back in to the photoreceptor outer segment for re-association with opsin.

1.2 Clinical assessment

Assessment of visual function and examination of ocular pathology are readily achieved in the clinical setting. Visual acuity, colour vision and fields are objective measurements of visual deficit. Slit lamp biomicroscopy through a dilated pupil permits direct visualisation of fundus changes which may be more apparent on retinal imaging.

1.2.1 Visual function

Visual acuity is a measurement of the ability to discriminate 2 points at a distance. The greatest acuity is found in the central fovea where the resolving power can reach 14 seconds of arc, greater than the angle subtended by a single cone partly due to complex retinal neuron processing and higher cortical processing.⁵¹ In infancy, visual acuity is reduced due to a lack of foveal maturation with foveal cone density rapidly increasing over the first 8 months of life.⁵² In addition, infants are hypermetropic due to the relatively small eyeball size with the process of emmetropisation occurring as the eye grows. High refractive errors are frequently found in retinal dystrophies possibly reflecting abnormal emmetropisation due to reduced vision.⁵³

Methods for assessing visual acuity are dependent on age and the presence of developmental delay. Optotypes are standardised pictures or letters for testing vision that represent the minimum distance between 2 points that the average person can resolve, specifically 1 minute of arc which is the thickness of the lines used in each optotype when viewed at a fixed distance.⁵⁴

In infants, forced-choice preferential looking cards are used which have a black and white grating pattern.⁵² The Cardiff acuity test, employ a similar preferential looking system but with vanishing optotypes using recognisable shapes such as a fish or a ship and are used from 6 months up to 2 years of age (figure 1-3). Once children are verbal and able to recognise pictures, usually from the age of 2 years, Kay pictures are used of varying size to represent specific visual acuity levels.⁵⁵ Once able to read, Snellen or logarithm of the Minimum Angle of Resolution (logMAR) visual acuity charts are used with decreasing sizes of optotypes. Patients are tested unilaterally with refractive correction and additionally with a pinhole. Snellen charts have a number of limitations including non-uniform progression in letter size and a different number of letters per line, the logMAR chart is more accurate in this regard.⁵⁶ Within this thesis, variable methods of visual acuity measurements over time were frequently found. To enable comparison, all acuities were converted between Snellen and logMAR using a conversion table (table 1-1).



Figure 1-3: Examples of visual acuity tests

Adapted from www.kaypictures.co.uk and www.haagstreituk.com. From left to right; the Cardiff acuity test, Kay picture test, logMAR chart.

Colour vision is routinely tested with either the Ishihara or Hardy-Rand-Rittler (HRR) tests, which are both pseudoisochromatic. The latter is the most accurate in identifying colour defects consistent with cone abnormalities as it tests all 3 components of colour vision including tritan function and can be performed in young children.⁵⁷ Reduced visual acuity can limit testing but only once worse than 0.72 logMAR for Ishihara plates and 1.10 logMAR for HRR plates.⁵⁸

Snellen visual acuity	log MAR visual acuity
6/3.8	-0.2
6/4.8	-0.1
6/6	0.0
6/7.5	0.1
6/9	0.18
6/9.5	0.20
6/12	0.3
6/15	0.4
6/18	0.48
6/19	0.50
6/24	0.60
6/30	0.70
6/38	0.80
6/48	0.90
6/60	1.00
6/75	1.10
6/90	1.18
6/95	1.20
6/120	1.30
6/150	1.40
6/190	1.50
6/240	1.60
6/600	2.00

Table 1-1: Conversion between Snellen and logMAR visual acuity

Adapted from Gregori 2010⁵⁹

Visual field testing permits an assessment of central regions of missing vision (scotomas) or of peripheral field defects. Visual fields to confrontation are also used as a rapid screening method for deficits. Formal visual fields are an objective method for monitoring progression over time and in addition are used to assess eligibility to drive. Within the clinic two main types of testing are used; the first a type of kinetic unocular visual field (Goldmann, Haag Streit, Bern, Switzerland) with a moving stimulus of varying brightness and size; the second with a static stimulus using the Humphrey Field Analyzer II (Carl Zeiss Meditec AG, Oberkochen, Germany) to produce unocular Humphrey 24-2 and 30-2 threshold visual fields or suprathreshold binocular (driving) Esterman visual fields. Goldmann visual field defects have been shown to correlate with wide-field autofluorescence imaging defects in patients with retinal dystrophy.⁶⁰

1.2.2 Ophthalmoscopy and retinal imaging

Binocular biomicroscopy with a slit lamp permits a stereoscopic, magnified examination of the eye with a double aspheric high-power positive lens used to focus on the fundus. Colour fundus photography allows accurate documentation of fundus changes and can

be performed in cooperative young children with a variety of cameras as described in methods. Particularly useful in the assessment of retinal dystrophy patients are fundus autofluorescence (FAF) imaging and optical coherence tomography (OCT). FAF can demonstrate areas of retinal dysfunction or atrophy not necessarily apparent on colour images. OCT provides a high resolution cross-sectional image of the retinal layers to allow quantifiable assessment of any changes in thickness or atrophy, as well as any intraretinal cystoid macular oedema, a frequent complication of RCD.⁶¹ These imaging techniques are further described in methods.

1.3 Molecular genetics

The human mitochondrial genome was first deciphered in 1981 but it was only in 2004 that a near complete human nuclear genome was published.^{62, 63} The Human Genome Project involved more than 20 groups across 6 countries from 1990 to 2004 at an estimated cost of 3 billion dollars.⁶⁴ Approximately 99% of the 3.1 gigabase genome was covered with the remainder consisting mainly of heterochromatin, a permanently condensed, transcriptionally inactive and highly repetitive DNA that is particularly challenging to sequence.⁶⁵ With the development of new sequencing technologies, the cost of a whole genome is now available for less than £1000.⁶⁴

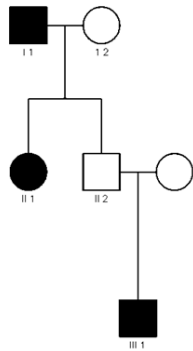
The emergence of new sequencing technology has greatly changed the approach to the molecular investigation of patients with parallel sequencing of multiple copies of fragmented DNA allowing a rapid and cost-effective approach to investigation. Previously Sanger sequencing of candidate genes, linkage analysis and arrayed primer extension (APEX) microarray screening were the only investigative options. Subsequently, NGS became routinely available with a large number of patients investigated by gene panels (Manchester Centre for Genomic Medicine), WES and WGS. In the research setting, we have performed WES on >100 patients with EORD. We have been able to recruit patients in to national research projects employing NGS techniques thus providing a funded route for investigating patients. This has included the National Institute for Health Research (NIHR) BioResource funded Specialist Pathology: Evaluating Exomes in Diagnostics (SPEED) study based at the Cambridge Biomedical Centre to which >500 patients have been contributed from Moorfields. Initially WES was performed but the majority of patients have undergone WGS as the cost difference became minimal. A second project to which large numbers of patients are being recruited is the 100,000 Genomes Project. This was devised in 2012 to sequence 100,000 whole genomes from 70,000 people with rare diseases and cancer with the aim of driving research, developing a genomic medicine service for the NHS and improving diagnosis and treatment (www.genomicsengland.co.uk). I was involved in running the pilot phase of this project in November 2013.

Within this thesis, patients have been molecularly solved by a variety of methods including Sanger sequencing, a tool which still provides a rapid and cheap screening approach for panels of unsolved patients and for confirmation of variants found by other methods.

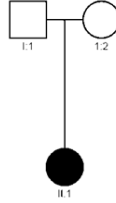
1.3.1 Mendelian inheritance

The approach to the investigation of the majority of EORD patients relies on the assumption of Mendelian or monogenic inheritance in which an alteration in the genetic code at a single locus leads to an abnormal phenotypic expression. A trait or condition that follows Mendelian inheritance may demonstrate a recognisable pedigree pattern to determine likely inheritance. There are a number of caveats to this. An autosomal dominant pedigree may not be apparent if there is variable expressivity or *de novo* disease, features found in *CRX* related retinal dystrophy, or if there is variable penetrance as found in *PRPF31* related RCD (figure 1-4).^{7, 66} In autosomal recessive inheritance, a pedigree may appear pseudo-dominant if the condition is common in the population or if there is extended consanguinity within the family. X-linked dominant disease may resemble a dominant pedigree except that there can be no male to male transmission. The pedigree may resemble that of mitochondrial inheritance with only female transmission possible but both males and females affected. If the condition is fatal in utero to males then only females within the pedigree will be affected as typically found in conditions such as incontinentia pigmenti.⁶⁷ In X-linked recessive disease, there is also no male to male transmission and in theory only males should be affected. However, female carriers can have phenotypic manifestations of disease due to skewed X-inactivation. This is apparent in conditions such as X-linked RCD.⁶⁸

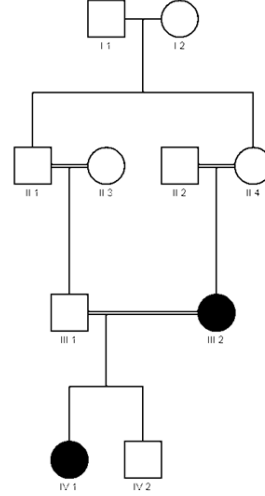
Autosomal dominant disease with variable penetrance or mild asymptomatic expressivity



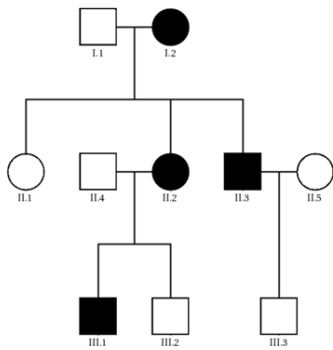
Autosomal dominant disease with *de novo* mutation



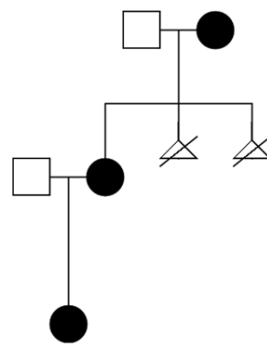
Autosomal recessive disease with pseudo-dominant pedigree due to multiple consanguinity



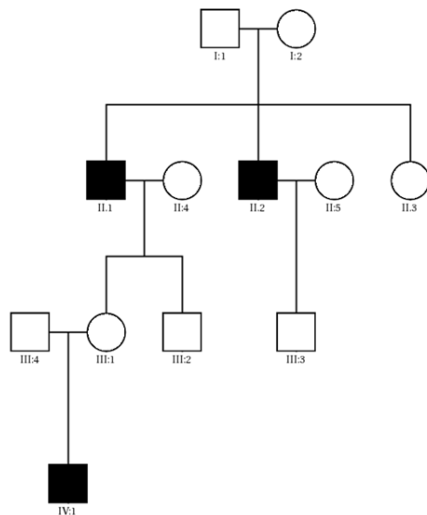
X-linked dominant disease, no male to male transmission



X-linked dominant disease, fatal *in utero* to males



X-linked recessive disease, no male to male transmission



X-linked recessive disease, affected female due to skewed X-inactivation

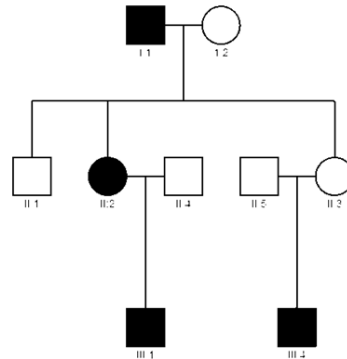


Figure 1-4: Pedigree examples

1.4 Types of retinal dystrophy

1.4.1 Leber congenital amaurosis

At the most severe end of the spectrum is Leber Congenital Amaurosis (LCA, MIM# 204000), a clinically and genetically heterogeneous condition characterised by onset at birth or in infancy, nystagmus and an absence of photoreceptor responses on ERG.⁶⁹ It was first described by Theodore Leber a German Ophthalmologist in 1869.⁷⁰ It accounts for at least 5% of all retinal dystrophies and 20% of children attending schools for the visually impaired with an estimated incidence of 1 in 81000 to 1 in 30000 live births.⁷¹ LCA may be isolated to ocular involvement or arise as part of a syndrome. The prognosis depends on the underlying genetic defect. For instance, patients with *RPE65* related disease have a better prognosis than *GUCY2D*.^{69, 72}

In LCA, at least 17 genes have been identified to date. All are recessively inherited apart from *CRX* which is predominantly dominant with a high rate of *de novo* mutations and 3 reports of sporadic heterozygous *IMPDH1* related LCA.⁷³⁻⁷⁵ Disease manifests by variable mechanisms (table 1-2). The regulation of phototransduction by intracellular cGMP is abnormal in LCA due to mutations in *GUCY2D* which encodes a membrane bound guanylate cyclase in photoreceptor outer segments.⁵⁰ Phototransduction is also affected by mutations in *RPE65*, *RDH12* and *LRAT* which encode enzymes essential in the retinol metabolism pathway.^{43, 45, 76} Abnormal photoreceptor development and survival arises in *CRX* related disease.⁷⁷ Abnormal cilia metabolism or protein trafficking is found in *AIPL1*, *LCA5*, *RPGRIP1*, *CEP290*, *SPATA7*, *TULP1*, *RD3* and *IQCB1* disease.^{12, 78-85} Abnormal function of the RPE inwardly rectifying potassium channel Kir7.1 is found in *KCNJ13* related disease leading to an abnormal membrane resting potential.⁸⁶ Mutations in *IMPDH1* may be pathogenic by impairing regulation of translation at polyribosomes.⁸⁷

Patients with LCA present with profound visual loss from birth or within the first few months of life, with a typical final visual acuity of 3/60 Snellen to perception of light.^{69, 72} Other features include pendular nystagmus, roving eye movements, sluggish or absent pupillary responses, high refractive error and the oculodigital sign where repetitive eye poking leads to loss of orbital fat, enophthalmos and eventually cataract and keratoconus. Photoattraction may be noted and conversely, although less commonly photodysphoria (extreme photophobia), a feature of *GUCY2D* related disease.⁷² Of note, visual function (acuity and fields) can vary significantly between visits and this is of particular relevance when considering clinical trials as the inter-test variability needs to be taken in to account.⁸⁸

Pheno-type, MIM #	Gene symbol, MIM	Chromo somal locus	Protein name (and function)	Key defining clinical features	First published
LCA1 204000	<i>GUCY2D</i> 600179	17p13.1	Guanylate cyclase 2D (hydrolysis cGMP)	Very poor vision, severe photoaversion, normal fundus early on	Perrault 1996 ⁵⁰
LCA2 204100	<i>RPE65</i> 180069	1p31.3- 1p31.2	Retinoid isomerohydrolase (phototransduction)	Relatively good early vision early on, featureless fundus, low autofluorescence	Marlhens 1997 ⁴³
LCA3 604232	<i>SPATA7</i> 609868	14q31.3	Spermatogenesis-associated protein 7 (cilial protein trafficking)	Retinal atrophy, attenuated vessels	Wang 2009 ⁸⁹
LCA4 604393	<i>AIP1</i> 604392	17p13.2	Aryl-hydrocarbon-interacting protein-like 1 (PDE6 chaperone)	Atrophic maculopathy, severe early visual loss	Sohocki 2000 ⁹⁰
LCA5 604537	<i>LCA5</i> 611408	6q14.1	Lebercilin (cilial transport)	Macula dysplasia/atrophy	den Hollander 2007 ⁷⁸
LCA6 613826	<i>RPGRIP1</i> 605446	14q11.2	Retinitis pigmentosa GTPase regulator-interacting protein (cilial transport)	Severe vision loss, initial normal fundus progresses to pigmentary retinopathy	Dryja 2001 ⁷⁹
LCA7 613829	<i>CRX</i> 602225	19q13.33	Cone-rod homeobox protein (photoreceptor development and survival)	Severe vision loss, macula atrophy, AD or sporadic	Freund 1998 ⁷⁷
LCA8 613835	<i>CRB1</i> 604210	1q31.3	Crumbs homolog 1 (Müller cell photoreceptor interaction and photoreceptor cell structure)	Nummular pigmentation, para-arteriolar RPE sparing, thickened and disorganised retina, Coat's like response	Lotery 2001 ⁹¹
LCA9 608553	<i>NMNAT1</i> 608700	1p36.22	Nicotinamide mononucleotide adenylyltransferases 1 (NAD+ biosynthesis and neuroprotection)	Atrophic macular lesions	Falk ⁹² , Perrault ⁹³ , Chiang ⁹⁴ , Koenekoop ⁹⁵ , all 2012
LCA10 611755	<i>CEP290</i> 610142	12q21.32	Centrosomal protein of 290 kDa (cilial transport)	Minimal fundus abnormalities in infancy	den Hollander 2006 ¹²
LCA11 146690	<i>IMPDH1</i> 146690	7q32.1	Inosine-5'-monophosphate dehydrogenase 1 (guanine synthesis and translation regulation)	Diffuse RPE mottling, no pigmentary deposits	Bowne 2006 ⁷⁴
LCA12 610612	<i>RD3</i> 180040	1q32.3	Protein RD3 (trafficking of guanylate cyclase 1)	Atrophic macular lesion	Friedman 2006 ⁹⁶
LCA13 612712	<i>RDH12</i> 608830	14q24.1	Retinol dehydrogenase 12 (phototransduction)	Bone spicule pigmentation and maculopathy, may get Coats like response	Janecke 2004 ⁷⁶
LCA14 613341	<i>LRAT</i> 604863	4q32.1	Lecithin retinal acyltransferase (phototransduction)	Low autofluorescence	Thompson 2001 ⁴⁵
LCA15 613843	<i>TULP1</i> 602280	6p21.31	Tubby-related protein 1 (cilial transport)	Pigmentary retinopathy, reading vision in early stages	Hagstrom 1998 ⁹⁷ , Banerjee 1998 ⁹⁸
LCA16 614186	<i>KCNJ13</i> 603208	2q37.1	Inward rectifier potassium channel 13 (RPE potassium channel)	Early poor vision, gradual progression, posterior pole dense nummular RPE pigmentation	Sergouniotis 2011 ⁸⁶
SLSN5 609254	<i>IQCB1</i> 609237	3q13.33	IQ motif-containing protein B1 (cilial protein)	Relatively preserved central RPE and photoreceptors, peripheral granular RPE change	Estrada-Cuzcano 2011 ⁸⁵ , Stone 2011 ⁸⁴

Table 1-2: Reported LCA genes, protein function and key features

SLSN5, Senior-Loken syndrome 5

The fundus appearance may initially be normal or show macular atrophic change with a pigmentary retinopathy tending to develop over time. Other reported changes include disc pallor, vessel attenuation, optic disc drusen, optic disc oedema, flecked retina and nummular pigmentation. Fundus appearances vary by genetic cause (table 1-2).

Fundus imaging may be limited in LCA from poor fixation due to young age, low vision, nystagmus or photophobia or poor image quality from nystagmus. Imaging as part of an examination under anaesthesia can be achieved using handheld instruments for fundus photography, FAF imaging and OCT. FAF imaging may be normal in LCA, or more commonly show a ring of increased autofluorescence parafoveally indicating abnormal accumulation of lipofuscin in the post mitotic RPE cell, with reduced autofluorescence around the arcades indicating RPE atrophy.^{99, 100} In *RPE65* related disease, the fundus appearance is usually normal in childhood but the FAF is universally severely reduced throughout the retina due to a lack of lipofuscin production from abnormal retinol metabolism.¹⁰¹ Patients with LCA, poor vision and undetectable ERG may still have normal or minimally decreased autofluorescence. This suggests that the RPE–photoreceptor complex is, at least in part, functionally and anatomically intact. This finding would have implications for future treatment, indicating that photoreceptor function may still be rescuable in such patients.

Electrodiagnostic testing although technically difficult in early childhood, is a key investigation to distinguish LCA from other early onset inherited retinal dystrophies presenting with nystagmus and poor vision such as congenital stationary night blindness and achromatopsia.¹⁰² The ERG in LCA for both photopic and scotopic responses is undetectable or severely abnormal. In congenital stationary night blindness the ERG shows a diminished scotopic b wave in the presence of a normal a wave. In achromatopsia (which may present very similarly to *GUCY2D* related LCA with photoaversion) the photopic responses are generally non-recordable with preserved scotopic (rod specific) responses.

Systemic assessment and relevant investigations are necessary for all LCA patients to exclude an underlying syndromic diagnosis or potential associated systemic findings. These include learning difficulties, found in 19.8% of LCA patients, neurological disorders including epilepsy, cerebellar vermis hypoplasia, renal impairment and cardiomyopathy.^{12, 103-105} Syndromic features may not be present at diagnosis but may develop later. For instance, Senior-Loken syndrome characterised by nephronophthisis and LCA and linked to 5 genes, usually presents in the first decade, but renal failure may not present until the second decade, if at all.^{84, 85, 106} The advent of molecular diagnosis via NGS may impact on the approach to systemic investigation of patients. A molecular diagnosis of non-syndromic retinal dystrophy may indicate no further

investigations are needed but conversely the identification of a syndromic cause such as a gene causing Joubert syndrome would allow targeted systemic investigation.

1.4.2 Rod cone dystrophy

In RCD, also known as retinitis pigmentosa, patients generally present in childhood or adolescence with symptoms of nyctalopia, a pigmentary retinopathy often described as bone spicules from intra-retinal pigmentary migration and ERG abnormalities predominantly affecting rod function first.^{107, 108} Retinal degeneration starts in the mid-periphery with loss of photoreceptors and mid-peripheral field loss. As the condition progresses, degeneration advances anteriorly and posteriorly reducing the visual field and ultimately affecting the central vision. Loss of vision occurs in adult life at an age depending on the underlying genetic cause.¹⁰⁹ Age of onset and visual prognosis are very variable. Other features include vascular attenuation, waxy disc pallor, cataract and cystoid macular oedema.

From a large series, dominant disease accounted for 20% of cases, recessive (classified based on consanguinity or more than 1 affected sibling) for 15%, X-linked for 7%, with 43% sporadic/simplex cases.¹¹⁰ Sporadic cases are often assumed to be recessive in origin although a significant minority will represent de novo dominant disease, X-linked (for males), mitochondrial or uniparental isodisomy.¹⁰⁷ WES investigations of sporadic cases have identified mutations in dominant genes in 10-19%, which may result from de novo mutations or incomplete penetrance in parents.^{10, 13} The first reported genetic cause of any RCD was of a mutation in the *RHO* gene which encodes the visual pigment for rod photoreceptors and is associated with dominantly and recessively inherited RCD.^{4, 111}

Non-syndromic recessive RCD has been associated with more than 60 genes.^{107, 112, 113} Dominantly inherited RCD is most commonly found to be due to *RHO* in 25% of cases.¹⁰⁷ Incomplete penetrance in dominant disease (which may initially mask the true inheritance pattern when analysing the pedigree) has been reported with *RP1* and pre-mRNA splicing factors such as *PRPF31*.^{114, 115} X-linked RCD presents earlier, is associated with childhood myopia and progresses more rapidly than other forms of RCD.¹⁰⁹ It usually manifests severe disease only in males. The phenotype in carrier females can be very variable from no abnormalities through to severe disease presumed to be related to random X-inactivation. In most families, the examination of carrier females is informative with abnormalities of the retina including a tapetal reflex and sectoral peripheral bone spicule pigmentation.⁶⁸ Three genes have been associated with X-linked RCD, *RPGR*, *RP2* and *OFD1* although the latter has only been found in 1 family to date.¹¹⁶ 73% of cases are due to mutations in *RPGR* with

66% of these clustered in the ORF15 region.¹¹⁷ Mutations within the ORF15 region of *RPGR* have also been shown to cause X-linked COD.¹¹⁸

1.4.3 Cone rod dystrophy

COD is less common than RCD arising in 1 in 80,000 from one large population study.¹⁰⁸ Patients present in childhood at a mean age of 11 years with disturbance of central visual function manifesting with reduced visual acuity, symptoms of blur, reduced colour vision and central scotoma.^{119, 120} Bulls-eye maculopathy is an early finding with retinal thinning on OCT. As the disease progresses, nyctalopia occurs and peripheral pigmentation increases. Severe sight impairment occurs by a mean age of 35 years.¹²⁰ Recessive mutations account for 90% of COD cases with *ABCA4* the most commonly identified gene.^{120 119}

1.4.4 Macular dystrophy

Childhood onset macular dystrophies arise less frequently than pigmentary retinopathies. Most common are Stargardt disease and Best's disease with several other less common types including pattern dystrophy from *PRPH2* and X-linked retinoschisis from mutations in *RS1*.^{110, 121} Recessive mutations in *ABCA4* can cause COD or RCD but most commonly cause Stargardt disease, a juvenile onset macular dystrophy characterised by yellow pisciform fleck deposits in the posterior pole. In Stargardt approximately half of patients have full field ERG abnormalities which represent peripheral photoreceptor dysfunction and are used as a marker of severity of disease.¹²² Best's vitelliform macular dystrophy presents in the 2nd decade with reduced visual acuity, yellow macular lesions and an abnormal electrocyclogram due to *BEST1* mutations.¹²³ There is significant intra-familial variability in severity. Rarely, bi-allelic mutations in *BEST1* cause a vitelliform dystrophy which is multifocal and has ERG abnormalities in adulthood.¹²⁴

1.4.5 Abnormal retinal vasculogenesis

Inherited disorders of retinal vascular development include familial exudative vitreoretinopathy (FEVR) and incontinentia pigmenti (IP). FEVR presents in infancy or early childhood with reduced vision and photoreceptor dysfunction as a consequence of complications including macular ectopia, retinal detachment and exudation.^{125, 126} Mutations in genes of the Wnt signalling pathway *NDP*, *LRP5*, *TSPAN12* and *FZD4*, which regulate normal retinal vascular growth *in utero*, are associated with approximately 50% of familial exudative vitreoretinopathy (FEVR) cases.¹²⁵ FEVR is characterised by variable expression and inheritance patterns.¹²⁶ IP is a systemic disorder of ectodermal cells due to mutations in *IKBKG* important in inflammatory and

apoptotic pathways.⁶⁷ Retinal vascular abnormalities may be present from birth and can lead to retinal detachment and vision loss.¹²⁷

1.4.6 Syndromic retinal dystrophies

Children presenting to the ophthalmologist may have a known syndromic manifestation of disease or may develop syndromic manifestations. As such, routine paediatric assessment of EORD patients is important. Syndromic manifestations may be apparent at presentation, for instance sensorineural hearing loss in Ushers syndrome, polydactyly in Bardet-Biedl syndrome and lack of cutaneous pigmentation in oculocutaneous albinism. Systemic associations may develop later, for instance in juvenile neuronal ceroid lipofuscinosis due to mutations in *CLN3*, a rapidly progressive retinal dystrophy presenting age 6-8 years precedes the onset of neurological decline.¹²⁸

1.5 Thesis aims

Detailed phenotypic and molecular analysis is incomplete for many sub-groups of EORD. This clinical characterisation is important for an accurate and timely diagnosis; appropriate and selective investigations; family counselling of prognosis and recurrence risks and options for pre-implantation diagnosis or pre-natal diagnosis; understanding of rate and degree of degeneration to target potential treatments to effective treatment windows; understanding of disease pathways to identify potential novel treatment targets; and selection of molecularly confirmed patients for treatment trials. By investigating groups of similar patients both molecularly and clinically, using the latest techniques available, insight in to phenotypes and novel molecular aetiologies should be achieved.

The main aims of this thesis are to:

- Phenotypically characterise cohorts of patients defined by molecular cause (proven or likely) by detailed history, examination, retinal imaging, electrophysiology and where appropriate systemic investigations in conjunction with paediatricians and clinical geneticists
- Develop practical skills to enable molecular investigation including Sanger sequencing, cell studies and zebrafish studies
- Perform targeted molecular screening of patients and family segregation
- Investigate identified variants from WES
- Develop the skills to interrogate databases and utilise bioinformatic tools to interpret and investigate molecular data
- Investigate potential phenotype-genotype correlation

2 Methods

2.1 Clinical methods

Ethical approval was obtained from the Research Ethics Committee, Moorfields Eye Hospital (reference MOOA1014). The study protocol adhered to the tenets of the Declaration of Helsinki. Written, informed consent was obtained from all participants prior to their inclusion in this study with parental written consent provided on behalf of the children involved in this study.

Patients and their relatives were examined and investigated within the inherited retinal eye disease clinics at Moorfields Eye Hospital, London and Great Ormond Street Hospital, London. I examined the majority of patients reported in this thesis. When this was not possible, for instance the patients were no longer under the care of the hospital or lived too far away for further review to be logistically possible, the prior assessment by one of my 2 supervisors was used. Within each chapter, the role of the examiner is made clear.

When relevant, relatives would be examined and investigated. Examination of available relatives is particularly useful in retinal genetics clinics, where clues to the diagnosis and inheritance pattern may be found. For instance, in a male patient presenting in the first decade with nyctalopia, high myopia and fundus signs consistent with a rod-cone dystrophy, examination of his mother may be informative. Carrier females in X-linked RCD may have abnormalities of the retina including a tapetal reflex and sectoral peripheral bone spicule pigmentation.⁶⁸

2.1.1 History and examination

A detailed history provides vital information as to the possible type of retinal disease, its potential inheritance and its impact on the patient and their family. In taking a medical history I enquired about specific ocular presenting symptoms including: nyctalopia, field loss (difficulty on stairs, bumping in to things), central vision disturbance (reading, faces, colours), photophobia, photoattraction, eye poking, glasses, and previous ocular surgery (eg cataract). I also enquired about any signs or symptoms of syndromic disease such as extra digits/skin tags on hands or feet (or scars if removed), renal impairment, deafness, anosmia, learning difficulties, developmental delay, obesity, skeletal abnormalities (such as hip dysplasia, shortened ribs), poor balance, cardiomyopathy, peripheral neuropathy, pituitary failure and bleeding diathesis. Some syndromic features may not be apparent at presentation but develop later, such as LCA with renal failure due to nephronophthisis which usually

develops in the first decade but may not present until the second decade.⁸⁴ Additionally for children I enquired about birth history, development, schooling and support in place. For adults it was important to note employment and difficulties working, driving and support. When visual deterioration met the criteria, registration as sight impaired or severely sight impaired was discussed. A detailed family history was taken and a pedigree drawn. This was helpful in determining likely inheritance pattern. Consanguinity was always documented.

Ocular examination of the patient included best corrected visual acuity, colour vision, and visual fields (as described above). Slit lamp biomicroscopy of the anterior segment was performed specifically looking for any relevant signs such as keratoconus, iris transillumination, anterior segment dysgenesis, cataract or raised intra-ocular pressure. A dilated fundus examination permitted assessment of the appearance of the optic disc and vessels and the distribution, type and pattern of any pigmentary change. Additional features included macular lesions such as vitelliform lesions or flecks, exudation, telangiectasia, haemorrhage, and schisis. In children too young for slit lamp examination, a hand-held slit lamp and an indirect ophthalmoscope were used.

Systemic assessment included external examination of the patient for any apparent dysmorphic features such as saddle-nose, microcephaly, short stature, scars on hands/feet, extra digits or sparse scalp hair. Growth parameters in children were measured when relevant.

2.1.2 Retinal imaging

All patients, age permitting underwent retinal imaging which is useful for documentation of findings and for objective monitoring of progression. Colour fundus images were obtained by 35 degree (Topcon Great Britain Ltd, Berkshire, UK), ultra-widefield confocal scanning laser imaging (Optos plc, Dunfermline, UK), or RetCam imaging (Clarity Medical Systems Inc, California, USA).

Conventional Topcon white-light 35 degree images would typically be obtained in 9 positions of gaze to cover the entire fundus through a dilated pupil (figure 2-1). An Optos image covers 200 degrees and encompasses the peripheral retina, particularly useful in the paediatric setting and for patients with limited cooperation as a single image may be sufficient once the dilated pupil is properly aligned. Optos images were acquired by laser scanning ophthalmoscopy using 2 lasers, 532nm green (to image retina) and 633nm red (to image RPE and choroid, www.optos.com). The RetCam was used for examination of supine patients, most typically during examination under anaesthesia in theatre again through a dilated pupil. Images were acquired using a corneal contact probe with white light and a field of approximately 130 degrees.

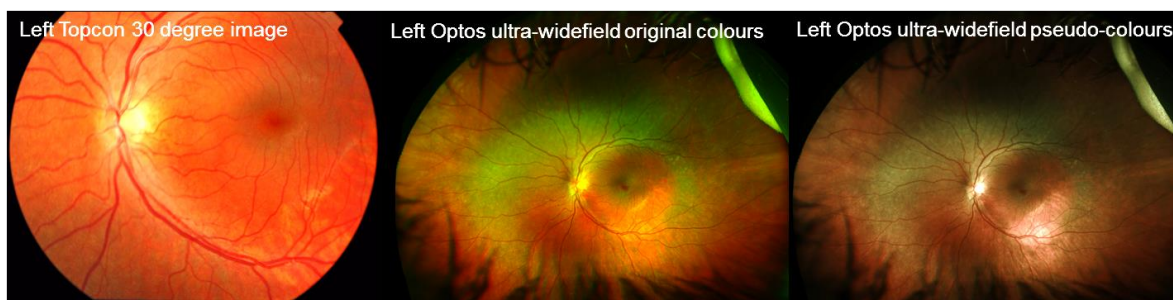


Figure 2-1: Example colour fundus imaging

Left eye of a 12 year boy with enhanced S-cone syndrome. Due to the wavelength of laser used, Optos images have an artificial appearance which can be altered to more realistic retinal colours using the product software. There are frequently artefacts from eyelashes (seen superiorly and inferiorly) and from fingers holding up eyelids (top right).

Fundus autofluorescence (FAF) imaging may highlight abnormalities in retinal dystrophy not visible ophthalmoscopically and can be a useful parameter for monitoring disease progression (figure 2-2). The RPE phagocytoses shed outer segments of photoreceptors with lipofuscin accumulating in lysosomes in the RPE as a by-product of this process.¹²⁹ When stimulated by blue light, the lipofuscin pigments naturally fluoresce. Normally, the optic disc and retinal vessels appear dark, the AF signal is most intense 5-15 degrees temporal to the fovea and the fovea itself appears dark due to the absorption of 488nm light by the macular pigments with some absorption by melanin granules in the RPE.¹³⁰ In early stages of retinal dystrophy, increased autofluorescence is indicative of RPE dysfunction prior to atrophy and in RCD is classically seen as a ring in the macula.¹³¹ Regions of reduced AF may be seen prior to any visible atrophic changes ophthalmoscopically. This loss of AF is indicative of severe damage to the retinal pigment epithelium (RPE) and subsequent atrophy of the overlying neurosensory retina. In this study, FAF imaging was most frequently performed using 30 or 55 degree imaging (Spectralis, Heidelberg Engineering Ltd, Heidelberg, Germany). The Spectralis is a confocal scanning laser ophthalmoscope which continually scans the retina. Laser excitation of 488nm was used with an emission detection filter of 500nm. The Optos ultra wide-field was also used for FAF imaging and these images can be used to estimate the visual field.⁶⁰

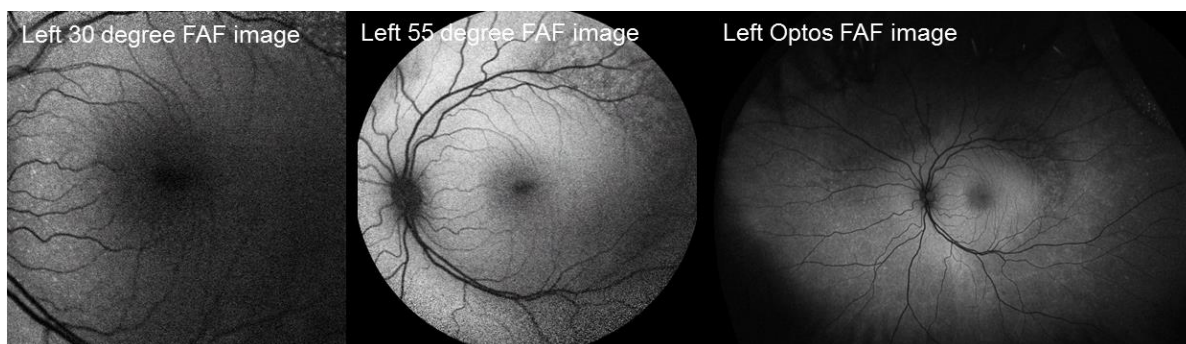


Figure 2-2: Examples of FAF imaging

Left eye of a 12 year boy with enhanced S-cone syndrome demonstrating different sizes of fields with different imaging modalities.

Spectral domain OCT scans (Spectralis) were used to create cross-sectional images of retinal layers, RPE and choroid (figure 2-3). An 870nm superluminescent diode was used across a 30 degree field with reflected light from a spectrum of wavelengths then measured. The speed of reflection and wavelength were processed to build up an image of the reflective surfaces. Images were measured at 40,000 A-scans per second giving a high axial resolution of 7 μm to a depth of 1.9mm (www.heidelbergengineering.com). OCT images demonstrate a number of features in retinal dystrophy, including loss of retinal layers, RPE or choroid, disorganised lamination, macular oedema and outer retinal tubulations (ORTs).¹³² In RCD, the inner segment ellipsoid (ISe) band is typically lost in the peripheral macula with progressive loss towards the fovea a marker of progression.¹³³



Figure 2-3: Example of OCT imaging with layer segmentation

Left OCT of patient with enhanced S-cone syndrome with individual layers labelled. Infrared image on left represents multiple scan positions with the highlighted arrow corresponding to the OCT image illustrated on the right. The outer segment/RPE band can be differentiated from the RPE in high quality scans only. Note, subfoveally the increased black space representing the increased outer segments in this region. Also note, nasally disrupted ISe band.

Fundus fluorescein angiography (FFA) is a technique to visualise retinal vessels and to a lesser extent the choroidal circulation (figure 2-4). Intravenous fluorescein is injected and consecutive fundus images taken with a blue excitation light of 488nm and a 500nm filter to isolate the fluorescence only. This technique is particularly useful in conditions where there may be abnormal vascular development such as familial exudative vitreoretinopathy, in telangiectasia and exudation and in choroidal neovascular membranes of the macula. FFAs can be performed using the Topcon system, Optos, RetCam or Spectralis. Optos FFA is particularly useful if peripheral images are needed. However, limited normative data can make interpreting these images challenging. Peripheral vascular abnormalities have been found in normal patients and areas of non-perfusion have been found in patients with high myopia.¹³⁴

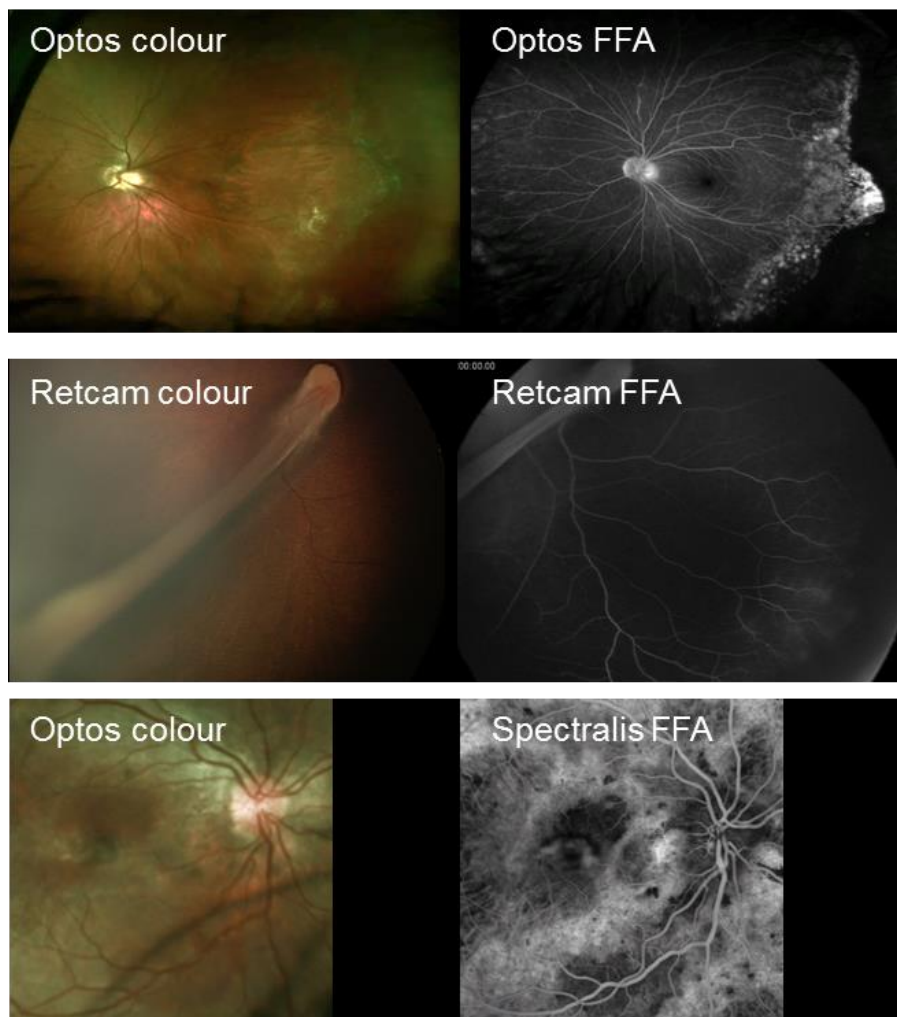


Figure 2-4: Examples of fundus fluorescein angiograms

Top, 31 year old untreated familial exudative vitreoretinopathy (FEVR); Optos image of left eye with temporal incomplete vascularisation and abnormal vascular malformations. Middle, 7 weeks old boy, poor eye contact, nystagmus and microcephaly; RetCam image of right retinal fold, incomplete peripheral vascularisation evident on FFA. Bottom, 11 year old with *PNPLA6* related chorioretinopathy and a secondary right choroidal neovascular membrane (CNVM); Optos colour image of right eye, Spectralis FFA of posterior pole, no leak from CNVM.

2.1.3 Electrophysiology

The majority of patients presenting with symptoms related to retinal dystrophy undergo electrophysiological testing to objectively assess the function of the visual pathways, localise disease and estimate visual disability. The interpretation of reporting of these is performed by Prof Graham Holder and Dr Anthony Robson, and the ERG figures and interpretations within this thesis have been provided by them.

Electrodiagnostic tests (EDTs) comprise the electroretinogram (ERG) which measures the mass response from photoreceptors and the inner retina; the pattern ERG (PERG) which measures the macula photoreceptor and retinal ganglion cell responses; the electrooculogram (EOG) for examining RPE function; and the visual evoked potential (VEP) which assesses intracranial pathways. In this thesis the main investigative

methods of relevance were the ERG, PERG and VEP. The ERG can be particularly useful in infants presenting with nystagmus and poor visual responses, to readily distinguish between LCA or less severe conditions such as achromatopsia. ERG responses can be pathognomonic of certain conditions including enhanced S-cone syndrome due to *NR2E3* mutations and cone dystrophy with supernormal rod ERG due to *KCNV2* mutations.¹³⁵

Recordings were performed to standards published by the International Society for Clinical Electrophysiology of Vision (ISCEV) to ensure the stimulus parameters and adaptive state of the eye at recording (dark or light adapted duration) were comparable and meaningful.^{136, 137} Recordings were performed with gold foil corneal electrodes but in infants and young children these were not usually tolerated and skin electrodes were used with modified protocols.¹³⁸ Abnormal retinal function was determined by reduced (or less commonly abnormally increased) amplitude and by delayed timing of responses.

The basic protocols for ERG recordings are broadly divided into 4 categories: dark adapted (DA) 0.01, DA 10.0, light adapted (LA) 30Hz and LA 3.0 (figure 2-5). Dark adaptation was performed by patching the eye for 20 minutes to obtain maximal information about rod-driven responses. Flash stimuli were delivered by a Ganzfeld bowl to achieve whole field, uniform illumination with units of candela-seconds per meter squared ($\text{cd}\cdot\text{s}\cdot\text{m}^{-2}$). DA 0.01 comprised a $0.01 \text{ cd}\cdot\text{s}\cdot\text{m}^{-2}$ dim stimulus generating a b-wave that reflects rod pathways. DA 10.0 comprised a $10.0 \text{ cd}\cdot\text{s}\cdot\text{m}^{-2}$ stimulus generating an a-wave which reflects combined photoreceptor responses and ON pathways, and a b-wave that reflects predominantly rod ON bipolar cells. In practice the DA 10.0 was predominantly used for interpreting rod and inner retinal cell dysfunction. Depending on the machine used, some recordings were with a $11 \text{ cd}\cdot\text{s}\cdot\text{m}^{-2}$ stimulus. Light adaptation was performed using a 30 cd m^{-2} stimulus from the Ganzfeld bowl for at least 10 minutes. LA 30Hz flicker was a $3.0 \text{ cd}\cdot\text{s}\cdot\text{m}^{-2}$ stimulus delivered at a frequency of approximately 30Hz, which generates a cone isolated response due to the poor temporal resolution of rods and rod-saturating background. LA 3.0 was a single flash $3.0 \text{ cd}\cdot\text{s}\cdot\text{m}^{-2}$ stimulus generating an a-wave reflecting predominantly cone function and a b-wave that reflects ON and OFF bipolar cells. Further specific testing was performed when indicated for instance S-cone specific ERG or ON and OFF bipolar cell recordings. ERGs were recorded with the pupil dilated except in young children/infants.

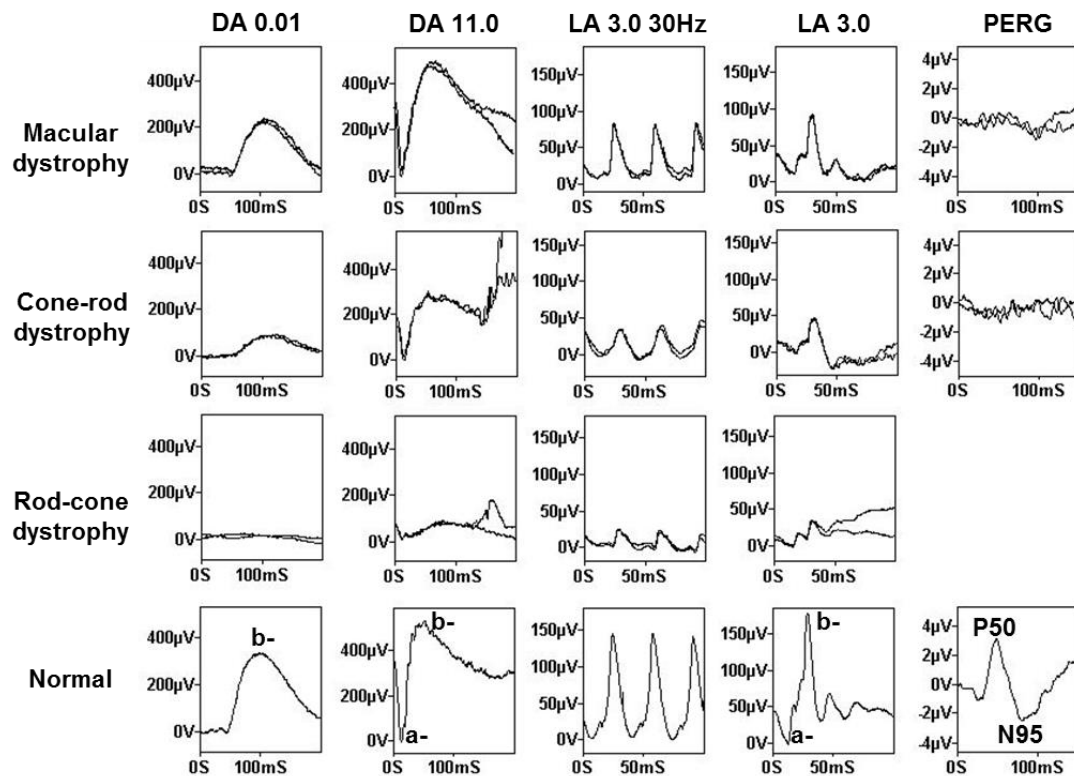


Figure 2-5: Electroretinogram and pattern electroretinogram examples

All patients shown have *CRX* mutations. Patient with macular dystrophy demonstrates subnormal PERG with normal ERGs for age (53 years at ERG). Patient with CORD, demonstrates subnormal rod and bright flash ERGs (DA 0.01; DA 11.0), delayed and subnormal cone flicker ERGs (LA 3.0 30Hz) and markedly subnormal single flash ERG (LA 3.0 2Hz) with undetectable PERG. Patient with RCD, demonstrates undetectable rod ERG (DA 0.01), severe reduction in the bright flash ERGs (DA 11.0) and markedly delayed and subnormal cone flicker and single flash ERGs (LA 3.0 30Hz; LA 3.0). PERG was unrecordable due to nystagmus.

PERG recordings were performed with a black and white checkerboard of constant mean luminance with an undilated pupil and refractive correction. The test required central fixation for good quality recordings. Recordings measured the response of the retina stimulated by this contrasting image reflecting function of the central macula. It is useful for assessing macular involvement in a retinal dystrophy (figure 2-5) and in differentiating macula or ganglion cell related visual loss.¹³⁹ Two main components were measured, the P50 at approximately 50msec which reflects the function of the macula and the N95 component reflecting retinal ganglion cell function.

The VEP was recorded using occipitally placed skin electrodes with monocular stimulation from a black and white checkerboard.¹⁴⁰ Relevant applications include; investigating demyelinating optic nerve disease in which the pattern VEP is delayed in the presence of a normal PERG; assessing chiasmal misrouting in oculocutaneous albinism in which the majority of optic nerve fibres decussate contralaterally; and demonstrating normal responses and objective visual acuity in non-organic visual loss.^{141, 142}

2.2 Molecular genetic methods

For the majority of patients reported within this thesis, I performed molecular investigations with Sanger sequencing. Patients were either undiagnosed and for candidate gene screening or they had undergone NGS and were for further investigation and co-segregation. Within each chapter, my role in the genetic investigations is detailed.

2.2.1 DNA isolation and quantification

Genomic DNA was isolated from peripheral blood lymphocytes, saliva or buccal swabs, using the Puregene kit (Gentra Puregene Blood and Tissue Extraction Kit, QIAGEN, Manchester, UK) by colleagues within the Institute (Beverley Scott and Naushin Waseem). DNA samples may have already been obtained. Otherwise patients and relatives were contacted for samples or recruited within clinic. I performed the majority of this additional sampling.

Extracted DNA was quantified using a spectrophotometer (NanoDrop 2000, Thermo Fisher Scientific, Waltham, MA, USA) and 1µl of the DNA sample. The spectrophotometer uses a wide spectral range of light stimulation from ultraviolet to visible light (190-840nm) and a photodetector to measure the absorbance of a sample. DNA has a peak absorbance at 260nm, protein at 280nm. The transmittance of a substance is related to its optical depth and its absorbance; this is known as the Beer-Lambert law and this principle is used to calculate the concentration of a sample based on a 50µg/ml DNA sample at 260nm absorbance having an optical density of 1. The quality of DNA was also assessed using a purity ratio, A260/A280 with an optimal ratio of 1.8 indicating low amounts of contaminating protein and values below 1.6 indicating high protein contamination. DNA was diluted to 50ng/µl for use in reactions.

2.2.2 Polymerase chain reaction

In vitro cloning of DNA fragments by polymerase chain reaction (PCR) is a rapid, and sensitive method of amplifying even tiny amounts of DNA.⁶⁵ Within the laboratory, PCR was performed to selectively amplify a region of DNA under investigation using specifically designed oligonucleotide sequences (primers) acting at target sequences surrounding an exon. Primers were designed in a 5' to 3' direction to direct synthesis of a complementary DNA strand towards the other primer binding site. Each newly synthesised strand thus acting as a template for further reactions, creating an exponential reaction for DNA production.

There are 3 steps to the PCR process (figure 2-6):

- 1) Denaturation: DNA is heated to a temperature sufficient to break the hydrogen bonds and separate the double-stranded DNA in to 2 complementary strands
- 2) Primer annealing: primers bind to complementary sequences on the single-stranded DNA
- 3) DNA synthesis: DNA polymerase initiates the synthesis of new DNA strands by the addition of synthetic deoxynucleoside triphosphates (dNTPs), specifically dATP, dCTP, dGTP and dTTP.

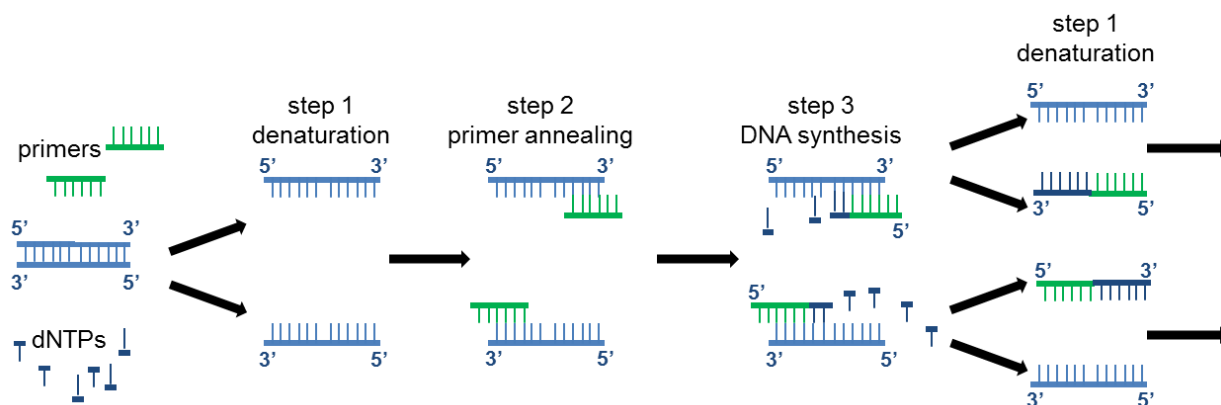


Figure 2-6: Polymerase chain reaction

The process was repeated for approximately 30 cycles to generate sufficient DNA to sequence (table 2-1). PCR was performed in a thermal cycler (Bio-Rad C1000, Bio-Rad Laboratories, California, USA). The reagents comprised DNA, Taq DNA polymerase, reaction buffer, magnesium chloride ($MgCl_2$), dNTPs and primers.

Standard PCR reaction, 20 μ l vol	
Step	Condition
1	95°C 300 secs
2	95°C 30 secs
3	X°C 30 secs
4	72°C 60 secs
Go to step 2, 34 times	
5	72°C 420 secs
6	4°C 120 secs

Table 2-1: PCR protocol

X is the PCR specific temperature

Taq polymerases are heat resistant DNA polymerases derived from a microorganism, *Thermus aquaticus* that exists in naturally hot environments. These enzymes can withstand the initial 95°C denaturation step. The standard Taq polymerase used in the lab was BIOTAQ (BIOTAQ™ DNA Polymerase, Bioline, London, UK, table 2-2). In

cases where PCR reactions were weak or sub-optimal, MyTaq (MyTaq™ DNA Polymerase, Bioron) was used (table 2-2). MyTaq has increased affinity for DNA.

BIOTAQ mix, total vol 20µl			Final concentration			MyTaq mix, total vol 20µl			Final concentration		
10x reaction buffer	2µl	1x				5x reaction buffer	4µl	1x			
Primer forward (10µM)	0.8µl	0.4µM				Primer forward (10µM)	0.8µl	0.4µM			
Primer reverse (10µM)	0.8µl	0.4µM				Primer reverse (10µM)	0.8µl	0.4µM			
BIOTAQ (5 units/µl)	0.2µl	1 unit/reaction				MyTaq (5 units/µl)	0.2µl	1 unit/reaction			
dNTPs (2mM)	2µl	0.2mM				DNA	50ng	-			
MgCl ₂ (50mM)	0.6µl	1.5mM				Water	13.2µl	-			
DNA	50ng	-									
Water	12.6µl	-									

Table 2-2: BIOTAQ and MyTaq protocols for PCR

The ammonium based reaction buffers (containing ammonium sulphate and Tris-hydrochloride) and MgCl₂ provided optimal reaction conditions. The MyTaq 5x reaction buffer contains dNTPs and MgCl₂. For those PCR products with an unavoidably high GC content (typically >60%), 8% dimethyl sulphoxide (DMSO) was added to the protocol. DMSO is thought to reduce the formation of secondary structures by binding the major and minor grooves of DNA strands.¹⁴³

Primers (typical 18-25 nucleotides) were designed using open-source software at Primer3plus.com with gene sequences from Ensembl accessed at <http://www.ensembl.org>.¹⁴⁴ Primer pairs were selected based on similar predicted melting temperatures, an optimal GC content (<60%) and an amplicon size <1000 base pair (bp) to avoid difficulties in amplification and sequencing. Primers with high GC content would be more likely to dimerise or form secondary structures. Primer pairs were run through *in silico* PCR software at UCSC genome browser (<https://genome.ucsc.edu/cgi-bin/hgPcr>) to ensure they would specifically anneal only to the area of interest without any other alternative binding sites in the genome. Lyophilised primers were re-suspended in sterile water at 100mM and stored at -20°C with a working stock of 200µl of 10mM primer stored at 4°C.

PCR reactions were first optimised using a temperature gradient protocol to determine the optimal primer annealing temperature to minimise non-specific amplification and ensure a high yield of PCR product. The temperature gradient would typically be run

from 50-65°C (figure 2-7). The resulting PCR products were separated by size using agarose gel electrophoresis. 4µl of PCR product was mixed with 1µl of loading buffer (bromophenol blue/xylene cyanol/Ficoll) and electrophoresed for 30-40 minutes at 150V constant voltage through a 2% agarose gel containing 5µl/100ml of SafeView reagent (Applied Biological Materials Inc, Richmond, BC, Canada) in TBE (Tris/borate/EDTA, Thermo Fisher Scientific) buffer. An appropriate molecular weight marker was used, most typically HyperLadder IV (Biolone Reagents Limited, London, UK). The gel was imaged using an ultraviolet transilluminator and photographed using an orange filter.

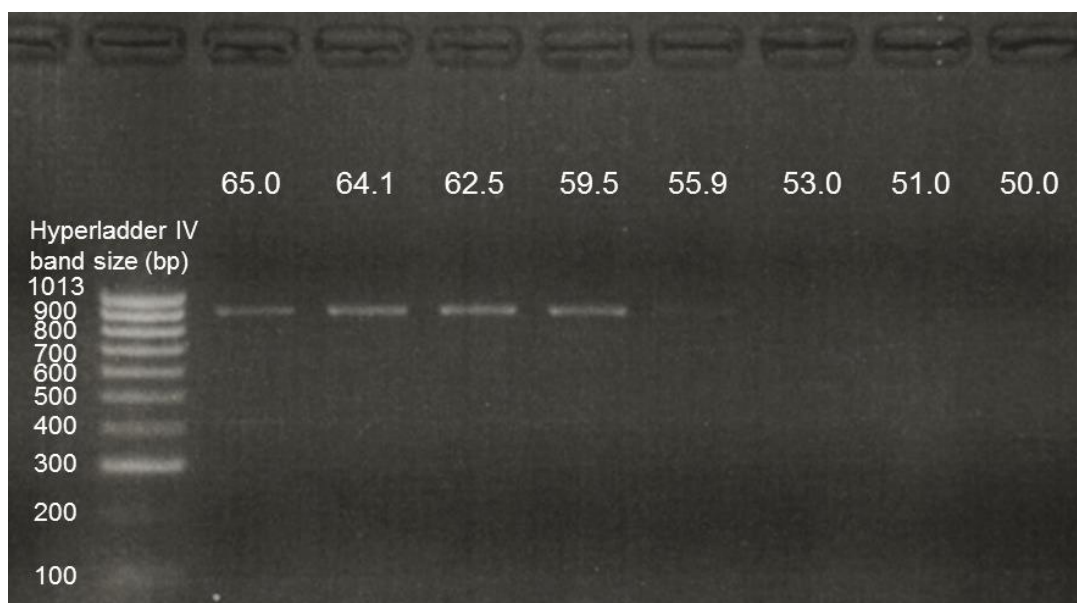


Figure 2-7: Temperature gradient optimisation example

Agarose gel electrophoresis image of *RDH12* exon 7 run with BIOTAQ. 65°C was the optimal temperature chosen from this experiment as it was the highest temperature with a clear band.

2.2.3 Sanger sequencing

Dye-terminator dideoxynucleotide DNA sequencing, more commonly known as Sanger sequencing, is an enzymatic process for interpreting the nucleotide order within a specific length of DNA.⁶⁵ The original method as described in the 1970s generated newly synthesised DNA strands of sequential lengths depending on the incorporation of a dideoxynucleotide chain terminator in to the new strand, that could be separated on a polyacrylamide gel.¹⁴⁵ Automated sequencing machines are now used with 4 fluorescent labels of differing emission wavelengths that are detected as the DNA sample migrates past a laser and camera at a fixed point during electrophoresis through a polyacrylamide gel capillary.¹⁴⁶

The PCR product was sequenced in a number of steps. Prior to sequencing, unincorporated primers and nucleotides were removed to avoid contamination of

downstream sequencing reactions or alteration of the dNTP:dye-terminator ratio. The product was cleaned up of primers and free dNTPs using a combination of Exonuclease I (ThermoFisher Scientific) and FastAP shrimp alkaline phosphatase (ThermoFisher Scientific). The former removes primers and acts on single stranded DNA such that the double stranded PCR product is not digested; the latter inactivates the dNTPs by dephosphorylating them. 3.2µl of enzyme mix containing 2 units of Exo I and 2 units of FastAP was added per PCR reaction and incubated for 60 minutes at 37°C followed by inactivation for 20 minutes at 80°C then cooled to 4°C for 5 minutes.

Sequencing of the amplified product was performed using BigDye terminator chemistry (table 2-3, BigDye Terminator Cycle Sequencing Kit, v.3.1; Thermo Fisher Scientific). This kit contains a DNA polymerase and fluorescently labelled dNTPs.

BigDye reaction		Step	Condition
		1	96°C 120 secs
Mix, total 10µl		2	96°C 10 secs
BigDye	1µl	3	50°C 5 secs
Template	1.5µl	4	60°C 240 secs
Primer	0.5µl		Go to step 2, 24 times
Water	7µl	5	4°C 120 secs

Table 2-3: BigDye reaction

Free nucleotides and enzyme were then cleaned up by using sequencing clean-up filter plates (Montage SEQ₉₆, Millipore Ltd, Watford, UK) with a vacuum pump according to manufacturer instructions and then re-suspended in 12µl of sterile water. Finally, the samples were loaded on to an automated capillary sequencer (Applied Biosystems 3730 DNA Analyzer) run by colleagues within the Institute (Naushin Waseem and Beverley Scott).

2.2.4 Next generation sequencing

2.2.4.1 Massively parallel sequencing

Patients were selected for WES based on prior molecular investigations including candidate gene screening, APEX microarray, single nucleotide polymorphism (SNP) microarray, homozygosity mapping and NGS gene panel screening. WES was predominantly performed at AROS Applied Biotechnology (Aarhus, Denmark), with alignment and variant calling performed by a colleague (Vincent Plagnol) at the UCL Genetics Institute. Further variant filtering and interpretation was predominantly performed by the post-doctoral fellow within the laboratory, Dr Gavin Arno as well as by

Prof Andrew Webster. WES was performed using SureSelect XT Human All Exon capture (Agilent Technologies Inc., Santa Clara, USA). In brief, for this type of massive parallel sequencing, patient DNA was digested in to randomly sheared, adaptor-ligated and PCR-amplified fragments.¹⁴⁷ These were mixed with a pool of biotinylated RNA capture probes (designed to cover the whole exome) that then attached to streptavidin-coated magnetic beads. These were then selectively PCR amplified with paired-end sequencing performed using the Illumina HiSeq2500 sequencer (Illumina, San Diego, CA). The fluorescence emitted for each incorporated dNTP was recorded to determine the sequence. Approximate read-depths and coverage were 30x minimum for 75% of the exome and 10x minimum for 90% of the exome.

2.2.4.2 Variant call alignment and analysis

The resulting raw data required extensive processing. The raw FASTQ files containing FASTA formatted text-based sequence and quality data for each read were aligned to the Genome Reference Consortium human genome build 37 (GRCh37) using Novoalign (Novocraft Technologies, Selangor, Malaysia) version 2.08.03. Duplicate reads were identified using Markduplicates (Picard Tools, Broad Institute, Cambridge, Ma, USA, <http://broadinstitute.github.io/picard>). The Haplotype Caller module of the Genome Analysis ToolKit (GATK, version 3.3-0, Broad Institute, www.broadinstitute.org/GATK) was used to identify sequence variants. The resulting genomic variant call format (VCF) file was further analysed using the GenotypeGVCFs module (of GATK) for final variant calling. Variant quality scores were recalibrated according to GATK best practice separately for single nucleotide variants and insertions/deletions. Finally, the resulting variants were annotated using ANNOVAR (www.openbioinformatics.org) based on Ensembl gene and transcript definitions. Candidate variants were filtered based on function (non-synonymous missense, presumed loss of function, splicing defined as intronic sites within 5 bp of exon-intron junction) and a minor allele frequency (MAF) <0.5% (as compared with an internal control group of 3000 clinical exomes, UCL-exomes consortium and the NHLBI GO Exome Sequencing Project dataset, EVS, Seattle, WA available at <http://evs.gs.washington.edu/EVS/>). Variants in know retinal dystrophy genes would be investigated first with this analysis predominantly performed by Dr Arno and Prof Webster and to a lesser extent by myself. If potentially pathogenic variants in known retinal dystrophy genes were not found, the other variants were investigated to try and identify candidate genes. This approach would involve investigating known reports of protein function, animal models, orthologues and human paralogues.

2.2.4.3 Whole genome sequencing

In WGS, there is no targeted capture of regions of interest and no PCR step. This results in less bias, improved coverage of regions difficult to PCR such as repetitive regions or GC rich first exons, allows investigation of deep intronic variants and regulatory regions that may not be covered with other methods and better identifies copy number variants (CNVs).¹⁴⁸ In practice, the coverage is approximately 95% of the genome with a lower read-depth than WES at 15x.

WGS was performed as part of the NIHR BioResource Rare-diseases SPEED study using the Illumina TruSeq DNA PCR-Free Sample preparation kit (Illumina Inc.) and sequenced using an Illumina HiSeq 2500. Alignment and variant calling was performed by Dr Keren Carss (NIHR BioResource - Rare Diseases, Department of Haematology, University of Cambridge, Cambridge, UK). Reads were aligned to the Genome Reference Consortium human genome build 37 (GRCh37) using Isaac Genome Alignment Software (version 01.14, Illumina Inc.).¹⁴⁹ Single nucleotide variations and small insertion deletions were identified using Isaac Variant Caller (version 2.0.17).¹⁴⁹

2.2.5 Other molecular investigations

NGS of the coding regions of 105 retinal genes (table 2-4) and subsequently 176 retinal genes (table 2-5) was performed at the Manchester Centre for Genomic Medicine (Manchester, UK) with enrichment using a SureSelect Target Enrichment Kit (Agilent Technologies Inc., Santa Clara, USA) then sequenced on the HiSeq 2500 (Illumina Inc., San Diego, CA).¹⁴ Sequenced reads were aligned to the human reference sequence hg19 (build GRCh37) with the Burrows-Wheeler aligner (BWA v0.6.2).¹⁵⁰ The genome analysis tool kit (GATKlite v2.0.39) was used for base quality score recalibration and indel realignment prior to variant calling using the UnifiedGenotyper.¹⁵¹ This gene panel was frequently used for screening undiagnosed patients as a rapid and cost-effective method from clinic with variant interpretation performed by the Manchester Centre providing a variant list from their analysis and most likely causative candidates.

Autozygosity mapping has frequently been used within the department for consanguineous families. The underlying principle is that non-random mating leads to inheritance of identical ancestral alleles. Regions of homozygous DNA >5Mb are generally not seen in non-consanguineous mating; larger homozygous tracts are identical by descent, and indicate parental consanguinity.¹⁵² For recessive disease, the degree of consanguinity is directly correlated to the risk of disease. Homozygosity mapping of multiple family members can highlight a candidate gene for sequence analysis. This investigation of homozygous regions was performed using a SNP

microarray containing 730,525 SNPs (OmniExpress, Illumina Inc., San Diego, Ca, USA) at the Institute of Child Health (London, UK) and was additionally performed on exome data.

<i>ABCA4</i>	<i>CEP290</i>	<i>GNAT2</i>	<i>NDP</i>	<i>RBP3</i>	<i>SAG</i>
<i>ADAM9</i>	<i>CERKL</i>	<i>GPR98</i>	<i>NR2E3</i>	<i>RD3</i>	<i>SEMA4A</i>
<i>AIPL1</i>	<i>CHM</i>	<i>GUCA1A</i>	<i>NRL</i>	<i>RDH12</i>	<i>SNRNP200</i>
<i>ARL6</i>	<i>CLRN1</i>	<i>GUCA1B</i>	<i>OTX2</i>	<i>RDH5</i>	<i>SPATA7</i>
<i>BBS1</i>	<i>CNGA1</i>	<i>GUCY2D</i>	<i>PCDH15</i>	<i>RGR</i>	<i>TEAD1</i>
<i>BBS10</i>	<i>CNGA3</i>	<i>IDH3B</i>	<i>PDE6A</i>	<i>RGS9</i>	<i>TIMP3</i>
<i>BBS12</i>	<i>CNGB1</i>	<i>IDH3B</i>	<i>PDE6B</i>	<i>RHO</i>	<i>TOPORS</i>
<i>BBS2</i>	<i>CNGB3</i>	<i>IMPDH1</i>	<i>PDE6C</i>	<i>RIMS1</i>	<i>TRIM32</i>
<i>BBS4</i>	<i>CRB1</i>	<i>IMPG2</i>	<i>PDE6G</i>	<i>RLBP1</i>	<i>TTC8</i>
<i>BBS5</i>	<i>CRX</i>	<i>KCNV2</i>	<i>PITPNM3</i>	<i>ROM1</i>	<i>TULP1</i>
<i>BBS7</i>	<i>DFNB31</i>	<i>KLHL7</i>	<i>PRCD</i>	<i>RP1</i>	<i>UNC119</i>
<i>BBS9</i>	<i>DHDDS</i>	<i>LCA5</i>	<i>PROM1</i>	<i>RP1L1</i>	<i>USH1C</i>
<i>BEST1</i>	<i>EFEMP1</i>	<i>LRAT</i>	<i>PRPF3</i>	<i>RP2</i>	<i>USH1G</i>
<i>C1QTNF5</i>	<i>ELOVL4</i>	<i>LRP5</i>	<i>PRPF31</i>	<i>RP9</i>	<i>USH2A</i>
<i>CA4</i>	<i>EYS</i>	<i>MERTK</i>	<i>PRPF6</i>	<i>RPE65</i>	<i>ZNF513</i>
<i>CACNA2D4</i>	<i>FAM161A</i>	<i>MKKS</i>	<i>PRPF8</i>	<i>RPGR</i>	
<i>CDH23</i>	<i>FSCN2</i>	<i>MKS1</i>	<i>PRPH2</i>	<i>RPGRIP1</i>	
<i>CDHR1</i>	<i>FZD4</i>	<i>MYO7A</i>	<i>RAX2</i>	<i>RS1</i>	

Table 2-4: List of 105 retinal genes in Manchester panel

Note, ORF15 region of *RPGR* poorly covered

<i>ABHD12</i>	<i>CDH3</i>	<i>GPR179</i>	<i>LZTFL1</i>	<i>PEX1</i>	<i>TSPAN12</i>
<i>ACBD5</i>	<i>CEP164</i>	<i>GRM6</i>	<i>MFRP</i>	<i>PEX2</i>	<i>TUB</i>
<i>ADAMTS18</i>	<i>CIB2</i>	<i>HARS</i>	<i>MVK</i>	<i>PEX7</i>	<i>VCAN</i>
<i>AHI1</i>	<i>CLN3</i>	<i>HMX1</i>	<i>NEK2</i>	<i>PHYH</i>	<i>VPS13B</i>
<i>ARL2BP</i>	<i>CNNM4</i>	<i>IFT140</i>	<i>NMNAT1</i>	<i>PLA2G5</i>	<i>WDR19</i>
<i>BB1P1</i>	<i>CSPP1</i>	<i>IMPG1</i>	<i>NPHP1</i>	<i>PRPF4</i>	<i>ZNF423</i>
<i>C21orf2</i>	<i>CYP4V2</i>	<i>INPP5E</i>	<i>NPHP3</i>	<i>RAB28</i>	
<i>C2ORF86</i>	<i>DTHD1</i>	<i>INVS</i>	<i>NPHP4</i>	<i>RBP4</i>	
<i>C8ORF37</i>	<i>EMC1</i>	<i>IQCB1</i>	<i>NYX</i>	<i>RPGRIP1L</i>	
<i>CABP4</i>	<i>FLVCR1</i>	<i>ITM2B</i>	<i>OAT</i>	<i>SDCCAG8</i>	
<i>CACNA1F</i>	<i>GNAT1</i>	<i>KCNJ13</i>	<i>OFD1</i>	<i>SLC24A1</i>	
<i>CAPN5</i>	<i>GNPTG</i>	<i>KIAA1549</i>	<i>PANK2</i>	<i>TMEM237</i>	
<i>CC2D2A</i>	<i>GPR125</i>	<i>KIF11</i>	<i>PCYT1A</i>	<i>TRPM1</i>	

Table 2-5: List of additional retinal genes in 176 gene panel

APEX microarray screening (Asper Biotech Ltd.), was performed on patients prior to my study using a genotyping microarray containing specific disease causing variants and common polymorphisms. For LCA this comprised >300 variants for 8 retinal dystrophy genes (*AIPL1*, *CRB1*, *CRX*, *GUCY2D*, *RPE65*, *RPGRIP1*, *LRAT* and

MERTK) with an autosomal recessive RCD screen containing >700 disease causing variants for 28 retinal dystrophy genes (*ABCA4*, *AIPL1*, *CERKL*, *CNGA1*, *CNGA3*, *CNGB3*, *CRB1*, *EYS*, *GRK1*, *IMPG2*, *LRAT*, *MERTK*, *PDE6A*, *PDE6B*, *NR2E3*, *PROM1*, *RBP3*, *RDH12*, *RGR*, *RHO*, *RLBP1*, *RP1*, *RPE65*, *SAG*, *TULP1*, *CLRN1* and *USH2A*).^{153, 154}

2.2.6 Variant analysis and functional predictive tools

Variants were interrogated using the GenBank accession number from the National Institute for Health publically available genetic sequence database with nucleotide position 1 corresponding to the A of the ATG translation initiation codon.¹⁵⁵

2.2.6.1 Determining novelty

Variants were identified as novel if not previously reported in the literature and if absent from open-source variant databases namely dbSNP available at <http://www.ncbi.nlm.nih.gov/projects/SNP/>, EVS, 1000 genomes project available at <http://www.1000genomes.org/> and the Exome Aggregation Consortium (ExAC, Cambridge, MA) available at <http://exac.broadinstitute.org>.¹⁵⁶ The ExAC database became publically available in late 2014 and comprises >60,000 exomes collated to determine MAF of a variant. Frequently, a pathogenic variant not previously reported in an affected patient, would be identified in the ExAC database but at a very low frequency (<0.0001) consistent with rare disease.

2.2.6.2 Predicting pathogenicity

Various *in silico* tools were used to estimate the pathogenicity of novel variants. These included the open-source predictive algorithms for missense variant of 'Sorting Intolerant from Tolerant' (SIFT) available at <http://sift.jcvi.org> and Polymorphism Phenotyping v2 (PolyPhen2) available at <http://genetics.bwh.harvard.edu/pph2> with a score <0.05 indicating pathogenicity for SIFT and a score of ≥ 0.90 -<0.95 indicating possibly damaging and ≥ 0.95 probably damaging for Polyphen2.^{157, 158} For splice site variants, Splice Site Prediction by Neural Network at http://www.fruitfly.org/seq_tools/splice.html and Human Splicing Finder (HSF) at www.umd.be/HSF3 were used.^{159, 160} Conservation of residues between orthologues and between human paralogues was analysed using Clustal Omega accessed at <http://www.ebi.ac.uk/Tools/msa/clustalo/> with protein sequences to be aligned identified from Ensembl.¹⁶¹ Conservation across species indicates importance of that residue in protein function. Both SIFT and Polyphen2 work in part by analysing conservation.

2.2.6.3 Protein modelling

A polypeptide may be subject to post-translational modification such as the methylation of cone transducin.¹⁶² The secondary structure motifs such as the α -helix may be partially predicted from the amino acid sequence but the three-dimensional tertiary structure of a protein may only be deduced experimentally. This includes X-ray crystallography or nuclear magnetic resonance spectroscopy with this information curated, annotated and made freely available within the Protein Data Bank (www.pdb.org).¹⁶³ The UniProt Knowledgebase (www.uniprot.org) is an open-source resource of protein sequence and functional information with manual curation of the Swiss-Prot section.¹⁶⁴ For proteins without experimental data, modelling of the crystalline structure can be performed using tools such as Visual Molecular Dynamics (VMD accessed at <http://www.ks.uiuc.edu/Research/vmd/>) based on paralogues and sequence information. VMD is developed with NIH support by the Theoretical and Computational Biophysics group at the Beckman Institute, University of Illinois at Urbana-Champaign, USA.

Complex structural motifs form protein domains essential for protein function and interactions. Mutations leading to altered residues within these domains may introduce structural change to the shape of the protein, may alter protein interactions or may be tolerated.

2.3 Cell studies

Under supervision by a colleague (Nicholas Owen) within our lab at the Institute of Ophthalmology, an *in vitro* experiment was designed to perform transient plasmid transfection of hTERT-RPE1 cells. I performed all experiments. This necessitated learning how to first transform XL1-Blue Supercompetent cells to synthesis plasmid DNA; perform Maxiprep, site directed mutagenesis and Miniprep; grow, split, freeze, resurrect and transfect cells using a class II biological safety cabinet; immunostain; and use a confocal microscope.

2.3.1.1 Plasmid transformation of cells

The initial experiment required transforming XL1-Blue Supercompetent cells (#200236, Agilent Technologies, Santa Clara, Ca, USA) with a WT and mutated (E664K) pCMV-IFT140-Myc-DDK plasmid (#RC207528, Origene, Rockville, MD, USA, both gifted from a colleague in France) in order to make large quantities of plasmid DNA. All procedures were performed using sterile plasticware on the laboratory bench using a Bunsen burner to minimise contamination.

Transformation was performed according to the following protocol:

1. LB agar plates: 400ml water and 16g LB agar was autoclaved in a 500ml conical flask, once cooled slightly antibiotic was added (100 µg/µl, ampicillin for pUC18 control, kanamycin for IFT140 plasmid), poured in to plates, stored agar side up
2. XL1-blue cells (from -80 °C freezer) were rapidly thawed by hand and added to labelled microcentrifuge tubes on ice, 50µl per experiment (plus 2 controls, pUC18 plasmid, known efficiency of $\geq 1.0 \times 10^9$ colony forming units/µg, and no DNA)
3. 0.85µl of β-mercaptoethanol was added to each tube and gently swirled
4. This was placed on ice for 10 minutes and swirled gently every 2 minutes
5. 50ng DNA plasmid (at 100ng/µl) was added (or 0.1ng (1µl) of pUC18), and swirled gently
6. Ice 30 minutes
7. Samples were heat pulsed at 42°C for 45 seconds exactly (water bath used)
8. Ice for 2 minutes
9. 200µl S.O.C. medium was added
10. Incubated for 1 hour at 37°C with shaking at 225-250rpm
11. Plated on LB agar plates using sterile technique with Bunsen burner, glass rod and 100% ethanol, 50µl and 150µl volumes both used per experiment
12. Incubated at 37°C overnight
13. Colonies counted next day- efficiency assessed by counting pUC18, expect >100 colonies per 1µl plated

This resulted in <10 colonies per plate, with no colonies on the control negative DNA plate and initially, <10 on the pUC18 plate indicating low efficiency. This markedly improved with practice until there were >100 colonies on the pUC18 plate.

2.3.1.2 Culture of single colonies

Due to the low numbers of colonies, all were cultured and sequenced:

1. Under sterile conditions 3-4ml of sterile LB broth + 3-4 µl kanamycin were added to a 50ml conical centrifuge tube
2. A single colony, was picked using a 10µl pipette tip with the whole tip placed in to the conical tube
3. Incubated at 37°C at 225rpm for 6 hours minimum
4. Under sterile conditions, 1.5ml was taken from the tube and added to a 50ml LB broth bottle, 2 made per experiment
5. Incubated overnight at 37°C at 225rpm
6. A glycerol stock was made of the resulting mix for storage in -80°C freezer for future source of original clone: 0.5ml of overnight mix + 0.5ml 8% sterile glycerol in a 1.5 ml microcentrifuge tubes

Maxiprep was then performed on the overnight culture using the EndoFree plasmid Maxi kit (QIAGEN, Dusseldorf, Germany) and an adapted manufacturer's protocol. This resulted in >900ng/μl of plasmid DNA per plasmid type with an overall approximate volume of 0.7ml per plasmid.

2.3.1.3 Sequencing of plasmid open reading frame

Primer pairs were designed to sequence the open reading frame (ORF) of the plasmid (table 2-6). Gradient optimisation of primer pairs was performed with template at 100ng/μl. VP1.5 and XL39 are plasmid specific primer sequences located before and after the ORF respectively.

Name	Primer forward 5' → 3'	Primer reverse 5' → 3'
VP1.5/IFTORF1R	GGACTTTCCAAAATGTCTG	AGTGCCTCCCTCTTCTCCAT
IFTORF 2	GAAGGGCAAGACCACTCAGG	TCCACTGATGTGCATGTCCG
IFTORF 3	TGTCGTCACACTTCCACCAG	CTTCGCATACAAACAGCCGG
IFTORF 4	GCAAGAGACTAATAAGAGCCACC	CATGTTCCCCAGGCACACC
IFTORF 5	TCAAAAGTGAGGCCGTCTGG	CTCCTCCTGGCTCTCGTACT
IFTORF 6	CTTCTCCCTGGTCCGCATC	CGTGTACTTCTTGGTGGCCA
IFTORF 7F/XL39	GAGCATCACCGAGGAGATGG	ATTAGGACAAGGCTGGTGGG

Table 2-6: Primer pairs for sequencing plasmid open reading frame

All reactions were performed with BIOTAQ DNA polymerase at 68°C. Both WT and E664K plasmids were checked for the correct sequence. This identified 2 additional variants in the E664K plasmid; both were synonymous.

2.3.1.4 Site directed mutagenesis

Four plasmid clones were generated by site directed mutagenesis (SDM) using a PCR based method. Primer pairs were designed to be complementary, 25-40bp length with the desired mutation central to the primer sequence, terminating with either a G or C and a total GC content not more than 40% (table 2-7). Primers were PAGE (Polyacrylamide gel purification) purified to give the highest percentage of mutagenized clones. The melting temperature (T_m) was checked to be approximately 10°C above the extension temperature where $T_m = 81.5 + 0.41(\%GC) - 675/N - \%mismatch$ (N, primer length, bps).

SDM was performed using Turbo DNA polymerase (Agilent Technologies, table 2-8 and 2-9, figure 2-8).

Plasmid mutant	Primer forward 5' → 3'	Primer reverse 5' → 3'
c.1319 T>C (p.Leu440Pro)	CATGTCGGTGCGCGGGCTGTGT GCGAC	GTCGCACACAGCCCCGCGCACCGA CATG
c.1451C>T (p.Thr484Met)	GGACCTTCTTGTGTGAGATGCC TGTGTTAGCAATGC	GCATTGCTAACACAGGCATCTCAC ACAAGAAGGTCC
c.2330T>G (p.Leu777Arg)	GAAGCTGAAGTGCGCATGGCG TCCCG	CGGGACGCCATGCGCCACTTCAG CTTC
c.2815T>C (p.Ser939Pro)	GCAGGTCCTCCGGCAGCATCCT GGG	CCCAGGATGCTGCCGGAGGACCT GC

Table 2-7: Primer pairs for site directed mutagenesis

Component	Volume	Final concentration
10x PCR Buffer	5 µl	1x
10mM dNTP	1 µl	0.2mM
DNA template	1/2/8 µl (5/10/40ng)	-
Turbo DNA polymerase 2.5 units/µl	1 µl	2.5 units/reaction
Primer forward, 10µM	1.1 µl	0.22µM
Primer reverse, 10µM	1.1 µl	0.22µM
Water	39.8/38.8/32.8 µl	-
Total volume	50 µl	

Table 2-8: Reaction mix for SDM

SDM procedure:

Step	Temperature	Time
1 Denature	95°C	30 seconds
2	95°C	30 seconds
3 Annealing/extension	50°C	1 minute
4	68°C	2 minutes/kb of plasmid
Go to step 2, 11 times		
5 Terminate	Ice	2 minutes

Table 2-9: Reaction steps for SDM

From each sample, 10 µl of PCR product was reserved. To the PCR reaction mix 1 µl of DpnI restriction enzyme (10 units/ µl, Thermo Fisher Scientific, Waltham, MA, USA) was added and incubated at 37°C for 1 hour to cleave the parental dsDNA. Samples were then run on an agarose gel, with each quantity of DNA template (10 µl product

with 2 μ l dye) both digested and undigested, aiming to see a difference between the two to select the DNA quantity that optimally worked.

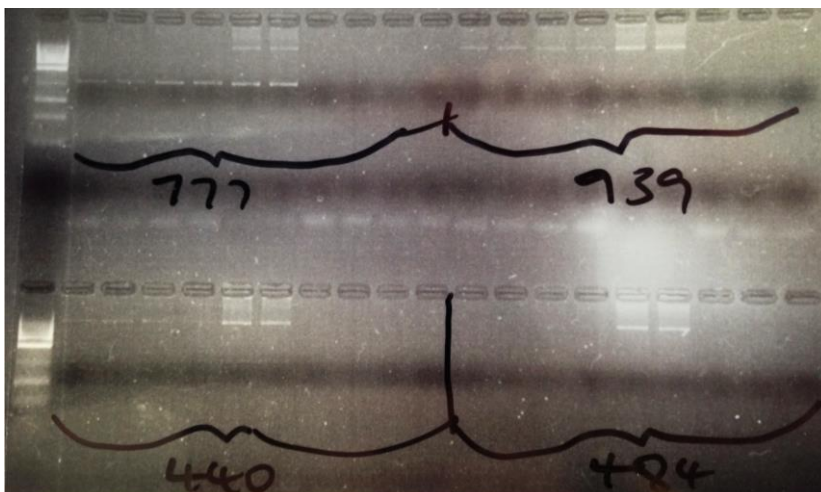


Figure 2-8: Agarose gel of PCR site directed mutagenesis

For each generated mutant, samples were run with undigested and digested products for each of 5ng, 10ng, 40ng, no polymerase and no template giving a total of 10 wells per mutant.

Following this XL1-blue cells were transformed with the PCR product using the same procedure as above, but using 5 μ l of the digested product. The initial attempt at transformation failed for all products. SDM was repeated for the L440P and L777R. Repeat transformation worked for all products with 2-5 colonies grown per plate (figure 2-9, example of the 5ng S939P agar plate with 2 colonies grown). For large numbers of colonies, colony PCR using restriction enzymes would have been used to identify correctly mutated colonies. However, given the small number of colonies, each colony was cultured. Single colony culture was performed as above followed by Miniprep of each colony for DNA extraction and sequencing. Miniprep was performed using the (QIAprep Spin Miniprep Kit (QIAGEN) and an adapted manufacturer's protocol with the resulting isolated DNA sequenced (table 2-6).

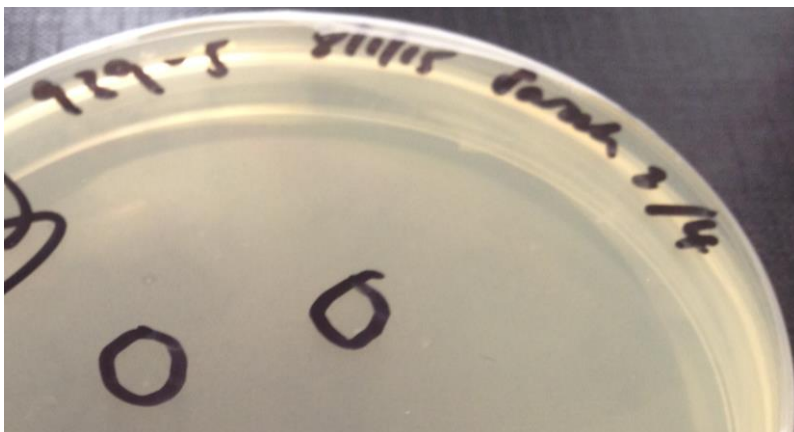


Figure 2-9: Overnight LB agar plate culture of XL1-blue supercompetent cells

From sequence results, the colony with successful mutagenesis was identified and an overnight culture performed from the glycerol stock (all under sterile technique):

1. 50ml flat bottomed tube with 4ml LB broth and 4µl kanamycin was prepared
2. Using a 10µl pipette tip, a sample was scraped from the top of the glycerol stock and dropped in to the tube
3. Incubated at 37°C, 220rpm for 6 hours
4. 1.5ml of started culture was added to each of 2 conical flasks with 50ml LB broth + 50µl kanamycin
5. Incubated at 37°C, 220rpm overnight

Maxiprep was then performed to again yield >900ng/µl of plasmid DNA per plasmid type with an overall approximate volume of 0.7ml per plasmid.

2.3.1.5 Culture of hTERT-RPE1 cells

Cultured hTERT-RPE1 cells (gifted from colleague in lab) were stored in an incubator at 37°C with 5% CO₂. To work with cells, a class II biological safety cabinet was used, with all equipment sterilized with 70% alcohol prior to use. Cells were used at passage 16 (p16) to p28, therefore a frozen stock was made at an early passage of p16.

Cell culture protocol:

1. DMEM (DMEM/F12 GlutaMAX, Thermo Fisher Scientific) containing 50ml FBS (foetal bovine serum, Labtech, Uckfield, UK) was warmed in a 37°C incubator, a 5ml trypsin (trypsin-EDTA, phenol red, Thermo Fisher Scientific) aliquot was taken out of the -20°C freezer to thaw
2. Cells were inspected under microscope
3. In hood, DMEM+FBS was removed
4. Cells were washed with 10ml HBSS (Thermo Fisher Scientific), wash was removed
5. 5ml trypsin was added to lift cells off flask surface
6. Incubated 5-10 minutes at 37°C, ensuring minimum time was used
7. 5-6ml DMEM+FBS was added to flask then all contents were removed to 15ml tube
8. Cells were counted with a haemocytometer: 25µl of sample were added to top and bottom, central 5x5 grids counted with top and right-sided lines only counted for cells touching sides of boxes, average number from 2 central grids were counted eg 200 equivalent to 200×10^4 (20×10^5).
9. A new flask containing 20ml DMEM+FBS was then re-seeded at cell concentration required, typically 1×10^5 to allow twice weekly splitting, eg from count above 1ml was added to give an approximate 1 in 20 ratio, cell confluence was required quicker, 1.5ml was added etc.

10. The flask was labelled with passage, sprayed with 70% ethanol and placed in incubator
11. Confluency, debris and infection check were performed daily
12. Remainder of cells were used to seed cover slips/ frozen

Freezing of cells:

1. From cell splitting, cells were pelleted in a 15ml tube in a centrifuge at high speed, for 5 minutes
2. Resuspended in freeze medium (table 2-10), volume to make 1×10^6 concentration
3. Frozen in 1ml aliquots in cryogenic tubes, 3 hours in -20°C then moved to -80°C

Component	Volume
10% DMSO	1ml
60% FBS	6ml
DMEM+FBS	3ml
Total	10ml (scale as appropriate)

Table 2-10: Freeze medium components

Resurrecting cells:

1. DMEM+FBS medium was warmed and 10ml added to a 15ml tube
2. Cells were removed from -80 freezer, rapidly thawed in hand
3. 1ml cells was added to 10ml medium
4. Spun at 1000rpm for 8 minutes
5. Medium was tipped off and pellet flicked to re-suspend
6. 10ml medium was added and pipetted to mix
7. Added to a flask already containing 10ml medium

2.3.1.6 Transient transfection of hTERT-RPE1 cells

Transient transfection was achieved using Lipofectamine[®] LTX Reagent with PLUS[™] (Thermo Fisher Scientific). A 12 well plate was used for which the surface area per well is 4cm^2 requiring 1ml volume of plating medium. The experiments were designed to include each plasmid under investigation with 2 control wells per plasmid; the first control contained no DNA, the second control contained both no DNA and no primary antibody.

1. In a class II biological safety cabinet, single round cover slips were sterilised (using 100% ethanol and flame) and placed in to each well

2. Cultured hTERT-RPE1 cells were seeded at 1×10^5 /well in 1ml of DMEM+FBS medium and incubated in a sterile incubator at 37°C with 5% CO₂
3. 50-80% confluency was required before transfection (approx. 24 hours)
4. The medium was removed and 800 µl warmed OptiMEM-I reduced serum medium (Thermo Fisher Scientific) added per well
5. For each experiment, in a 1.5ml microcentrifuge tube, plasmid DNA was diluted in 200 µl OptiMEM-I reduced serum medium, and mixed gently
6. PLUS reagent was added to the diluted DNA
7. This was mixed gently, then incubated for 5 minutes at room temperature
8. Lipofectamine LTX was added (avoiding tube sides), and mixed thoroughly, then incubated for 30 minutes at room temperature
9. DNA-lipid complexes were added drop-wise to the wells, mixed by gently rocking
10. Wells were incubated in 5% CO₂ incubator at 37°C
11. After 4-6 hours if cells dying then the medium was changed to DMEM+FBS
12. After 24 hours serum starvation was performed in order to ciliate cells, by removing OptiMEM-I, washing with 1ml DMEM (no FBS) and then adding 1ml DMEM (no FBS) and incubating for 24 hours

Fixation/permeabilisation

1. All steps were performed at room temperature, culture media was removed and each well washed with 1ml phosphate buffered saline (PBS, Sigma-Aldrich) 3 x 10 minutes
2. Fixed for 10 minutes using 4% fresh/thawed paraformaldehyde (PFA, Sigma-Aldrich) in PBS
3. Washed with PBS 3 x 10 minutes
4. Permeabilised with 0.5% Triton X-100(Sigma-Aldrich) in PBS, 15 minutes
5. Washed with PBS 3 x 10 minutes

Immunostaining

1. Cells were blocked with 400µl 5% normal donkey serum (NDS, Abcam, Cambridge, UK) diluted in PBS for 1 hour at room temperature
2. Primary antibodies were prepared in 1% NDS + PBS, 300 µl per well
3. Blocking solution was removed and replaced with antibody dilutions
4. The 12-well plate was sealed and incubated overnight at 4°C
5. Next day, solutions were removed and washed with PBS 3 x 10 minutes
6. The following steps were all performed in dim lighting at room temperature
7. Secondary antibodies were prepared in 1% NDS + PBS, typically at 1:300
8. Final wash solution was removed and secondaries added

9. If low on antibody stock, cover slips were removed from the well and 140 μ l solution dropped carefully on to each slip
10. Incubated 1 hour
11. Washed with PBS 3 x 10 minutes
12. Mounted with Prolong Gold Antifade Mountant with DAPI (Thermo Fisher Scientific)
13. Allowed to dry minimum 2 hours, preferably overnight before imaging

Cells were immunostained with primary antibodies to the C-terminal Myc-DDK tag of the plasmid (1:5000 rat Anti-DYKDDDDK Tag Antibody, 200473, Agilent Technologies), basal body (1:1000 rabbit anti-pericentrin, Sigma-Aldrich, Dorset, UK) and secondarily stained with 1:300 donkey Alexa Fluor® 488 conjugated anti-rat (Thermo Fisher Technologies) and 1:300 donkey Alexa Fluor® 647 conjugated anti-rabbit (Thermo Fisher Technologies). In addition, primary antibody to cilia was initially used (1:1000 mouse anti-acetylated tubulin, Sigma-Aldrich) with secondary 1:300 donkey Alexa Fluor® 594 conjugated anti-mouse (Thermo Fisher Technologies).

Optimisation experiments were performed initially with 1 μ g of WT plasmid to determine optimal dilution of anti-FLAG antibody, then the amount of plasmid DNA was further optimised based on transfection efficiency (tables 2-11, 2-12).

Well	Plasmid name	Plasmid amount, μ g	LTX amount, μ l	PLUS amount, μ l	Anti-FLAG antibody dilution
1	WT	1	2	1	1:1000
2	WT	1	2	1	1:2000
3	WT	1	4	1	1:5000
4	WT	1	4	1	1:10000
5	WT	0	2	1	1:1000
6	WT	0	2	1	No primary

Table 2-11: Optimisation of anti-FLAG antibody

Well	Plasmid name	Plasmid amount, μ g	LTX amount, μ l	PLUS amount, μ l
1	WT	0.25	2	1
2	WT	0.5	2	1
3	WT	1	2	1
5	WT	0	2	1
6	WT	0	2	1

Table 2-12: Optimisation of wild-type *IFT140* plasmid quantity

This determined that 1 µg plasmid DNA was optimal for transfection. Ciliation was successful for the control sample without plasmid DNA (figure 2-10) and was observed with 0.25 µg and to a lesser extent with 0.50 µg of DNA. However transfection efficiency was low for these amounts. At 1 µg, ciliation was inhibited but transfection efficiency was reasonable (approximately 38%). Therefore the ciliation step and anti-acetylated tubulin antibody primary were removed from the transfection procedure.

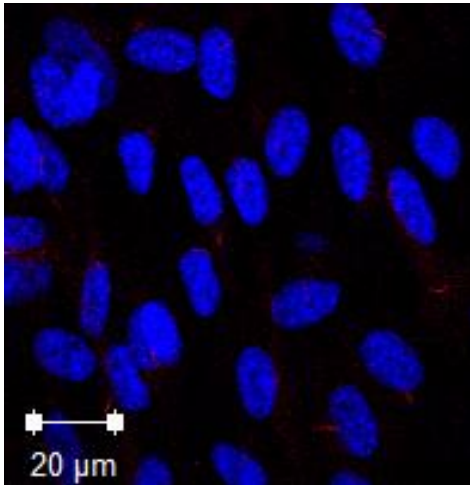


Figure 2-10: hTERT-RPE1 ciliated cells

Cells were imaged with confocal pinhole laser-scanning microscopy (Zeiss LSM 700, Carl Zeiss Microscopy GmbH, Jena, Germany) using 4 solid-state excitation lasers (405/444, 488, 555 and 633 nm) with 2 reflection channels simultaneously detected. Image processing was performed with ZEN software (2012, Carl Zeiss Microscopy GmbH). The percentage of transfected cells with localisation of IFT140 to the basal body was calculated from a mean of 3 independent experiments with >100 cells counted per experiment (statistical analysis with a one-way analysis of variance and post hoc comparison using a Bonferroni correction, IBM® SPSS® Statistics version 22). It was noted that a large degree of non-specific cytoplasmic staining was present for the majority of transfected cells with a minority of cells expressing IFT140 at a low level that was focal and could be localised. This low level expression was counted in the experiment and this approach double checked with French colleagues who had initially published the experiment.

Further clarification of observed IFT140 staining was achieved by investigating endogenous IFT140 staining in these cells with 1:50 and 1:200 anti-IFT140 antibody and 1:300 donkey Alexa Fluor® 647 conjugated anti-rabbit as above. This identified non-specific endogenous nuclear staining which would have precluded interpretation of expression differences.

2.4 Zebrafish studies

Colleagues within the laboratory already working with zebrafish helped with the investigation of an *ift140* zebrafish morphant; their roles were in breeding and maintaining the zebrafish, performing the microinjections, fixing and embedding, retinal histology and Western blots. I designed the experiments, performed retinal cryosections, immunohistochemistry, tunel assay and embryo length measurements.

Wild type (wt) AB zebrafish were bred and maintained in the University College London animal facility according to standard protocols and the guidelines of the ARVO Statement for the Use of Animals in Ophthalmic and Vision Research.¹⁶⁵

Microinjection of 3ng ATG start site translation blocking

(ATCAAATACACAGCCATGAGCTAC, GeneTools, Philomath, OR, USA) and mismatch (MM, ATAAAATAAACAACCATAAGATAC) morpholino, both modified with a 3' end with carboxyfluorescein, was performed into the yolk sac of 1-2 cell stage wt embryos. The morphant embryos were grown at 28.5°C, observed for morphological changes at 3 and 5 days post-fertilisation (dpf) with wholemount alcian blue (Sigma-Aldrich) staining to highlight cartilage structure.¹⁶⁶ Successful knockdown of *ift140* was confirmed by western blot of morphant (both ATG and MM) and wt fish (n=20 per group, 30ug total protein) using an IFT140 antibody (1:500 rabbit polyclonal IFT140 antibody, 17460-1-AP, Proteintech, Manchester, UK) with a beta-actin positive antibody control (Sigma-Aldrich). In addition, simultaneous knock-down of both *Tp53* and *ift140* were performed to ensure that any observed phenotype was not an off-target apoptotic effect.¹⁶⁷

For histological analysis, embryos were fixed in 4% PFA, embedded, sectioned and stained with toluidine blue (Sigma-Aldrich) according to previously published protocols.¹⁶⁸

2.4.1.1 Retinal immunohistochemistry

Immunohistochemistry was performed on 12 µm retinal cryosections that had been fixed in 4% PFA, cryo-protected with 30% sucrose (Sigma) and embedded in Tissue-Tek® O.C.T. Compound (Sakura Finetek Europe, Alphen aan den Rijn, The Netherlands).

A cryostat (Leica Biosystems, Nussloch, Germany) was used to make the retinal cryosections for immunohistochemistry. Separate experiments were performed to test primary antibodies against green/red double cones (1:500 mouse anti-zpr-1, ZIRC, Oregon, USA) and axons to demonstrate inner retinal layers (1:400 mouse anti-acetylated tubulin, Sigma-Aldrich). Sections were secondarily stained with donkey

Alexa Fluor® 488 conjugated anti-mouse (Thermo Fisher Scientific). Immunostaining procedure was as follows:

1. Slides of retinal cryosections either used fresh or if from -80°C freezer, allowed to dry for 1-2 hours
2. Washed with PBS for 10 minutes x 3
3. Blocked at room temperature for 1 hr using 20% NDS in PBS with 0.5% Triton x100
4. Removed block and covered with primary antibodies diluted in 1% NDS (in PBS with 0.5% Triton x100) and incubated at 4°C overnight
5. Washed with PBS for 10 minutes x 3
6. Covered with secondary antibody (in dark), incubated room temperature 2-4 hours
7. Washed with PBS for 10 minutes x 3
8. Dried at room temperature
9. Mounted with ProLong Gold Antifade Mountant with DAPI and coverslips
10. Imaged with confocal microscopy (Zeiss LSM 700).

2.4.1.2 Tunel assay

For investigation of apoptosis levels, 12 µm cryosections were stained according to manufacturer instructions using the ApopTag® Fluorescein In Situ Apoptosis Detection Kit (Merck Millipore, Billerica, USA) and then mounted with ProLong Gold Antifade Mountant with DAPI and imaged with confocal microscopy (Zeiss LSM 700).

2.4.1.3 Rescue experiments

For the rescue experiments, embryos were co-injected with *ift140* ATG MO and 0.1 µg/µl of wt RNA or mutant mRNAs (L440P, T484M) and compared with both wt fish and a control group injected with *ift140* ATG MO only ($n \geq 100$ live embryos counted per experiment). The mRNA was generated from plasmid constructs, linearized by SfoI restriction enzyme digest (New England Biolabs, Inc., Hitchin, UK) followed by T7 driven *in vitro* transcription (mMESSAGE, mMACHINE T7 transcription kit, Life Technologies) according to manufacturer protocols. Phenotypes were quantified at 5dpf based on morpholino length measured from snout to end of notochord using ImageJ (statistical analysis with a 2-tailed, paired t-test, IBM® SPSS® Statistics version 22) and as a secondary measure the vertical eye diameter was also measured.^{169, 170} The fish were anaesthetised with 0.003% tricaine before imaging (Nikon stereoscopic microscope). The E664K plasmid repeatedly failed transcription and so rescue was attempted with wt, L440P and T484M RNAs only.

3 Retinal dystrophy due to mutations in the cone-rod homeobox gene

3.1 Introduction

The cone-rod homeobox gene *CRX* (MIM #602225) encodes a transcription factor vital for both the development and survival of photoreceptors.¹⁷¹⁻¹⁷³ It is expressed predominantly in photoreceptors and the pineal gland and has a high homology to the OTX family of homeobox genes.^{171, 173} It acts by binding to promoter enhancer regions of specific retinal genes; this role is particularly important in retinal development. It is co-expressed in the retina with other transcription factors including NRL and NR2E3.^{173, 174}

A locus for autosomal dominant CORD (CORD2, MIM #120970) was identified in 1994 and mapped to 19q13.¹⁷⁵ The gene responsible for CORD at this locus was identified as *CRX*.¹⁷¹ Subsequently it became evident that mutations in *CRX* may be associated with a range of different retinal phenotypes including CORD, LCA, RCD and COD.^{77, 176, 177}

CRX mutations are rare with the majority of mutations arising de novo.⁷³ Prior to the research outlined in this thesis, 42 probable disease causing mutations and 1 whole exon deletion had been reported, all in the heterozygous state except for 3 case reports of homozygous disease in LCA and severe RCD.^{16, 73, 75, 77, 171, 176-199}

In this study of *CRX* related retinal dystrophy, the phenotypic heterogeneity was investigated. This identified a previously unreported association with adult-onset 'bull's-eye' macular dystrophy.

3.2 Methods

3.2.1 Ascertainment of patients

WES in a cohort of unsolved macular dystrophy patients identified 2 patients with heterozygous *CRX* mutations, with this novel finding prompting further study of this gene. From interrogation of the genetic database, I identified 65 unsolved probands with adult-onset macular dystrophy or CORD and performed targeted Sanger sequencing of all exons and intron-exon boundaries of *CRX*. CORD was included to ensure all macular involving dystrophies were investigated. This identified 3 families. In addition, from the database, 6 further molecularly solved families with LCA or childhood onset retinal dystrophy were identified.

3.2.2 Clinical assessment

Each patient with a *CRX* mutation underwent a full clinical examination including visual acuity and dilated fundus examination. The majority of examinations were performed by myself, but in a few patients were performed by one of my supervisors. Age permitting, retinal fundus imaging was obtained with electrophysiology performed in all patients.

3.2.3 Molecular investigations

In total, 11 families were solved by a combination of candidate gene Sanger sequencing of all exons and intron-exon boundaries (5 families), APEX microarray (2 families), Manchester 105 retinal gene panel (1 family) and WES (3 families).

Confirmatory bi-directional Sanger sequencing of affected exons was performed by myself on all 11 identified probands with segregation in available relatives. DNA was amplified using specifically designed primers (table 3-1).

Exon	Primer forward 5' → 3'	Primer reverse 5' → 3'	Enzyme	Annealing temp (°C)	Amplicon size (bp)
2	TCACATACCTAAGAGGAGAAGGAGG	TGACATACATTTTCAGATGAACCC	BIOTAQ	64	389
3	TGAGGTGTAGAAGGGCAGGG	TCCAGATAGAGGAAACTGAGTGC	MyTaq	64	564
4.1	TGCAAAGTAGACAGATGTGAACCC	TGAAATAGGAGCTCGGAGACCC	BIOTAQ	64	518
4.2	TGGAGCCCAGCCTCAGAGTCC	TCTCTGTAAGCTGAACACCGAGC	MyTaq	64	564

Table 3-1: Primer pairs for sequencing of *CRX*

Mutation nomenclature was assigned in accordance with GenBank Accession number NM_000554.4.

Phenotype-genotype correlation

Age of presentation was used as a surrogate and approximate metric of severity in order to test associations between mutation position and phenotype severity. First, a quantitative analysis was performed of the mutations by plotting the mutation position against age of presentation. Using the same data, the hypothesis that mutations affecting residues earlier in the gene are generally more severe than others was tested by computing the non-parametric Spearman correlation coefficient. Second, a qualitative comparison was performed by dividing the mutations into two mutually exclusive groups: missense variants affecting the homeodomain, and those that were premature termination codons (PTCs) in the carboxyl end of the gene. A comparison of

the median age of the two groups was made, and tested for significance using the Mann-Whitney test. Statistical analysis was performed using IBM® SPSS® Statistics version 22.

Conservation of CRX homeodomain residues between species and between paralogues within humans was analysed using Clustal Omega. The locations of mutations arising within the homeodomain were plotted against the consensus sequences.

3.3 Results

The clinical data are summarized in table 3-2 with pedigrees shown in figure 3-1. From the screened cohorts, 11 affected patients were ascertained with a further 7 affected relatives from 5 families recruited giving a total of 18 affected patients from 11 families. There were 6 simplex cases of which *de novo* disease could be confirmed in 3 (19090, 19512 and 20046). A dominant pedigree was evident in 4 families.

Twelve patients had generalized photoreceptor dysfunction with clinical diagnoses of LCA (n=4), RCD (n=2), CORD (n=5) and COD (n=1). An unexpected group of adult onset macular dystrophy in 6 patients was identified with initial identification of this phenotype from WES of 2 patients. Two were asymptomatic with their disease identified incidentally. One (patient 17489.2) was identified after all family members of patient 17489.1 were examined in the clinic and the other (patient 19161.1) was identified after routine visual field testing at the optometrist showed centrocaecal scotomas. This patient still had acuity of 0.0 logMAR (6/6 Snellen) after 6 years of follow-up. Deterioration of acuity with time was documented in 3 cases. Patient 4663, the most severely affected of the macular dystrophy group, deteriorated from 0.2 logMAR (20/32 Snellen) each eye to right 1.3 logMAR (20/400 Snellen) and left 1.5 logMAR (20/630 Snellen) during 16 years follow up. Patient 16711 had incidental peripapillary changes similar to angioid streaks without any other identifiable features in the fundus or systemically (figure 3-2); this was thought to be an incidental finding unrelated to his macular dystrophy.

A common fundus feature in all phenotypes was that of macular atrophy, present in 14 of 18 cases. It was not present in 2 LCA patients (examined at a young age), nor in both members of family 17489, although these latter cases did have ISe band disruption at the maculae on OCT (figure 3-2). Three of the 4 LCA cases had noticeably blonde fundi at presentation.

Retinal dystrophy due to mutations in the cone-rod homeobox gene

Family, gender	Age onset	Age last rv	Diagnosis	Fundus	Age at last electrophysiology, key findings	Latest VA, logMAR, (Snellen), refraction if known
19090 (f)	Birth	2 yrs	LCA	Blonde	11 mths: probably undetectable	R NPL L NPL
19512 (m)	3 mths	2.5 yrs	LCA	Blonde fundus, central macular atrophy, thin peripheral retina	9 mths: undetectable	R&L NPL R&L +3.00 DS
20046 (f)	Birth	7 mths	LCA	Blonde fundus	7 mths: markedly attenuated	R&L PL R&L +3.50 DS
5126.1 (m)	12 yrs	50 yrs	CORD	Macular & peripheral atrophy, bone spicules, attenuated arterioles, pale optic discs	47 yrs: very severe generalized retinal dysfunction	R HM L CF R +3.25/-2.00x165 L +3.75/-3.50 x5
5126.2 (m)	12 yrs	27 yrs	CORD	Macular atrophy, subtle peripheral RPE mottling	25 yrs: undetectable PERG, generalized retinal dysfunction, cone deterioration	R 1.0 (6/60) L 1.1 (6/75) R +1.25/-2.75 x29 L +1.25/-3.00 x174
5126.3 (f)	14 yrs	25 yrs	CORD	Macular atrophy, peripheral retinal RPE pigment change	15 yrs: undetectable PERG, subnormal rod, moderately severe reduction cone	R 1.0 (6/60) L 0.8 (6/38) R +6.5/-3.50 x 175 L +6.00/-3.50 x 20
17489.1 (m)	3.5 yrs	16 yrs	RCD	Yellow spots R macula, pale optic discs, attenuated arterioles, mid peripheral hypopigmentation	11 yrs: Undetectable PERG and rod ERG, markedly subnormal cone specific ERG	R 1.0 (6/60) L 1.2 (6/95) R +0.50 DS L +0.50 DS
17489.2 (f)	53 yrs	53 yrs	MD	Mild disc pallor only	53 yrs: Bilateral macular dysfunction, normal ERGs	R 0.3 (6/12) L 0.5 (6/19)
18280.1 (f)	49 yrs	56 yrs	MD	Ring of RPE atrophy in maculae	52 yrs: PERG not definitely detectable, normal ERGs	R 0.2 (6/9.5) L 0.3 (6/12) R +0.25/0.25 x180 L +0.25/0.25 x45
18280.2 (f)	50 yrs	56 yrs	MD	Ring of RPE atrophy in maculae	51 yrs: Undetectable PERG, normal ERGs	R 0.6 (6/24) L 0.3 (6/12) R +1.00/-0.75 x90 L +0.50 DS
18280.3 (m)	32 yrs	42 yrs	CORD	Ring RPE atrophy in maculae with peripheral RPE pigmentary change	35 yrs: Undetectable PERG, subnormal rod, markedly subnormal cone ERG	R&L 1.0 (6/60) R -2.50/-0.50 x180 L -3.50/-0.50 x180
19161.1 (f)	50 yrs	56 yrs	MD	Mild RPE mottling maculae	52 yrs: Markedly reduced PERG, normal ERGs	R&L 0.0 (6/6) Hyperopic
19161.2 (f)	45 yrs	52 yrs	CD	Ring of RPE atrophy in maculae	48 yrs: Severely reduced PERG, cone ERGs reduced/delayed	R 0.5 (6/19) L 0.2 (6/9.5) R&L +1.75 DS
19990.1 (f)	6 yrs	27 yrs	RCD	Macular atrophy, peripheral extensive pigmentary retinopathy	26 yrs: Severe generalised loss of photoreceptor function	R&L PL
19990.2 (f)	Birth	2 yrs	LCA	Ring of RPE atrophy in maculae, mottled peripheral RPE change	20 mths: undetectable PERG and ERG	R&L HM R +6.00/-2.00x180 L +2.00/-1.25 x180
712 (f)	11 yrs	73 yrs	CORD	Pale discs, blonde posterior pole, attenuated arterioles, peripheral pigmentary clumps	60 yrs: PERG undetectable on L, residual on R, severe cone dysfunction with rod involvement	R 0.8 (6/38) L 1.0 (6/60) R -11.00/-1.00 x10 L -9.50/-2.00 x175
4663 (f)	42 yrs	67 yrs	MD	Macular atrophy	67 yrs: extinguished PERG, normal ERGs	R 1.3 (6/120) L 1.5 (6/190) Hyperopic
16711 (m)	35 yrs	63 yrs	MD	Macular atrophy	54 yrs: undetectable PERG, normal ERGs	R&L 1.0 (6/60)

Table 3-2: Key phenotypic features of patients

NPL, no perception of light; DS, dioptre sphere; PL, perception of light; HM, hand movements; CF, counting fingers

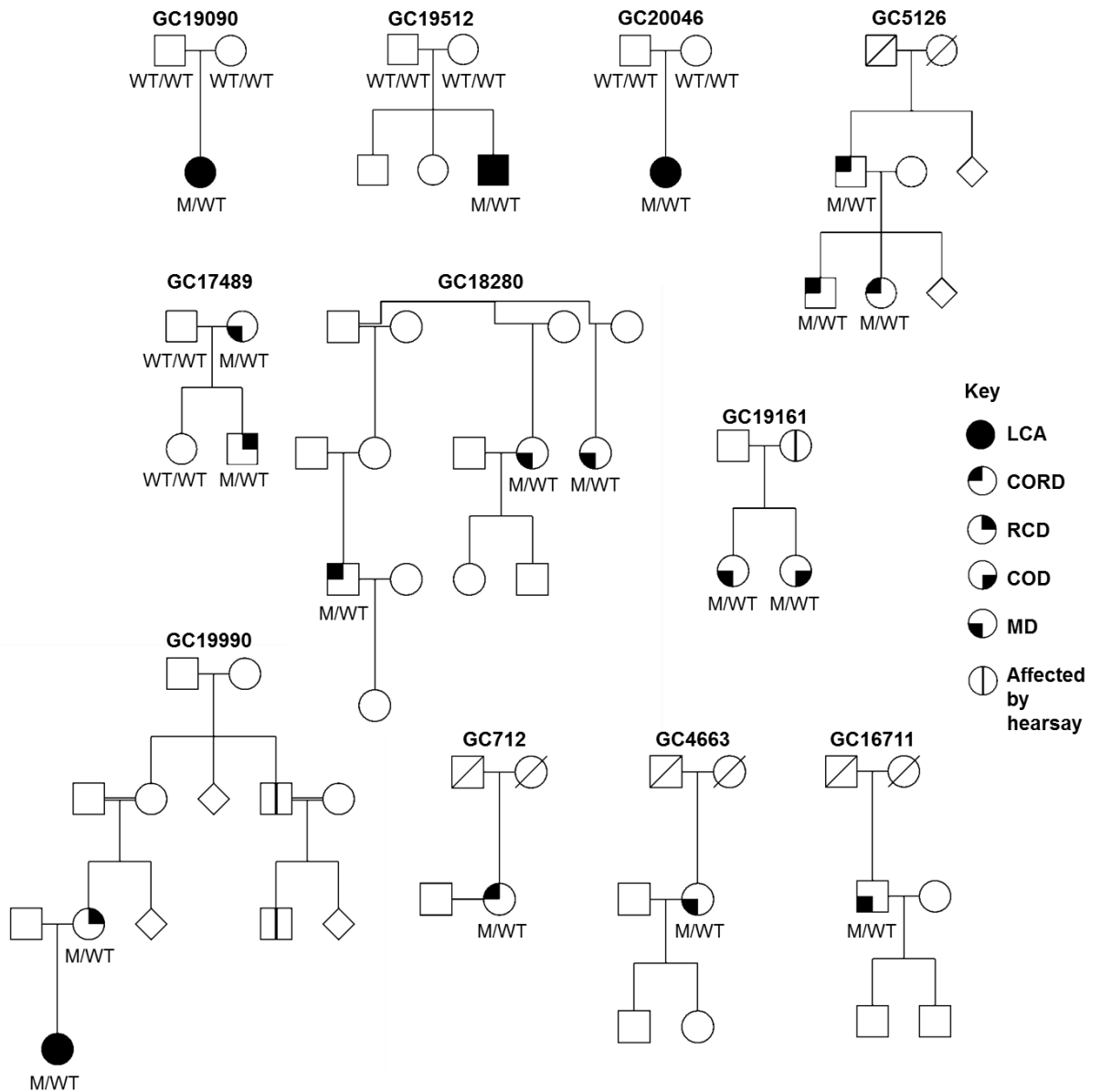


Figure 3-1: Pedigrees

FAF imaging and OCT scans were available in 12 of 18 patients; the LCA patients were all too young for imaging and FAF and Spectralis OCT was unavailable in the COD patient. FAF imaging demonstrated a reduced ring of autofluorescence parafoveally in the CORD patients, an extensive loss of autofluorescence in the RCD patients and a ring of increased autofluorescence at the macula with loss of autofluorescence within the ring in all macular dystrophy patients.

On OCT, 4 of the CORD patients had loss of the ISe band with outer retinal thinning at the macula on OCT, with patient 9 showing disruption of the ISe band but no macular thinning. The 2 patients with RCD had loss of outer retina and ISe band at the maculae on OCT. The macular dystrophy patients had disruption of the ISe band at the maculae on OCT with patient 17489.2 the least affected.

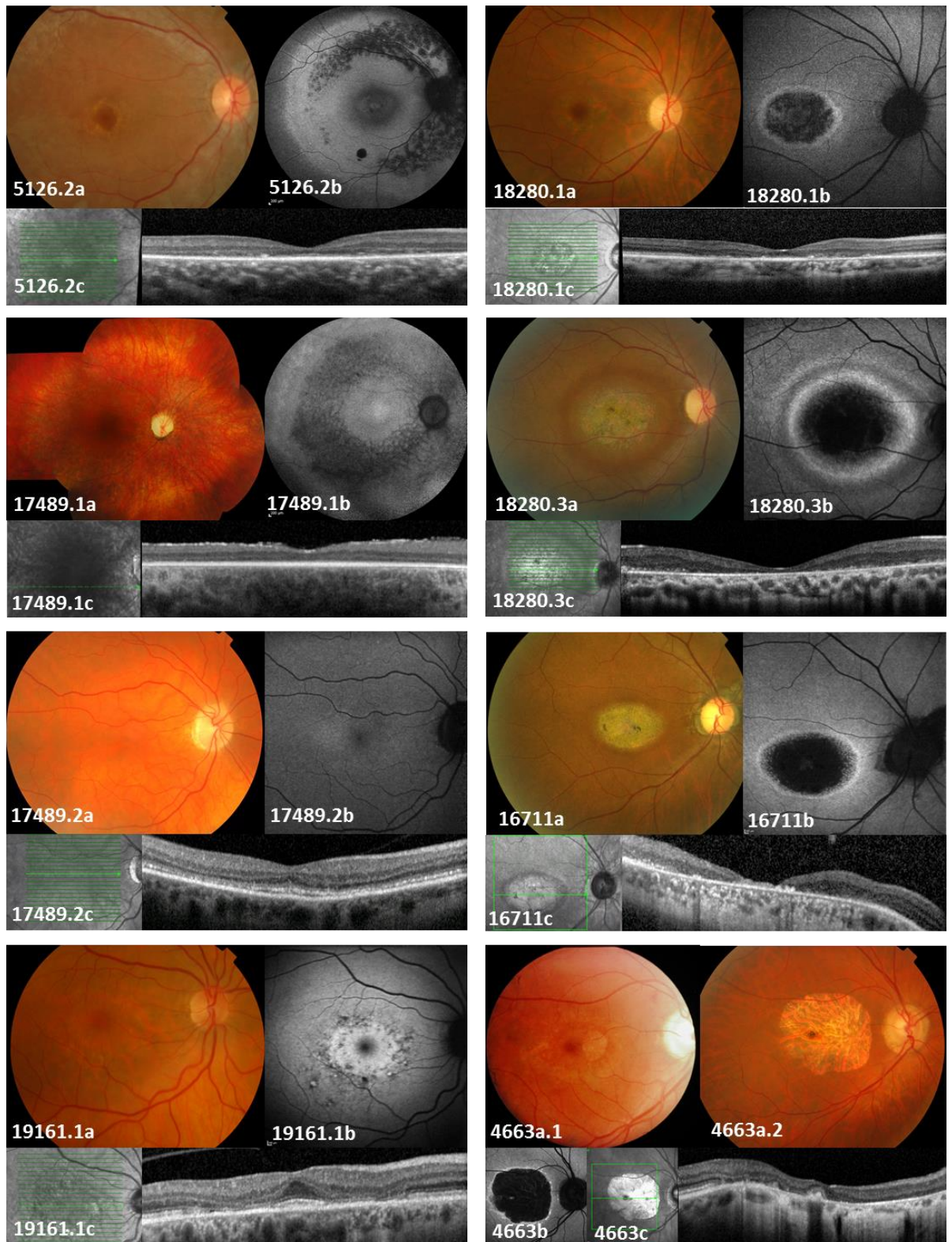


Figure 3-2: Retinal imaging in *CRX* related retinal dystrophy

Fundus imaging of patients 5126.2, 17489.1, 17489.2, 19161.1, 18280.1, 18280.3, 16711, 4663: (a) right fundus photograph, (b) right 30 or 55 degree FAF imaging, (c) right OCT. Patient 4663, (a.1) fundus photograph from 1998, (a.2) fundus photograph from 2014

Electrophysiology was performed in all patients (figure 3-3, table 3-2). Patients with LCA had an undetectable ERG, whereas those with later onset generalised

photoreceptor dystrophy had subnormal and delayed full field ERGs. The PERG was universally reduced in the macular dystrophy patients, with normal full field ERGs.

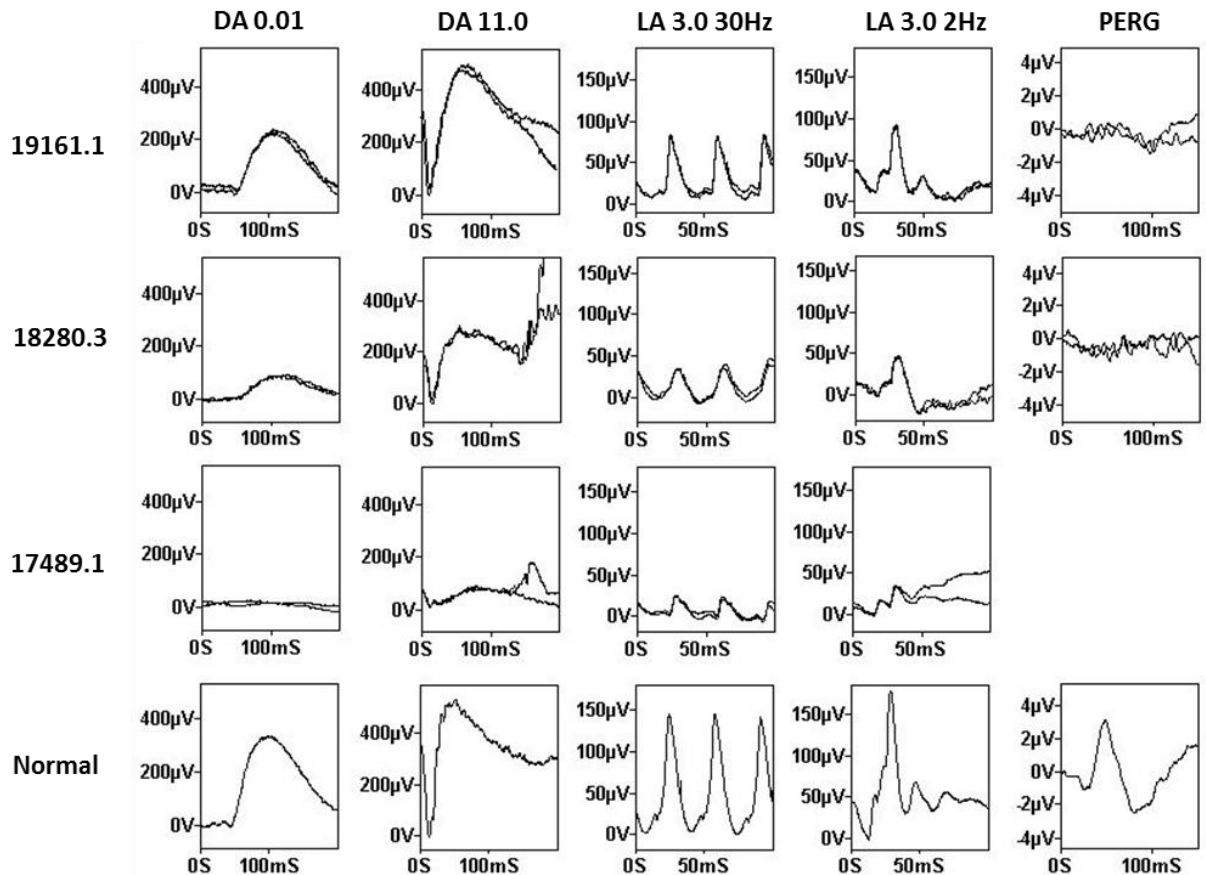


Figure 3-3: Electoretinography features

One eye of patients 19161.1, 18280.3, 17489.1 and normal control (age 24). Patient 19161.1, macular dystrophy, demonstrates subnormal PERG with normal ERGs for age (53 years at ERG).^{200, 201} Patient 18280.3, cone-rod dystrophy, demonstrates subnormal rod and bright flash ERGs (DA 0.01; DA 11.0), delayed and subnormal cone flicker ERGs (LA 3.0 30Hz) and markedly subnormal single flash ERG (LA 3.0 2Hz) with undetectable PERG. Patient 17489.1, rod-cone dystrophy, demonstrates undetectable rod ERG (DA 0.01); severe reduction in the bright flash ERGs (DA 11.0) and markedly delayed and subnormal cone flicker and single flash ERGs (LA 3.0 30Hz; LA 3.0 2Hz). PERG was unrecordable due to nystagmus.

Four families demonstrated intra-familial phenotypic heterogeneity (figure 3-1). Family 17489 segregated macular dystrophy and RCD; family 18280 macular dystrophy and CORD; family 19161 macular dystrophy and cone dystrophy; and family 19990 RCD and LCA. Family 17489 is particularly unusual as the son had early onset retinal dystrophy with rod-cone dysfunction, the mother a mild, asymptomatic macular dystrophy and the daughter optic atrophy with normal ERGs that presented age 3. Both she and her father screened negative for mutations in *CRX*. The identified heterozygous mutation in this family has previously been reported.¹⁷⁸ Phenotypic homogeneity was present in only 1 family (5126), all affected members having CORD.

Molecular analysis was performed on all patients and available family members (table 3-3). Seven novel mutations were identified, 6 PTCs in exon 4, and 1 missense mutation in exon 3. The novel missense mutation is predicted to be pathogenic based on SIFT and Polyphen2 scores. Segregation analysis confirmed *de novo* mutations in 3 of the LCA cases.

Family	Diagnosis	Variant: nucleotide, protein	Predicted effect	Segregation	First report
19090	LCA	c.570delC (p.Tyr191Metfs*3)	PTC	Both parents negative	This paper
19512	LCA	c.571delT (p.Tyr191Metfs*3)	PTC	Both parents negative	Rivolta 2001 ¹⁹⁴
20046	LCA	c.570delC (p.Tyr191Metfs*3)	PTC	Both parents negative	As above
5126	CORD	c.568_590del (p.Pro190Glyfs*38)	PTC	Present in all 3 affected patients, other family DNA unavailable	This paper
17489	RCD, MD	c.121C>T (p.Arg41Trp)	Pathogenic SIFT 0, Polyphen2 1.0	Present in affected patient and affected mother, absent in father and sister	Swain 1997 ¹⁷⁸
18280	MD, CORD	c.774T>A (p.Tyr258*)	PTC	Present in all 3 affected patients, further family DNA unavailable	This paper
19161	MD, CD	c.605delG (p.Cys202Sfs*17)	PTC	Present in both affected patients, further family DNA unavailable	This paper
19990	RCD, LCA	c.624T>G (p.Tyr208*)	PTC	Present in affected patient and daughter, further family DNA unavailable	Stone 2007 ⁷³
712	CORD	c.821delG (p.Gly274Alafs*97)	PTC	No other DNA available	This paper
4663	MD	c.582delC (p.Tyr195Thrfs*23)	PTC	No other DNA available	This paper
16711	MD	c.272G>A (p.Arg91Lys)	Pathogenic SIFT 0, Polyphen2 0.992	No other DNA available	This paper

Table 3-3: Mutations in CRX found in this patient series

Nine further missense variants in 11 patients were identified (table 3-4). Based on predictive algorithms, previous reports and the presence of the variant in control population databases, 8 of these most likely represent benign changes with the ninth predicted to be damaging but not segregating with known disease within the family. Four of these 9 variants are novel and include 2 synonymous changes, c.355A>C (p.Arg119Arg) and c.561C>T (p.Thr187Thr), and 2 non-synonymous changes, c.127C>T (p.Arg43Cys) and c.526C>T (p.Arg176Trp). The novel synonymous changes

are predicted to be tolerated on SIFT analysis, arise more than 100 base pairs from any intron-exon boundary and are not predicted to affect splicing *in silico*. Variant c.365G>A, found in 2 patients with macular dystrophy and cone dystrophy, onset childhood and early 30's respectively, has been previously reported as an apparently benign variant.²⁰² Variants c.472G>A and c.101-12A>G were found in 2 patients both with predominantly macular dystrophy and mild full field ERG abnormalities. Both variants have been previously reported in normal controls.¹⁷⁸ The c.526C>T variant was identified in a RCD patient hemizygous for a novel *RPGR* splice site mutation (identified in the same exome sequencing experiment) and segregation analysis found the same heterozygous *CRX* change in the mother, who had normal acuity, fundus examination and electrophysiology at the age of 35. The c.127C>T variant predicted to be damaging was identified in a macular dystrophy patient on exome-analysis and subsequently also identified in her older brother and mother, both of whom are asymptomatic but unavailable for further examination. Age of onset in this patient was 22 years old with visual acuity at last review age 27 of 1.0 logMAR each eye (20/200 Snellen)

Patient details	Variation	SIFT	Polyphen2	ExAC database	First reported
Family 19090, father	c.355A>C (p.Arg119Arg)	0.43	N/A	N/A	This paper
Family 20046, patient and mother	c.196G>A (p.Val66Ile)	1.0	0.033	358 in 121402	Vallespin 2007 ²⁰³
Family 17489, patient 17489.1 ,	c.100+12C>T	N/A	N/A	17164 in 114812	Swain 1997 ¹⁷⁸
Patient with CORD	c.561C>T (p.Thr187Thr)	0.75	N/A	N/A	This paper
Two patients cone dystrophy and macular dystrophy	c.365G>A (p.Gly122Asp)	0.35	0.080	1092 in 119584	Schocki 2001 ²⁰²
Patient macular dystrophy with mild cone and rod involvement	c.472G>A (p.Ala158Thr)	0.62	0.012	981 in 119300	Swain 1997 ¹⁷⁸
Patient macular dystrophy with mild rod and cone involvement	c.101-12A>G	N/A	N/A	358 in 121402	rs73941294
Patient with rod cone dystrophy	c.526C>T (p.Arg176Trp)	0.22	0.974	4 in 119782	ExAC
Patient with macular dystrophy	c.127C>T, p.Arg43Cys	0.03	1.000	N/A	This paper

Table 3-4: Identified *CRX* variants of uncertain pathogenicity

A quantitative analysis was performed of the mutations by plotting the mutation position against age of presentation. A more severely affected subset of patients could be expected to have a lower median age of presentation than the remainder of the cohort.

Such an analysis would be expected to demonstrate critical gene regions after which severity might change thus exposing clinically significant functional domains.²⁰⁴ On plotting the position of mutation against age of presentation (figure 3-4) there was no evident position after which severity differed, nor was there a correlation between position and severity (Spearman correlation coefficient $r_s = 0.093$, $p = 0.787$). A comparison of median age of presentation in those with homeodomain missense versus PTC mutations showed no statistical difference (Mann-Whitney test, $U = 7.00$, $p = 0.634$).

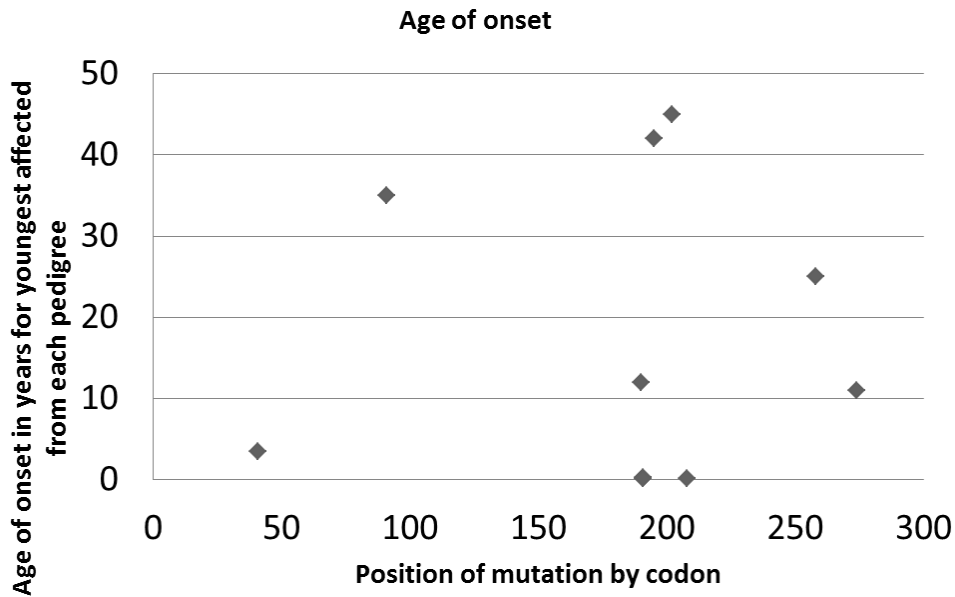


Figure 3-4: Mutation codon position against age of onset

Forty three mutations of possible pathogenicity have been previously reported (table 3-5). A further 4 variants were excluded from further analysis for the following reasons: the first was from a single report of a mutation in exon 2, c.24dupG (p.Pro9Alafs*61) in a patient with LCA but the mutation did not segregate with disease and the patient in question also had severe bilateral sensorineural hearing loss, a feature not otherwise reported with *CRX* mutations¹⁹⁶; 2 mutations, c.720_742dup23 (p.Gln248Profs*19) and c.753delC (p.Ser252Profs*119), are part of a screen on a microarray are also excluded as they are unpublished and no further information is provided as to patient phenotype¹⁵³; the fourth, c.351dupC (p.Lys118Glnfs*56) is also unpublished.¹⁸³

Retinal dystrophy due to mutations in the cone-rod homeobox gene

Mutation- heterozygous unless specified	Protein	SIFT score	Polyphen2 score	First report
c.121C>T	p.Arg41Trp	0	1.0	Swain 1997 ¹⁷⁸
c.122G>A	p.Arg41Gln	0.04	0.998	Swain 1997 ¹⁷⁸
c.124G>A	p.Glu42Lys	0.03	0.997	Li 2011 ¹⁷⁹
c.166G>A	p.Ala56Thr	0.23	0.96	Lotery 2000 ¹⁸⁰
c.193G>C, homozygous	p.Asp65His	0	0.999	Jin 2008 ¹⁸¹
c.238G>A	p.Glu80Lys	0	0.991	Sankila 2000 ¹⁸²
c.239A>C	p.Glu80Ala	0	0.991	Freund 1997 ¹⁷¹
c.239A>G	p.Glu80Gly	0.03	0.997	Huang 2012 ¹⁸³
c.264G>T	p.Lys88Asn	0	0.999	Nichols 2010 ¹⁸⁴
c.268C>T, homozygous	p.Arg90Trp	0	1.000	Swaroop 1999 ¹⁸⁵
c.344G>A	p.Arg115Gln	0.58	0.999	Sohocki 2001 ²⁰²
c.413delT	p.Ile138Thrfs*48	N/A	N/A	Nichols 2010 ¹⁸⁴
c.421delT	p.Ser141Profs*46	N/A	N/A	Zou 2013 ¹⁸⁵
c.429_430delTCinsA	p.Ser143Argfs*44	N/A	N/A	Stone 2007 ⁷³
c.436_447del	p.Leu146_Pro149del	N/A	N/A	Sohocki 1998 ¹⁷⁶
c.447dupC	p.Ser150Leufs*24	N/A	N/A	Lines 2002 ¹⁸⁷
c.458delC	p.Pro153Glnfs*34	N/A	N/A	Ziviello 2005 ¹⁸⁸
c.460delA	p.Thr154Profs*33	N/A	N/A	Arcot Sadagepan 2013 ¹⁹⁹
c.463_464insGGCA	p.Thr155Argfs*20	N/A	N/A	Stone 2007 ⁷³
c.495delAinsTTT	p.Ala166Leufs*22	N/A	N/A	Kohl 2012 ¹⁸⁹
c.502delG	p.Glu168Serfs*19	N/A	N/A	Freund 1997 ¹⁷¹
c.503_504delAG	p.Glu168Valfs*6	N/A	N/A	Freund 1998 ⁷⁷
c.512delT	p.Leu171Cysfs*16	N/A	N/A	Perrault 2003 ¹⁹⁰
c.520delG	p.Ala174Argfs*13	N/A	N/A	Nakamura 2002 ¹⁹¹
c.529delG	p.Ala177Leufs*10	N/A	N/A	Koenekoop 2002 ¹⁹²
c.541delG	p.Ala181Profs*6	N/A	N/A	Zhang 2001 ¹⁹³
c.570dupC	p.Tyr191Leu*45	N/A	N/A	Stone 2007 ⁷³
c.571delT	p.Tyr191Met*3	N/A	N/A	Rivolta 2001 ¹⁹⁴
c.573T>A	p.Tyr191*	N/A	N/A	Chen 2013 ⁷⁵
c.585C>A	p.Tyr195*	N/A	N/A	Stone 2007 ⁷³
c.585dupC	p.Ala196Argfs*40	N/A	N/A	Sohocki 1998 ¹⁷⁶
c.587-590delCCCC	p.A196Gfs*22	N/A	N/A	Swain 1997 ¹⁷⁸
c.615delC	p.Ser206Profs*13	N/A	N/A	Itabashi 2004 ¹⁹⁵
c.624T>G	p.Tyr208*	N/A	N/A	Stone 2007 ⁷³
c.636delC	p.Ser213Profs*6	N/A	N/A	Kitiratschky 2008 ¹⁷⁷
c.650delG	p.Gly217Alafs*2	N/A	N/A	Freund 1998 ⁷⁷
c.709dupC	p.Leu237Profs*30	N/A	N/A	Stone 2007 ⁷³
c.709delC	p.Leu237Serfs*134	N/A	N/A	Silva 2000 ¹⁹⁶
c.789delC	p.Val264Trpfs*107	N/A	N/A	Rivolta 2001 ¹⁹⁴
c.816delCACinsAA	p.Thr273Argfs*98	N/A	N/A	Paunescu 2007 ¹⁹⁷
c.887T>G	p.Phe296Cys	0	0.999	Preising 2007 ¹⁹⁸
c.899A>G	p.*300Trpext*118	N/A	N/A	Eisenberger 2013 ¹⁶
c.85-?_299+?del	Unknown	N/A	N/A	Eisenberger 2013 ¹⁶

Table 3-5: Previously reported mutations in CRX

Analysis of the 43 remaining likely pathogenic mutations indicates a pattern of missense mutations in exon 3 and PTCs in exon 4 (figure 3-5). There are 2 exceptions to this, c.344G>A (p.Arg115Gln) located early in exon 4 and reported in a single patient with limited phenotype and segregation data; and c.887T>G (p.Phe296Cys), located in the extreme C terminal and reported in a single family with CORD that is predicted to be damaging.^{198, 202} There is a single report of a whole exon deletion of *CRX*, identified in a sibling pair with LCA who had bi-allelic disease with a compound heterozygous missense mutation on the other allele.¹⁶

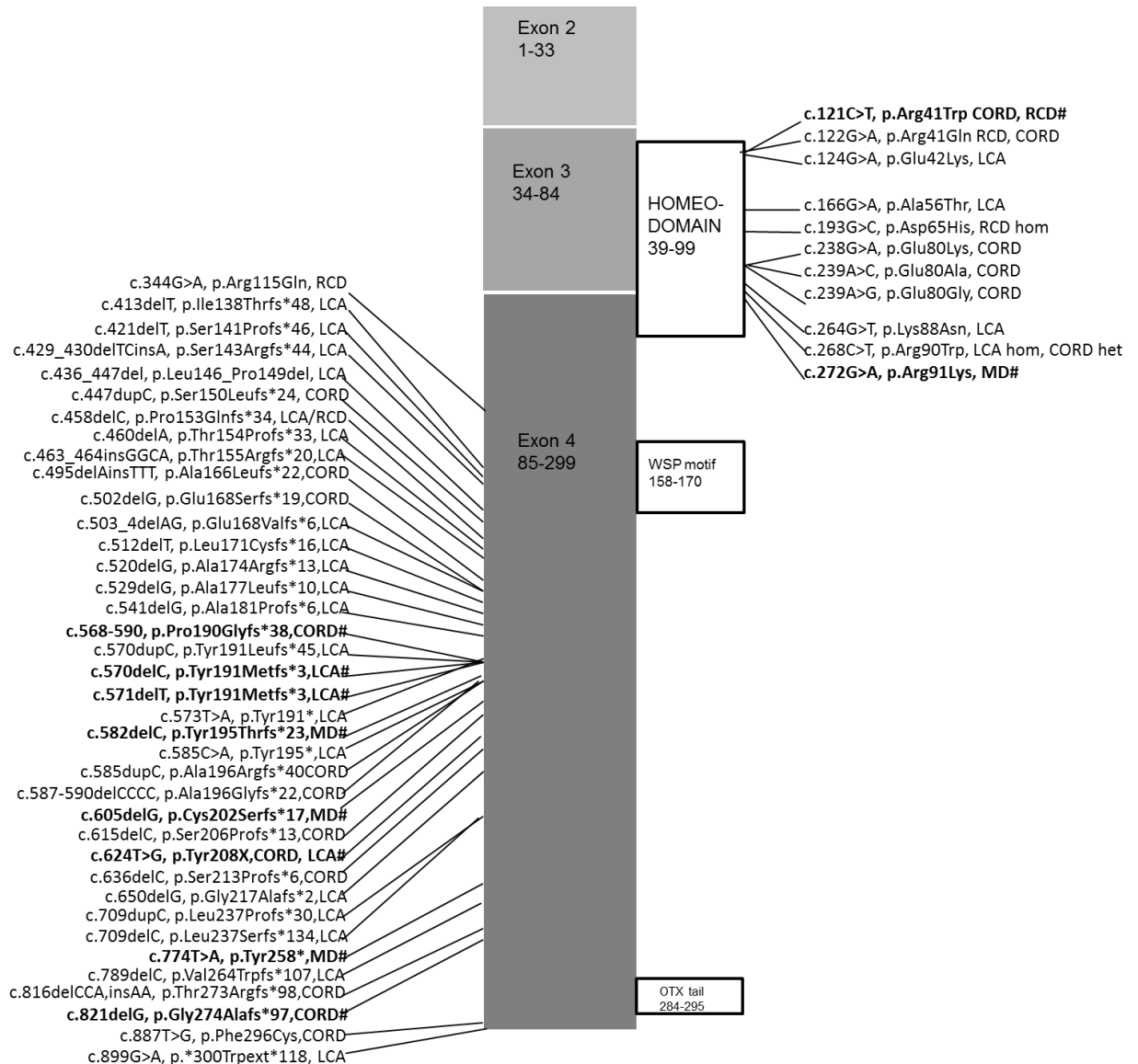


Figure 3-5: Schematic diagram of CRX structure and mutations

All published likely pathogenic mutations and 7 novel mutations from this series positioned along gene schematic. Mutations in bold with # for patients in this series.

The CRX homeodomain is highly conserved throughout species (figure 3-6) with all reported homeodomain mutations arising within highly conserved residues. Analysis of the homeodomain between human paralogues reveals that 4 reported mutations arise

in residues that are not conserved (figure 3-7); p.Glu42Lys reported to cause LCA, p.Ala56Thr reported to cause LCA, p.Asp65His reported to cause RCD in a homozygous state and p.Lys88Asn reported to cause LCA. All mutations found within the homeodomain that are associated with LCA therefore alter amino acid residues that are not conserved between paralogue human proteins.

```

      ##          #          #          #          #          #
fruitfly  QRRERTTFTRAQLDVLEALFGKTRYPDIFMREEVALKINLPESRVQVWFKNRRAKCRQQQLQ
mouse    QRRERTTFTRSQLEELEALFAKTQYPDVYAREEVALKINLPESRVQVWFKNRRAKCRQQRQ
rat      QRRERTTFTRSQLEELEALFAKTQYPDVYAREEVALKINLPESRVQVWFKNRRAKCRQQRQ
guinea   QRRERTTFTRSQLEELEALFAKTQYPDVYAREEVALKINLPESRVQVWFKNRRRA-----
human    QRRERTTFTRSQLEELEALFAKTQYPDVYAREEVALKINLPESRVQVWFKNRRAKCRQQRQ
macaque  QRRERTTFTRSQLEELEALFAKTQYPDVYAREEVALKINLPESRVQVWFKNRRAKCRQQRQ
cow      QRRERTTFTRSQLEELEALFAKTQYPDVYAREEVALKINLPESRVQVWFKNRRAKCRQQRQ
zebrafish  QRRERTTFTRTQLDILEALFQKTRYPDIFMREEVALKINLPESRVQVWFKNRRAKCRQQQQ
pufferfish  QRRERTTFTRAHWNVLEALFSKTRYPDIFMREEVALKINLPESRVQVWFKNRRAKCRQQQQ
frog     QRRERTTFTRAQLDILEALFAKTRYPDIFMREEVALKINLPESRVQVWFKNRRAKCRQQQQ
lizard   QRRERTTFTRAQLDILEALFAKTRYPDIFMREEVALKINLPESRVQVWFKNRRAKCRQQQQ
*****: : ***** **:***: : *****
    
```

Figure 3-6: Conservation of missense variants across species

Affected residues in this study highlighted with residue change underneath. * (asterisk) indicates positions which have a single, fully conserved residue, a : (colon) indicates conservation between groups of strongly similar properties, a . (period) indicates conservation between groups of weakly similar properties.

```

          Glu42Lys      Ala56Thr      Asp65His      Lys88Asn
          ##          #          #          #          #          #
DMBX1   QRRSRTAFTAQQLALEAKTFQKTHYPDVMRERLACTNLPEARVQVWFKNRRAKFRKKQR
CRX     QRRERTTFTRSQLEELEALFAKTQYPDVYAREEVALKINLPESRVQVWFKNRRAKCRQQRQ
OTX2    QRRERTTFTRAQLDVLEALFAKTQYPDIFMREEVALKINLPESRVQVWFKNRRAKCRQQQQ
OTX1    QRRERTTFTRSQLDVLEALFAKTRYPDIFMREEVALKINLPESRVQVWFKNRRAKCRQQQQ
HESX1   GRRPRTAFTQNQIEVLENVFRVNCYPGIDIREDLAQKLNLEEDRIQIWFQNRRAKLRSHR
GSC2    TRRHRTIFSEEQLQALEALFVQNQYPDVSTREERLAGRIRLREERVEVWFKNRRAKWRHQKR
GSC     KRRHRTIFTDEQLEALENLFQETKYPDVGTRQLARKVHLREEKVEVWFKNRRAKWRQKR
PITX3   QRRQRTHTFSQQLELEATFQRNRYPDMSSTREEI AVWNTNLTEARVRVWFKNRRAKWRKRE
PITX2   QRRQRTHTFSQQLELEATFQRNRYPDMSSTREEI AVWNTNLTEARVRVWFKNRRAKWRKRE
PITX1   QRRQRTHTFSQQLELEATFQRNRYPDMSMREEI AVWNTNLTEPRVRVWFKNRRAKWRKRE
VSX2    KRRHRTIFTSYQLEELEKAFNEAHYPDYAREMLAMKTELPEDRIQVWFQNRRAKWRKRE
VSX1    KRRHRTVFTAHQLEELEKAFNEASHYPDYAREMLAVKTELPEDRIQVWFQNRRAKWRKRE
UNCX    RRRTRTNFTGWQLELEKAFNESHYPDVFMRREALALRLDLVESRVQVWFKNRRAKWRKREN
MIXL1   QRRKRTSFSAEQLQLELVFRRTYPDIHLRERLAAALTLLPESRIQVWFQNRRAKSRRQSG
PROP1   RRRHRTTFSPVQLEQLESAFGRNQYPDIWARES LARDTGLSEARIQVWFQNRRAKQRKQER
          ** ** *: *: ** * ** : ** :* ** * :.:**:*:*:*:
    
```

Figure 3-7: Conservation of missense variants across human paralogues

3.4 Discussion

This series of 18 patients with retinal dystrophy consequent on *CRX* mutations represents the largest series studied and identified a new associated macular dystrophy phenotype. A group of patients with an autosomal dominant macular dystrophy presenting in their 3rd to 5th decades is described. There was documented progression of the macular disease. Two cases were asymptomatic at presentation.

At the severe end of the *CRX* disease spectrum are the LCA cases presenting in infancy with severe loss of vision. RCD presented within the first decade of life, CORD

Retinal dystrophy due to mutations in the cone-rod homeobox gene in the 2nd-3rd decades and macular dystrophy in adulthood, with a range of 35 to 53 years. The macular dystrophy was characterized by a 'bull's-eye' appearance similar to that observed in other macular dystrophies including the autosomal dominant form associated with *PROM1*.²⁰⁵ Variable expressivity is also a feature of *PROM1* with some patients manifesting generalized retinal dysfunction.

Macular atrophy was present in 14 of 18 cases. Also commonly found was a disrupted ISe band on OCT, identified in all investigated patients. Electrophysiology further characterised the phenotypes demonstrating a normal ERG in all macular dystrophy cases confirming that the dysfunction was confined to the macula. Two cases with macula dystrophy have normal ERG age 60 and 67 years indicating no evidence for peripheral retinal dysfunction developing with time. In families 17489 and 18280 who co-segregate macular dystrophy with generalised retinal dysfunction, it is noted that the older affected family members have the mildest phenotype.

There are 4 exons in *CRX*, the first non-coding, producing a 299 amino acid protein. The protein has strong homology to OTX1 and OTX2 in 3 regions; the homeodomain at residues 39-99 which binds to DNA, the 13 residue WSP motif at residues 158-170, which is of unknown function, and the OTX tail at residues 284-295, a specific carboxyl terminus motif, of unknown function.¹⁷¹ Broadly, the mutations that arise in the homeodomain are missense mutations; those in the remainder of the last exon, exon 4 are PTCs with no mutation reported within the OTX tail (figure 3-5). In all cases, it is predicted that abnormal protein is produced, as avoidance of nonsense mediated decay (NMD) would be predicted for the premature terminations according to the classical rules for this phenomenon.²⁰⁶ The significance of the two distinct classes of mutation in the different protein regions is not clear. As noted, no clear genotype-phenotype association could be deduced from the complete data set or from the cases newly reported here.

All but 1 reported homeodomain mutation arise within the alpha helices that are important in binding to the major groove of DNA via several hydrogen bonds, the exception being a homozygous mutation, c.193G>C (p.Asp65His).^{181, 184} One homeodomain mutation associated with LCA, c.264G>T (p.Lys74Asn) has been demonstrated to disrupt DNA binding in a molecular model as well as interfere with the normal function of co-expressed transcription factors such as NRL in vitro, by a postulated dominant-negative effect¹⁸⁴. The homeodomain mutations arise in residues fully conserved in *CRX* between species but not fully conserved in human paralogues of the *CRX* protein. Interestingly, all LCA associated mutations were located in non-conserved residues in these paralogues suggesting importance of these residues in *CRX* specific function.

There have been 3 reports of bi-allelic *CRX* disease. Two siblings with LCA have been reported with compound heterozygous mutations, the first a missense mutation that removes the normal translation termination codon, the second a deletion of exon 4.¹⁶ The carrier parents were asymptomatic but not examined. Two homozygous, missense mutations have been reported, both in the homeodomain; c.193G>C (p.Asp65His) in a sporadic patient with severe RCD and asymptomatic parents unavailable for examination and c.268C>T (p.Arg90Trp) in a patient with LCA, his heterozygous carrier parents having subtle cone abnormalities on ERG.^{181 185} *In vitro* studies of DNA binding compared the p.Arg90Trp mutation to p.Arg41Trp which had been identified in *CRX* related CORD.¹⁸⁵ DNA binding was more severely affected by p.Arg41Trp. This was thought to be consistent with the more severe symptoms found in heterozygous p.Arg41Trp related CORD compared to the heterozygous p.Arg90Trp asymptomatic carrier parents. However, in the series of patients reported in this thesis, affected members of family 17489 were heterozygous for p.Arg41Trp manifesting with severe RCD in the son and asymptomatic macular dystrophy in the mother which would not fit with this theory. The reason for the variable severity of mutations is still to be elucidated.

Heterozygous knockout mice (+/-) have no retinal phenotype at 6 months of age whereas homozygous knockout mice (-/-) have severe loss of rod and cone function, but neither types model the dominant human disease.²⁰⁷ A spontaneous mouse mutant, *Crx*^{Rip/+} was then identified in which a dominant PTC on one allele produced a truncated protein and a phenotype similar to congenital, blinding, dominant *CRX* retinal dystrophy in humans.²⁰⁸ There is a lack of normal photoreceptor differentiation in the *Crx*^{Rip/+} mouse, with arrested development at an early stage and inactive and immature photoreceptors identified histologically. There were 2 main mechanisms by which this mutant caused disease: firstly by a lack of normal DNA binding by the *CRX* mutant compared to wild type leading to loss of normal transactivation of photoreceptor genes and secondly by a dominant negative effect of this mutant allele whereby mutant *CRX* blocks the binding of wild type *CRX* to target genes and of *OTX2* to the *Nrl* promoter preventing transactivation of *Nrl* and in turn the transactivation of essential rod and cone gene expression. Ectopic *Nrl* expression in the *Crx*^{Rip/+} mouse partially rescued the poorly differentiated rod photoreceptor precursors. Reported knock-in mouse models have severely reduced retinal function and demonstrated the association of *CRX* expression level on disease severity as well as the ability of the mutant allele to interfere with wild type function.²⁰⁹ One model with a truncating mutation had more severe disease than another, with a missense mutation mirroring the reported human phenotypes for those specific mutations. These mouse models may provide excellent opportunities for further functional analysis of *CRX* related disease and the

investigation of potential treatments. The evidence to date, including this study and the mouse models, suggests that haploinsufficiency of *CRX* is not, in itself, disease-causing. Instead, an allele has to be both non-functional and expressed (hence the lack of PTCs early in the gene), such that the abnormal protein partly abrogates the normal one expressed from the other allele.

Seven novel mutations were identified; 1 missense in exon 3 with 6 PTCs in exon 4. Four families demonstrated the large degree of clinical variability that can occur between those sharing the same *CRX* mutant allele. This heterogeneity may be due to i) the influence of polymorphisms in the *CRX* promoter region; ii) polymorphisms in co-expressed transcription factors such as *Nrl*; iii) the impact of environmental factors; iv) stochastic factors, that is small perturbations of *CRX* function causing larger and later effects on the degree of degeneration; v) variable levels of expression of the mutant allele which in a mouse model has been correlated with variable severity or vi) variable levels in expression of the wild-type allele which in *PRPF31* related disease has been correlated with variable penetrance.^{114, 209} Study of the promoter region and of RNA transcripts may help to elucidate this further.

A further novel mutation, c.127C>T, in a patient with macular dystrophy did not segregate with known eye disease in the family, with the asymptomatic mother and brother heterozygous for the variant. Given the examples in this series of asymptomatic presentation, it cannot be concluded that these other family members are not affected. Unfortunately, examination and retinal imaging was not possible in the family members to clarify this issue. The patient presented at age 22, younger than the other macular dystrophy patients in this series, and also has a more severe reduction in visual acuity than the other macular dystrophy patients.

Only 3 of the 11 reported families had a family history of possible retinal dystrophy in antecedent generations prior to this study. Parental sequencing in 3 of the 8 other families confirmed *de novo* mutations. DNA was unavailable from antecedents in the remaining 5 families, although the observed pedigrees make it possible that these mutations may also have arisen *de novo*. Alternatively, given the relatively mild presentation of the macular dystrophy phenotype, disease in antecedents might have been unreported. These 8 families highlight the difficulties in genetic counselling in patients with apparent simplex retinal disease. The possibility of *de novo* mutation, or mild unreported disease in antecedents, suggests a greater risk in subsequent generations than if autosomal recessive inheritance was assumed. It would also affect the risk to other siblings. Clinicians should therefore have a low threshold for screening *CRX* in patients presenting with any of the phenotypes consistent with those presented here.

4 Enhanced S-cone syndrome in children

4.1 Introduction

Enhanced S-cone syndrome (ESCS, MIM #268100) is a rare, autosomal recessive retinal dystrophy first described in 1990.²¹⁰ It is one of the few disorders in which the electrophysiological findings are pathognomonic.^{135, 210} Patients present with symptoms of nyctalopia from the first decade with or without reduced vision; the visual loss may be associated with foveal schisis.^{211, 212} The disorder is probably slowly progressive and deterioration of the ERG has been demonstrated.^{212, 213} Adults with the disorder characteristically show nummular pigmentary deposition at the level of the RPE outside of the vascular arcades with or without foveal schisis-like cystic changes.²¹² There are few reports of the presentation of ESCS in children: case reports of early findings describe a normal fundus or early changes of white dots at the level of the RPE.²¹⁴⁻²¹⁶ This prompted further investigation of a series of children with a diagnosis of ESCS from Moorfields.

Defects in a nuclear receptor gene, *NR2E3*, were linked to ESCS in 2000. Mutations in *NR2E3* leading to loss of function of the transcription factor are theorised to be pathogenic by the abnormal differentiation of post-mitotic photoreceptor precursor cells, so altering their cell fate from rod to S-cone.^{217, 218} To date, at least 49 mutations have been reported with resultant phenotypes of ESCS, Goldmann-Favre syndrome and both autosomal dominant and autosomal recessive RCD.^{212, 218-239} An atypical form or ESCS due to bi-allelic *NR2E3* variants has been reported in 3 patients with residual rod function.^{229, 233, 240}

4.2 Methods

4.2.1 Patient ascertainment

Nine patients (2 simplex cases, 2 sibling pairs and 1 sibling pair and half cousin) were ascertained from the inherited retinal disease clinics based on a clinical and molecular diagnosis of ESCS.

4.2.2 Clinical assessment

Each confirmed patient underwent a full clinical examination including visual acuity and dilated ophthalmoscopic examination. I examined all patients. One patient declined further investigations apart from molecular testing but their sibling had undergone full investigation. All other patients had electrophysiological testing and dilated fundus

imaging. Additional S-cone ERGs were recorded, when possible, to a 5ms blue stimulus (445 nm, 80 cd.m⁻²) on a bright orange background (620nm, 560 cd.m⁻²); ON-OFF ERGs were recorded to an orange stimulus (duration 200ms) on a green background (530nm, 150 cd.m⁻²).^{241, 242}

4.2.3 Molecular investigations

Patients identified as clinically typical for ESCS had already been screened by colleagues within the lab for disease causing mutations. Family 2 declined further molecular testing on the affected children, the father having already been identified as having a homozygous variant causing his Goldmann-Favre syndrome and the related mother being heterozygous for the same variant. This consanguineous family, who demonstrate pseudo-dominant inheritance, has been previously reported.^{211, 212, 243} I confirmed those parental mutations and performed segregation within all other families by direct sequencing of the relevant exons and intron/exon boundaries of *NR2E3* (table 4-1). Mutation nomenclature was assigned in accordance with GenBank Accession number NM_014249.3 with nucleotide position 1 corresponding to the A of the ATG initiation codon. The gene was not covered on the ExAC database.

Ex-on	Primer forward 5' → 3'	Primer reverse 5' → 3'	Enzyme	Annealing temp (°C)	Amplicon size (bp)
1	TGGTAATGCTGCAGGTGTGGC	TCCTTCCATGGTCCCTGCGAACC	BIOTAQ	60	482
2-3	GCGTGGGTTTCGTTCAAATGCGG	CTCTCCCACTCACCATCCTCT	BIOTAQ	60	837
4-5	TGACAAGAAATGGGCAGCGGGAC	ATACTGGCGTGGGGATGTGTGTG	BIOTAQ	60	712
6-7	TCCTTGGGTGCCTGAGATGGTG	TGGGAGAGTGTGGGAGAGGCAGA	BIOTAQ	60	894
8	AATTCCTCCTGACCCACTCTGG	CTTTCGGTGGGCATTTCTGCTG	BIOTAQ	60	393

Table 4-1: Primer pairs for sequencing of *NR2E3*

4.3 Results

Clinical findings are summarized in table 4-2. Nine children (5 female, 4 male) from 5 families were assessed. Mean age at last review was 10.8 years (median 11 years, range 7-15 years). Diagnostic ERG was performed in 8 patients at a mean age of 8.6 years (median 8 years, range 3-14 years). Geographic/ethnic origin was white British in 4 families and the Kashmir region of Pakistan in 1 family.

Patient (gender) family	Age last rv	Fundus	FAF	OCT	Latest VA, log MAR	Refraction
1.1 (f) GC 19824	9	White dots and nummular pigmentation along arcades	Diffuse paracentral hyperfluorescence, multiple small high density foci along arcades, hypofluorescence outside of the arcades	Normal	R 0.80 L 0.90	R +8.00/-3.50 x 5 L +8.50/-3.50 x 160
1.2(f)	9	White dots and nummular pigmentation along arcades	Diffuse paracentral hyperfluorescence, multiple small high density foci along arcades, hypofluorescence outside of the arcades	Foveal sparing cysts BE	R 0.50 L 0.36	R +10.50/-1.00 x 70 L +10.00/-1.00 x 80
1.3(m)	12	Few white dots and RPE mottling along arcades	Diffuse paracentral hyperfluorescence with multiple small high density foci along arcades	Normal	R 0.14 L 0.74 (L amblyopia)	R +3.00/-0.50 x 10 L +4.50 DS
2.1(f) GC 15494	15	Subtle RPE mottling along arcades	Small foci of high density along arcades	Foveal sparing cysts BE	R 0.1 L 0.1	R +2.50/-1.25 x 180 L +2.25/-1.25 x 180
2.2(m)	11	Normal	Small foci of high density along arcades	Normal	R 0.00 L 0.08	R +1.00/-1.00 x 15 L +2.50/-2.25 x 170
3.1(m) GC 19784	7	Few white dots along superior arcades	-	-	R 0.05 L 0.10	R +2.25/-1.00 x 180 L +3.00/-1.00 x 180
3.2(m)	9	RPE mottling along arcades	Diffuse paracentral hyperfluorescence with multiple small high density foci along arcades	Normal	R 0.14 L 0.00	R +3.50 DS L +2.50 DS
4(f) GC 19940	14	White dots and nummular pigmentation along arcades	Diffuse paracentral hyperfluorescence, multiple small high density foci along arcades, hypofluorescence outside of the arcades	Foveal involving cysts BE	R 0.86 L 1.20	R +3.50/-0.50 x 21 L +3.50/-1.00 x 145
5(f) GC 16715	11	Normal	Small foci of high density along arcades	Normal	R 0.10 L 0.125	R +3.50/-1.50 x 20 L +4.00/-1.50 x 165

Table 4-2: Key clinical features

Longitudinal data were available in 8 patients (mean follow up 3 years; range 1-10 years). All patients reported nyctalopia although patient 3.1 only reported this from the age of 7. No patient had nystagmus. Visual acuity ranged from 0.0 to 1.2 logMAR. Reduced vision in both eyes (≥ 0.3 logMAR) with deterioration over time was recorded in patients 1.1, 1.2 and 4, the rest retaining good visual acuity with appropriate refractive correction. Only patient 4 had evidence of intra-retinal cysts involving the fovea. This patient was intolerant of both topical and oral carbonic anhydrase inhibitors. All patients had a hyperopic refractive error with mean spherical equivalent at presentation of +4.40 D (range +1.40 D to +11.75 D) and at last review a mean of +4.00 D (range +0.50 D to +10.00 D).

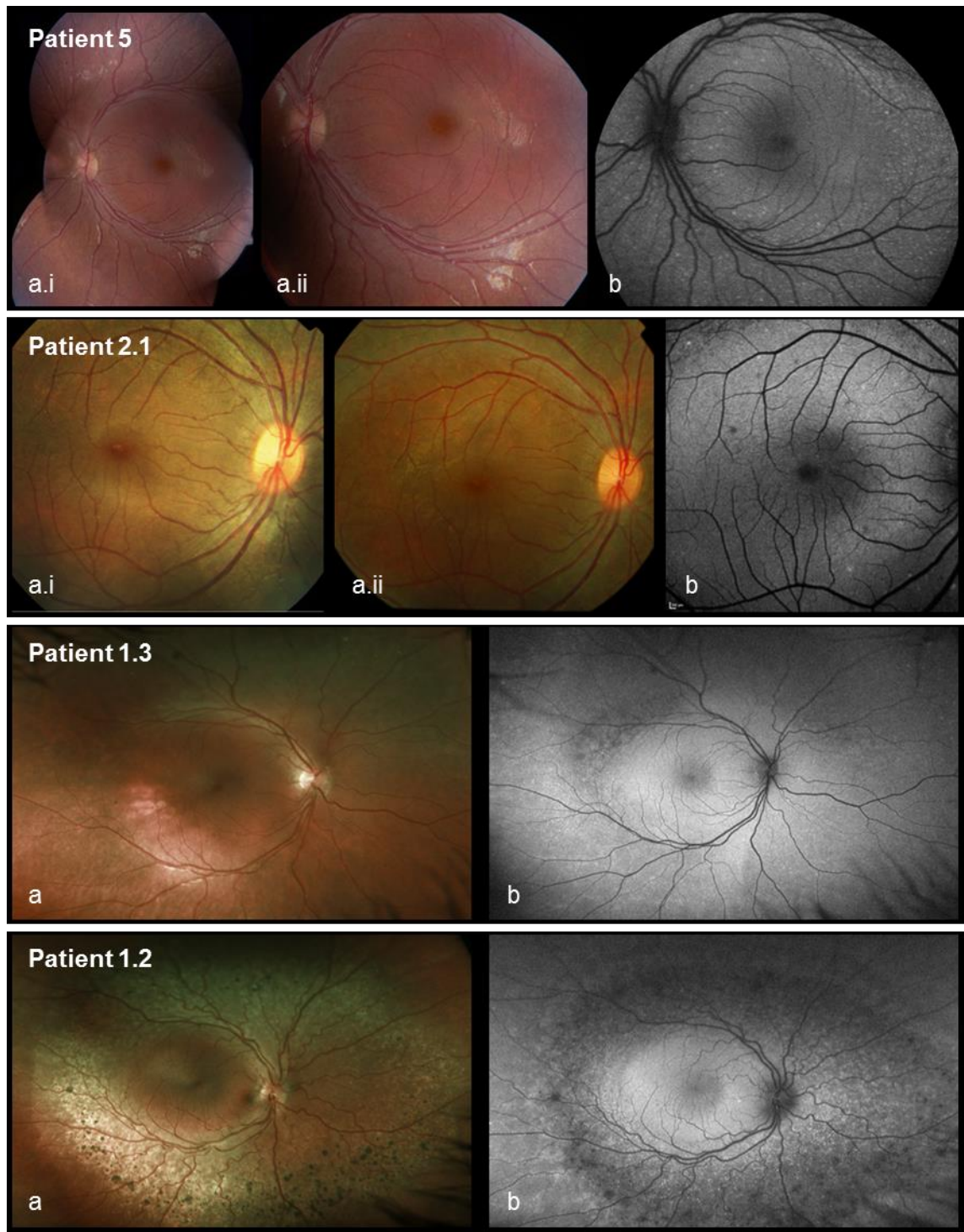


Figure 4-1: Fundal abnormalities in paediatric enhanced S-cone syndrome

Patient 5, (a.i) and (a.ii) left normal fundal photographs, (b) abnormal fundus autofluorescence (FAF) imaging with high density foci; Patient 2.1, (a.i) right normal fundal photograph 2006 (a.ii) right fundal photograph 2011 with RPE mottling present (b) right FAF imaging with high density foci; Patient 1.3, (a) right Optos fundus photograph with RPE mottling and a few white dots, (b) FAF imaging showing diffuse paracentral hyperfluorescence and small high density foci along arcades; Patient 1.2, (a) right Optos fundus photograph demonstrating white dots and extensive nummular pigmentation, (b) FAF imaging demonstrating diffuse paracentral hyperfluorescence, small high density foci and a hypofluorescent ring outside of the arcades.

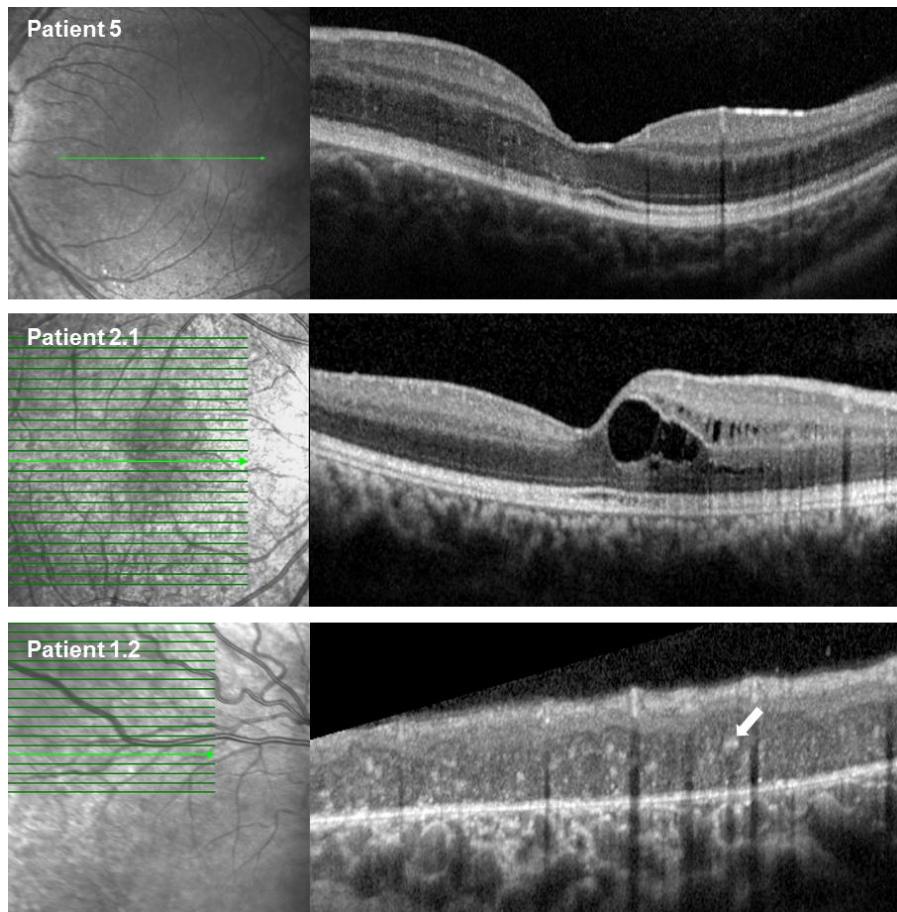


Figure 4-2: Optical coherence tomography scans

Patient 5, left normal macular OCT; Patient 2.1, right abnormal macular OCT with intra-retinal cysts; Patient 1.2, right abnormal superior arcade OCT demonstrating disorganized architecture and multiple hyper-reflective lesions in the outer nuclear layer (white arrow).

Two patients had a normal biomicroscopic appearance to their fundi although their FAF imaging demonstrated foci of high density around the arcades (figure 4-1). Two had RPE mottling only and 2 had RPE mottling with white dots. The typical adult ESCS feature of nummular pigmentary deposits along the arcades was present in 3 patients. There was phenotypic variability within family 1 which was independent of age; a female patient and her female half cousin (patients 1.1, 1.2) had extensive nummular pigmentation not present in her older male half cousin (patient 1.3, figure 4-1).

Progression of ophthalmoscopic changes was recorded in 4 patients. Patient 2.1 who presented at age 6 years with a normal fundus appearance showed subtle RPE mottling along the arcades at age 11 years (figure 4-1). Patient 3.1 had subtle RPE mottling at presentation aged 4 years, and subsequently developed white dots along the arcades from age 6. Patients 1.1 and 1.2 had nummular pigmentary lesions along the arcades which increased during follow up periods of 2 and 3 years respectively.

FAF imaging was abnormal in 8 of 8 patients. Three patients had multiple fine foci of increased autofluorescence associated with the arcades. Two of these patients had a

normal fundus appearance; the third had subtle RPE mottling only. Diffuse paracentral hyperfluorescence within the arcades in conjunction with multiple fine high density foci alongside the arcades, was present in 5 patients. In 3 of these patients with more severe disease, reduced autofluorescence was noted outside of the arcades in the mid peripheral retina.

Eight patients underwent OCT; 5 had normal OCTs, 2 had evidence of macular intra-retinal cysts without foveal involvement and 1 had fovea-involving cysts (figure 4-2). Extended OCT scanning, to include the superior arcades, was performed in 2 patients. There was loss of normal retinal architecture and small hyper-reflective lesions throughout the outer nuclear layer.

ERGs demonstrated the characteristic features of ESCS (figure 4-3).

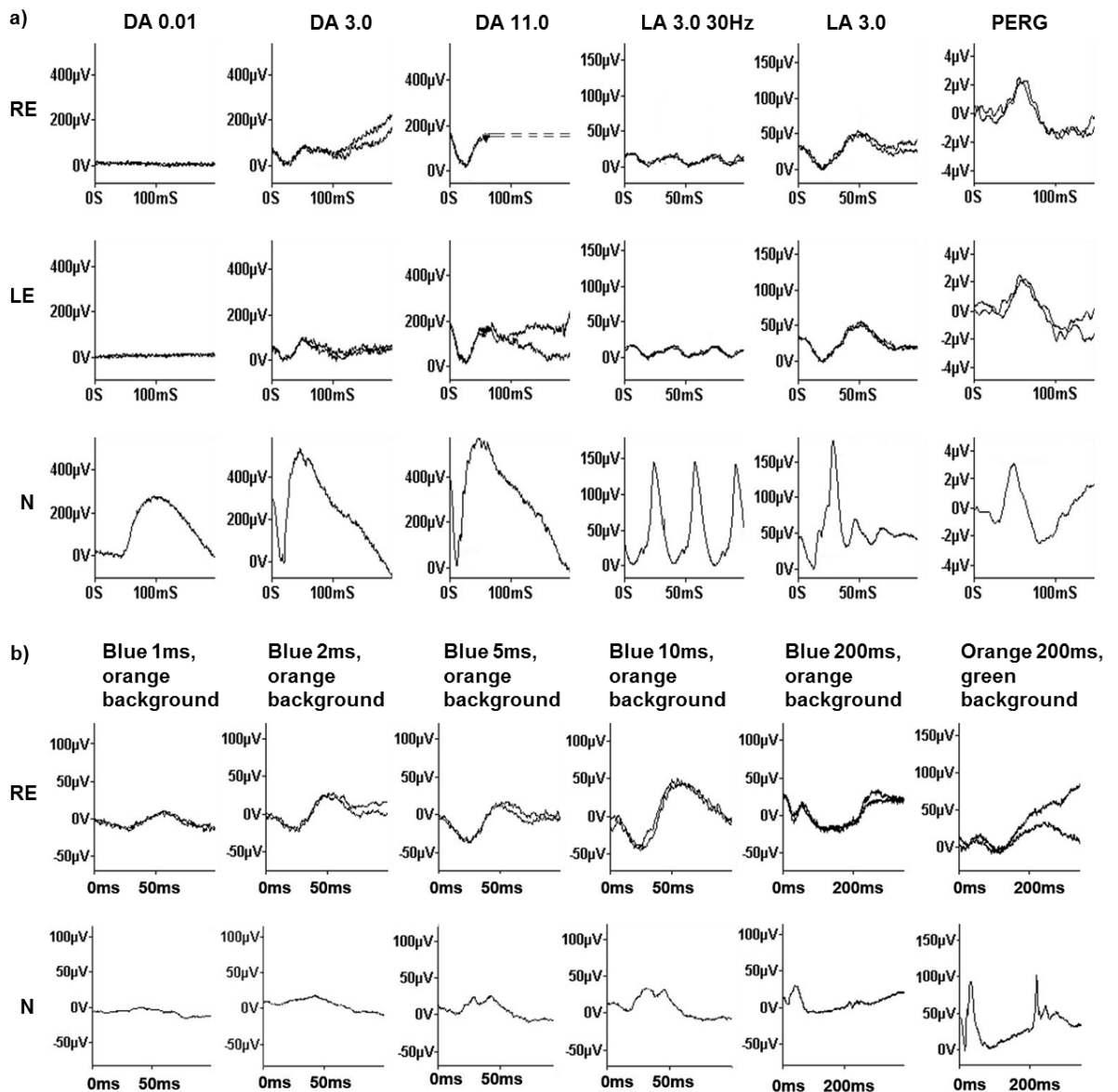


Figure 4-3: Electrophysiology in enhanced S-cone syndrome

a) Full-field and pattern ERGs in patient 2.1. b) Extended S-cone ERGs from the right eye of patient 2.1. N, normal.

The rod-specific DA 0.01 response was undetectable; brighter flash dark adapted ERGs (DA 3.0 and DA 11.0) were of simplified, delayed waveform (figure 4-3). The responses to the same stimuli under scotopic (DA 3.0) and photopic adaptation (LA 3.0) were of similar waveform; the 30Hz flicker ERG was profoundly delayed and additionally was of lower amplitude than the single flash LA 3.0 ERG a-wave. S-cone specific testing was possible in 5 children, and showed high amplitude, delayed and simplified responses in keeping with origins in short wavelength sensitive cones, and of similar waveform to those obtained to white light stimulation. Extended S-cone ERGs from patient 2.1 is shown in figure 4-3b. The 200ms blue stimulus response shows some OFF- activity, as occurs in some but not all ESCS patients.²¹² The photopic ON-OFF- response in the patient (200ms orange flash) is markedly reduced, of simplified waveform, and shows delay in all components.

The PERG P50 component, used to assess macular function, was within normal amplitude limits in 2 patients, subnormal without delay in 2, delayed without amplitude reduction in 1, and delayed and subnormal in 1 patient. PERG data from one patient was excluded due to high levels of physiological noise. One patient did not have electrodiagnostic testing due to parental preference but his brother has typical electrophysiology and both have genetically confirmed disease.

Molecular genetic analysis

Mutations identified and segregation are shown in table 4-3 and figure 4-4.

Mutation	Family	SIFT	Polyphen2	First reported
119-2A>C, aberrant splicing	1 and 3	N/A	N/A	Haider 2000 ²¹⁸
c.1194delT (p.Pro399Glnfs*44)	1	N/A	N/A	This series
c.310C>T (p.Arg104Trp)	2	0.00	1.00	Haider 2000 ²¹⁸
c.1025T>C (p.Val342Ala)	3	0.00	0.996	This series
c.305C>A (p.Ala102Asp)	4	0.00	0.999	This series
c.767C>A (p.Ala256Glu)	4 and 5	0.02	0.998	Sharon 2003 ²⁴⁴
c.994G>A (p.Glu332Lys)	5	0.04	0.912	This series

Table 4-3: Identified mutations in *NR2E3*

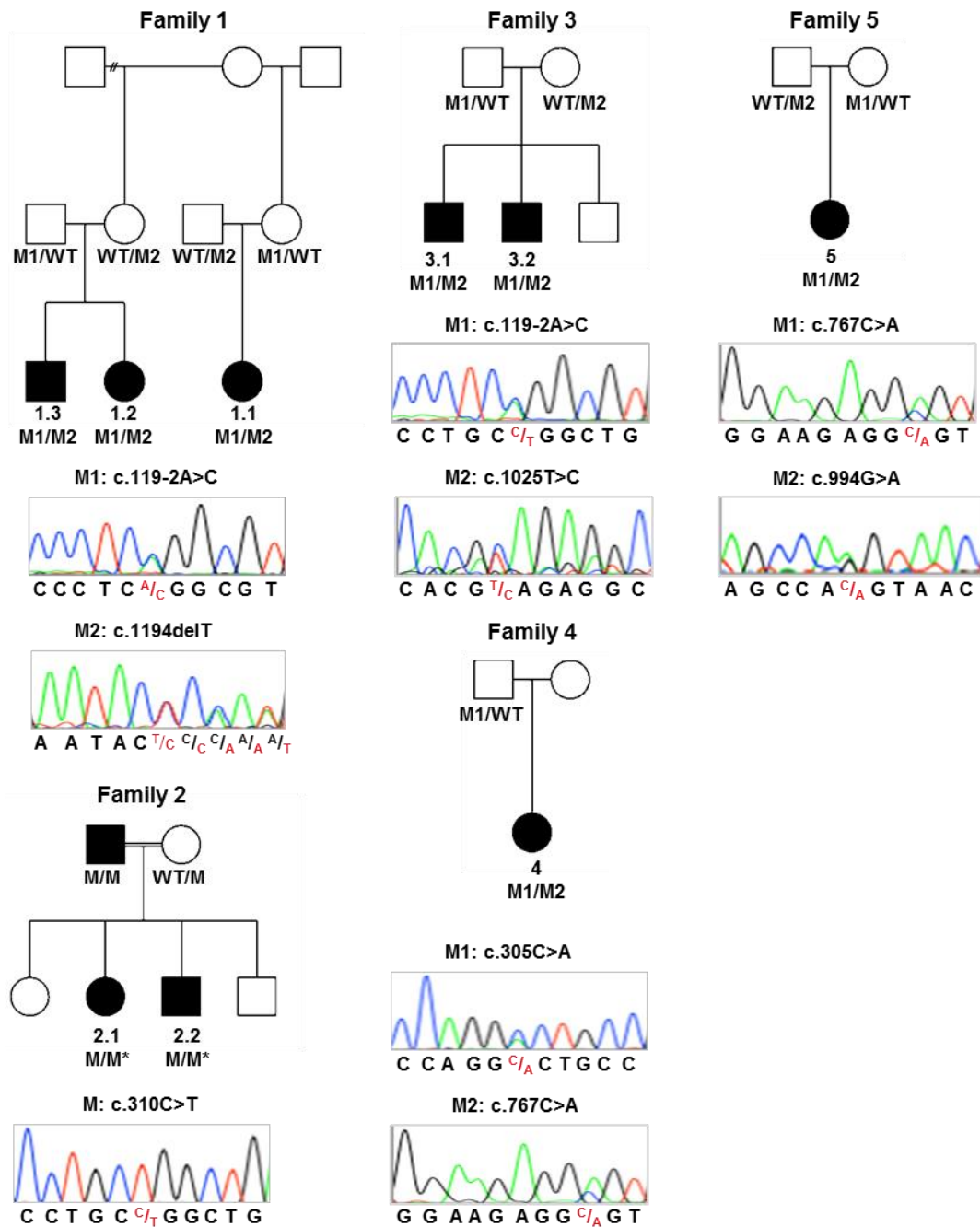


Figure 4-4: Pedigrees and mutation distribution for the 5 affected families

* presumed genotype, DNA unavailable for testing

Family 1, a brother and sister pair and their cousin have the same compound heterozygous change; c.119-2A>C (paternal), predicted to cause aberrant splicing and the most common mutation reported in ESCS, and a novel PTC, c.1194delT (p.Pro399Glnfs*44, maternal). Additional novel mutations identified were all missense, c.1025T>C (p.Val342Ala), c.305C>A (p.Ala102Asp) and c.994G>A (p.Glu332Lys). All novel missense mutations are predicted to be pathogenic *in silico* (table 4-3). They all arise in amino acids highly conserved throughout evolution as confirmed by Clustal Omega (figure 4-5).

	Ala102Asp Arg104Trp
cod	ADSSSGKHGYIHACNGCSGFFKRSIRRRLLIYRCQTGTGTCCVVDKAHRNQCAACRLQRCLQ
rat	GDSSSGKHGYIYACNGCSGFFKRSVRRRLIYRCQVAGMCPVDKAHRNQCAACRLKKCLQ
mouse	GDSSSGKHGYIYACNGCSGFFKRSVRRRLIYRCQVAGMCPVDKAHRNQCAACRLKKCLQ
microbat	GDSSSGKHGYIYACNGCSGFFKRSVRRRLIYRCQVAGMCPVDKAHRNQCAACRLKKCLQ
cow	GDSSSGKHGYIYACNGCSGFFKRSVRRRLIYRCQVAGMCPVDKAHRNQCAACRLKKCLQ
human	GDSSSGKHGYIYACNGCSGFFKRSVRRRLIYRCQVAGMCPVDKAHRNQCAACRLKKCLQ
monkey	GDSSSGKHGYIYACNGCSGFFKRSVRRRLIYRCQVAGMCPVDKAHRNQCAACRLKKCLQ
platyfish	GDTSSGKHGYIYACNGCSGFFKRSVRRRLIYRCQAGTGMCVVDKAHRNQCAACRLKKCLQ
lizard	GDTSSGKHGYIYACNGCSGFFKRSVRRRLIYRCQAGTGMCVVDKAHRNQCAACRLKKCLQ
flycatcher	GDTSSGKHGYIYACNGCSGFFKRSVRRRLIYRCQAGTGLCPVDKAHRNQCAACRLKKCLQ
	.*:*****:*****:.*:.*:****:.*: * *****:****
	Ala256Glu
cod	PKREQSQAPC-SLSPVRPELDHVSARLLFMVAVRWAKNMPVFSHLPFRDQVILLEEAWSE
rat	PEFPA-----SPCNLDGIHETSARLLFMVAVKWAKNLPVFSNLPFRDQVILLEEAWNE
mouse	PEFPA-----SPCSDGIHETSARLLFMVAVKWAKNLPVFSNLPFRDQVILLEEAWNE
microbat	PEFPSSPHSS--SPCGVDSIHETSARLLFMVAVKWAKSLPVFSNLPFRDQVILLEEAWSE
cow	PEFPSSPYSS--SPCALDSIHETSARLLFMVAVKWAKNLPVFSNLPFRDQVILLEEAWSE
human	PEFPSSPYSS--SPCGLDSIHETSARLLFMVAVKWAKNLPVFSNLPFRDQVILLEEAWSE
monkey	PEFPSSPYSS--SPCGLDSIHETSARLLFMVAVKWAKNLPVFSNLPFRDQVILLEEAWSE
platyfish	PERASSEYHMALYPSS-SENVYETSARLLFMSVKWAKNLPVFSNLPFRDQVILLEEAWSE
lizard	PERPGGEAHVSPYPTASPEVYETSARLLFMVAVKWAKNLPVFSNLPFRDQVILLEEAWSE
flycatcher	PERAAGEYQVAPYPAAGPENIYETSARLLFMVAVKWAKNLPVFSNLPFRDQVILLEEAWSE
	*: : ..**:*:*:*:*:*:*:**** *****:*
	Glu332Lys Val342Ala
cod	FACLKAIIVLFKPEARGLKDPDQVENLQDQSQVLLGQHIHSLHPSQSARFGRLLLLLPSFLH
rat	FACLKALVLFKPETRGLKDPDHVEALQDQSQVMLKQPPR-LPPSQPVR-----
mouse	FACLKALVLFKPETRGLKDPDHVEALQDQSQVMLSQHSAKHHPSQPVRFGKLLLLLPSLR
microbat	FACMKALVLFKPETRGLKDPDHVEALQDQSQVMLSQHSAKHHPSQPVRFGKLLLLLPSLR
cow	FACMKALVLFKPETRGLKDPDHVEALQDQSQVMLSQHSAKHHPSQPVRFGKLLLLLPSLR
human	FACMKALVLFKPETRGLKDPDHVEALQDQSQVMLSQHSAKHHPSQPVRFGKLLLLLPSLR
monkey	FACMKALVLFKPETRGLKDPDHVEALQDQSQVMLSQHSAKHHPSQPVRFGKLLLLLPSLR
platyfish	FACLKAIIVLFKPETRGLKDPDQVENLQDQSQVMLGQHIRSHYPTQPARFGKLLLLLPSLR
lizard	FACMKAIIVLFKPETRGLKDPDQVENLQDQSQVMLGQHNRSHYPTQPARFGKLLLLLPSLR
flycatcher	FACMKAVVLFKPETRGLKDPDQVENLQDQSQVMLGQHNRSHYPTQPARFGKLLLLLPSLR
	:**:**:*****:.* *****:.* * : * * *

Figure 4-5: Conservation of missense mutations

4.4 Discussion

In this study, the characteristic retinal features of ESCS in children was investigated and compared with adults with the disorder. Appropriate investigations, in particular ERG and FAF imaging, were found to be clinically most helpful in diagnosis. Variability of presentation and visual disability both across and within families was identified.

Most children initially lack the deep nummular pigmentation typically seen in adults, and fundus examination may be normal at presentation in keeping with previous reports of the paediatric phenotype in ESCS.^{215, 216} Patient 2.1 in this series, previously reported to have a normal fundus appearance, now has subtle RPE mottling.^{211, 212} Isolated, subtle RPE changes along the arcades are a finding not previously noted in ESCS but apparent in this series. Sub-retinal white dots without nummular pigmentation in children have been previously reported in a series of 3 patients.²¹⁴ Whilst the white dots are characteristic of ESCS, they are not diagnostic and have also been reported in *NR2E3* related autosomal recessive RCD with clumped pigmentation.²⁴⁴ Previously reported complications in ESCS of choroidal neovascular membrane or sub-retinal fibrosis were not evident in any of the present series.^{210, 215, 245}

This series of children suggests a sequence of fundal change from normal appearance, followed by RPE mottling along the arcades, and then the development of white dots

followed by deep nummular pigmentary deposition. FAF imaging is particularly useful in highlighting subtle abnormalities along the arcades in children with a normal fundus appearance. High density foci along the arcades on FAF imaging with a normal fundal appearance has previously been reported in an 8 year old child.^{211, 215} A practical application is in determining whether other (younger) family members are affected. The high density foci on FAF imaging do not always correspond to white dots seen ophthalmoscopically.²¹⁵ Four patients in the present series demonstrated high density foci on FAF without white dots. These foci have been shown in a murine model to originate from accumulations of microglial cells between the outer nuclear layer and the RPE.²⁴⁶ Microglial cells are known to play a central role in chronic degenerative conditions of the central nervous system. In adults, FAF imaging may demonstrate a ring of relatively increased hyperfluorescence within the arcades as seen in 5 cases in this series, a spoke-like hyperfluorescence in the macula in the presence of foveal schisis and/or a reduction in autofluorescence anterior to the arcades in the mid periphery of the retina.²¹² This latter sign was found in 3 cases in this series all of whom have more severe disease and is thought to represent loss of photoreceptor cells. It corresponds well to reported histology in advanced ESCS which demonstrated relative preservation of photoreceptors in the macula and the far periphery of the retina with loss of photoreceptors in the mid periphery.²¹³ Monitoring of disease progression with FAF imaging in particular the loss of autofluorescence in the mid periphery can therefore be used as a marker of photoreceptor loss.

Intra-retinal cysts in the macula similar to adult disease, can occur in children and can lead to loss of vision.^{211, 212} The majority of patients in the present series maintained good visual acuity in keeping with other reported ESCS cases, but in 3 patients vision deteriorated.^{210, 247} One case had intra-retinal cysts involving the fovea that could explain the reduction in acuity and one had para-foveal cysts. However, these 3 cases also had more advanced ophthalmoscopic changes with nummular pigmentation.

Two patients underwent extended OCT outside of the macula. There were intra-retinal, hyper-reflective lesions in the outer nuclear layer, with a disorganized retinal architecture and loss of normal lamination. This has been previously described in a child with ESCS in the mid-periphery, and may be a useful adjunct in diagnosis and monitoring.^{215, 248} The OCT findings are consistent with the previously described histological data which found a loss of normal retinal lamination and disorganisation of the retina.²¹³ The disorganised retinal lamination has been suggested not to be developmental but acquired either from ongoing proliferation in the *NR2E3* deficient retina or as a secondary proliferative response to cell death.²⁴⁸ Extended OCT studies also identified thickening of the retina in particular the outer nuclear layer in a ring

around the arcades, with thinning evident in end-stage disease.²⁴⁸ In *CRB1* related retinal dystrophy there is thickening and disorganisation evident throughout the retina including the macula, a finding thought most likely to be developmental.²⁴⁹ Although this has been observed at an early age it has not yet been proven to be developmental.

Electrophysiology remains the most useful investigation in ESCS due to the pathognomonic ERG abnormalities. Additional non-standard ERG testing provides further evidence of the disorder with S-cone specific ERGs several times the magnitude of normal, also showing a waveform similar to that of the conventional Ganzfeld ERG.¹³⁵ Pattern ERGs were abnormal in 4 of 6 cases but were generally better preserved than in affected adults; a previous study revealed abnormal pattern ERGs in 16 of 16 adults including 5 with undetectable responses.²¹² Pathognomonic ERGs facilitate targeted molecular diagnosis.

NR2E3 encodes a 410 amino acid, 8 exon, ligand dependent transcription factor important in the determination of photoreceptor cell fate. NR2E3, in cell studies and the *RD7* murine model, acts in tandem with CRX to promote rod photoreceptor differentiation and suppress the formation of cone cells.^{174, 250} Histopathological and immunocytochemical analysis of a post mortem eye of one elderly patient with ESCS showed a degenerate retina with no rods and approximately twice the number of cones, 92% of which were short-wavelength cones.²¹³ The NR2E3 protein constitutes a DNA binding domain (DBD, amino acid residues 45-131) and a ligand binding domain (LBD, amino acid residues 222-410).²⁵¹ The DBD is a highly conserved region comprising 2 'zinc finger' -like structures that specifically bind to consensus sites in the promoter regions of target genes.²⁵¹ Interaction of the DBD with the homeodomain of CRX enables NR2E3 transactivation of target genes.^{174, 251} Mutations in the DBD have been shown to abolish DNA binding.²⁵² Some but not all mutations in the LBD have been shown to disrupt homo- and heterodimerisation.²⁴⁰ Reported mutations in *NR2E3* are evenly split between the DBD and the LBD without any obvious clustering. Four novel mutations are reported in this study, three of which are missense mutations predicted to be damaging *in silico*; p.Ala102Asp arising within the DBD and p.Glu332Lys and p.Val342Ala located within the LBD. The novel deletion, c.1194delT; p.Pro399Glnfs*44, also located in the LBD, is a PTC that creates an alternative reading frame predicted to result in a new 43 amino acid chain followed by a stop codon.

All but 1 family in this series were found to be compound heterozygous for mutations in *NR2E3*, limiting the possible phenotype-genotype correlations that could be made based on a specific type or location of mutation. At present the prognosis related to a specific genotype is unknown and the molecular diagnosis does not alter the patient's management.

5 Non-syndromic retinal dystrophy due to bi-allelic mutations in *IFT140*

5.1 Introduction

The outer segments of photoreceptors are highly modified, photosensitive cilia, which lack any capability for protein production.²² Thus, they are reliant on the intraflagellar transport (IFT) system, which comprises large protein complexes for transport from the cell body to cilium tip and back driven by the motors kinesin-2 and dynein-2 respectively.²³ The IFT-B complex is essential for cilium assembly and anterograde transport whereas the IFT-A complex is responsible for retrograde transport, with additional roles in anterograde transport by connecting kinesin to the IFT complex, and in facilitating entry of proteins in to the cilium.^{253, 254} *IFT140*, a subunit of IFT-A, is vital for both the development and the maintenance of outer segments, and has a specific role in opsin transport across the connecting cilium.²³

Mutations in *IFT140* have been associated with Jeune asphyxiating thoracic dystrophy and Mainzer-Saldino syndrome, ciliopathies forming part of a spectrum of skeletal dysplasias now collectively termed short rib thoracic dysplasia 9 with or without polydactyly (SRTD9, MIM#266920).²⁵⁵⁻²⁵⁸ First described in 1970, patients have variable skeletal features including shortened ribs, short stature, cone-shaped phalangeal epiphyses (pre-pubertal), brachymesophalangy, and acetabular spurring or metaphyseal defect of the femoral head.²⁵⁹ Non-skeletal features in the majority of patients include a severe early-onset retinal dystrophy, and end stage renal failure secondary to nephronophthisis by teenage years with cerebellar ataxia, epilepsy, facial dysmorphism, learning difficulties and cholestasis also reported.²⁵⁵⁻²⁵⁷

IFT140 mutations have now been identified in patients with isolated retinal dystrophy.^{260, 261} Prior to these reports, 2 families from this centre were identified from WES with non-syndromic RCD due to bi-allelic *IFT140* variants and further functional investigation of this novel finding was then planned. A further 3 families were subsequently identified, 2 from the Manchester 176 retinal gene panel and 1 from WGS as part of the SPEED study. Detailed characterisation of the ocular phenotype was performed and functional analysis of 2 identified variants with protein localisation studies in hTERT-RPE1 cells performed to support their pathogenicity. In addition, characterisation of a zebrafish morpholino was performed as a potential animal model of the human disease.

5.2 Methods

5.2.1 Patient ascertainment

Two probands were initially identified by colleagues from whole exome sequencing. Variants in *IFT140* were identified as the most likely cause of their retinal dystrophy with no other pathogenic variants in known retinal dystrophy genes. Both probands were assessed and examined by myself and their extended family in Pakistan and New Zealand contacted for DNA samples and segregation. All patients provided written, informed consent. A colleague in Pakistan was able to review 2 of the affected family members there. Three further probands were later identified, 2 from the Manchester NGS gene panel test and the fifth from WGS as part of the SPEED study.

5.2.2 Clinical investigations

A total of 8 affected patients were studied with full ophthalmic examination (2 by myself, 4 by my supervisors and 2 by a colleague in Pakistan) and retinal imaging. Seven of 8 patients underwent renal function testing, 5 of 8 patients had hand x-rays. One patient was no longer contactable despite multiple attempts and therefore unavailable for renal function testing.

5.2.3 Molecular investigations

Patient 1.1 had been previously investigated by a negative APEX microarray. He was then found negative by targeted NGS of the coding regions of 31 retinal dystrophy genes performed at Bioscientia Center for Human Genetics (Ingelheim, Germany). WES was then performed (AROS). Patient 2 was initially investigated as part of the UK National Collaborative Usher study due to the co-existence of hearing loss with retinal dystrophy with negative bidirectional Sanger sequencing of 9 Usher genes (*MYO7A*, *CDH23*, *PCDH15*, *USH1C*, *USH1G*, *USH2A*, *GPR98*, *WHRN*, *CLRN1*) and a candidate gene *SLC4A7* as part of the UK National Collaborative Usher Study as previously described.²⁶² WES was then performed as above. Patients 3.1 and 4 underwent NGS of the coding regions of 176 retinal genes (Manchester). Patient 5 underwent WGS as part of the SPEED study.

Bi-directional Sanger sequencing of involved exons and intron-exon boundaries of *IFT140* was performed by my colleague in the lab for family 1, by myself on family 2, by Manchester Genomics centre for families 3 and 4 and as part of the NIHR SPEED study on family 5. Segregation was confirmed in available relatives. I obtained blood samples on relatives from Pakistan and New Zealand to enable segregation. DNA was amplified using specifically designed primers by polymerase chain reaction (PCR) and the resulting fragments were sequenced using standard protocols (table 5-1).

Exon	Primer forward 5' → 3'	Primer reverse 5' → 3'	Enzyme	Annealing temp (°C)	Amplicon size (bp)
13	CAGTTCCTGTGCCTCAGAG	ACCCGGTCTCAGGTAGTTCT	BIOTAQ	65	409
19	TCTGACCATTGCCAGTGACC	TGGGCAGCATTTTCATCGAGT	BIOTAQ	65	548
22	GTGCTCAGGGTCTGCAGAG	TGGCTTTGTCCAAAGGGAGG	BIOTAQ	65	423

Table 5-1: Primer pairs for Sanger sequencing of *IFT140* in families 1 and 2

Nomenclature was assigned in accordance with GenBank Accession number NM_014714.3.

5.2.4 Cell studies

Under supervision by a colleague (Nicholas Owen) within our lab at the Institute of Ophthalmology, an *in vitro* experiment was designed to perform transient plasmid transfection of hTERT-RPE1 cells to further investigate missense variants identified in the original 2 families. I performed all experiments as described in methods section 2.3.

5.2.5 Zebrafish studies

Investigation of a zebrafish morphant was performed as described in methods section 2.4. There was limited published data on this morphant, and we hypothesised that rescue experiments may provide further evidence of pathogenesis of the missense variants studied.

5.3 Results

Ophthalmological and systemic findings

Five families were studied (figure 5-1). Clinical details are summarised in table 5-2. All patients had a retinal dystrophy characterised by nyctalopia and progressive field loss, with fundus features and electrophysiology (available in 3 patients) consistent with a rod-cone dystrophy.

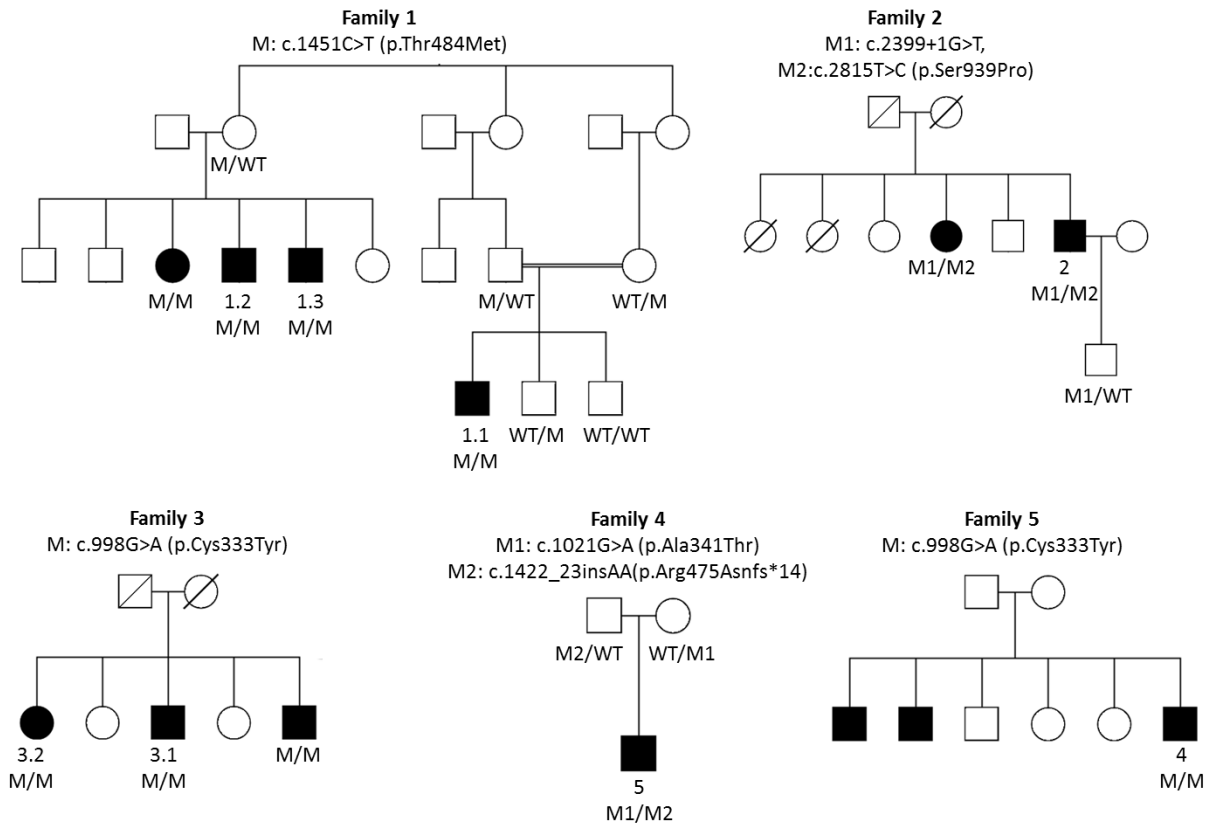


Figure 5-1: Pedigrees of 5 families with mutation segregation

Family 1 of Northern Pakistan origin was comprised of the proband (patient 1.1) and his 3 affected second cousins, 2 of whom (patients 1.2 and 1.3) were available for clinical examination. Patient 1.1 was born at full term to consanguineous parents. He was noted to have reduced night vision at 2 years of age. Fundus examination demonstrated mild mid-peripheral retinal changes only (figure 5-2). Electroretinography (ERG) performed age 8 demonstrated a relatively severe rod-cone dystrophy with marked bilateral macular involvement which had progressed when repeated age 13 years. Systemically, patient 1.1 was well with no dysmorphic features and normal growth parameters (age 13, height 50th-75th centile, weight 75th centile, head circumference 25th centile). His fingers were noted to be long and he had no skeletal abnormalities. Hand and hip X-rays were normal (figure 5-3). He had a history of congenital right pelvico-ureteric junction obstruction and secondary hydronephrosis, which required surgical correction at 4 years of age. Renal and liver function blood tests were normal at age 13 years. Renal ultrasound demonstrated a normal left kidney, with global cortical thinning and loss of normal corticomedullary differentiation on the right consistent with the history of hydronephrosis.

Non-syndromic retinal dystrophy due to mutations in *IFT140*

Pt	Age of onset	Age at last review, logMAR visual acuity (Snellen), refractive error	Key fundus findings	Other findings	ERG, PERG	Serum creatinine $\mu\text{mol/L}$ (70-120)	eGFR, L/min/m ² (>90 normal)
1.1 GC 17830	2 years	13 years R 0.0 (6/6) L 0.0 (6/6) R +0.25/-1.25 x40 L -5.50/-0.50 x140	Mid-peripheral hypopigmented dots, mild RPE atrophy	Humphrey VF 24-2: extensive loss periphery, central 10° preserved Ishihara: 17/17 BE	Age 13, residual PERG activity, severe loss both rod and cone systems	N	N
1.2	<10 years	45 years R 0.7 (6/30) L 0.5 (6/19)	Mid-peripheral RPE hypopigmentation with intra-retinal pigmentary migration, macular atrophy	Early cataract RE, L cataract surgery age 44	Not done	N	N
1.3	<10 years	44 years R 0.3 (6/12) L 0.3 (6/12)	Mid-peripheral RPE hypopigmentation, early macular atrophy	Early lens opacity	Not done	N	N
2 GC 1558	16 years	67 years R HM L PL	Posterior pole chorioretinal atrophy, extensive mid-peripheral pigmentation, severely attenuated vessels	Confrontation VF: <5° BE Cataract surgery BE late 40's, myopic prior	Not done	76	95
3.1 GC 4303	Late 20's	53 years R 0.7 (6/30) L 1.8 (1/60)	R cystoid macular oedema with epiretinal membrane, B macular atrophy, attenuated vessels extensive pigmentary change	Confrontation VF: 20° on R, 10° on L Early cataract	Age 45, undetectable PERG and rod specific ERG, markedly subnormal cone	115	61
3.2	Early 30's	57 years R 0.2 (6/9.5) L 0.2 (6/9.5)	Marked vessel attenuation, nasally occluded vessels, extensive atrophy particularly posterior pole, mid-peripheral pigmentary change	Early cataract BE Ishihara: R 2/17 L 4/17	Not done	91	56
4 GC 21161	28 years	31 years R 0.0 (6/6) L -0.1 (6/4.8)	Attenuated vessels, mid-peripheral RPE mottling	Confrontation VF: full Ishihara: 17/17 BE	Not done	77	109
5 GC 20552	14 years	26 years R 0.3 (6/12) L 0.2 (6/9) R -2.50/-0.75 x15 L -1.75/-1.25 x10	Bilateral mild epiretinal membrane, mild RPE change in mid-periphery	Early subcapsular cataract Ishihara: R 7/17 L 17/17	Age 25, subnormal PERG, rod responses undetectable, subnormal cone	NA	NA

Table 5-2: Clinical summary of patients with *IFT140* related retinal dystrophy
eGFR, estimated glomerular filtration rate; NA, not available

Both patients 1.2 and 1.3 developed visual symptoms in childhood with preservation of central vision until their 40's. They had retinal changes of RCD with attenuated vessels, macular atrophy and mid-peripheral pigmentary change, worse in the older brother. Neither brother had any syndromic features. Specifically, hand X-rays did not demonstrate shortened phalanges, and renal and liver functions were normal.

Patient 2, of Caucasian British origin, first noticed nyctalopia aged 16 years with peripheral field loss noted in his mid-20's when he was diagnosed with RCD. Loss of central vision occurred by 50 years of age with fundus features of a severe and extensive pigmentary retinopathy. There was no history of skeletal or renal abnormalities. Hand X-ray did not identify shortened phalanges, and renal function blood tests were normal age 67 years. There was a history of progressive hearing loss noted at the age of 4 years, which required hearing aids. Audiometry revealed symmetrical bilateral high frequency loss and bilateral plateau loss of 25-30db in 250-2000 kHz frequencies. The hearing loss was atypical for Usher syndrome. There was no other medical history of note. His younger sister also has RCD but without hearing loss. Clinical examination was not possible but a DNA sample was obtained.

Family 3 are from the Gujarat region of India. The proband, 3.1, noted nyctalopia in his late 20's and problems with glare. He noted reduced left vision at age 44 years. Fundus examination revealed extensive pigmentary change and vessel attenuation. ERG was consistent with severe generalised retinal dysfunction in both eyes. Patient 3.2, presented with nyctalopia and progressive peripheral field loss in her early 30's. When last reviewed age 57, visual acuity was still good at 0.2 logMAR each eye (Snellen 20/32) despite marked vessel attenuation and generalised atrophy of the posterior pole. Neither patient has any systemic manifestations. Both patients have normal serum creatinine but estimated glomerular filtration rates (eGFR) that are borderline and under review. Both are hypertensive on oral medications. Patient 3.2 has had stable creatinine and eGFR over 6 years of monitoring.

Family 4 are British Caucasian. The proband noted difficulty with dark and light adaptation in his late 20's but otherwise remains without symptoms. At last review age 31 years, visual acuity was excellent with mild retinal changes only. Systemically well, skeletal survey, renal function and renal ultrasound were all normal.

Family 5 are from the Punjab region of Pakistan. The proband developed nyctalopia in early teenage years without any other noticeable symptoms. When last reviewed age 26 years, the patient was systemically well with no clinically apparent syndromic features of disease. Further investigations were unfortunately not possible as the patient is no longer contactable.

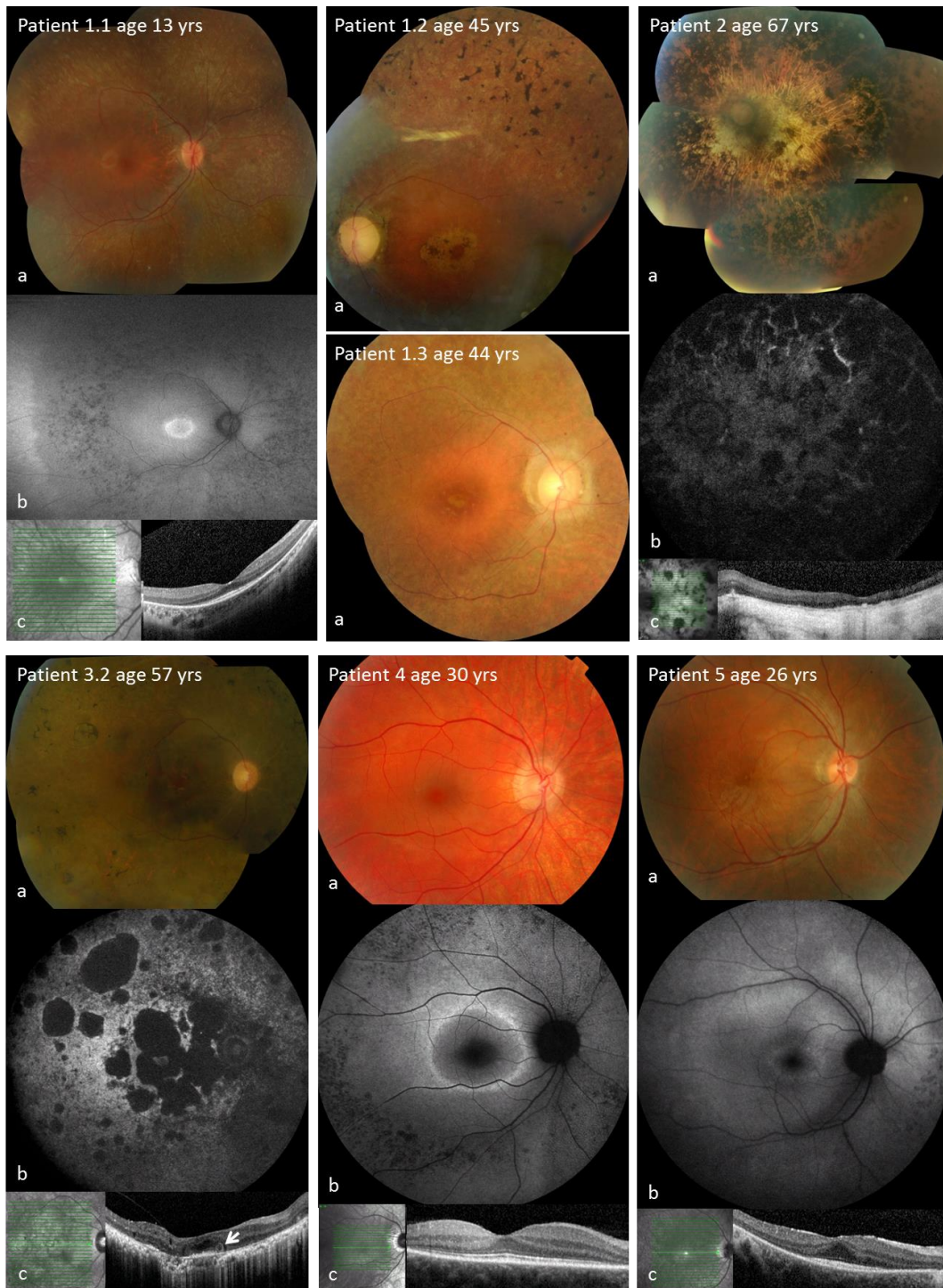


Figure 5-2: Retinal imaging in *IFT140* related rod-cone dystrophy

(a) colour fundus photographs, (b) FAF imaging, (c) OCT.

Patient 1.1, RE (a) diffuse, mid-peripheral white dots, para-foveal atrophy in macula, (b) ring of increased autofluorescence in macula, reduced mid-peripherally (c) centrally preserved ISE band. Patient 1.2, LE (a) central macula atrophy, peripheral intra-retinal pigmentary migration in regions of depigmentation. Patient 1.3, LE (a) central macular atrophy with mid-peripheral hypopigmentation. Patient 2, LE (a) posterior pole atrophy with heavy mid-peripheral pigmentation, (b) extensive loss of autofluorescence, (c) loss of outer retina and inner choroid. Patient 3.2, RE. (a) macular atrophy, mid-peripheral RPE atrophy and pigment change, marked vessel attenuation, nasal vessel occlusion, (b) reduced autofluorescence particularly in posterior pole, (c) disorganised retina with loss of outer retina and ORT (arrowed). Patient 4, RE. (a) attenuated vessels, mid-peripheral RPE hypopigmentation, (b) ring of increased autofluorescence in macula, speckled reduction mid-periphery (c) ISE band preserved centrally. Patient 5, RE. (a) mild mid-peripheral RPE atrophy, (b) ring of increased autofluorescence in macula with small dots of reduced autofluorescence nasally, (c) ISe band preserved centrally



Figure 5-3: Skeletal imaging in *IFT140*

Patient 1.1 anteroposterior (AP) x-rays of left hand and pelvis, patient 2, AP and lateral x-rays of left and right hands. All x-rays normal.

Molecular investigations

In family 1, WES identified a homozygous variant, c.1451C>T (p.Thr484Met), with segregation in 5 unaffected and 3 affected family members supporting causality (figure 5-1). This variant has now been reported.²⁶⁰ No other predicted pathogenic variants were identified in known retinal genes. In family 2, WES identified a splice site variant c.2399+1G>T, that has been previously reported in 4 syndromic patients and a novel missense variant, c.2815T>C (p.Ser939Pro) predicted to be tolerated *in silico*.^{255, 256} Patient 2's affected sister also carries both variants with his son carrying the missense variant only, confirming that the mutations are in *trans*.

A targeted gene panel of 176 genes identified c.998G>A (p.Cys333Tyr) in the third proband. This was also present in 2 other affected family members with 1 unaffected sibling not harbouring the variant. It is therefore possible, in this non-consanguineous family, that the affected patients are hemizygous with a deletion on the other allele. This variant has not been reported in an affected patient before but is present in 2 of 121,370 alleles on ExAC.

Patient 4 also underwent targeted sequencing of 176 retinal genes identifying 2 variants. The first, c.1021G>A (p.Ala341Thr) has an allele frequency of 10 in 119,692 on ExAC and is predicted to be damaging *in silico* (SIFT 0.03, Polyphen2 1.00). The

second, is a novel frameshifting mutation, c.1422_1423insAA (p.Arg475Asnfs*14).

Segregation in his parents confirmed the mutations to be in trans.

WGS in patient 5 identified the same homozygous variant as found in family 3. Affected and unaffected family members overseas were unavailable for further testing.

Conservation of the missense variants identified in this study was compared to syndromic missense variants across a diverse range of orthologues (figure 5-4).

Ala341Thr, Thr484Met and Ser939Pro are not conserved, Cys333Tyr is fully conserved. Six of 9 syndromic missense mutations are fully conserved; 3 are not conserved.

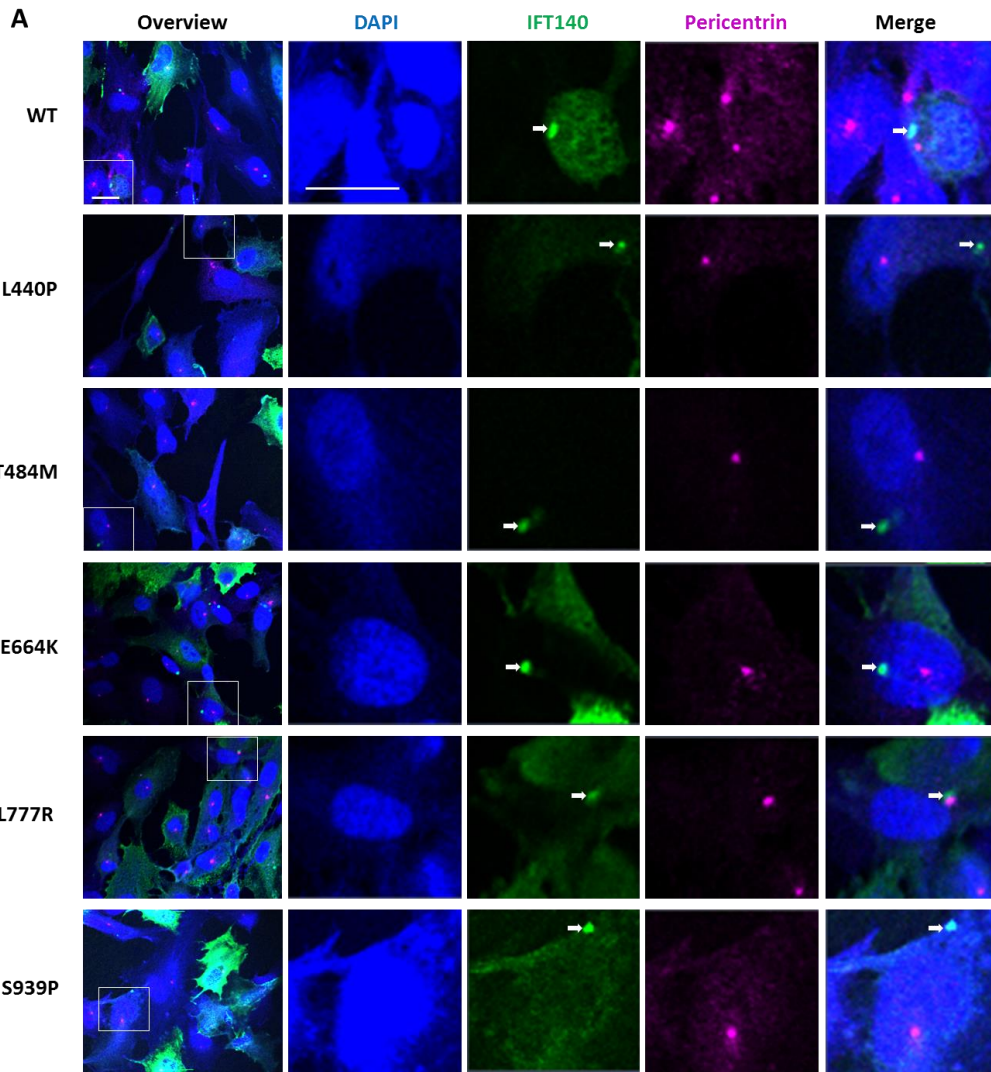
	Leu152Phe	Gly212Arg	Ile233Met	Val292Met	Tyr311Cys	Cys333Tyr	Ala341Thr
Rabbit	EYGKHLTRCIF	VSLADGTVHYV	STDGSIQTMFY	:EDSLLVTALGE	.GREENYVLSLE	NCVCYCAVKGLLAAGTDRG	
Human	EYGKHLTHCIF	VSLMDGTVHYV	SADSTIQMLFY	:EGSLLVMAVGE	.ERGENYILSPD	NCVCYCKVKGLLAAGTDRG	
Macaque	EYGKPLTHCIF	VSLMDGTVHYV	SADSAIQMLFY	:EGSLLVMAVGE	.ERGENYILSPD	NCVCYCVQVKGLLAAGTDRG	
Cow	EYGQPLTHCIF	VSLTDGTVHHV	STDSSIQTIFY	:DGSLLVTAIGE	.ERGENYVLSPE	NCVSYCKVKGLLAAGTDKG	
Mouse	EYGKALTHCIF	VSLMDGTVHYV	STDSSIQTIFY	:EGSLLVTAIGE	.ERGENYILSLQ	NCVCFCKAKGLLAAGTNKG	
Microbat	EYGRHLTHCIF	VSLMDGTVHYV	STDSSIQTIFY	:EGSLLVTAIGE	.EGGENYVLSPE	NCVSYCKIKGLLAAGTDKG	
Anole	EYGKHLNCCIF	ISTTDGTVHYV	TTESPVQKLLFI	:DHSLLITATGE	.ERGENYVVSLD	NCISYCSAKGLLSGGTDKG	
Flycatcher	EYGKCLCHCVF	VTLTDGTVHYV	STDLSVRKLLLI	:DRSLVVTALGE	.DRDENYVLSLD	NCVSYCSAKGVLAAGTSKG	
Cod	DYGKALSCCIF	VSTVDGKVHSV	ALDSPVQKLFYI	:ESGLLFTATGE	.ERDDNYVLSLD	NCVSYCSAKEVLAAGTSLG	
Zebrafish	DYSRPLTCCIF	ISTADGSVYSV	SVESAVHKMWY	:EGLLITASGE	.ELDDHYALSLD	NCVSFCTSKQVLAAGTSRG	
	:*.: *	*:* ::	**.*: *	: :. ::	: :.*: *	*:* : *	*:*:*: *

	Leu440Pro	Thr484Met	Gly522Glu	Glu664Lys	Ser939Pro	Cys1360Arg
Rabbit	STGAAHSLRTDMHV	AFLCETPVLAV	FSENEGPNCF	PRLFVCEAVQVTP	EVPRMLSEDLQAL	KESVRQCELLLQE
Human	STGVAHSLRTDMHI	TFLCETPVLAM	FSETEGNPCF	PRLFVCEAVQETP	EVPRMLSEDLPSL	KESIKQCELLLEE
Macaque	STGVAHSLRTDMHI	TFLCETPVLAM	FSETEGNPCF	PRLFVCEAVQETL	EVPRMLSEDLPSL	KESIKQCELLLEE
Cow	STGVTHSLRTDMHV	SFLCESPVLAM	FSESEGNPCF	PRLFVCEAVREVP	EVPRMLVEDLQAL	KGSVRQCQLLLEE
Mouse	STGGTHSLRTDMHI	TFLCETSVLAM	FSETEGSPCF	PRLFVCEALQEAP	EVPRMLSEDLQSL	KESLRQCELLLEE
Microbat	STGLTYNLRTDMHI	TFLCESPVLAM	FSETEGNPCF	PRLFVCEAVREAT	EVPRMLSEDLQSL	KESVKQCELLLEE
Anole	SDKMTENLRIDMRV	SFSCDSPVLAM	FSESEGNPCF	PRLFICETALDPN	EVPRMLSEDLQAL	REARQCELLLEE
Flycatcher	STGTTHSLRIDMNA	SFLCDSPLVSV	FSEAEGNPCL	PRLFVCEAIPESG	EVPRMLSEDLQAL	EEAVRQCELLLAE
Cod	AEEPPLALRTHIHI	GFQCDSQVLAV	FSEAEGNPVL	ARLLVCETVPVGA	EVPRMLQDSDGSL	GEAMSLCDALLEE
Zebrafish	TSNTHITFNTDTHI	SFQCESPALAL	FSEAEGNPTL	PRLFVCETVSVNS	EVPRMLMEDNVSL	VEAVRLCESLLEE
	:	:. . .	* *:*: .*::	*** **.* :	**:*:*:	***** .* :*

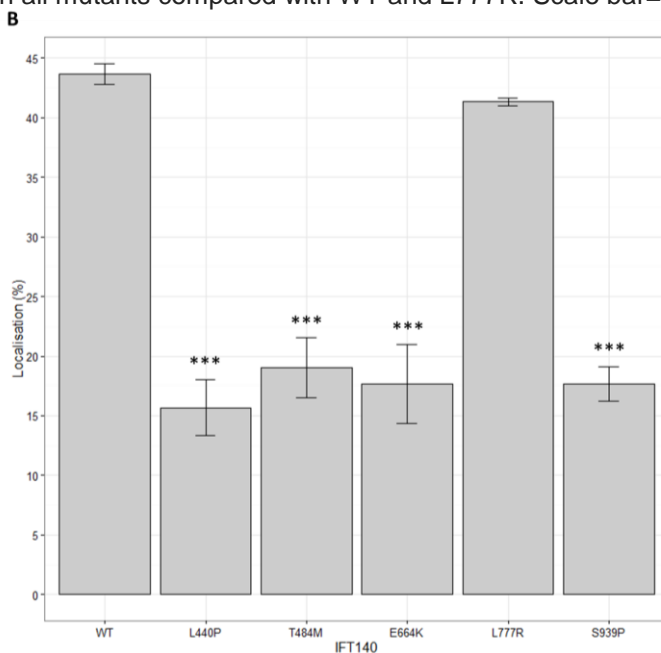
Figure 5-4: Conservation of missense variants

Transient cell transfection studies

Site directed mutagenesis using mutation specific complementary primer pairs generated 4 plasmid clones. A total of 6 plasmids were used in cell transfection experiments: 2 contained non-syndromic mutations c.1451C>T (p.Thr484Met, T484M) and c.2815T>C (p.Ser939Pro, S939P); one a previously unreported mutation, c.1319T>C (p.Leu440Pro, L440P), from a patient with Leber Congenital Amaurosis and renal failure (personal communication Isabelle Perrault); a previously reported plasmid with a syndromic mutation c.1990G>A (p.Glu664Lys,E664K);²⁵⁵ the WT plasmid; and a polymorphism, c.2330T>G (p.Leu777Arg, L777R), rs34535263. Following transient transfection of *IFT140* and mutants in hTERT-RPE1 cells and subsequent immunostaining, analysis of aberrant IFT140 localisation with the basal body was performed (figure 5-5).



(A) Transient transfection was performed with 6 Myc-DDK-tagged IFT140 plasmid constructs. Cells were immunostained with primary antibodies to the IFT140 plasmid and basal body and secondarily stained. Expressed IFT140 (white arrow) and basal body localisation was reduced in all mutants compared with WT and L777R. Scale bar= 20µm.



(B) The percentage of transfected cells with localisation of IFT140 to the basal body was calculated from a mean of 3 independent experiments (n>100 cells).

A statistically significant difference was found between WT and E664K, L440P, T484M and S939P (***) $p < 0.0001$). There was no statistically significant difference found between WT and L777R, nor between the syndromic mutants, E664K and L440P and the non-syndromic mutants T484M and S939P ($p=1$).

Figure 5-5: Aberrant localisation of IFT140 with basal bodies in transiently transfected hTERT-RPE1 cells.

Transfection efficiency was 38% with generalised cytoplasmic staining frequently observed. Those cells with specific basal body labelling by IFT140 were counted. Statistically significant aberrant localisation was found for T484M, S939P, L440P and E664K compared to WT and L777R ($p < 0.0001$). No significant difference was found between any of the 4 pathogenic mutations (T484M, S939P, L440P and E664K, $p = 1$) nor between the syndromic mutants L440P and E664K when compared to the non-syndromic mutants T484M and S939P ($p = 1$). Two control experiments using secondary antibodies and either no plasmid DNA or no plasmid DNA and no primary antibodies were performed each time to check for contamination (figure 5-6).

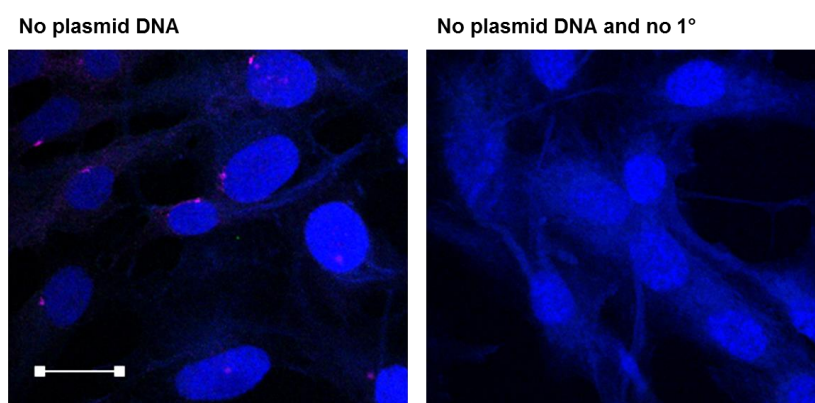


Figure 5-6: Control experiments

No aberrant staining with secondary antibodies. Scale bar = 20 μ m.

Characterisation of an *ift140* zebrafish morphant

Colleagues within the lab performed microinjection of an *ift140* translation blocking morpholino (*ift140* ATG MO) with embryos analysed at 3 and 5 dpf (figure 5-7). They identified changes in the gross morphology with normal body axis curvature but shorter length and smaller eyes for both *ift140* ATG MO 3dpf and 5dpf morphants but with abnormalities most obvious in the 5dpf group. In addition, there was a variable lack of swim bladder for *ift140* ATG MO at 5dpf. They performed Western blot to confirm successful knockdown of *ift140*. Simultaneous knock-down of both *Tp53* and *ift140* at 3dpf demonstrated that the observed phenotype was still present indicating that this was not an off-target apoptotic effect. Alcian blue cartilaginous stain was similarly distributed between morphant and wt although development appeared either delayed or the cartilaginous structures reduced in size in morphants. Retinal histology demonstrated mild thickening of the inner plexiform and ganglion cells layers at 5dpf. Apoptosis assay found no apparent difference between wt and morphant at both 3dpf and 5dpf stages. Immunohistochemistry demonstrated reduced anti-zpr-1 (red-green double cone staining) for 5dpf MO. Anti-acetylated tubulin was similarly distributed and intense for wt and MO; an increased ganglion cell layer was occasionally found.

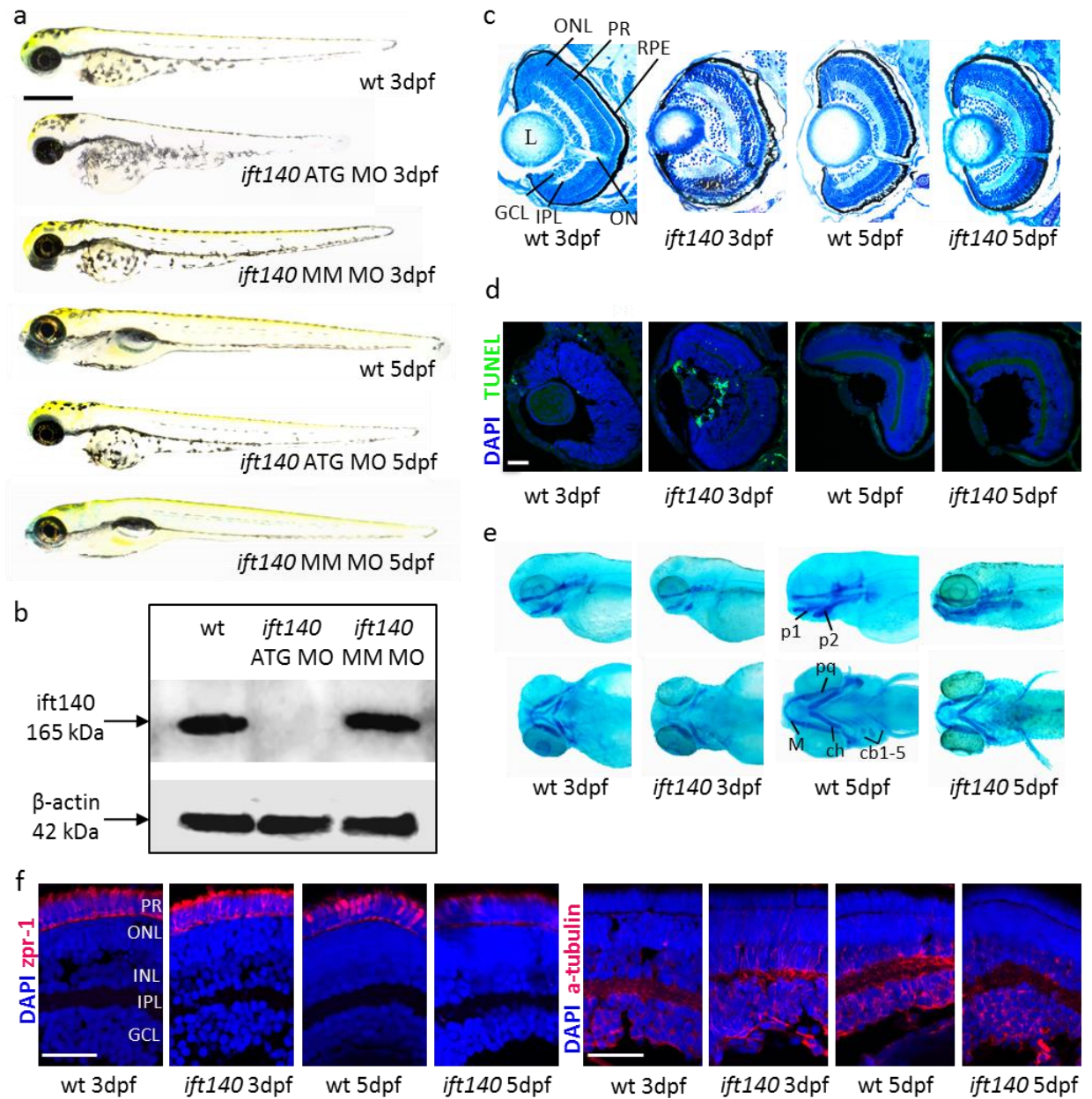


Figure 5-7: Characterisation of an *ift140* zebrafish morphant

(a) Gross morphology of 3 and 5 dpf wt *ift140* ATG morphant MO, and *ift140* MM MO demonstrating similar body axis curvature but shorter length, smaller eye and variable lack of a swimbladder (5dpf only) for the ATG MO compared to the wt and MM. Scale bar = 500µm.

(b) Western blot analysis of wt, *ift140* ATG MO and *ift140* MM MO (n=20 for each, 30 µg) demonstrating successful knockdown of *ift140* translation for the ATG MO.

(c) Retinal histological sections demonstrating thickening of both inner plexiform layer (IPL) and ganglion cell layer (GCL) in MO morphants at both 3 and 5 dpf (PR, photoreceptors; ONL, outer nuclear layer; ON, optic nerve; RPE, retinal pigment epithelium).

(d) Apoptosis assay demonstrating similar numbers of TUNEL+ve cells between wt and MO. Scale bar= 20 µm.

(e) Alcian blue stain of lateral and transverse whole-mount zebrafish demonstrating similar cartilage staining although structures are reduced in size for the *ift140* MO (p1, pharyngeal arch 1; p2, pharyngeal arch 2; M, Meckel's cartilage; pq, palatoquadrate; ch, ceratohyal; cb1-5, ceratobranchials 1-5).

(f) Transverse cryosections through wt and MO retina stained with either mouse anti-zpr-1 or mouse anti-acetylated tubulin. Mild thickening of IPL and GCL observed for anti-acetylated tubulin 5dpf *ift140* MO. Scale bar= 20 µm.

Further investigation of missense variants was performed by attempted rescue of morphant phenotype. I generated wt, L440P and T484M mRNAs having first checked that there was no consensus between injected morpholino and the mRNAs using Blast. Colleagues performed co-injection of zebrafish embryos with *ift140* ATG MO and wt or mutant mRNAs. I performed the analysis at 5dpf. As the previously described lack of swim bladder phenotype was not found on these repeat experiments, length of fish and vertical eye diameter were instead measured. This identified significantly smaller lengths of 5dpf morphant fish for all mRNA types compared to wt and failed to demonstrate rescue of phenotype with wt mRNA (figure 5-8). The eye diameter was significantly smaller for all mRNA types with the morphant also smaller but not reaching statistical significance ($p=0.0641$). However the numbers in the eye diameter group were much smaller than the length group as only those fish with full lateral orientation on photographs could be measured accurately.

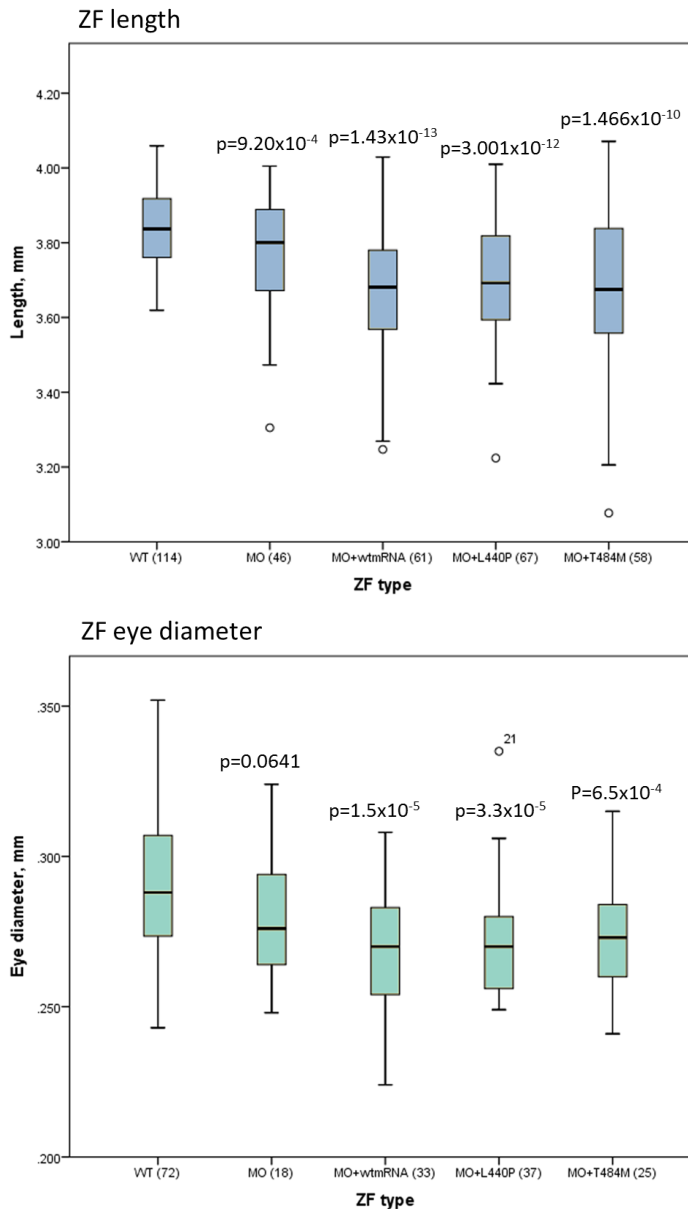


Figure 5-8: mRNA rescue experiments of morphant phenotype

5.4 Discussion

This series of patients with *IFT140* mutations and non-syndromic retinal dystrophy underwent detailed ophthalmic phenotyping. Systemic investigation was performed in all but 1 patient. Five patients were in their 5th-7th decades, far older than any previously reported patients. The patients have typical features of RCD presenting from early childhood to the 4th decade and all are developmentally normal, with no apparent skeletal or neurological abnormalities. Cone-shaped epiphyses are universally found pre-pubertally in *IFT140* related disease. This abnormality is not apparent in adults, although shortening of the phalanges can still be detected.²⁶³ Hand X-rays in patients 1.2, 1.3 and 2 did not identify shortened phalanges but it remains possible that X-rays during childhood could have revealed evidence of the cone shape abnormality. Renal function was normal in the tested patients except for patients 3.1 and 3.2 with borderline renal function age 53 and 57 years respectively. It is possible that this mild renal impairment is related to *IFT140* but given their age and hypertension, it may be unrelated. Patient 1.1 had unilateral congenital pelvico-ureteric obstruction which has not been reported in *IFT140* related disease; it is likely that this is an incidental finding. His 2 affected older second cousins have normal renal function in their 40s.

All but one of the previously reported syndromic patients with *IFT140* mutations had a severe, early-onset retinal dystrophy and undetectable or severely attenuated ERG.²⁵⁵⁻²⁵⁷ The exception, a patient homozygous for c.699T>G (p.Ile233Met), had no evidence of retinal dystrophy age 2 years but did have skeletal and renal manifestations.²⁵⁵ Of 7 patients recently reported with isolated retinal dystrophy due to *IFT140*, 5 have RCD with onset of nyctalopia ranging from 7 to 33 years old, and 2 have severe early-onset retinal dystrophy.²⁶⁰ There was no evidence of renal or skeletal involvement, but one patient had hypogonadism and fatty liver which have been reported in other ciliopathies.^{264, 265} It was not clear if all patients underwent systemic investigation and renal function. A further report of 12 patients, focused on the ophthalmic phenotype, describing it as severe with infantile onset, hyperopia and flat ERG (age <2 years-20 years). The patients reported in this present series have milder and later onset retinal dystrophy than the majority of those previously reported with fundus features consistent with RCD. Refraction, available in 2 patients was myopic.

All reported patients with syndromic *IFT140* related ciliopathy, have developed end stage renal failure by their second decade with the exception of 10 families homozygous for p.Glu664Lys (reported ages 10 months -17 years).^{255-257, 261} The affected children in those families presented in infancy with severe EORD consistent with a diagnosis of LCA and with additional syndromic findings including epilepsy, hypotonia and developmental delay. In all patients in whom hand x-rays were

performed, cone-shaped epiphyses were identified. Systemic investigations were unavailable for 4 families.²⁶¹ The lack of overt renal dysfunction suggests a possible genotype-phenotype correlation for this specific mutation.^{255, 257, 261} However, there has been 1 reported patient homozygous for this variant with renal failure and a kidney transplant age 17 years raising the possibility that renal dysfunction may still occur with this allele but perhaps later than with other syndromic disease alleles.²⁶¹

Phenotypic heterogeneity of several ciliopathy genes has been well established including *CEP290*, *IQCB1*, *IFT172*, *BBS1* and *BBS3*.^{11, 12, 85, 266, 267} In the case of *CEP290*, there is evidence for a dosage-dependent phenotype with bi-allelic loss of function mutations associated with Joubert syndrome and the common c.2991+1655A>G splicing mutation in which a small amount of protein is still produced, associated with LCA.¹² In addition, *CEP290* mutations in functionally critical regions, despite predicted residual protein production, were associated with a more severe phenotype.²⁶⁸ Three non-syndromic families in this report have bi-allelic missense mutations, as do several of the previously reported syndromic families (table 5-3).²⁵⁵⁻²⁵⁷ This would suggest that phenotypic variability is not related to the type of mutation. Only 1 patient with bi-allelic premature termination codons has been reported which may indicate an essential developmental role for *IFT140*.²⁶¹ Mice homozygous for *Ift140^{null1}* die mid-gestation indicating embryonic lethality for a null phenotype.²⁶⁹

IFT140 is a 1462 amino acid protein encoded by 31 exons and consists of 2 types of domain; 5 WD repeats and 9 tetratricopeptide repeats.¹⁶⁴ Reported mutations arise throughout the gene with no clustering or domain preference (table 5-3). Of the 4 missense variants in this report, p.Cys333Tyr and p.Ala341Thr arise within the WD5 domain but the other 2 are not located within known functional domains. Of the previously reported syndromic mutations, 2 arise within functional domains (p.Val292Met and p.Tyr311Cys in WD4) and the remaining 7 do not. Conservation of missense amino acid residues in orthologues demonstrates a lack of conservation of 3 of the non-syndromic residues, with 1 fully conserved. Three of 9 syndromic mutations are not conserved precluding any conclusion (figure 5-4). The Cys333Tyr allele was identified in 2 families and it would suggest that this may be a retina-specific allele. The variant Thr484Met was recently identified in conjunction with a 2nd missense variant in a patient with non-syndromic LCA indicating that this allele may also be retina-specific. The non-conserved Ala341Thr variant was identified in a patient with a novel frameshifting variant; neither have been reported in an affected patient before. The non-conserved Ser939Pro residue is predicted to be tolerated *in silico* and arises in conjunction with a splice site variant previously reported in syndromic disease. These

results may indicate that the Ala341Thr and Ser939Pro variants are less deleterious to protein function such that there is a non-syndromic manifestation of disease.

Diagnosis	Allele 1	Exon	Allele 2	Exon
Perrault 2012²⁵⁵				
MSS	c.2399+1G>T	Intron 19	c.1990G>A ; p.Glu664Lys	17
MSS	c.932A>G ; p.Tyr311Cys	9	c.857_860del ; p.Ile286Lysfs*6	8
MSS	c.1990G>A ; p.Glu664Lys	17	c.1990G>A ; p.Glu664Lys	17
MSS	c.1990G>A ; p.Glu664Lys	17	c.1990G>A ; p.Glu664Lys	17
MSS	c.634G>A ; p.Gly212Arg	7	c.3916dupG ; p.Ala1306Glyfs*56	29
MSS	c.699T>G ; p.Ile233Met	7	c.699T>G ; p.Ile233Met	7
JATD	c.2399+1G>T	Intron 19	c.634G>A ; p.Gly212Arg and/or alteration exon 6 donor splice site	7
MSS	c.1565G>A ; p.Gly522Glu	14	2 nd allele not found	
MSS	c.874G>A ; p.Val292Met	8	2 nd allele not found	
MSS	c.1727G>A ; p.Arg576Gln	15	2 nd allele not found	
MSS	c.489C>T ; p.Gly163Gly, and c.488_491del (p.Glu164Thrfs*10) from creation donor splice site	5	2 nd allele not found	
Schmidts 2013²⁵⁶				
JATD	c.1380delC ; p.Asn460Lysfs*28	12	c.874C>T ; p.V292M	8
JATD	c.1565G>A ; p.Gly522Glu	14	c.874C>T ; p.V292M	8
JATD	c.454C>T ; p.Leu152Phe	5	c.454C>T ; p.Leu152Phe	5
JATD	c.1565G>A ; p.Gly522Glu	14	c.874C>T ; p.Val292Met	8
JATD	c.2278C>T ; p.Arg759*	19	2 nd allele not found	
MSS	c.2399+1G>T	Intron 19	c.4078T>C ; p.Cys1360Arg	30
MSS	c.418G>A ; p.Gly140Arg and c.800A>G ; p.Glu267Gly	5, 7	c.490G>T ; p.Glu164*	6
JATD	c.2399 +1C>A	Intron 19	2 nd allele not found	
JATD	c.4058 G>C ; p.Pro1353Arg	30	2 nd allele not found	
JATD	c.2360 T>C ; p.Asp787Gly	19	2 nd allele not found	
JATD	c.1541 A>T ; p.Leu514His (rs150903791)	14	2 nd allele not found	
JATD	c.329G>A ; p.Arg110His	4	2 nd allele not found	
JATD	c.481C>A ; p.Pro161Thr	5	2 nd allele not found	
JATD	c.481C>A ; p.Pro161Thr	5	2 nd allele not found	
Khan 2014²⁵⁷				
MSS	c.1990G>A ; p.Glu664Lys	17	c.1990G>A ; p.Glu664Lys	17
MSS	c.1990G>A ; p.Glu664Lys	17	c.1990G>A ; p.Glu664Lys	17
Xu 2015				
RP	c.4196T>C (p.L1399P)	31	c.1898_1901delATAA (p.N633Sfs*10)	17
RP	c.3826G>A (p.G1276R)	28	c.1989C>G (p.C663W)	17
RP	c.650_651delTG (p.V217Gfs*2)	7	c.212C>T (p.P71L)	4
RP	c.2611C>T (p.R871C)	21	c.1377G>A (p.W459*)	12
RP	C.1252G>C (p.A418P)	11	c.2921C>T (p.A974V) NB presumed in <i>trans</i>	23
LCA	c.1452C>T (p.T484M)	13	c.985T>C (p.C329R)	9
LCA	c.2368G>A (p.E790K)	19	c.1655_1656delAG (p.E522Gfs*6)	14
Bifari 2015				
MSS	c.1990G>A ; p.Glu664Lys	17	c.1990G>A ; p.Glu664Lys	17
EORD	c.1990G>A ; p.Glu664Lys	17	c.1990G>A ; p.Glu664Lys	17
EORD	c.1990G>A ; p.Glu664Lys	17	c.1990G>A ; p.Glu664Lys	17
EORD	c.1990G>A ; p.Glu664Lys	17	c.1990G>A ; p.Glu664Lys	17
MSS	c.1990G>A ; p.Glu664Lys	17	c.1990G>A ; p.Glu664Lys	17
EORD	c.1990G>A ; p.Glu664Lys	17	c.1990G>A ; p.Glu664Lys	17
MSS	c.1990G>A ; p.Glu664Lys	17	c.1990G>A ; p.Glu664Lys	17
EORD	c.1541_1542delinsAA	14	c.1541_1542delinsAA	14
MSS	c.1990G>A ; p.Glu664Lys	17	c.1990G>A ; p.Glu664Lys	17

Table 5-3: Previously reported mutations in *IFT140*

JATD: Jeune asphyxiating thoracic dystrophy, MSS: Mainzer-Saldino syndrome, EORD: early-onset retinal dystrophy

Transient expression of IFT140 in hTERT-RPE1 cells transfected with a Myc-DDK-tagged IFT140 plasmid, demonstrated that localisation of IFT140 with the basal body was significantly reduced in mutant cells compared with WT and L777R cells ($p < 0.0001$). No difference was found between the 2 missense variants from families in this report and the 2 reported syndromic missense variants indicating a deleterious effect on protein trafficking *in vitro* for all mutants studied. This supports causality of these 2 non-syndromic missense variants *in vitro*.

Characterisation of an *ift140* zebrafish morphant demonstrated mild abnormalities only, indicating that in early embryonic development *Ift140* is not an essential component for ciliary development in this specific model organism. Retinal characteristics of *ift140* morphant zebrafish have not previously been reported but other features consistent with a weak phenotype in particular a lack of abnormal body axis shape and olfactory ciliary defects have been described for both translation-blocking and splice site *ift140* morphants.²² A more severe phenotype may present later than 5 dpf. There are limited other animal models. Homozygous knockout *Ift140*^{null/null} mice are embryonically lethal with severe multi-system abnormalities including skeletal defects.²⁷⁰ Mice with selective knockout in the renal collecting ducts (from HoxB7-Cre-driven depletion) have very shortened or missing cilia at birth with subsequent cyst development and renal dysfunction.²⁶⁹ CRISPR/CAS or Talen generated transgenic animal models may be useful for future studies. Transgenic zebrafish generated by CRISPR/CAS would permit investigation of the phenotype in the adult fish.

In this series, 5 families with apparently isolated RCD due to *IFT140* mutations are characterised. Given the potential for systemic complications, children with apparently isolated retinal dystrophy due to *IFT140* mutations, may need long-term systemic investigation and renal function monitoring. However it is likely that some patients will have isolated retinal disease and as more patients are reported, specific allele phenotypes may emerge.

6 Knobloch syndrome

6.1 Introduction

Knobloch syndrome is a rare, recessively inherited disorder first described in 1971 in a family with 5 of 10 children affected by vitreoretinal degeneration, retinal detachment, high myopia, occipital encephalocele and lens subluxation.²⁷¹ The phenotypic description has subsequently evolved with additional ocular features of cataract, smooth irides and persistent foetal vasculature.²⁷²⁻²⁷⁴ Limited electrophysiological characterisation has been reported in 3 patients.^{275, 276} Neuroradiological imaging has revealed a variety of developmental brain anomalies including occipital skull defects with or without encephalocele, polymicrogyria, sub-ependymal nodules and cerebellar vermis atrophy.^{275, 277-280} Additional systemic findings include epilepsy, developmental delay, and renal abnormalities.^{272-274, 277, 280-284}

The Knobloch locus was mapped to 21q22.3 in 1996 and *COL18A1* was subsequently identified as the causative gene.^{285, 286} *COL18A1* encodes Collagen alpha-1(XVIII) chain, ubiquitously expressed in vascular and epithelial basement membranes.^{287, 288} It has multiple functions in ocular and neurological development including angiogenesis, maintenance of basement membranes and in the Wnt/ β -catenin signalling pathway.²⁸⁷

Following identification of families with this rare syndrome in the retinal genetics clinics and review of the literature, the lack of complete published phenotypic data prompted further study. I ensured all had neuroradiological imaging and examined all families to ascertain key clinical, electrophysiological and molecular data. This identified novel features including pigment dispersion syndrome and glaucoma, and cone-rod dysfunction on electroretinography. Two patients had normal neuroradiology highlighting the fact that some affected individuals have isolated ocular disease. Patients may initially present to the ophthalmologist and awareness of the ocular phenotype will aid early diagnosis, appropriate genetic counselling and monitoring for potential complications.

6.2 Methods

6.2.1 Ascertainment of patients

Five families were ascertained from inherited retinal clinics. Four were diagnosed with Knobloch syndrome based on clinical features and underwent *COL18A1* Sanger sequencing by colleagues. The fifth, was diagnosed after WES identified a homozygous, previously reported variant in *COL18A1* and re-examination of the

phenotype supported Knobloch syndrome. Investigation of patient phenotype and molecular results were conducted by myself.

6.2.2 Clinical assessment

All patients underwent retinal imaging, electrophysiology and radiological imaging of the brain, either Magnetic Resonance Imaging (MRI) or Computed Tomography (CT) examinations.

6.2.3 Molecular investigations

Bi-directional Sanger sequencing by colleagues in the laboratory of all 41 exons and intron-exon boundaries of the medium isoform of *COL18A1* (NM_030582.3) was performed in an affected proband from families 1-4 and segregation confirmed in the affected sibling and available relatives. Patients 1.1 and 5 had previously undergone APEX microarray. Patient 5 underwent WES (AROS) with identified variants then confirmed by Sanger sequencing in the affected proband and available relatives. A diagnosis of Knobloch syndrome had not been clinically suspected in patient 5 prior to WES. Two potentially pathogenic homozygous variants were identified in *COL18A1* and *RPGRIP1*. I segregated the *RPGRIP1* variant (primers table 6-1)

Exon	Primer forward 5' → 3'	Primer reverse 5' → 3'	Enzyme	Annealing temp (°C)	Amplicon size (bp)
18	GTTGTAAACTACCAGCTTG	GGGACACTACAACCCACAA	MYTAQ	60	301

Table 6-1: Primer pair for sequencing *RPGRIP1*

Databases were interrogated for novel variants in *COL18A1* using both the medium isoform (NM_030582.3) and the alternate short isoform, also reported in the literature (NM_130445.2). GenBank accession number NM_020366 was used for the *RPGRIP1* variant.

6.3 Results

Key clinical features are summarised in table 6-2. Nine patients from 5 families (figure 6-1) were evaluated; ages at last review ranged from 2 to 38 years (mean 15.7, median 14). The ethnic origins were Indian, British Caucasian (2 families), Slovak and Arab. All patients had presented in infancy with nystagmus and variable convergent or divergent squints except for patient 3.2 who was orthophoric. All patients had severe visual impairment with best corrected visual acuity in each eye at last review ranging from 1.06 log MAR (Snellen 6/75) to no perception of light. Patient 1.2 had stable vision of

1.3 log MAR (Snellen 6/120) in the right eye from first review age 9 years to last review age 21 years; patient 5 also had stable vision of 1.0 log MAR each eye over a 36 year review period. All patients had high myopia (≥ -6 dioptres) in at least 1 eye with high myopia reported in patients 4.2 and 5 prior to cataract extraction. Five patients were anisometropic with high myopia in 1 eye and hyperopia in the other. This was related to lens subluxation in 2 patients (2.2 and 3.1), unilateral retinal detachment with hyperopic shift in 1 patient (2.1) and unilateral high myopia in the right eye with near emmetropia in the left eye from infancy in two siblings unrelated to retinal detachment (1.1 and 1.2). These siblings had asymmetrical axial lengths as measured by B scan ultrasound age 8 years for patient 1.1 and age 19 years for patient 1.2 when the length of the myopic eyes were 26.7mm and 27.9mm and the emmetropic 20.7mm and 21.1mm respectively. These siblings were previously reported when children; new data in this report, 15 years later, include visual acuity, repeat ERG, anterior segment and fundus features and neuroradiology.²⁸⁹

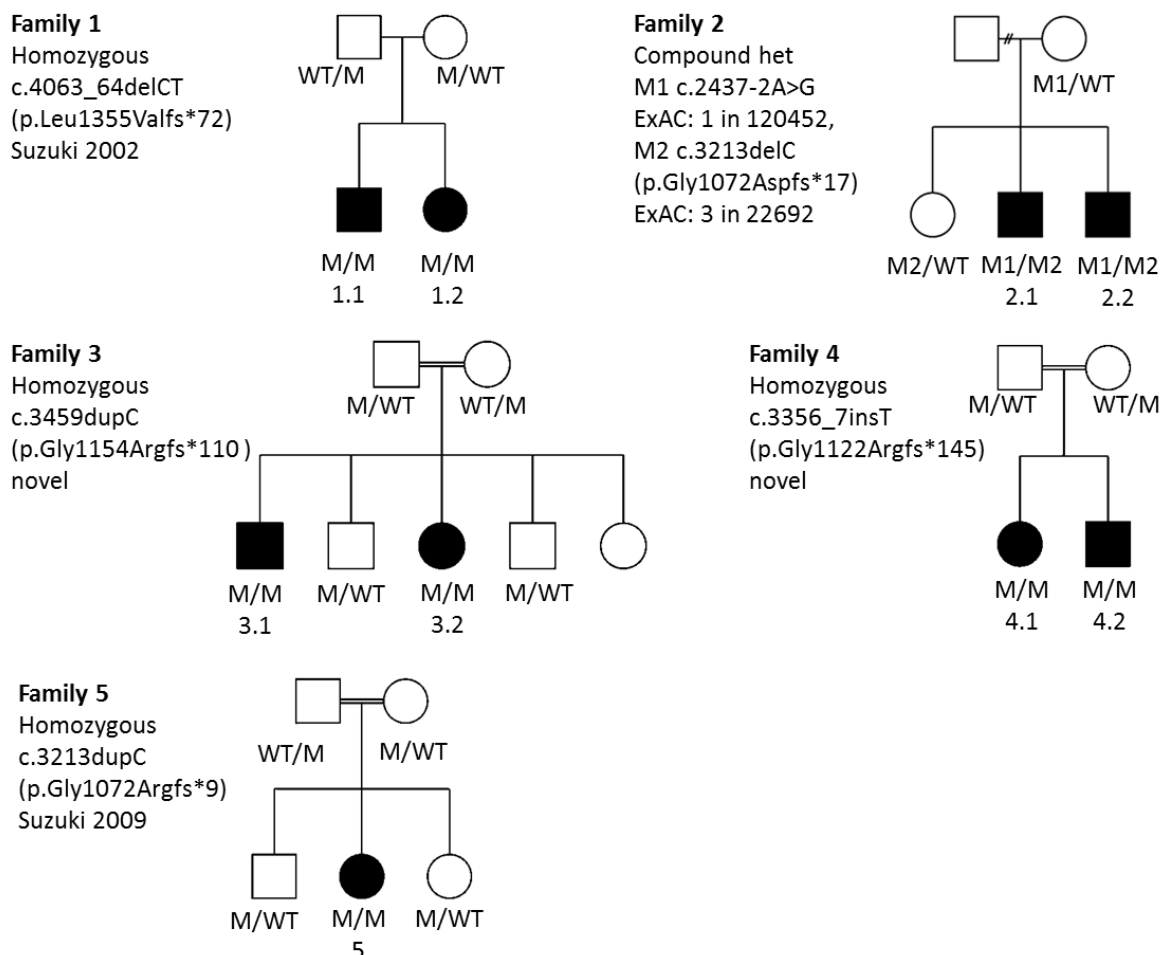


Figure 6-1: Pedigrees and mutation segregation

Patient No./ Gender/ Ethnic origin/ Genetic Database no.	Age at last rv, yrs	Visual acuity, logMAR (Snellen equivalent)	Refraction, under cycloplegia unless otherwise stated	Anterior segment features							Posterior segment features	
				Absent iris crypts	Persistent pupillary membrane	Poor pupillary dilatation	Iris transillumination	Cortical lens opacity	Lens subluxation	Retinal detachment		Macular features
1.1/M Indian GC14449	23	R NPL L CF	R -17.50DS L +1.0 DS (atropine 1998)	+		+					+	R para-central, circumscribed C-R atrophy, L generalised retinal/RPE atrophy
1.2/F	21	R 1.3 (6/120) L PL	R -13.5/-1.00 x180 L +0.75/-1.00 x180 (subjective 2002)	+	+	+						R para-central, circumscribed C-R atrophy, L generalised retinal/RPE atrophy
2.1/M British Caucasian GC19526	14	R 1.9 (6/480) L NPL	R -18.00/-2.00 x15 L +9.00DS		+	+	+				+	Generalized, ill-defined macular C-R atrophy BE
2.2/M	11	R 1.6 (6/240) L 1.4 (6/150)	R -24.00/-2.00 x10 L +3.00/-1.50 x15		+	+	+			+		Para-central well-defined C-R atrophy BE
3.1/M Slovak GC20422	17	R 1.6 (6/240) L 1.4 (6/150)	R +12.00/-2.00 x100 L -10.00/-6.00 x110 (subjective 2014)	+		+		+	+			Para central ill-defined retinal/RPE atrophy BE
3.2/F	11	R 1.2 (6/95) L 1.4 (6/150)	R -20.00/-2.00 x100 L -19.00/-2.00 x180	+		+		+	+			Para-central C-R atrophy, well-defined on R, ill-defined on L
4.1/F Arab GC20693	4	R 2.1 (<6/600) L 2.1 (<6/600)	R -12.00/-2.00 x10 L -12.50 DS									Central, ill-defined C-R atrophy BE
4.2/M	2	R PL L NPL	Not performed						+		+	Central, ill-defined C-R atrophy BE
5/F British Caucasian GC18840	38	R 1.06 (6/75) L 1.06 (6/75)	R -35 DS L -28 DS (pre lens removal)			+	+	+	+			Para-central well-defined deep large C-R atrophy on R, smaller and ill-defined on L

Table 6-2: Key ophthalmic features in Knobloch syndrome

C-R, chorioretinal

Anterior segment abnormalities were present in all patients except patient 4.1, examined at age 4 years (figure 6-2). Abnormalities included poor pupillary dilatation (6 patients), absence of crypts associated with a featureless iris (5 patients), iris transillumination (3 patients) and persistent pupillary membrane (3 patients).

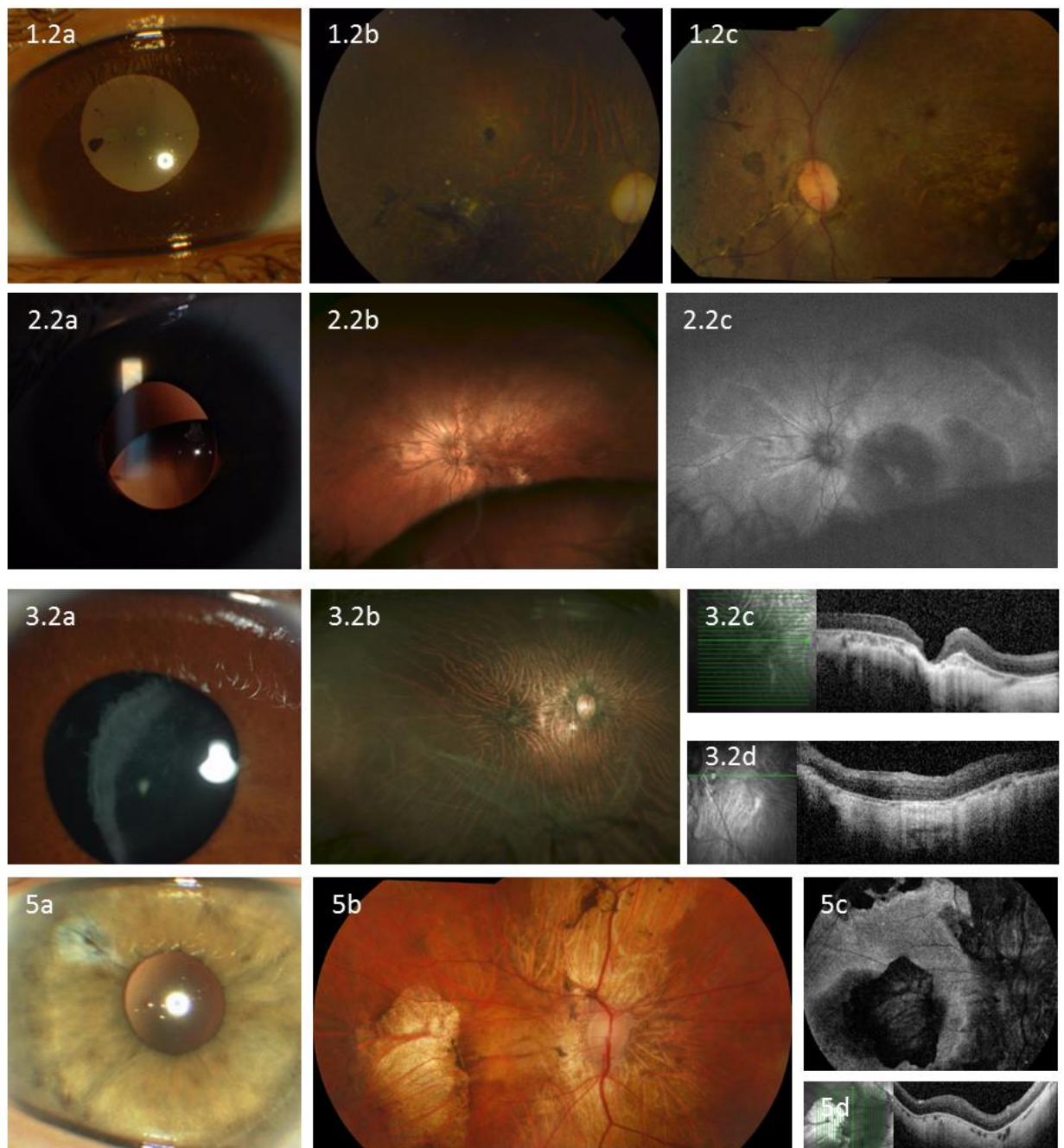


Figure 6-2: Anterior segment and retinal imaging in Knobloch Syndrome.

Patient 1.2, 21 year old female, (a) LE, featureless iris with ectropion uveae and persistent pupillary membranes, (b) RE and (c) LE colour fundus photographs, bilateral macular atrophy and hyperpigmentary change, R tessellated fundus; Patient 2.2, 14 year old male, (a) L inferotemporal lens subluxation (b) L Optos widefield colour and (C) L Optos autofluorescence imaging features of peripapillary atrophy, macula atrophy, tessellated blonde fundi, circumscribed loss of autofluorescence in posterior poles, inferotemporal artefact in fundus image from subluxated disc; Patient 3.2, age 11 years, RE (a) right featureless iris, cortical lens opacity with inferotemporal lens subluxation, (b) left Optos wide-field imaging demonstrating disc pallor, attenuated vessels, thin retina, abnormal collapsed vitreous, (c) R (d) L OCT demonstrating extensive atrophy of outer retina, RPE and choriocapillaris in both eyes; Patient 5, 38 year old female, RE (a) pseudophakia with peripheral laser iridotomy, (b) Topcon fundus photograph demonstrating attenuated vessels, macular and peripapillary atrophy and increased retinal pigment, (c) autofluorescence imaging with reduced autofluorescence corresponding to atrophy and (d) loss of outer retina, RPE and choroid on OCT.

Five patients had cataract with 2 requiring cataract extraction. Three patients had lens subluxation in the inferotemporal direction with patient 5 reported to have lens subluxation prior to cataract extraction. All 3 patients of Northern European origin (families 2 and 5), had iris transillumination with all developing raised intraocular pressure. Glaucomatous disc cupping was identified in one eye of patient 2.1 at age 11 years without lens subluxation. No increased pigment was noted on gonioscopy of patients 2.1 and 2.2. Patient 5, in addition to iris transillumination, had endothelial pigment (Krukenberg spindles), pigment on the lens capsule and heavily pigmented angles on gonioscopy, all consistent with a diagnosis of pigment dispersion syndrome.

All highly myopic eyes had disc pallor, attenuated vessels, a markedly tessellated appearance with prominent choroidal vessels, peripapillary atrophy and occasional pigmented spots (figure 6-2); two eyes had staphylomas. The emmetropic left eyes of patients 1.1 and 1.2 were heavily pigmented. Abnormal vitreous condensations were noted in 6 patients. Macular atrophy was present in all eyes (table 6-2). The atrophy was chorioretinal in most patients, involving outer retina, RPE and choroid. In 10 eyes the atrophy was para-central being well-circumscribed in 6 of 10 eyes; in 8 eyes it was central and ill-defined (figure 6-2). In those patients without central macular atrophy, poor foveal reflexes were noted. Patients 1.1 and 4.2 developed bilateral retinal detachments and patient 2.1 unilateral detachment. OCT scanning of the posterior pole was available in 6 patients. All showed lack of foveal pits, extensive loss of outer retinal structure and in 4 patients, additional atrophy of the RPE and choroid. Fundus autofluorescence imaging, available in 5 patients, demonstrated well-circumscribed loss of posterior pole autofluorescence.

Electroretinography showed cone-rod dysfunction in 14 eyes of 8 patients, and severely reduced/undetectable responses in 4 eyes of 3 patients (figure 6-3). Patients 1.1 and 1.2 at initial testing in 2002 had undetectable ERGs in their emmetropic left eyes with cone more than rod dysfunction in their myopic right eyes. Repeat ERG in 2014 in patient 1.1 showed undetectable ERGs in both eyes, the right eye having developed a total retinal detachment and the left a peripheral shallow detachment only. Repeat ERG in patient 1.2 showed marked deterioration, particularly of cone responses in the right eye, but with stable visual acuity. ERG was undetectable in patient 4.2 who was tested under general anaesthesia with silicone oil in situ in both vitreous cavities.

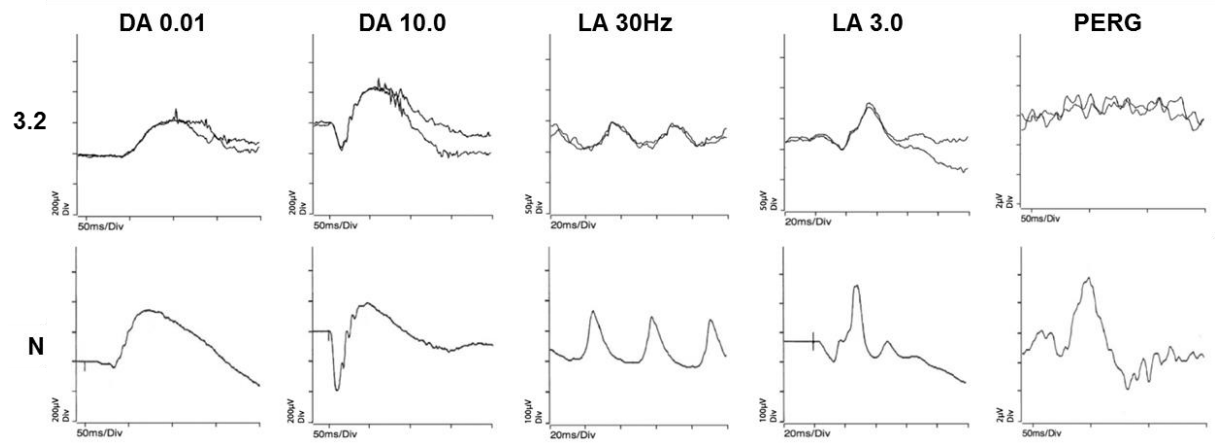


Figure 6-3: Cone-rod dysfunction in Knobloch syndrome

Left eye of patient 3.2 with normal (N) for comparison. Rod specific (DA 0.01) ERG is mildly subnormal; bright flash (DA 11.0) a-wave amplitude is subnormal; cone flicker (LA 30Hz) and single flash (LA 3.0) ERGs are markedly subnormal and delayed (note the differences in calibration compared to the normal); PERG is undetectable.

Neuroradiology was performed in all patients (table 6-3, figure 6-4). Imaging was normal in 2 patients. Four patients had occipital skull defects and only patient 2.2 had occipital encephalocele. Minor abnormalities in 2 patients comprised an occipital subgaleal fat pad and a corticated (covered in cortical bone) small channel in the occipital lobe, possibly representing an atretic encephalocele. Three patients had polymicrogyria. The imaging results differed between siblings in all families except family 4.

Pt no.	Neurological features	Systemic features
1.1	Subgaleal fat pad, polymicrogyria	Epilepsy, developmental delay
1.2	Midline occipital defect, atretic encephalocele, polymicrogyria	None
2.1	Normal	Hypermobile joints
2.2	Resected occipital encephalocele, polymicrogyria	Hypermobile joints
3.1	Midline occipital defect	Learning difficulties
3.2	Occipital lobe corticated channel	None
4.1	Midline occipital defect	Congenital hydronephrosis, hypermobile joints
4.2	Midline occipital defect	Hypermobile joints
5	Normal	Unilateral duplex kidney/bifid ureter, hamstring sarcoma

Table 6-3: Neuroradiological and systemic features

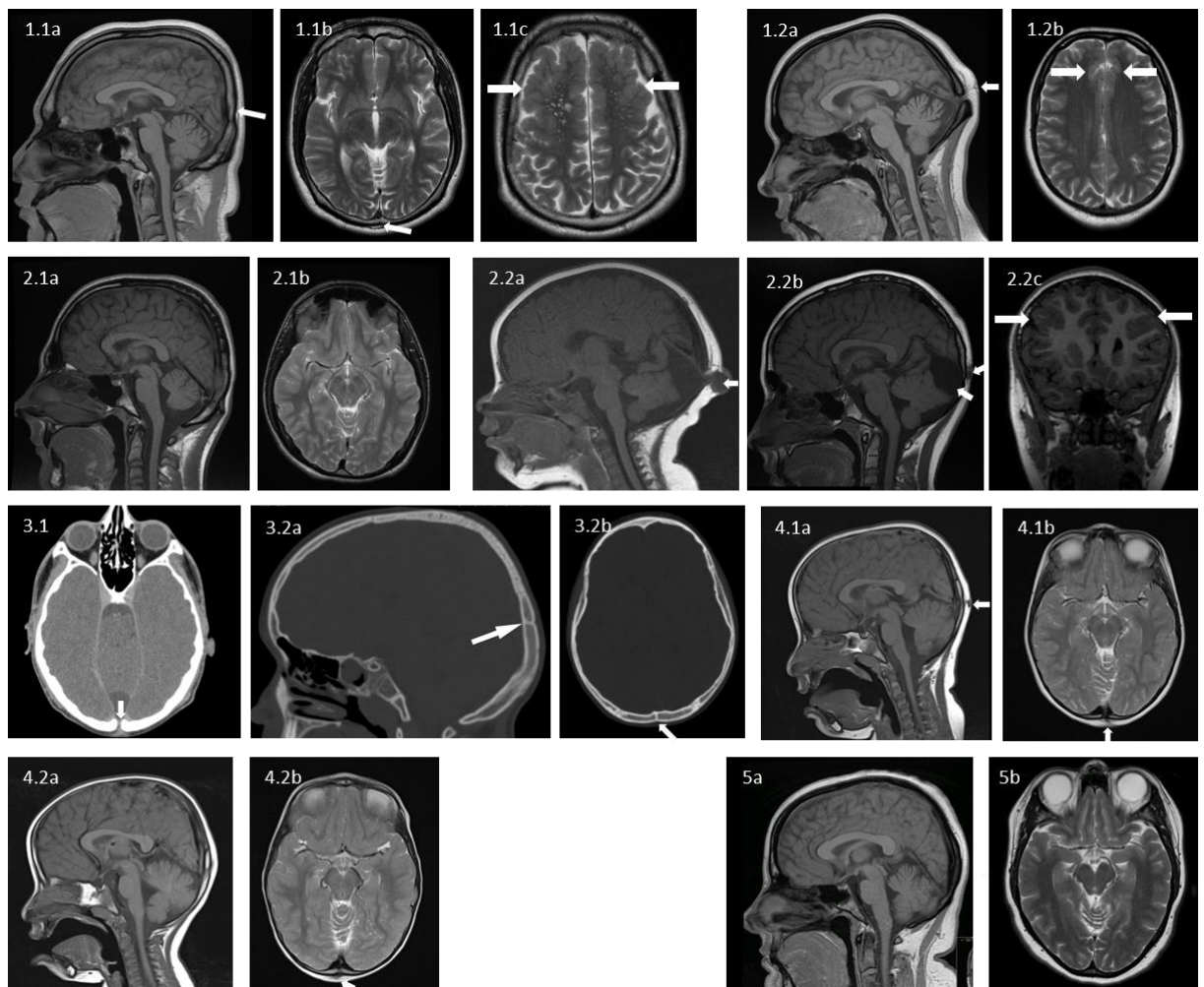


Figure 6-4: Neuroradiological findings in Knobloch syndrome

Intracranial sagittal and coronal T1- and axial T2- weighted MRI acquisitions of patients 1.1, 1.2, 2.1, 2.2, and 4.1 as well as CT of patient 3.2. Patient 1.1 (a), (b), subgaleal fat pad (arrowed) overlying occipital bone, (c) extensive bifrontal polymicrogyria (arrowed); Patient 1.2 (a) small occipital bone defect (arrowed) with atretic encephalocele/meningocele, (b) medial bifrontal polymicrogyria (arrowed); Patient 2.1 (a) and (b) no abnormalities; Patient 2.2 (a) MRI aged 6 months with occipital encephalocele (arrowed), (b) MRI aged 11 years occipital scarring and retained retrocerebellar arachnoid cyst at site of previous surgery (arrowed), (c) MRI aged 11 years bilateral inferior frontal polymicrogyria (arrowed); Patient 3.1, midline occipital bony defect above occipital protuberance (arrowed); Patient 3.2 (a) small, well corticated channel in the midline of the occipital lobe (arrowed); Patient 4.1 (a) small bony occipital defect (arrowed) with meningeal tissue communicating to subcutaneous tissue through the defect; Patient 4.2 (a), (b) small bony occipital defect (arrowed) with fibrous band extending from meningeal lining to subcutaneous tissue; Patient 5 (a) and (b) no abnormalities.

Cutaneous occipital abnormalities were present in 4 patients including a palpable swelling, alopecia and a patch of white hair. Systemic abnormalities included learning difficulties, epilepsy, congenital hydronephrosis from a ureteric abnormality and duplex kidney with bifid ureters in patient 5 who additionally had undergone treatment for a hamstring sarcoma.

Bi-allelic variants in *COL18A1* predicted to be pathogenic were identified in all 5 families. Segregation was confirmed in available family members (figure 6-1).

Two novel mutations were identified with a further 3 mutations not previously reported in an affected patient but found at a very low mean allele frequency in the ExAC database (figure 6-1). Six mutations, 5 that create PTCs and a splice site mutation were identified in total. The splice site mutation, c.2437-2 A>G, very rare on ExAC (1 in 120452), disrupts the canonical acceptor site for exon 17. WES on patient 5 also identified a missense homozygous variant in *RPGRIP1* c.3064C>T, p.Leu1022Phe (rs367899074) which also segregated with disease in the family. This was not thought to be causative based on predicted tolerance *in silico* (SIFT score 0.7, Polyphen2 score 0.049), phenotype of the patient in particular the anterior segment abnormalities and due to the identified *COL18A1* variant having been previously reported in 3 families with Knobloch syndrome.^{290, 291} Variant c.3213delC (p.Gly1072Aspfs*17) identified in family 2 was reported at an allele frequency of 0.004 on EVS, but this appears to be an artefact. It was absent in 1000genomes and dbSNP, and on contacting the EVS team, the area had poor coverage and the results were most likely spurious. Subsequently, the ExAC database was released in which the variant has an allele frequency of 3 in 22692 but with only a relatively small number of individuals covered. Finally, the variant was found in a single allele only of a control group of 2000 exomes (UCL consortium).

6.4 Discussion

The classical description of Knobloch syndrome includes myopia, retinal detachment and occipital encephalocele, but more recent publications have described an increasingly variable ocular and systemic phenotype.^{275, 280, 291} This series with detailed retinal imaging, ERGs and neuroradiology in all patients, has allowed a detailed assessment of the clinical phenotype.

All patients presented in infancy with nystagmus and had high myopia in at least 1 eye. Three patients had inferotemporal lens subluxation consistent with a previous report.²⁷⁵ Iris abnormalities were also common. Absence of iris crypts and a single case of iris atrophy have been described previously.^{273-275, 291} In a knockout mouse model *COL18a1*^{-/-}, there was disruption of the posterior iris pigment epithelial cell layer and release of melanin granules that resembled the human pigment dispersion syndrome.²⁹² Three patients in this series had clinical features of pigment dispersion syndrome with 1 associated glaucoma.²⁹³ This suggests potential increased risk of pigmentary glaucoma in Caucasian patients with Knobloch syndrome.

Many of the retinal changes noted in this series are consistent with high myopia and are not specific to the syndrome.²⁹⁴ These include peripapillary atrophy and the tessellated fundus appearance with prominent choroidal vessels. Although vitreous

abnormalities are seen in high myopia, the collapsed abnormal vitreous present in these patients from a young age may relate to the underlying disorder. Macular atrophy was identified in all patients. This can also occur in high myopia with diffuse atrophy or focal areas of atrophy; the latter shown to develop in the 5th decade in a large natural history study.²⁹⁵ The young age of the present patients suggest the atrophic lesions, are likely to be a consequence of mutations in *COL18A1*. Macular atrophic lesions and abnormal vitreous condensations have been previously reported and may be key features of the disorder.^{275, 277, 291}

Previous electrophysiology reports in Knobloch syndrome are limited; delayed and depressed photopic and scotopic ERGs were reported in 2 children in one report but few details on technique or amplitude of responses were given; an undetectable ERG was described in one patient in another report.^{275, 276} This series with detailed electrophysiology of all affected patients, demonstrates both cone and rod dysfunction. Repeat ERG in patient 1.2 showed deterioration but with stable visual acuity. It therefore remains unclear whether this disorder represents a progressive dystrophy of photoreceptors or a stable dysfunction but progression, if present, appears asymptomatic and slow. In our patients with long term follow up, there was little deterioration in visual acuity unless complicated by retinal detachment.

COL18A1 encodes collagen alpha-1(XVIII) chain, highly expressed throughout the human eye including the iris, ciliary body, trabecular meshwork, Schlemm's canal, the inner limiting membrane (ILM), retinal vessels, basement membrane of the retinal pigment epithelium (RPE) and Bruch's membrane but not in photoreceptors.²⁸⁸ The ILM and vitreous body are important regulators of eye size in a chick embryo model with disruption of these structures leading to eye enlargement. This could explain the high myopia seen in Knobloch syndrome as evidenced by the high axial length measured in the myopic eyes of family 1.²⁹⁶ In mice, lack of ColXVIII causes abnormal vitreous separation, consistent with the abnormal vitreous and retinal detachment found in human disease.²⁹⁷ The underlying pathogenesis of photoreceptor dysfunction is not clear from animal models but the abnormal Bruch's membrane, RPE and ILM would be predicted to have secondary effects on the photoreceptors.²⁹⁷ Alternatively the distribution and function of ColXVIII may differ in the human eye.

Occipital encephalocele/meningocele is reported to be common in Knobloch syndrome but was only identified in one patient in this series.²⁹⁸ Normal neuroimaging has previously been reported in 2 patients; the additional minor abnormality of a subgaleal fat pad is a novel observation.^{277, 282} Four patients had externally observable occipital findings, ranging from soft tissue swellings to hair abnormalities, emphasising the importance of occipital scalp examination if Knobloch syndrome is suspected. In one

patient, a cutaneous scalp abnormality was identified in the absence of neuroradiological abnormality. This has been previously reported in a single patient; usually there is an associated neuroradiological abnormality when scalp defects are present.^{277, 280, 282, 283, 299} Polymicrogyria was identified on MRI in 3 patients (1.1, 1.2 and 2.2); a feature now reported in several Knobloch patients.^{273, 278-280}

Type 18 collagen is found in many different tissues and it is unsurprising that mutations in *COL18A1* may result in a varied systemic phenotype. Systemic associations in the present series include epilepsy, learning difficulties, congenital hydronephrosis and unilateral duplex kidney with bifid ureter. There are several reports of epilepsy in Knobloch.^{275, 277, 280, 284, 291, 300} Renal abnormalities in Knobloch are unusual with 2 previous reports of congenital duplex kidney and bifid ureter.^{272, 283} Sarcoma, present in one subject, has not been previously reported in Knobloch syndrome although there has been one case of acute lymphoblastic leukemia.²⁹⁹ Those reports and the present series highlight the importance of systemic assessment.

COL18A1 consists of 43 exons with 3 main alternate isoforms produced.^{287, 301} There have been 22 previously reported, likely pathogenic mutations in *COL18A1* leading to recessively inherited disease, 17 of which lead to PTCs, 2 large deletions encompassing at least a whole exon and 3 splice site mutations, which may indicate that this syndrome represents a null phenotype (table 6-4). The c.4063_4064delCT mutation is the most common, found in a total of 14 families to date.^{279, 280, 284, 290, 291, 299, 300, 302} The diverse ethnic origins of the reported families include Indian, Brazilian, North American, Saudi, Irish, Pakistani and Turkish in keeping with a mutational hotspot not a founder effect. A further 4 disease causing mutations were identified in the current series.

Knobloch syndrome is a systemic disorder with variable neurological involvement and severe visual impairment from early childhood. It may be undiagnosed without careful examination of the anterior segment and awareness of the potential lack of scalp and/or intracranial occipital abnormalities. The diagnosis might be considered in any patient with infantile onset high myopia, developmental abnormalities of the anterior segment and evidence of cone-rod dysfunction on ERG. A timely diagnosis not only ensures that patients are aware of the potential complications of the disorder, such as lens subluxation, retinal detachment and glaucoma, but may facilitate targeted molecular sequencing and informed genetic counselling.

	Mutation NM_030582.3 (AF18081)	Mutation NM_130445.2 (AF18082)	Exon no of 43	Reported papers, (no of families)
1	In 5' UTR (-50,112 nucleotides)	c.12-2A>T	Intron 1	Sertie 2000 ²⁸⁶ Suzuki 2002 ²⁸⁴
2	c.895delG (p.Val299Serfs*)	c.355delG p.Val119Serfs*5	4	Aldahmesh 2011 ³⁰⁰
3	c.1469-2A>G	c.929-2A>G	Intron 7	Suzuki 2009 ²⁹⁰
4	c.1604insC p.Gly538Argfs*55	c.1064insC p.Gly355Argfs*55	9	Caglayan 2014 ²⁸⁰
5	c.1761_2054del, p.Asp589_Gly686del	c.1221_1514del, p.Asp409_Gly506del	9-14	Aldahmesh 2013 ²⁹¹
6	c.1778-9insA p.Asp593Glufs*58	c.1238-1239insA, p.Asp413Glufs*58	10	Suzuki 2002 ²⁸⁴
7	c.2325_2326delCCinsA, p.Pro777Leufs*127	c.1785_1786delCCinsA p.Pro597Leufs*127	17	Aldahmesh 2011 ³⁰⁰
8	c.2416C>T (p.Arg806*)	c.1876C>T (p.Arg626*)	18	Passos-Bueno 2006 ²⁹⁸ Williams 2008 ²⁸³
9	c.2645delT p.Leu882Profs*22	c.2105delT p.Leu702Profs*22	23	Suzuki 2002 ²⁸⁴
10	c.2658dupC p.Gly887Argfs*23	c.2118dupC p.Gly707Argfs*23	23	Aldahmesh 2013 ²⁹¹
11	c.2797C>T p.Arg933*	c.2257C>T p.Arg753*	26	Aldahmesh 2013 ²⁹¹
12	c.3213dupC (p.Gly1072Argfs*9)	c.2673dupC (p.Gly892Argfs*9)	33	Suzuki 2009 ²⁹⁰ (2) Aldahmesh 2013 ²⁹¹
13	c.3283C>T (p.Arg1095*)	c.2743C>T (p.Arg915*)	35	Aldahmesh 2011 ³⁰⁰ (2)
14	c.3363_3364insC, (p.Gly1122Argfs*32)	c.2823_2824insC, (p.Gly942Argfs*32)	35	Menzel 2004 ²⁸²
15	c.3364_3371delGGCCCCC (p.Gly1125Argfs*142)	c.2824_2831delGGCCCCC (p.Gly945Argfs*142)	35	Suzuki 2009 ²⁹⁰
16	c.3509-3518delCAGGGCCCCC (p.Pro1170Glnfs*38)	c.2969-2978delCAGGGCCCCC (p.Pro990Glnfs*38)	36	Suzuki 2002 ²⁸⁴
17	c.3544+3A >C	c.3004+3A>C	Intron 36	Keren 2007 ²⁷⁸
18	c.3811C>T (p.Gln1273*)	c.3271C>T (p.Gln1091*) c.3277C>T reported	40	Suzuki 2002 ²⁸⁴
19	delEx41	delEx41	41	Suzuki 2009 ²⁹⁰
20	c.4063_4064delCT (p.Leu1355Valfs*72) reported as c.4054-4055delCT (p.Leu1352Valfs*72)	c.3523-3524delCT (p.Leu1175Valfs*72)	41	Suzuki 2002 (3) ²⁸⁴ , Paisan- Ruiz 2008 ²⁷⁹ , Suzuki 2009 ²⁹⁰ , Joyce 2010 ³⁰² , Mahajan 2010 ²⁹⁹ , Aldahmesh 2011 ³⁰⁰ , Aldahmesh 2013 (3) ²⁹¹ , Caglayan 2014 (2) ²⁸⁰
21	c.4374_4387del (p.Ser1459Alafs*9)	c.3834_3847del (p.Ser1279Alafs*9) reported as p.Ser1276Alafs*9	43	Haghighi 2014 ²⁷⁶
22	c.4494_4497insTGCC (p.Ala1499Cysfs*14)	c.3954_3957insTGCC (p.Ala1319Cysfs*14)	43	Caglayan 2014 ²⁸⁰

Table 6-4: Previously reported mutations in COL18A1

7 Preserved visual function in retinal dystrophy due to hypomorphic *RPE65* mutations

7.1 Introduction

RPE65 (Retinal Pigment Epithelium-Specific Protein, MIM# 180069), located on 1p31.3-p31.2, encodes a retina-specific, 65kD visual cycle protein, retinoid isomerohydrolase, a vital component of the visual cycle.⁴² Recessive mutations in *RPE65* are associated with severe EORD including LCA and account for approximately 11% of early onset RCD.^{43, 44} Patients usually present in infancy or early childhood with reduced central vision, with or without nystagmus. Nyctalopia is a prominent feature and some patients also demonstrate photoattraction.³⁰³ Myopia is found in at least half of patients.³⁰⁴ Visual acuity, although significantly reduced in childhood is usually sufficient to enable a sighted education.^{303, 305} The fundus appearance is usually normal in infancy but small subretinal white dots may appear later in childhood, possibly as a result of abnormal accumulation of retinyl esters.^{53, 306} Retinal imaging reveals a variable thinning of the outer nuclear layer on OCT and a characteristically low signal on FAF imaging.¹⁰¹ Electrophysiology demonstrates absent rod function but there may be residual cone function in childhood.³⁰⁵ This may reflect the alternative source of 11-*cis* retinol that cones obtain from Müller cells.³¹ Gene therapy trials using subretinally administered recombinant adeno-associated viral vectors expressing *RPE65* have so far achieved promising, albeit largely unsustainable improvements in retinal function.³⁰⁷⁻³⁰⁹

Recessive *RPE65* related disease may present atypically with mild phenotypes due to presumed hypomorphic alleles; a single patient with a fundus albipunctatus phenotype has also been reported.^{8, 303, 310-312} Dominant disease resembling choroideraemia with variable penetrance has also been reported in 2 families.⁸ I identified 4 patients (4 families) who were known to have early onset retinal dystrophy with preserved visual function in to adulthood. Molecular screening including *RPE65* had already been performed and likely pathogenic variants identified. This group of patients were further analysed and the underlying molecular mechanisms explored in this study.

7.2 Methods

7.2.1 Ascertainment of patients

Patients had been recruited from the inherited retinal clinics of Moorfields based on a diagnosis of EORD. Molecular screening had been completed by colleagues prior to

my investigation of the patients. Proband 1 and 2 with some features of retinal dystrophy due to *RPE65*, but better visual acuity than previously reported, were screened for *RPE65* mutations by Sanger sequencing. Subsequent to the discovery of a putative hypomorphic allele (p.Arg515Trp) in patient 2 and the finding of the same allele in a previous report, a panel of 190 unrelated probands with adult-onset recessive RCD were Sanger sequenced for exon 14 of *RPE65*.³¹¹ This yielded one further proband (patient 3), heterozygous for this mutation. Sanger sequencing of all exons and intron-exon boundaries was undertaken in this patient to determine a second allele. Finally, Sanger sequencing of *RPE65* was performed in patient 4, with a retinal appearance similar to fundus albipunctatus, following a report of this phenotypic appearance being associated with *RPE65*; mutations in both *RLBP1* and *RDH5* had already been excluded.³¹³ Segregation to establish bi-allelic mutations was not possible for families 2 and 3 in whom family DNA was unavailable.

7.2.2 Clinical assessment

Each patient had undergone full clinical examination by one of my supervisors within the retinal genetics clinics. Electroretinography was obtained in 3 patients using gold foil electrodes to incorporate the ISCEV standards; ERG recording in patient 3 was performed elsewhere at age 3 years with surface electrodes. Suprathreshold binocular (driving) Esterman visual fields and unioocular Humphrey 24-2 and 30-2 threshold visual fields were performed using the Humphrey Field Analyzer II (Carl Zeiss Meditec AG).

A control group of 5 patients with typical *RPE65* related early onset retinal dystrophy, and a recorded visual acuity age 18 years, were selected from the genetics database in order to statistically compare the median visual acuities in the better eye between the hypomorphic group and the control group. Statistical analysis was performed using IBM® SPSS® Statistics version 22.

7.2.3 Molecular investigations

Molecular screening had been performed as described above and the identified variants further analysed as part of this study. Mutation nomenclature was assigned in accordance with GenBank Accession number NM_000329.2. Protein modelling of the crystalline structure of RPE65 was performed using Visual Molecular Dynamics with Protein Data Bank number 4F3A.³¹⁴ Mutations were plotted on this model including hypomorphic mutations from this paper, previously reported hypomorphic mutations, and non-hypomorphic missense mutations in order to investigate any potential pattern for position of mutations.

7.3 Results

Four patients from 4 families were investigated (figure 7-1). Clinical data are summarised in table 7-1.

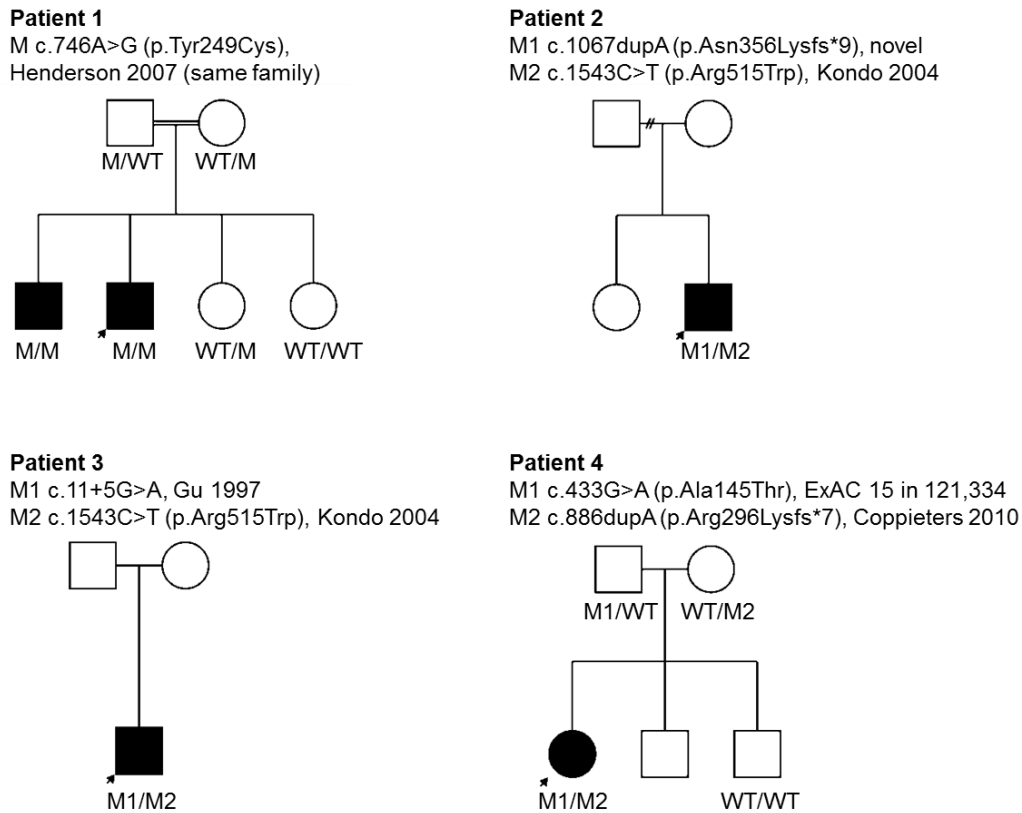


Figure 7-1: Pedigrees and segregation of *RPE65* variants

Patient 1 presented with mild nyctalopia without nystagmus in early childhood; there was no subjective deterioration over time. VA was 0.2 logMAR each eye at age 13 years, R 0.2 logMAR and L 0.3 logMAR at age 22 years with a highly myopic correction. Fundus examination demonstrated myopic changes with peripapillary atrophy and visible choroidal vasculature. There were a few white dots in the posterior pole and extensive granularity of the retinal mid-periphery that had a white flecked appearance. OCT imaging revealed a normal ISe band at the macula with para-foveal disruption and temporal retinal thinning in both eyes consequent upon thinning of the ONL (figure 7-2). On FAF imaging, there was generalised hypofluorescence with irregular almost radial bands of relative hyperfluorescence in the macula which did not correspond to the disrupted ISe band on OCT. Binocular Esterman visual fields age 18 years were full except for an extreme left scotoma outside 70 degrees eccentricity (figure 7-3). Unocular 24-2 Humphrey visual fields age 22 years demonstrated central scotoma. ERG at age 13 years showed generalized retinal dysfunction, with cone ERGs more affected than rod ERGs (figure 7-4). PERG showed marked macular involvement. Repeat ERG age 20 years demonstrated no deterioration.

Pt, (gender) family	Age onset (yrs)	Age last rv (yrs)	Length f-up (yrs)	Fundus	Age at last EDTs, key findings	Latest VA, logMAR (Snellen) and refractive error	Other findings
Pt 1 (m) GC16768	2	22	9	Peripheral small white dots level of RPE, later mid-peripheral RPE atrophy	19 yrs: cone-rod dysfunction; marked macular involvement; no deterioration over 7 yrs	R 0.2 (6/9.5) L 0.3 (6/12) R -15.50/-3.50 x169 L -16.50/-3.75 x30	Binocular Esterman visual fields well-preserved age 18, Humphrey 24-2 central scotoma age 22
Pt 2 (m) GC14577	3	19	0	Mild peripheral RPE hypopigmentation	17 yrs: rod-cone dysfunction with severe macular involvement	R 0.0 (6/6) L 0.0 (6/6) R -0.50/-3.00 x175 L -0.50/-3.25 x175	Minimal exophoria with good recovery Binocular Esterman fields well-preserved age 17
Pt 3 (m) GC130	3	35	13	Widespread pigmentary change with attenuated vessels, pale discs	3 yrs: severe generalised rod-cone dysfunction	R CF L 1.0 (6/60) Myopic	Central visual loss in 20's
Pt 4 (f) GC15862	7	26	15	Extensive round white-yellow dots	26 yrs: rod-cone dysfunction, partial recovery after prolonged dark adaptation; mild worsening of rod function and PERG over 12 yrs	R 0.0 (6/6) L 0.1 (6/7.5) R -4.50 DS L +1.00/-1.25	Intermittent left exotropia Ishihara age 22, 17/17 each eye, age 26, R 12/17 L 16/17 Binocular Esterman fields full age 18, Humphrey 30-2 age 26 paracentral scotomas

Table 7-1: Summary of clinical data

Patient 2 presented with mild nyctalopia and photophilia before the age of 5 years with no nystagmus and no deterioration in symptoms over time. When reviewed, age 18 years, VA was 0.0 logMAR in each eye with low myopic correction. Fundus examination revealed mild mid-peripheral RPE hypopigmentation and white dots. Time-domain OCT demonstrated a normal ISe band throughout the macula. There was a ring of relatively increased autofluorescence in the macula on FAF imaging with the background signal otherwise markedly reduced. This ring did not correspond to any ISe band abnormalities on OCT and as such likely represents relative preservation of normal autofluorescence rather than abnormally increased autofluorescence. Binocular Esterman visual fields were full age 17 years except for bilateral extreme scotoma outside of 70 degrees eccentricity (figure 7-3). ERG demonstrated undetectable rod responses but small cone responses in keeping with a RCD. PERG was undetectable indicating severe macular involvement (figure 7-4).

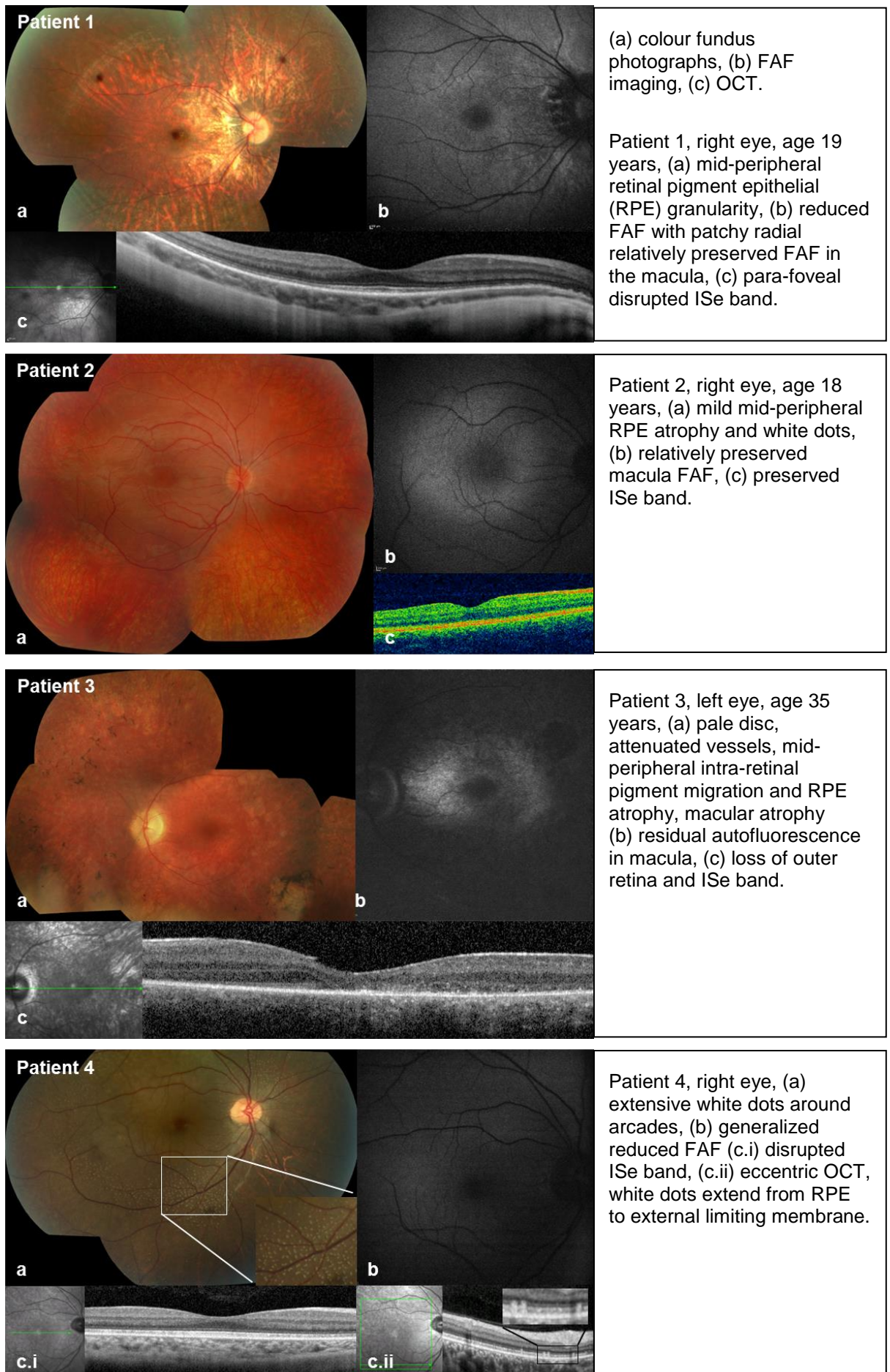


Figure 7-2: Retinal imaging in hypomorphic *RPE65* related dystrophy

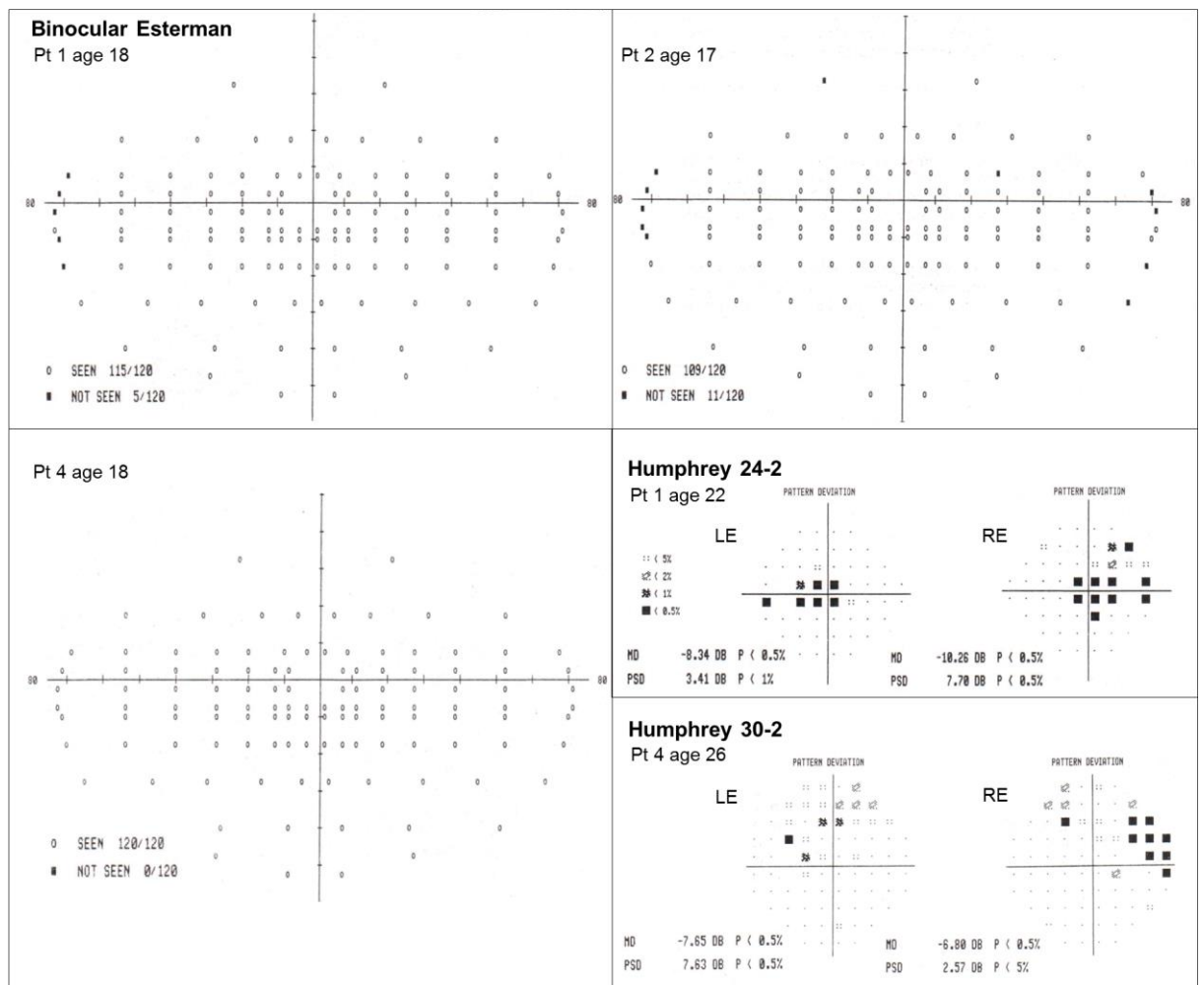


Figure 7-3: Visual fields for patients 1, 2 and 4

Binocular Esterman suprathreshold fields and Humphrey uniocular threshold fields: patient 1, well-preserved Esterman field age 18 years, central scotoma on uniocular Humphrey 24-2 age 22 years; patient 2 well-preserved Esterman field age 17 years; patient 4 well-preserved Esterman field age 18 years, arcuate defects on uniocular Humphrey 30-2 age 26 years.

The third patient also described nyctalopia at a young age with reported good visual acuity into his 20s and onset of central blur from his late 20's only. Visual acuity age 30 was R 0.6 logMAR and L 1.0 logMAR but at last review age 44 was R HM, L CF with irregular nystagmoid like movements. On fundus examination, there was disc pallor, attenuated vessels, mid-peripheral intraretinal pigment migration, and RPE atrophy of both macula and mid-periphery (figure 7-2). There was loss of the ISe band and outer retina on OCT particularly centrally and temporally. FAF imaging demonstrated loss of autofluorescence para-foveally and throughout the peripheral retina with a ring of preserved autofluorescence in the macula. ERG age 3 years was reported to demonstrate severe rod-cone dysfunction (performed elsewhere).

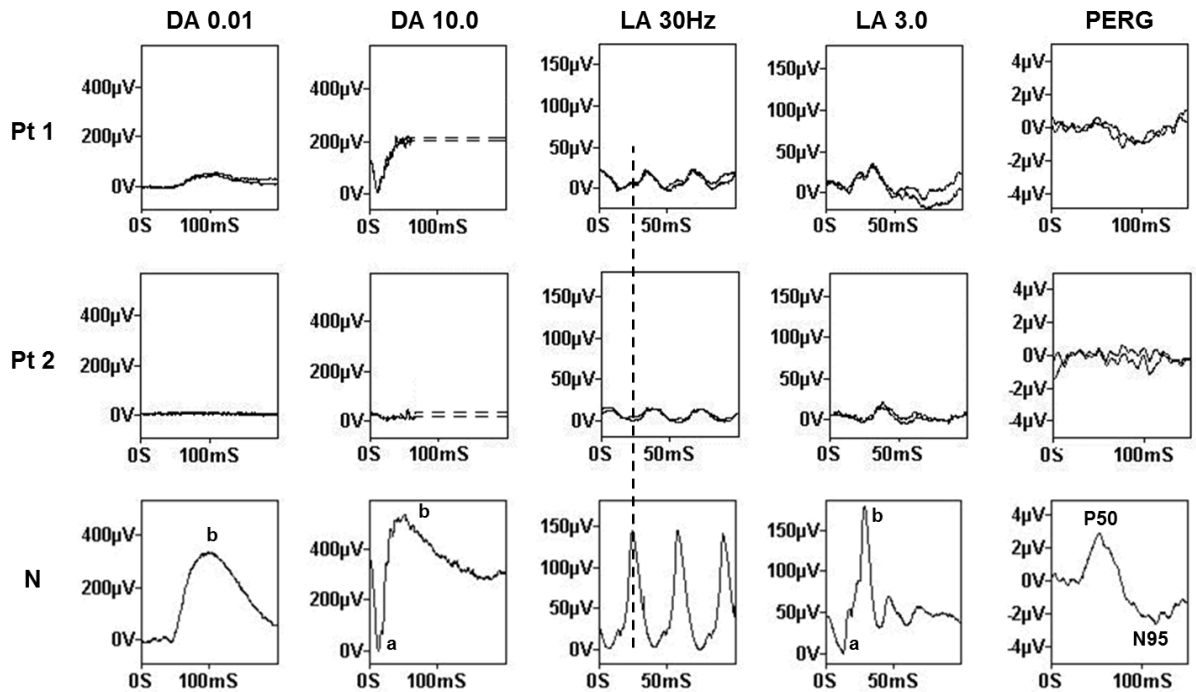


Figure 7-4: Electrophysiology for patients 1 and 2.

RE of patients 1 (age 19 years) and 2 (age 18 years) with N for comparison: patient 1 rod specific ERG (DA 0.01) markedly subnormal with DA 11.0 moderately subnormal, cone specific (LA 30Hz and LA 3.0) markedly delayed and subnormal, PERG markedly subnormal, in keeping with a CORD of moderate severity; patient 2 undetectable rod function with markedly delayed and subnormal cone responses and undetectable PERG, in keeping with a RCD.

Patient 4 presented with nyctalopia at age 7 years but no nystagmus. Visual acuity was R 0.0 logMAR and L 0.1 logMAR at last review age 26 years with deterioration of nyctalopia and colour vision. Fundus examination revealed widespread discrete white dots both round and ovoid in shape throughout the mid-periphery of both eyes predominantly around the arcades reminiscent of fundus albipunctatus (figure 7-2). The number and distribution of the dots remained stable over 12 years of imaging although occasional dots were observed to fade in size. On OCT the white dots extended from the RPE to the level of the ELM. The ISe band was disrupted but present throughout the macula. FAF imaging demonstrated generalised reduction of autofluorescence with a discrete area of further reduction infero-nasal to the optic disc in the right eye only, suggestive of RPE atrophy (55 degree FAF imaging, not shown). The white dots were not hyperautofluorescent. Binocular Esterman visual field age 18 years was full (figure 7-3). Unocular, Humphrey 30-2 visual fields age 26 years demonstrated paracentral scotoma in both eyes with MD -7.65 DB right and -6.80 DB left. Electrophysiology age 21 years demonstrated a generalised rod more than cone pattern of abnormality with severe rod-system dysfunction (figure 7-5). There was some recovery of rod-dominated ERGs after prolonged dark adaptation but they did not normalise. The ERG showed mild worsening of rod function over 12 years of testing. PERG was normal age 15 years with deterioration indicating macular dysfunction evident at age 21 years.

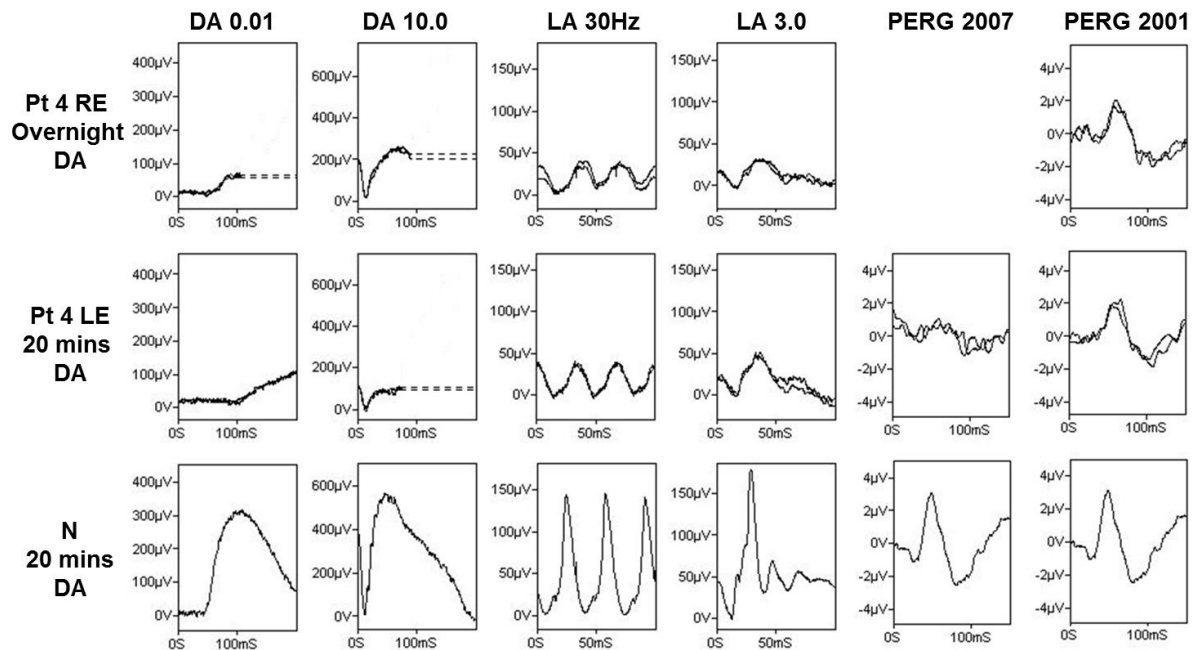


Figure 7-5: Electrophysiology for patient 4

RE (dark adapted, DA, overnight) and left eye (LE, DA for 20 minutes) of patient 4 (age 27 years) with N for comparison (DA 20 minutes); rod specific ERG is detectable from the RE but not from the LE, cone specific responses are profoundly reduced and delayed with the PERG from the LE markedly subnormal, PERG age 15 years normal both eyes. Findings are in keeping with marked retinal dysfunction of both rod and cones with partial recovery of rod function after prolonged dark adaptation.

Molecular screening of *RPE65* in the first patient identified a homozygous variant in *RPE65*, c.746A>G (p.Tyr249Cys), predicted to be damaging *in silico*. This patient's molecular result has been previously reported.³¹⁵ Segregation was confirmed in the family with an affected brother (unavailable for clinical assessment) also homozygous for this variant and their parents and sisters heterozygous. Two mutations in *RPE65* were found in the second patient; c.1067dupA (p.Asn365Lysfs*9), a novel PTC, and c.1543C>T (p.Arg515Trp) which has been previously reported as a hypomorphic allele.³¹¹ This allele was also identified in patient 3 as well as a second mutation, c.11+5G>A, previously reported as one of the commonest variants found in *RPE65* related disease.³⁰³ Screening of *RPE65* in patient 4 identified compound heterozygous mutations, c.433G>A (p.Ala145Thr, paternal), not previously associated with disease, predicted to be tolerated *in silico* (SIFT 0.13, Polyphen2 0.41) and found in 15 of 121,334 alleles on ExAC and c.886dupA (p.Arg296Lysfs*7, maternal) which has been previously reported.³¹⁶

Two groups were assessed for a significant difference in visual acuities at age 18 years, the first comprising patients 1,2 and 4 (VA age 18 unavailable for patient 3) and the second group of 5 molecularly proven *RPE65* patients without known hypomorphic alleles. A comparison of the median visual acuity of the two groups was made, and

A review of a further 26 molecularly-confirmed *RPE65* families attending the clinics found no other cases harbouring the missense changes reported here. Analysis of the conservation of missense residues throughout a broad range of vertebrate and invertebrate classes was performed with Clustal Omega; all arose in completely conserved residues (figure 7-7).

Assessment of the position of mutations on the 3 dimensional crystalline structure of RPE65 did not demonstrate an observable difference between hypomorphic and non-hypomorphic residues (figure 7-8).

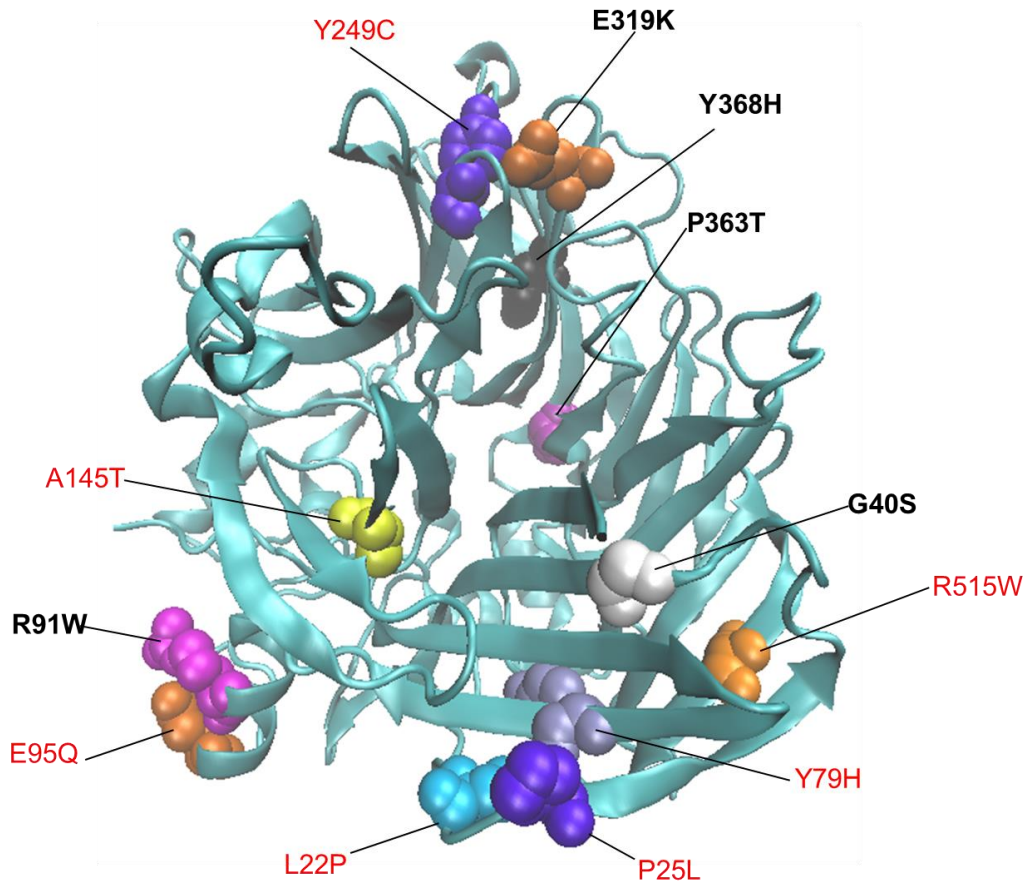


Figure 7-8: Crystalline structure of RPE65 labelled with mutations

Hypomorphic missense mutations both from this series and previously reported (red), and non-hypomorphic missense mutations (black). This image was made with VMD software support and PDB number 4F3A.

7.4 Discussion

Although the majority of patients with mutations in *RPE65* have severe visual impairment, this series of 4 patients with *RPE65* mutations have good visual acuity and preserved visual fields into adulthood. Compared to other patients with typical *RPE65* related EORD, visual acuity is statistically better at age 18 years.

Four hypomorphic patients with homozygous or compound heterozygous missense mutations in *RPE65* have previously been reported with nyctalopia from early childhood, but normal visual acuity until 6 to 24 years.^{303, 310-312} The first with reduced central vision in the 2nd decade carried 2 missense variants, p.Leu22Pro and p.His68Tyr.³¹² He had end-stage disease with a barely detectable photopic ERG and undetectable scotopic ERGs when examined age 40 years. The 2nd was still able to read age 40 years and had 2 missense variants, p.Tyr79His and p.Glu95Gln; no further information was given on the retinal appearance or ERG.³⁰³ The 3rd homozygous for p.Arg515Trp, developed central vision loss age 24 years and had end-stage disease with an undetectable ERG when examined age 54 years.³¹¹ The 4th homozygous for p.Pro25Leu had good visual acuity when last reviewed at age 7 years.³¹⁰ He had blonde fundi, residual rod function and relatively well preserved cone function on ERG and a low but detectable FAF. Apart from the 4th report, limited phenotypic data have been published.

In contrast, the patients reported herein had detailed phenotyping of both retinal structure and function. All patients had good visual acuity until at least age 19 years, with only mild visual field loss. Three have lengthy follow-up with evidence of a slow but definite progression based on visual acuity (patients 1 and 3), colour vision testing (patient 4) and ERG/PERG (patient 4). Patients 1 and 2 had minimal fundus changes at last review, similar to the previously reported young patient. In contrast, patient 3 showed the typical features of advanced photoreceptor degeneration age 35 years similar to the end-stage disease in 2 previously reported patients.³¹⁰⁻³¹² OCT imaging in patients 1, 2 and 4 demonstrated preserved para-foveal retinal thickness and minimally disrupted or intact ISe band; in patient 3 with advanced disease the OCT was markedly thinned.³¹⁷ Fundus autofluorescence was reduced but detectable in all patients.³¹⁰

Most patients with *RPE65* deficiency have undetectable rod function on ERG but may have residual cone function until late in the disease.³¹⁸ Patient 2 had absent rod function but patients 1 and 4 had residual rod function in keeping with milder disease with similarities to the previously reported 7 year old patient.³¹⁰ Unusually, patient 1 demonstrated relatively greater cone than rod dysfunction on ERG examination with no evidence of deterioration between ages 12 and 19 years.

Patient 4 had widespread white dots that extended from RPE to ELM. Fundus albigunatus due to compound heterozygous *RPE65* mutations (IVS1+5G>A and p.Ile115Thr) was previously reported in a patient who had deterioration of visual acuity by age 18 years.³¹³ Electroretinography was similar to that found in *RDH5* mutations with normalization of rod-system ERGs after prolonged dark adaptation. The patient in the present series has a similar retinal appearance but only partial recovery of rod

function following extended dark adaptation and excellent visual acuity at age 26 years. The dots in the previously reported patient were demonstrated on OCT to extend throughout the RPE up to the level of the ELM, similar to the patient in this report and to a previous report of OCT findings in an *RPE65* related severe EORD patient.³⁰⁶

Molecular analysis in patient 1 identified a homozygous p.Tyr249Cys variant, predicted to be pathogenic *in silico*. Patients 2 and 3 carried 2 variants including the p.Arg515Trp allele that has been previously reported in a similarly mildly affected patient.³¹¹ Patient 4 had a missense change, p.Ala145Thr, tolerated *in silico* and not previously reported in disease, but arising in a highly conserved residue. This was combined with a PTC mutation, previously reported in a patient with LCA and assumed to be null.³¹⁶ The analysis of mutations in this series of patients would indicate that p.Tyr249Cys, p.Arg515Trp and p.Ala145Thr are all hypomorphic alleles. One weakness of this study has been the lack of other family member DNA samples for segregation in families 2 and 3 but the finding of a previously reported hypomorphic mutation on one allele consistent with their phenotype would support likely pathogenicity.

RPE65 is a membrane-bound, iron-dependent enzyme that converts all-*trans*-retinyl esters to 11-*cis*-retinol, most likely in a dimeric state.³¹⁹ A previously reported *in vitro* assay system using purified RPE65 confirmed its isomerase function in the visual cycle and permitted quantitative analysis of enzymatic activity.³²⁰ Some hypomorphic *RPE65* alleles have been shown *in vitro* to produce RPE65 protein with sufficient residual activity for good photopic visual function in childhood. For example, p.Pro25Leu was found to have 7.75% residual isomerase activity *in vitro*, sufficient to maintain good visual acuity in a patient age 4.5 years.³¹⁰ In contrast, p.His68Tyr, associated with a severe phenotype, had less than 2% activity.

Investigation of the location of hypomorphic residues in the crystalline RPE65 structure revealed no apparent difference when compared to non-hypomorphic residues; the hypomorphic residues are surface located as are the majority of non-hypomorphic residues (figure 7-8). Previously, in an analysis of a parologue of RPE65, it was suggested that surface residues would have little effect on enzyme activity but residues located centrally near the substrate binding site would have a greater effect.⁴¹ However mutations of the surface residues in RPE65 clearly do have an effect on protein function. An investigation of RPE65 residues that are frequently affected in retinal dystrophy (Arg91, His182 and Tyr368) demonstrated that the amino acid side chains make specific interactions with surrounding residues and that the substituted residues are not structurally tolerated leading to misfolding.³¹⁹ In compound heterozygous patients with one hypomorphic allele and one severe mutant allele, the overall residual activity appears sufficient to regenerate physiologically significant levels of

chromophore, perhaps as the structural change in the hypomorphic residues are better tolerated. Further *in vitro* assessment would determine the precise impact on isomerase activity for the presumed hypomorphic alleles reported in our subjects.

It appears from the study of patients with hypomorphic alleles that low levels of isomerase activity are sufficient to maintain good foveal cone function in to adulthood despite ERG evidence of poor rod and cone function and marked macular dysfunction on PERG.³¹⁰ It is therefore surprising that improvement in visual acuity in *RPE65* gene replacement therapy trials have been limited despite good rescue of rod and extrafoveal cone function.³⁰⁷⁻³⁰⁹ In the patients in this series, low levels of RPE65 activity from birth is associated with normal visual acuity but markedly reduced rod and cone function. This suggests that the efficiency of transduction in human gene replacement trials may not be the limiting factor in improving visual acuity post treatment, but rather that gene replacement therapy should be given very early in childhood for optimal recovery of visual acuity.³⁰⁷

8 Familial exudative vitreoretinopathy and microcephaly

8.1 Introduction

Familial exudative vitreoretinopathy (FEVR) is a disorder of abnormal vasculogenesis with variable manifestations including incomplete peripheral vascularisation, retinal folds and total retinal detachment.¹²⁶ Approximately 50% of cases can be molecularly solved due to mutations in *LRP5* (AD, AR), *FZD4* (AD, AR), *NDP* (X-linked recessive), *TSPAN12* (AD, AR) and *ZNF408*.^{125, 321-327} Most of these are genes involved in the canonical Wnt signalling pathway, a transmembrane pathway that activates β -catenin/TCF transcription, involved in retinal development/angiogenesis.^{328, 329} The exception, *ZNF408* is a zinc finger transcription factor identified in 3 families to date.^{125, 327} There is variable severity within families but complete penetrance.¹²⁶

Rarely, FEVR has been reported in association with microcephaly.³³⁰⁻³³² *KIF11* has been reported as one cause of this association, allelic with microcephaly with or without chorioretinopathy, lymphedema or mental retardation (MCLMR, MIM#152950).^{333, 334} In addition, one patient with bi-allelic mutations in *TUBGCP6* has been reported with microcephaly, retinopathy and retinal folds.³³⁵ The aim of this study was to characterise a series of 12 children from 10 families with microcephaly and FEVR and investigate the extent of any genetic heterogeneity. Additionally, the potential benefits of a molecular diagnosis in informing both genetic counselling and relevant systemic investigations were studied.

8.2 Methods

8.2.1 Ascertainment of patients

Patients were all known to the paediatric genetic clinic at Moorfields, under the care of one of my supervisors. One patient was already molecularly solved. Patients were identified from the genetics database and from my supervisor as having FEVR and microcephaly. In 2 patients, microcephaly was only apparent after further review in clinic and measurement of the occipito-frontal circumference (OFC).

8.2.2 Clinical assessment

In total, 10 probands and 2 siblings were ascertained for detailed phenotyping including growth parameters. I was able to examine 8 patients, my supervisor the remaining patients. All patients had retinal imaging and systemic assessment by paediatric

colleagues. Systemic assessment included growth parameters of OFC, height and weight. Microcephaly was defined as an OFC more than 2 standard deviation (SD) below the mean (≤ -2 SD) for gender, age and ethnicity.³³⁶ Based on the growth charts used within UK practice, this corresponds to \leq the 2nd centile.³³⁷ When necessary, patients were referred for further specialist opinion such as endocrinology if *LRP5* mutations were identified which is known to be associated with reduced bone mass.³³⁸ Available parents were examined and FFA performed if indicated.

8.2.3 Molecular investigations

Six probands underwent WES, 5 screened by colleagues (Pia Ostergaard and Sahar Mansour) at St George's Hospital as part of a project investigating microcephalic patients and one as part of a trio with his parents (AROS). This latter proband was solved by WES. WES (St Georges) had initially also identified a novel, heterozygous variant in *LRP5*, c.2116G>A (p.Gly706Arg), in patient 7. Segregation found this variant to be homozygous in her unaffected mother making it likely to be a polymorphism. It had nevertheless prompted a screen of a series of FEVR microcephaly patients for *LRP5* variants.

In total, 8 probands had candidate gene Sanger sequencing including *LRP5* (n=7, by me), *KIF11* (n=7, St George's hospital colleagues), *FZD4* (n=1, by me), *NR2E3* (n=6 by me), *TSPAN12* (n=1, Carmel Toomes in Leeds), *NDP* (n=3, Leeds), and *TUBGCP6* (n=1, Prof Jackson, Edinburgh). This identified causative mutations in 4 probands. All identified mutations were segregated with available affected and unaffected family members. I designed primer pairs for screening of *LRP5* and *FZD4* (table 8-1). Mutation nomenclature was assigned in accordance with GenBank Accession numbers NM_2335.3 for *LRP5*, NM_012193.3 for *FZD4*, NM_004523.3 for *KIF11* and NM_020431.3 for *TUBGCP6*.

Exon	Primer forward 5' → 3'	Primer reverse 5' → 3'	Enzyme	Annealing temp (°C)	Amplicon size (bp)
<i>LRP5</i>					
1	TCCGCTCCCGCGCGCCAGCT	GCGGGGCCGCCC GGCCATT	MYTAQ +DMSO	70	311
2	GCAGTACCAGGAGTGCTCTG	TGGGCTCATGCAAATTCGAG	BIOTAQ	65	572
3	AGGGCAAGTTCACTGTCTGT	GAACGCCTTCAAAGCCCTG	BIOTAQ	65	364
4	GGTCAGCAGCAATGACTGACG	CCCACGCCCCCGCATC	MYTAQ	65	355
5	ATGAGGCAGGTGGAATGGTG	ACCCGCCAAGTGGATCATTT	BIOTAQ	65	432
6	TGAGTATTTCCCTTGCCCGG	TCCGGGTCTGATGCAAGAC	BIOTAQ	65	599
7	CTCTTGGCACTGGGGATGC	TGGCCAAATAGCAGAGCACA	BIOTAQ	65	355
8	TCTTGTGGGGCAGCTCAG	GGCACCTGAGCTCAACACTT	BIOTAQ	65	414
9	ACGGCAGCATTTCATTGTGTG	TTTGAGGCAGGAACAGAGGC	BIOTAQ	65	447
10	TGGGCAAGAAGAGCGAAACT	CTCTAATCACCGAGGGCCAC	BIOTAQ	65	427
11	GAAGAGGTGGGGACAGTTGC	TTGCAGGCCACAGGGTATG	BIOTAQ	65	373
12	GTTGAACCCTGGCTCACCC	AGAAGCTCCTTTCAGCGTCA	BIOTAQ	61	494
13	TTGTCGAGTGCGTGCTATC	GCCATCCTCTGTTTCTCCC	BIOTAQ	65	392
14	TTGAGAAGTGTGGCCTCTGC	ATCCCCAGGGTGGAAAGTCT	BIOTAQ	65	495
15	AATGTGACCTGTCAGCCTCG	TCACTCAGAACCCCAGCCTA	BIOTAQ	65	494
16	AAAGCATGGAATCCCCCAGG	CTCGGGACATTCGGACATGT	BIOTAQ	65	494
17	CAGGAGGGCCAGTTCTCATG	GAAACTGGATGCCACAGGGA	BIOTAQ	65	347
18	CTTTGAAGCCCAGTCACGC	AGAGCCCCTACTCCTGTGAG	BIOTAQ	65	413
19	CGCTGGTCTAGAAAGGGTC	GCACGTCTCCTCCCCTAAAC	BIOTAQ	65	318
20	CAAAGCCAGCCCCTTCAGG	TGTCTGCCACATGTGCAAGA	BIOTAQ	65	449
21	GGTAGTGGGAGCAGAGGAGA	AGCAGAAGGGTTTGAAAAGGGA	BIOTAQ	65	385
22	GAAGCCCTCTCTGCAAGGAA	TAGTGTGGTTGGCAGAGCAG	BIOTAQ	65	354
23	GACAGGCCTTTCCCGTTCA	CATCACAGTTCACATTTCTCATGTT	BIOTAQ	65	492
<i>FZD4</i>					
1	GCATCACACTCCCGTCCC	TGTCTCCTTCGGGCTAGGAT	MYTAQ	64	509
2a	AACTCAGCTTTGTGGGAGCA	TGACCCCATTTGAGTCCTGC	MYTAQ	64	805
2b	TGAAGAGGCAGCAGAACCTG	CAAATGCTGGCATTCCCCC	MYTAQ	64	818

Table 8-1: Primer pairs for sequencing *LRP5* and *FZD4*

8.3 Results

Twelve patients (8 male, 4 female) from 10 families were investigated (table 8-2, figure 8-1). All had FEVR of variable severity with visual impairment and nystagmus. In patients 4 and 10, there was a retinal fold in 1 eye, chorioretinal dysplasia in the other. Visual acuity was worse for patients with retinal folds and detachment, and mildest for peripheral retinal vascularisation (table 8-3). Age ranged from 4 months to 16 years at

last review. OFC ranged from far below the 0.4th centile to on the 2nd centile.

Developmental delay was present in 8/12 patients.

Patient, gender, family	Gene/ assay	Age last rv	Latest VA logMAR (Snellen)	Fundus features	Growth parameters, centile			Other findings
					OFC	Ht	Wt	
Pt 1 (M) GC16755	<i>LRP5</i>	9 yrs	R CF L NPL	RE tractional RD, nasally avascular, LE total RD with no fundal view	<<0.4 th	0.4 th -2 nd	2 nd - 9 th	Normal DEXA scan Normal MRI brain
Pt 2 (F) GC19160	<i>LRP5</i>	5 yrs	R 1.3 (6/120) L 1.4 (6/150)	BE retinal folds with partial retinal vascular preservation on FFA	<0.4 th	95 th	95 th	Reduced bone mass on DEXA scan, maternal OFC 95 th centile
Pt 3 (M) GC21489	<i>KIF11</i>	4 mths	Fixing and following	BE retinal folds with partial retinal vascular preservation on FFA. Rod-cone dysfunction on ERG	<0.4 th	9 th	2 nd	Normal MRI brain
Pt 4 (M) GC20377	<i>KIF11</i>	8 yrs	R 0.6 (6/24) L 1.6 (6/240)	RE chorioretinopathy with focal atrophy, LE retinal fold. Rod-cone dysfunction	<0.4 th	N/A	N/A	Developmental delay
Pt 5 (M) GC21033	<i>TUBGCP6</i>	17 yrs	R 0.56 (6/24) L 0.52 (6/19)	Loss of photoreceptors outside of fovea on OCT, lack of peripheral vascularisation with fibrotic ridge. Rod-cone dysfunction	<<0.4 th	2 nd	9- 25 th	Moderate learning difficulties
Pt 6 (F) GC21033	<i>TUBGCP6</i>	14 yrs	R&L 0.7 (6/30)	Lack of peripheral vascularisation on FFA with fibrotic ridge. Rod-cone dysfunction	<<0.4 th	9- 25 th	2 nd - 9 th	Moderate learning difficulties
Pt 7 (F) GC19713	WES negative, <i>LRP5</i> SNP	4 yrs	Fixing and following	RE Large temporal retinal fold, LE Large retinal fold with partial RD	<<0.4 th	N/A	N/A	Developmental delay Maternal OFC 9 th centile
Pt 8 (M) GC18797	<i>NDP</i> & <i>LRP5</i> negative	4 yrs	BEO 1.0 (6/60)	BE retinal folds. Reduced ERG responses R>L, tested age 6 weeks	2 nd	N/A	N/A	Normal MRI brain
Pt 9 (F) GC19208	WES, <i>LRP5</i> negative	11 yrs	R 1.0 (6/60) L NPL	RE macular atrophy, temporal peripheral non-perfusion, telangiectasia with shallow exudative RD, LE total RD	N/A	N/A	N/A	Developmental delay, learning difficulties
Pt 10 (M) GC19303	WES, <i>LRP5</i> negative	11 yrs	R NPL L 0.78 (6/38)	RE retinal fold with peripheral chorioretinal atrophy and pigment, LE focal chorioretinopathy	<<0.4 th	25 th	50 th	Normal MRI brain ERG R undetectable L rod-cone dysfunction
Pt 11 (M) GC20924	WES, <i>NDP</i> , <i>LRP5</i> negative	13 yrs	R 1.2 (6/95) L 1.4 (6/150)	RE retinal fold with exudate, LE retinal fold with macular scar	0.4 th	N/A	N/A	Parents normal FFAs, paternal OFC 91 st centile
Pt 12 (M) GC20924	Unsolved	9 yrs	R NPL L 1.6 (6/240)	RE total RD no fundal view, LE retinal fold, tractional RD/exudate	<0.4 th	N/A	N/A	Developmental delay

Table 8-2: Clinical summary for patients with FEVR and microcephaly

Ht, height; wt, weight; RD, retinal detachment; DEXA, dual energy X-ray absorptiometry

Patient 1 presented with eye poking at 2 months of age and was found to have a total detachment of the left eye with a retinal fold in the right eye. *NDP* screen was negative. Microcephaly was only identified at 9 years of age in the ophthalmology clinic and was then confirmed in the affected younger sister. Family 1 had previously undergone autozygosity mapping which identified a region of homozygosity at the *EVR1* locus which encompasses both *FZD4* and *LRP5*. Screening of *FZD4* did not find any mutation. Screening of *LRP5* with segregation identified a novel homozygous splice site variant c.4112-3C>G in the proband and his affected sister, and was heterozygous in the unaffected sister and parents. Due to the molecular diagnosis, bone density is under monitoring with a normal DEXA scan to date.

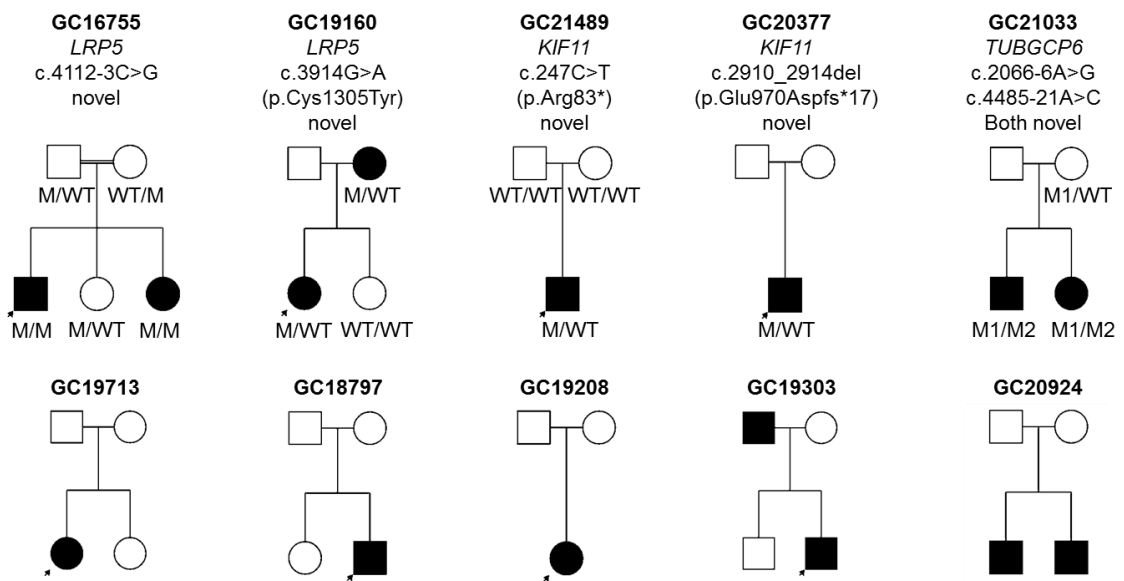


Figure 8-1: Pedigrees and mutations segregation for 10 FEVR families

Retinal abnormality	Number of eyes	Vision logMAR (Snellen)
Peripheral non-perfusion	5	0.52-0.70 (6/19-6/30)
Chorioretinal dysplasia	2	0.50-0.80 (6/19-6/38)
Retinal fold	12	1.2-NPL (6/95-NPL)
Retinal detachment	5	1.5-NPL (6/190-NPL)

Table 8-3: Visual acuity based on retinal phenotype

Patient 2 presented in early infancy with nystagmus, poor vision and bilateral retinal folds (figure 8-2). Microcephaly was observed at birth. On Sanger sequencing, a heterozygous novel missense mutation in *LRP5* was identified, c.3914G>A (p.Cys1305Tyr) which is predicted damaging *in silico* (SIFT 0, Polyphen2 1.0). This was also identified in the mother who had previously had a normal dilated fundus examination. Subsequent Optos widefield FFA in the mother identified subtle abnormal

peripheral retinal perfusion (figure 8-2). A bone density scan in the affected 5 year old child was abnormal with a z-score of -2.1 indicating osteoporosis and a similar scan is planned in the mother. Further family segregation was performed within an accredited NHS laboratory which found the proband's sister was not a carrier, and the 2 maternal aunts were not carriers. Further retinal screening for these at risk family members was therefore not needed.

Patient 3 presented in infancy with nystagmus, poor vision and microcephaly. Head circumference was reportedly normal at birth. Examination under anaesthesia at 6 months of age identified bilateral retinal folds, and rod-cone dysfunction with 'enhanced S-cone-like' features on ERG. These comprised the characteristic features of delayed 30Hz flicker of lower amplitude than the LA 3.0, the DA 3.0 and LA 3.0 responses having the same simplified and markedly delayed waveform.¹³⁵ This finding prompted screening of *NR2E3* in this patient and other unsolved FEVR/microcephaly patients without identifying any pathogenic variants. WES was subsequently performed on the proband and both parents. This identified a novel, de novo, nonsense mutation, c.247C>T (p.Arg83*) in *KIF11* as the likely causative mutation.

Patient 4 presented in infancy with reduced vision and was found to have a retinal fold in the left eye with areas of chorioretinal atrophy in the right eye (figure 8-2). Microcephaly was diagnosed in the Ophthalmology clinic at 6 years of age. ERG identified rod-cone dysfunction without any features of ESCS as described above. Screening of *KIF11* by Sanger sequencing identified a novel, heterozygous premature truncating codon, c.2910_2914del (p.Glu970Aspfs*17).

Patients 5 and 6 are siblings with learning difficulties, microcephaly and rod-cone dysfunction on ERG. Dilated fundus examination identified abnormal peripheral retinal vasculogenesis with peripheral scarred ridges in both eyes (figure 8-2). FFA in patient 6 identified abnormal vascular malformations anterior to this ridge. Treatment has not yet been required. Based on the combination of microcephaly, learning difficulties and rod-cone dysfunction, candidate gene sequencing was performed by colleagues in Edinburgh. They were found to have bi-allelic novel, mutations in *TUBGCP6*, c.2066-6A>G and c.4485-21A>C with RNA analysis confirming abnormal splicing (performed in Edinburgh).

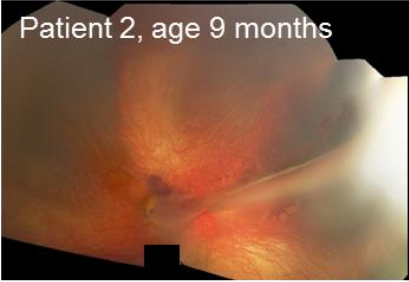
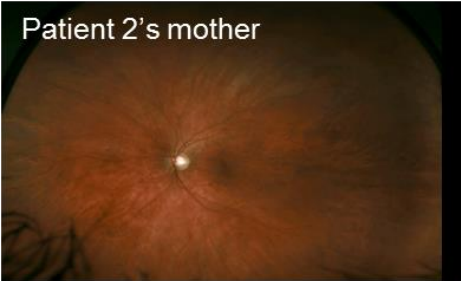
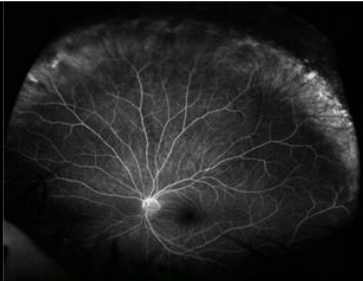
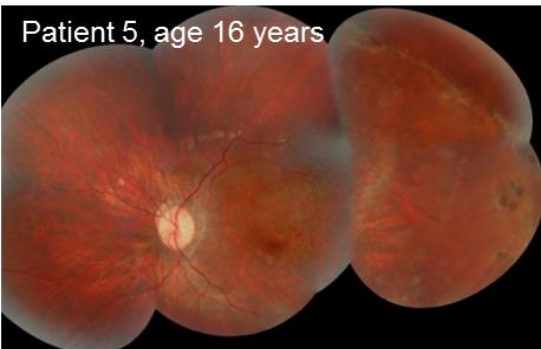
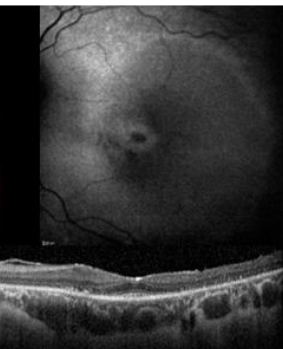
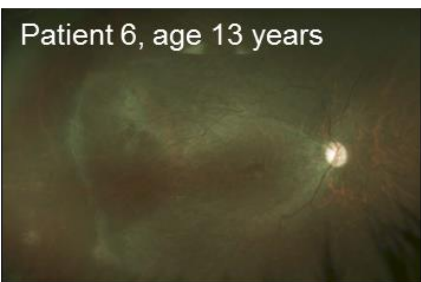
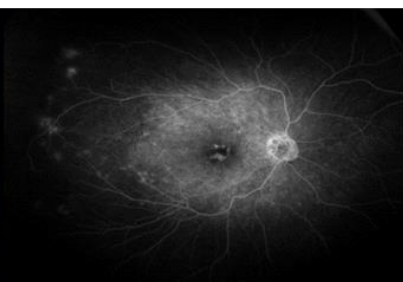
<p>Patient 2, age 9 months</p> 		<p>Patient 2, LE RetCam colour and FFA images demonstrating retinal fold from optic disc to ora serrata with limited retinal vascularisation elsewhere</p>
<p>Patient 2's mother</p> 		<p>Patient 2's mother, LE Optos colour and FFA images, no obvious abnormalities on colour, but abnormal peripheral vascularisation on FFA</p>
<p>Patient 4, age 7 years</p> 		<p>Patient 4, RetCam images, RE inferior, circumscribed chorioretinal atrophy lesions, LE retinal fold</p>
<p>Patient 5, age 16 years</p> 		<p>Patient 5, LE colour montage, mid-peripheral RPE hypopigmentation, peripheral scarred ridge, FAF imaging increased autofluorescence peri-foveally and in outer macular with loss of autofluorescence in-between, OCT, outer retinal atrophy with centrally preserved ISe band</p>
<p>Patient 6, age 13 years</p> 		<p>Patient 6, RE Optos colour and FFA demonstrating macular atrophy, peripheral scarred ridge with lack of vascularisation anterior to it and abnormal vascular malformations</p>
<p>Patient 11, age 13 years</p> 		<p>Patient 11, Optos colour images of RE retinal fold with exudative detachment, LE smaller retinal fold with macular atrophy</p>

Figure 8-2: Retinal imaging in FEVR with microcephaly

Six patients (5 families) all with microcephaly and FEVR remain unsolved despite WES in all but 1 family. Patient 7 remains unsolved having had a novel, heterozygous variant identified on WES in *LRP5*, c.2116G>A (p.Gly706Arg) which was likely to be a polymorphism. Segregation found this variant to be homozygous in her unaffected mother who had a normal dilated fundus examination and an OFC on the 9th centile. Patient 9 has a retinal fold in one eye and chorioretinal atrophy in the other. His father is also microcephalic and on dilated fundus examination has incomplete peripheral vascularisation. Screening of the most likely candidate gene, *KIF11*, has been negative. Patients 11 and 12 carry a copy number gain at 4q22.2 (0.68Mb) which is paternally inherited. This was found elsewhere by comparative genomic hybridization. Within this region are 7 genes (*HPGDS*, *PDLIM5*, *SMARCAD1*, *BMPR1B*, *UNC5C*, *PDHA2*, and *STPG2*). Only one of these has a known retinal developmental role, bone morphogenetic protein receptor type 1B (*BMPR1B*) which has been shown in a mouse model to be required for normal ventral ganglion cell axon targeting to the optic nerve head as well as controlling inner retinal apoptosis.³³⁹ Given the normal fundus examination and FFA in the father, it is unlikely that this copy number gain is pathogenic. WGS is planned on all unsolved families with available parents to be sequenced simultaneously.

8.4 Discussion

In this series of 12 patients with FEVR and microcephaly, half of the patients have been molecularly solved and half remain under investigation. This reflects a similar published solved rate for FEVR alone.¹²⁵ All patients presented in early childhood with nystagmus and visual impairment. Fundus features were variable in keeping with the known spectrum of FEVR from incomplete peripheral vascularisation to retinal fold to retinal detachment.¹²⁶ In addition, there were 2 patients with unilateral retinal folds and contralateral chorioretinal dysplasia which has been seldom reported in the literature before.^{332, 334} Visual acuity correlated with fundus feature, being most severe in those patients with retinal folds or detachment.

ERG was available in 5 patients, 2 with *KIF11* mutations, 2 with *TUBGCP6* mutations, and 1 unsolved patient and identified rod-cone dysfunction. The *TUBGCP6* patients have evidence of rod-cone dystrophy on retinal imaging with loss of photoreceptors on OCT and abnormal autofluorescence. For the other patients, it is unknown whether their ERG features are consistent with a rod-cone dystrophy as there has been limited retinal imaging possible due to the severe retinal abnormalities. Interval ERG would be helpful to demonstrate deterioration consistent with a rod-cone dystrophy. Previously reported ERG findings in FEVR are limited. A report of 3 patients from one family described abnormal ERG in 2 patients with reduced rod and cone responses.³⁴⁰ A

detailed characterisation of MCMLR due to *KIF11* mutations in 6 patients found rod and cone dysfunction with abnormal macular function in those with available PERG results.³⁴¹ It may be anticipated that in the majority of patients with FEVR, there would be measurable photoreceptor dysfunction based on abnormal retinal development but this hypothesis and determination of progressive retinal dysfunction need to be substantiated.

FEVR with microcephaly has been reported in association with *KIF11* and *TUBGCP6* but has not been previously reported with *LRP5*.^{333-335, 342} Microcephaly in this series ranged from the 2nd centile (-2 SD) to <<0.4th centile (<-5SD). In 2 patients it was only observed after measurements in the Ophthalmology clinic and should be specifically looked for in patients with FEVR. One drawback in this study is the lack of complete data on parental OFC and peripheral retinal examinations which may be helpful in filtering whole genome data from the unsolved families if the likely inheritance pattern is known.

LRP5 (MIM 603506) is a 23 exon gene initially found to cause osteoporosis-pseudoglioma syndrome a recessive disorder of severe retinal dysplasia and juvenile osteoporosis presenting with bone fractures in early childhood and subsequently also associated with dominant high bone density from missense variants located within the N-terminal YWTD-EGF domain.^{338, 343, 344} *LRP5* has been associated with both dominant and recessive forms of FEVR with mutations distributed throughout the gene and with evidence of non-penetrance in dominant disease.^{325, 345} In recessive disease, carrier parents can also have low bone mass.³³⁸ Of the 2 families identified with *LRP5* mutations in this study, one has recessive disease with a novel splice site mutation, and the other dominant disease. For patient 2 and her mother, evidence for the causality of the novel missense mutation which is predicted to be damaging *in silico*, includes the abnormal peripheral retinal vascular findings in the mother and the reduced bone density in the patient at age 5 years. For this family, the molecular diagnosis has enabled systemic monitoring of bone density to prevent fractures and screening for this mutation in the patients maternal aunts and younger sister, all of whom were negative. Given the possibility that a second variant including a copy number variant has been missed by Sanger sequencing, or alternatively that there is another molecular cause, whole genome sequencing is being performed.

Kinesin family member 11 (*KIF11* MIM 148760) encodes EG5, a microtubule motor involved in mitosis.³⁴⁶ Its exact role in retinal development has not yet been elucidated. Mutations were first identified in association with MCLMR and later with microcephaly and FEVR.³⁴⁶ However, not all patients have microcephaly.³³⁴ Patient 3 in this report has a *de novo*, novel, nonsense mutation. Patient 4 has a novel PTC with segregation

unavailable to determine if it was *de novo*. Previously reported mutations include missense, nonsense, splice and PTC and are found distributed throughout the gene without obvious mutational hotspots and without apparent difference in mutation distribution between patients with retinal folds and those with chorioretinal atrophy.^{333,}

³⁴² At least 40% of mutations arise *de novo*. Non-penetrance has been reported in carrier parents. For family 3, the molecular diagnosis identifying *de novo* disease has allowed accurate genetic counselling on the risk of recurrence in future children.

TUBGCP6 (MIM 610053) was first reported in a patient with microcephaly and chorioretinopathy without further ophthalmic detail provided.³⁴⁷ Subsequently it was identified in 4 patients all with extreme microcephaly (-7.2 to -11.1 SD), short stature (-2.3 to -3.45 SD) and retinopathy with one patient additionally described to have retinal folds.³³⁵ In one patient, ERG demonstrated absent rod and cone function. The siblings in this series have abnormal retinal vascularisation identified in conjunction with a rod-cone dystrophy but with less severe microcephaly and without short stature. Their novel mutations are both predicted to create cryptic splice sites with out of frame transcripts then created. Previously reported mutations include splice site, PTC and missense.^{335, 347} Detailed ophthalmic phenotyping of all *TUBGCP6* patients would be of particular interest to investigate the exact types of retinal involvement.

WGS in the 5 unsolved families is in progress with probands being sequenced in parallel with unaffected and other affected family members to aid interpretation of the results. This is particularly relevant when the inheritance can be recessive or dominant, with the potential for variable penetrance and *de novo* mutations.

9 Hermansky-Pudlak syndrome 6

9.1 Introduction

Oculocutaneous albinism is a recessive disorder of melanogenesis presenting in infancy with poor vision and nystagmus.³⁴⁸ It is characterised by iris transillumination, foveal hypoplasia, chiasmal misrouting on VEPs and variably reduced pigmentation of the fundus, hair and skin. OCA is a feature of certain syndromes including Hermansky-Pudlak syndrome (HPS, MIM#203300) associated with bleeding diathesis, pulmonary fibrosis and granulomatous colitis and Chediak-Higashi syndrome (MIM#214500) with immunodeficiency and neurological involvement.^{349, 350}

HPS is an inherited disorder of lysosomal organelle biogenesis most prevalent in Puerto Rico at a rate of 1 in 1800 due to founder mutations in *HPS1* and *HPS3*.^{351, 352} Nine HPS genes have been identified all encoding protein complexes involved in the biogenesis of lysosome related organelles (BLOC), including melanosomes in melanocytes and delta granules in platelets.³⁵³ *HPS6* is a subunit of the BLOC2 complex in addition to *HPS3* and *HPS5*. *HPS6* is an integral part of the retrograde motor complex for lysosomal transport from cell membrane to the perinuclear region.³⁵⁴ *HPS6* is a very rarely reported subtype with only six families reported to date; their *HPS6* related disease characterized by OCA with bleeding diatheses.³⁵⁵⁻³⁵⁷

There may be a delayed diagnosis of HPS if the systemic disease is mild as has been reported in *HPS3* related disease and as such the patients may initially have an isolated ophthalmic diagnosis of OCA or even ocular albinism.³⁵⁸ Consideration of HPS as a differential diagnosis by the ophthalmologist is important due to its systemic complications. In this investigation of 2 families with *HPS6* related disease, the diagnosis was delayed due to a mild systemic phenotype.

9.2 Methods

9.2.1 Ascertainment of patients

Two children from a distantly consanguineous family of Punjabi Afghan descent were recruited from the paediatric clinic at Moorfields to the inherited retinal disease study. They had both presented in infancy with nystagmus and reduced vision and were diagnosed with isolated foveal hypoplasia. WES of the proband when age 10 identified a homozygous variant in *HPS6* which prompted further investigation of the family by myself. I then also investigated an adult patient known to have a diagnosis of HPS and a mild systemic phenotype but no molecular diagnosis.

9.2.2 Clinical assessment

All patients were assessed and examined by myself at their most recent visit. All underwent full clinical examination and imaging including anterior segment and colour fundus photography, FAF and OCT as detailed in methods. ERG was performed using eyelid electrodes for the 2 children of family 1 as detailed in methods. In addition, both children underwent VEP recording to evaluate chiasmal routing. ERG/VEP recordings were not available for patient 3.

9.2.3 Systemic investigations

All patients underwent haematological assessment and investigation following referral to haematology colleagues. In addition the 2 children of family 1 were under the care of general paediatric colleagues.

9.2.4 Molecular investigations

The proband of family 1 had previously undergone screening of *SLC38A8*, which was at the time a candidate gene for isolated foveal hypoplasia under investigation by colleagues in Leeds.³⁵⁹ This did not identify a mutation. WES was then performed at AROS Applied Biotechnology.

A homozygous variant in *HPS6* was identified by colleagues as likely causative. Following my own review of the results, a single variant in *SLC38A8* was also identified and given the patient's phenotype further investigated. Both patients were clinically reviewed by myself and the rest of the family's blood samples taken for DNA extraction and segregation. I designed primers for bi-directional Sanger sequencing of the single exon of *HPS6* (4 primer pairs required due to size of exon) and the exon-intron boundaries as well as the affected exon 7 of *SLC38A8* (table 9-1).

Gene/ exon	Primer forward 5' → 3'	Primer reverse 5' → 3'	Enzyme	Annealing temp (°C)	Amplicon size (bp)
<i>HPS6-A</i>	GCTGGACCTGGGCAAAGC	CAGCAGGACGTGTGTGCG	MYTAQ + DMSO	65	600
<i>HPS6-B</i>	CTTTCAGCCACTGTGTGTGC	AAGATTCCCTCGGGTCTCCA	BIOTAQ	65	653
<i>HPS6-C</i>	GTACATCTGCTAGAACCGCCA	CTCCACACATCAGGGGGTG	MYTAQ	65	597
<i>HPS6-D</i>	CAACACCGTTTTCCAAGCCC	CCCTGAGTGTTCTGATGCCT	MYTAQ	65	840
<i>SLC38A8</i> exon 7	AGGACAGGAAAGCTTTGGGC	TGTGCCTGTTTCCTCCTGTC	BIOTAQ	65	441

Table 9-1: Primer pairs for sequencing of *HPS6* and *SLC38A8*

In the 3rd patient, I performed candidate gene investigation with Sanger sequencing of *HPS6* based on the mild systemic phenotype. In addition, given a reported history of parental consanguinity, autozygosity mapping using a SNP microarray (OmniExpress) was performed including all 9 HPS loci (table 9-2).

HPS subtype	Gene	Coordinates
HPS1	<i>HPS1</i>	10q24.2
HPS2	<i>AP3B1</i>	5q14.1
HPS3	<i>HPS3</i>	3q24
HPS4	<i>HPS4</i>	22q12.1
HPS5	<i>HPS5</i>	11p15.1
HPS6	<i>HPS6</i>	10q24.32
HPS7	<i>DTNBP1</i>	6p22.3
HPS8	<i>BLOC1S3</i>	19q13.32
HPS9	<i>BLOC1S6</i>	15q21.1

Table 9-2: Nine HPS genes and loci

Mutation nomenclature was assigned in accordance with GenBank Accession number NM_024747.5.

9.3 Results

Clinical details are summarised in table 9-3. Patient 1 was examined at age 12 years. She had reduced vision at R 0.48 logMAR, L 0.40 logMAR, fine horizontal nystagmus but no iris transillumination. Dilated fundus examination revealed reduced foveal reflexes but otherwise appeared normal (figure 9-1). Her younger sibling at age 4 years also had reduced vision R0.76 logMAR and L 0.70 logMAR with fine horizontal nystagmus and no iris transillumination. His dilated fundus examination also demonstrated reduced foveal reflexes and his fundi were noticeably blonder than his sisters. On careful comparison of hair and cutaneous pigment in the siblings and their parents, the proband's hair was noted to be slightly lighter than her parents; her younger brother on removal of his turban had noticeably lighter hair. Retinal imaging confirmed foveal hypoplasia with loss of the foveal pit and persistence of inner retinal layers over the expected anatomical position of the fovea (figure 9-1). Both patients had previously undergone electrophysiology, in the proband age 1 and repeated age 5 and in the younger brother at 8 months of age. In both, full field ERG was normal with VEPs finding no evidence of chiasmal misrouting.

Subsequent re-evaluation elicited a history of mild bruising at the time of immunisations for both children and for patient 1, nose bleeds every 1-2 weeks from the age of 6

years. Haematological investigation was consistent with a platelet storage pool disorder and HPS was confirmed (table 9-3).

Pt number, age last review, family number	Visual function		Haematology investigations		
	Visual acuity logMAR (Snellen)	Refraction	Platelet ATP:ADP ratio (0.9-2.3)	Platelet Function tests	Electron Microscopy
Pt 1 12 years GC18806	R 0.48 (6/19) L 0.40 (6/15)	R +7.00/-2.00 x 180 L +6.00/-1.00 x180	13.9	Normal aggregation Significantly reduced ATP release	Not done
Pt 2 4 years GC18806	R 0.76 (6/38) L 0.78 (6/38)	R +5.50/-3.00 x 180 L +5.50/-3.00 x 180	31.4	Reduced aggregation Significantly reduced ATP release	Not done
Pt 3 29 years GC15023	R 0.82 (6/38) L 0.94 (6/48)	R -1/-1.25 x 180 L -4/-3 x180	10.8	Reduced aggregation Absent ATP release	Reduced platelet dense granules

Table 9-3: Key molecular, visual and haematological findings

ATP, adenosine triphosphate; ADP, adenosine diphosphate

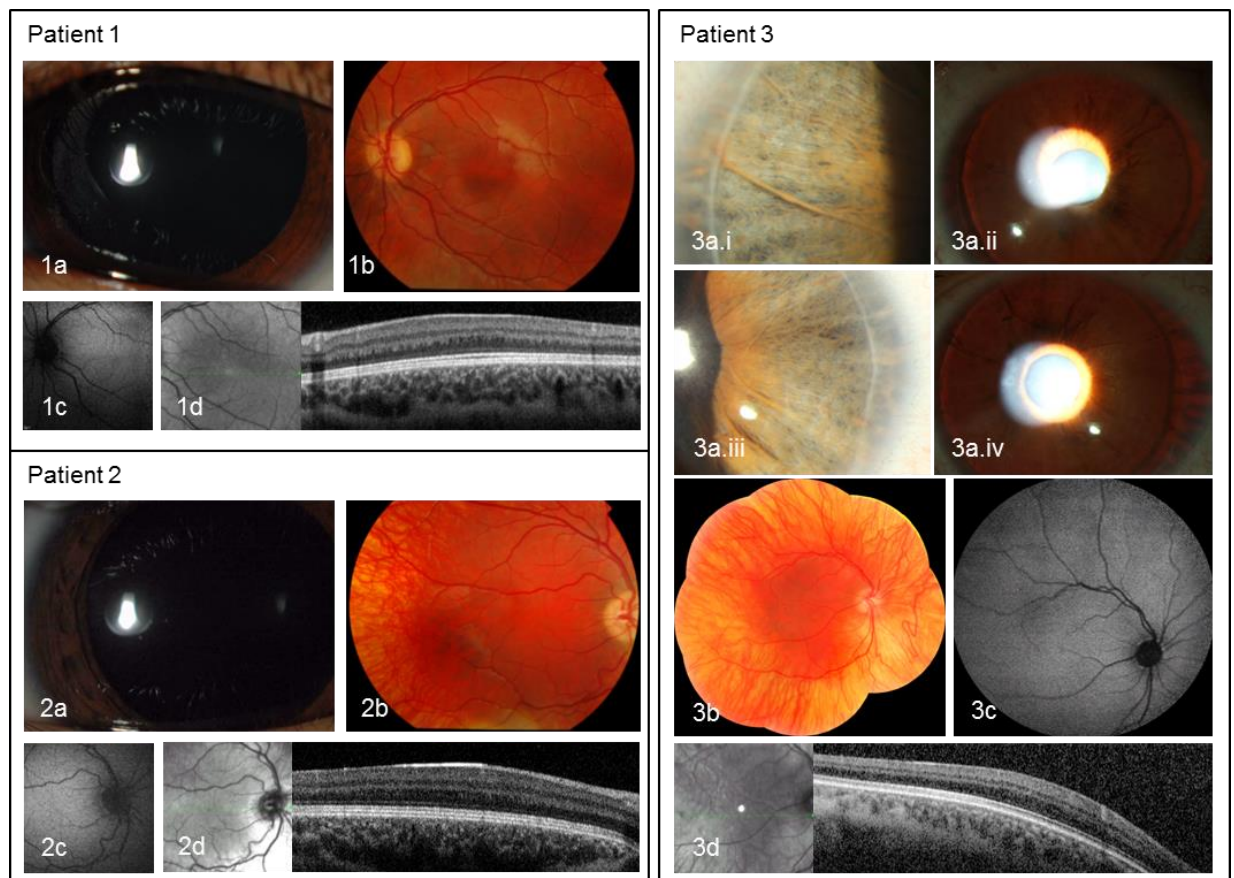


Figure 9-1: Anterior segment and retinal imaging in HPS-6

(a) anterior segment imaging, (b) colour fundus photographs, (c) FAF imaging, (d) OCT. Patient 1 and 2, no iris transillumination, peripherally blonde fundi more obvious in patient 2, no fovea on FAF or OCT imaging. Patient 3, right Axenfeld anomaly, left posterior embryotoxin, transillumination, blonde fundus and no fovea.

Patient 3, the second child of parents of Russian-Palestinian origin, presented at 3 months of age with reduced vision, nystagmus, iris transillumination and blonde fundi. In addition right Axenfeld anomaly and left posterior embryotoxin were noted (figure 9-1). An initial diagnosis of mild ocular albinism was made, amended to oculocutaneous albinism age 9 years due to likely inheritance pattern (ie not X-linked) and the observation of mildly reduced cutaneous/hair pigmentation.³⁶⁰ There were no complications from hernia surgery age 6 years but age 26 years there was prolonged bleeding for 3-4 hours following a dental extraction. Haematological investigations identified a platelet storage pool disorder consistent with HPS (table 9-3).

WES in patient 1 identified a novel, homozygous missense variant in *HPS6*, c.779G>A (p.Gly260Glu), predicted to be damaging *in silico* (SIFT 0.03, Polyphen2 1.00) and a novel heterozygous variant in *SLC38A8*, c.860C>G (p.Ser287Cys) which was predicted damaging *in silico* by Polyphen2 (1.00) but tolerated by SIFT (0.14). Sequencing of both variants in patient 2 supported causality of the *HPS6* variant with the *SLC38A8* variant not found. The parents were confirmed to be carriers of the *HPS6* variant (figure 9-2).

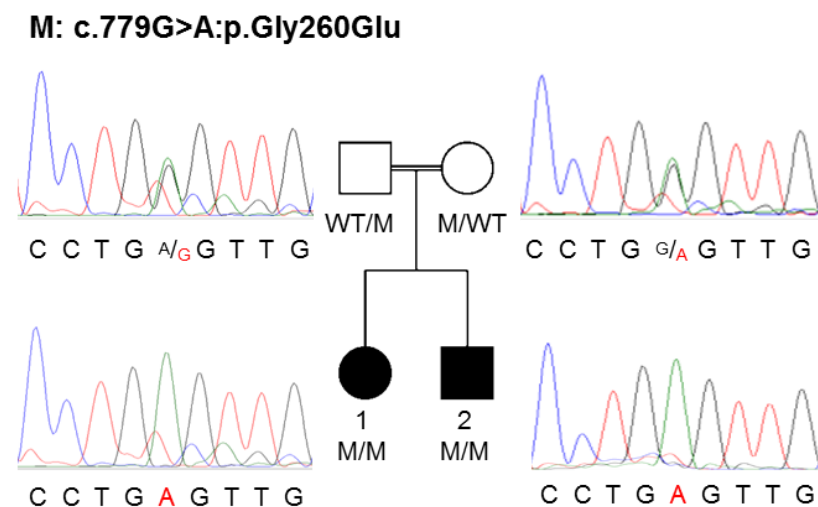
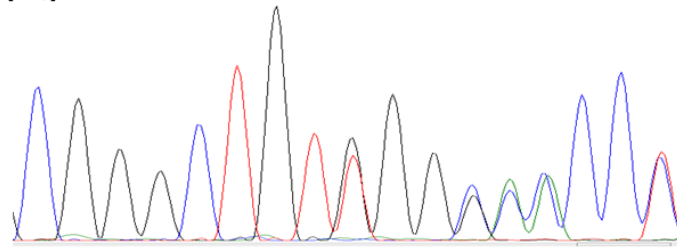


Figure 9-2: Pedigree of family 1 (patients 1 and 2) and *HPS6* chromatograms

Patient 3 had a mild systemic phenotype and as this was consistent with previous reports of *HPS6* related disease, candidate gene sequencing of *HPS6* was performed.³⁵⁷ This identified bi-allelic PTCs, c.902dupT (p.Thr303Hisfs*64) which was novel and c.1083dupC (p.Gly362Argfs*5), not reported in an affected patient before but with a very low allele frequency on ExAC (1 in 120260). Both variants resulted in predicted truncation of each allele at the same codon (figure 9-3). As both variants inserted a base and were within a single exon, they were identified as bi-allelic based on Sanger sequencing alone. Autozygosity mapping identified no regions of

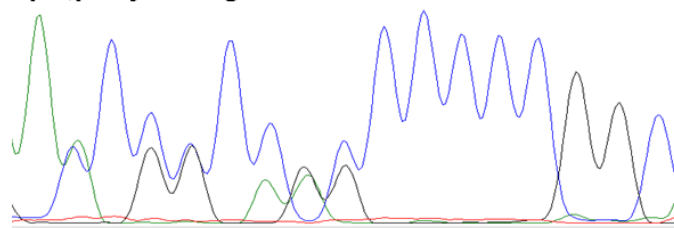
homozygosity over any of the 9 HPS loci and in general had few regions of homozygosity. This meant that the reported consanguinity in the family was unlikely.

M1: c.902dupT;p.Thr303Hisfs*64



Allele 1: 895 C G G G C T G T T G G G C A C C C 910
 Allele 2: 895 C G G G C T G T G G G C A C C C T 911

M2: c.1083dupC;p.Gly362Argfs*5



Allele 1: 1070 A A C C G C C A G C C C C C G G C 1086
 Allele 2: 1071 A C C G C C A G C C C C C C G G C 1086

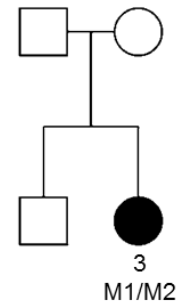


Figure 9-3: Pedigree of family 2 (patient 3) and *HPS6* chromatograms

9.4 Discussion

This study of 3 patients with HPS6 describes novel features including a lack of iris transillumination, normal VEPs and 2 novel mutations. Furthermore, it substantiates the previous reports of a mild systemic phenotype.

HPS6 was first reported in a single patient with OCA, bleeding diathesis but no pulmonary and gastrointestinal involvement.³⁵⁵ A further report identified *HPS6* as a cause of OCA with mild bleeding diathesis in an extended Israeli Bedouin pedigree, all affected members having classical features of OCA including iris transillumination.³⁵⁶ A detailed series of 4 patients with mutations in *HPS6* demonstrated variable degrees of albinism diagnosed in infancy; all had iris transillumination and bleeding diatheses.³⁵⁷ There have been no reported complications of pulmonary fibrosis or granulomatous colitis. This is similar to the present series of patients and to other BLOC2 subtypes, HPS3 and HPS5 which also manifest with milder systemic disease than the other forms of HPS.^{358, 361, 362} Although colitis may present within the first decade of life, the onset of pulmonary fibrosis is not until the 4th decade.^{363, 364} With the limited number of

HPS6 patients reported to date, there is the theoretical possibility that these complications could still be associated.

Patients 1 and 2 have an unusual presentation with a lack of iris transillumination and no chiasmal misrouting on VEPs which led to an initial diagnosis of isolated foveal hypoplasia. Isolated foveal hypoplasia has been reported in association with bi-allelic mutations in *SLC38A8*.³⁵⁹ One variant was found on WES in this gene and assuming a second variant was still to be found, this was further investigated. Segregation ruled out this variant as it was not present in the affected younger brother. A lack of iris transillumination has not been previously reported in HPS although the degree of iris defects can range from mild spoke like defects to complete transillumination.^{365, 366}

Abnormal chiasmal misrouting is regarded as a cardinal feature of OCA and the degree of misrouting has been shown to correlate with the loss of pigmentation.^{140, 367} VEP characterisation in HPS is limited; a report of 11 molecularly uncharacterised HPS patients identified aberrant chiasmal misrouting in all patients.³⁶⁸ The lack of misrouting in the siblings in this report may reflect the mildness of their hypopigmentation. Further investigation of VEPs in other HPS patients in particular the BLOC2 subtypes may demonstrate similar findings. The visual acuities were significantly reduced most likely related to foveal hypoplasia and nystagmus. The vision levels found were similar to those reported in other HPS6 patients.³⁵⁷

Patient 3 in this series has a similar ocular phenotype to previously reported HPS6 patients with iris transillumination, a blonde fundus and foveal hypoplasia. In addition she has features of anterior segment dysgenesis with Axenfeld anomaly and posterior embryotoxin, reported in up to a third of patients with HPS.³⁶⁵ Interestingly, she underwent abdominal surgery age 6 years without bleeding complications but had prolonged bleeding post dental extraction when 10 years of age.

HPS6 is a single exon gene encoding a 775 amino acid ubiquitously expressed protein for which no domain or tertiary/quaternary structure data is available.³⁵⁷ The unbiased platform of WES identified a novel missense variant in *HPS6* in family 1 (p.Gly260Glu) which is predicted to be damaging *in silico*. This directed further haematological assessment and investigation of platelet function. Only 1 of 9 previously reported pathogenic variants was missense (p.Thr272Ile).³⁵⁵⁻³⁵⁷ This was identified in a conjunction with a PTC in a patient diagnosed in early childhood with bleeding suggestive of HPS and typical ocular phenotypic features.³⁵⁷ Bi-allelic missense variants could manifest a milder phenotype as seen in family 1 if the protein function is less functionally impaired than truncating variants. However a large series of patients would be needed to substantiate this potential correlation. The PTCs identified in patient 3 are predicted to produce a truncated protein and not undergo NMD as there is

only a single exon of *HPS6*.²⁰⁶ This has been substantiated by mRNA investigation in the previously reported Bedouin family.³⁵⁶ Neither of these variants has been reported in an affected patient before although one variant is present at a very low level on ExAC. Both variants would truncate the protein at the same codon of 367 which is the same predicted truncation codon of a previously reported variant p.Leu356Argfs*11.³⁵⁶

This study demonstrates that *HPS6* can be associated with mild and late systemic manifestations and a diagnosis of HPS should therefore be considered in any patient presenting with foveal hypoplasia, ocular albinism or OCA. An accurate diagnosis will ensure appropriate precautions during surgical or dental procedures.³⁶⁹

10 CDH3 related congenital hypotrichosis with juvenile macular dystrophy

10.1 Introduction

CDH3 (Cadherin 3, MIM#114021) encodes P-cadherin, a regulator of both hair, retinal and limb development.^{370, 371} First described in 2 brothers in 1935, hypotrichosis, congenital, with juvenile macular dystrophy (HJMD, MIM#601553) presents with childhood onset central visual loss with an associated scalp hair abnormality due to bi-allelic mutations in *CDH3*.³⁷² The disorder is rare and has been reported in a total of 21 molecularly confirmed families to date with 15 reported variants.^{370, 371, 373-381}

Ectodermal dysplasia, ectrodactyly and macular dystrophy syndrome (EEMS) is an allelic disorder also arising due to bi-allelic *CDH3* variants.³⁸² The disorder is of variable severity and phenotype with ectodermal involvement including hypotrichosis, nail dysplasia and partial anodontia and limb defects including syndactyly (joined digits), campylodactyly (bent digits) or ectrodactyly (missing phalanges with a claw hand appearance the most severe manifestation). Only 6 molecularly confirmed patients have been reported in the literature, with 5 additional pathogenic variants identified.^{371, 376, 382, 383}

Apart from a series of 7 families focusing on electrophysiology characteristics, the previous descriptions of *CDH3* related macular dystrophy are limited.³⁸⁴ A single patient has been published with OCT and FAF imaging with single posterior pole colour images on 8 patients otherwise published.^{370, 373, 375, 376, 381, 384, 385} Following a result from WES of a homozygous *CDH3* mutation in a patient with macular dystrophy, the phenotype was studied and further patients identified with clinically similar presentations. A total of 7 patients have been identified and undergone detailed phenotyping including serial imaging and electrophysiology. All have bi-allelic *CDH3* mutations including 3 novel mutations.

10.2 Methods

10.2.1 Ascertainment of patients

Patients were identified from adult inherited retinal clinics. Two patients had WES, 1 patient already had a molecular diagnosis from elsewhere. An additional 9 patients were identified by myself and my supervisors as phenotypically similar, and I screened this cohort for *CDH3* mutations, which identified a further 4 patients.

10.2.2 Clinical assessment

All patients had undergone complete ophthalmic examinations and retinal imaging as part of their routine care. Serial imaging was available in patients 1, 3, 5, 6 and 7. Thickness of the central subfield region as defined by the Early Treatment Diabetic Retinopathy Study (ETDRS) was measured using the automated Heidelberg Spectralis viewing module (version 6.3.4.0) with the RPE basement membrane and the ILM layers checked for accuracy in each OCT slice and manually corrected if necessary.³⁸⁶ Size of the atrophic region was mapped for each FAF image with the region first highlighted using Adobe Photoshop Elements 14 (Adobe Systems Incorporated, San Jose, Ca, USA) and the area then calculated using the Threshold Colour plugin in Image J (National Institutes of Health, Bethesda, Md, USA). Only those images in which the atrophic region border could be clearly delineated were assessed, which was possible for patients 3 and 5. Five patients underwent EDTs.

10.2.3 Molecular investigations

Both WES results (AROS) were confirmed by Sanger sequencing with segregation performed in available relatives with specifically designed primers (table 10-1). In addition, all 16 exons and intron-exon boundaries of *CDH3* were screened in a panel of 9 patients. Mutation nomenclature was assigned in accordance with GenBank Accession number NM_001793.4.

Exon	Primer forward 5' → 3'	Primer reverse 5' → 3'	Enzyme	Annealing temp (°C)	Amplicon size (bp)
1-2	TCAAAGGGGCAAGAGCTGAG	CGCGGTCCACACCAAATG	MyTaq	65	507
3	TCTGCAGCCACTTAGCAGTC	CCTCTGAAGGGCTGACTTGG	BIOTAQ	65	322
4	AGGCTCATCTAGGTCTCCTCA	CTCTGTGAAGAGGGGCACTG	BIOTAQ	65	539
5-6	CAGTGCCCCTCTTCACAGAG	AGCATTAAAGGGTGTGGGCC	BIOTAQ	65	545
7	TGGAGTTGGAAGTGGGAGGA	GACGTGGGTCTCCTACTGTTC	MyTaq	65	343
8	CAGTGCTTCCTGGAGGTCAG	GGTCACACAGCCATAGTGCT	BIOTAQ	65	329
9	GACATCCTGCCGCTGTGTAT	GGACTTCCCAACACAAGAGTG	BIOTAQ	65	506
10	CTGTTGCTAGTGAGGGCCTC	AAATACCTGCCCCAAACCC	BIOTAQ	65	548
11	TGGTATGAGGAGGCCCTGAA	CCGGCCTAGGACCAGTCTTT	BIOTAQ	65	403
12	AGAATGATGGCTCAACTGGCA	AGATCATTGTCCCATGGCC	MyTaq	65	501
13	TCTCTGCATTGCCACATGT	GAGGCTGAGCTGGGAAGATC	BIOTAQ	65	549
14	GCTCTGGCTACTGAGTGAGG	GGCCAAAGAGACTACAGCA	BIOTAQ	65	422
15	TGCTGTAGTCTCTTTGGCC	AAAAGCTGGTTGGTGGTGGA	BIOTAQ	65	507
16	AGAGAGGGGCTCACAGAGAG	TGCTGAAGTCAAAGTGGCCA	BIOTAQ	65	504

Table 10-1: Primer pairs for *CDH3*

10.3 Results

Clinical data are summarised in table 10-2.

Patient, family number, variant	Age of onset, years	Age at last review (length of review), years	Initial VA logMAR (Snellen)	Latest VA logMAR (Snellen)	Latest refractive error, dioptres	Age at colour vision	Age at last electrophysiology, key findings
Patient 1 GC18250	11	18 (5)	R 0.4 (6/15) L 0.4 (6/15)	R 0.80 (6/36) L CF	R 0/-2.50 x 177 L -0.25/-2.25 x 162	13 years Ishihara R 5/17 L 6/17	14 years, subnormal PERG P50. Normal ERGs
Patient 2 GC19726	4-5	20 (0)	R 1.0 (6/60) L 1.2 (4/60)	n/a	Not performed	20 years, Ishihara 1/17 BE	20 years, undetectable PERG, subnormal rod and subnormal and mildly delayed cone ERGs
Patient 3 GC20690	5-6	24 (8)	R 0.30 (6/12) L 0.30 (6/12)	R 0.80 (6/36) L 0.30 (6/12)	R +0.50/-2.00 x 5 L emmetropic	22 years, HRR medium r/g defect, b/y normal	Age 22, undetectable PERG. Mildly subnormal rod ERGs on right. Other ERGs normal bilaterally.
Patient 4 GC22774	4	25	R 1.0 (6/60) L 1.2 (4/60)	n/a	Myopic	25 years, Ishihara R 3/21, L 0/21	Not done
Patient 5 GC18293	8-9	31 (20)	R 0.18 (6/9) L 0.18 (6/9)	R 0.18 (6/9) L 0.18 (6/9)	R -1.00/-1.00 x 170 L -1.00/-0.50 x 60	28 years, Ishihara R 15/17 L 12/17	18 years, markedly subnormal PERG P50. Subnormal rod ERGs and subnormal and delayed cone ERGs. 27 years, undetectable PERG; stable ERGs.
Patient 6 GC19948	17	36 (3)	R 0.6 (6/24) L 1.2 (4/60)	R 0.84 (6/38) L 1.20 (4/60)	R -0.50/-0.50 x 40 L +0.50/-2.50 x 180	33 years, Ishihara 1/17 BE	33 years, undetectable PERG. Rod and cone ERGs normal on the right; marginally subnormal on the left due to eye closure.
Patient 7 GC18996	10	57 (7)	R 1.3 (3/60) L 1.3 (3/60)	R 1.20 (4/60) L 1.20 (4/60)	Not performed	54 years, HRR 0/24 BE	Not done

Table 10-2: Summary of clinical features in CDH3 related macular dystrophy

Seven probands from 7 families (6 consanguineous) were identified with bi-allelic variants in *CDH3* (figure 10-1); 2 from WES, 4 from screening a panel of 9 phenotypically similar patients and one with an already identified homozygous variant found elsewhere by Sanger sequencing.³⁷⁴ All presented in childhood/teenage years, age range 4-17 years. Of the 5 patients that screened negative for *CDH3*, 2 were later found to carry likely pathogenic *ABCA4* mutations and one was found to have *CRB1* mutations.

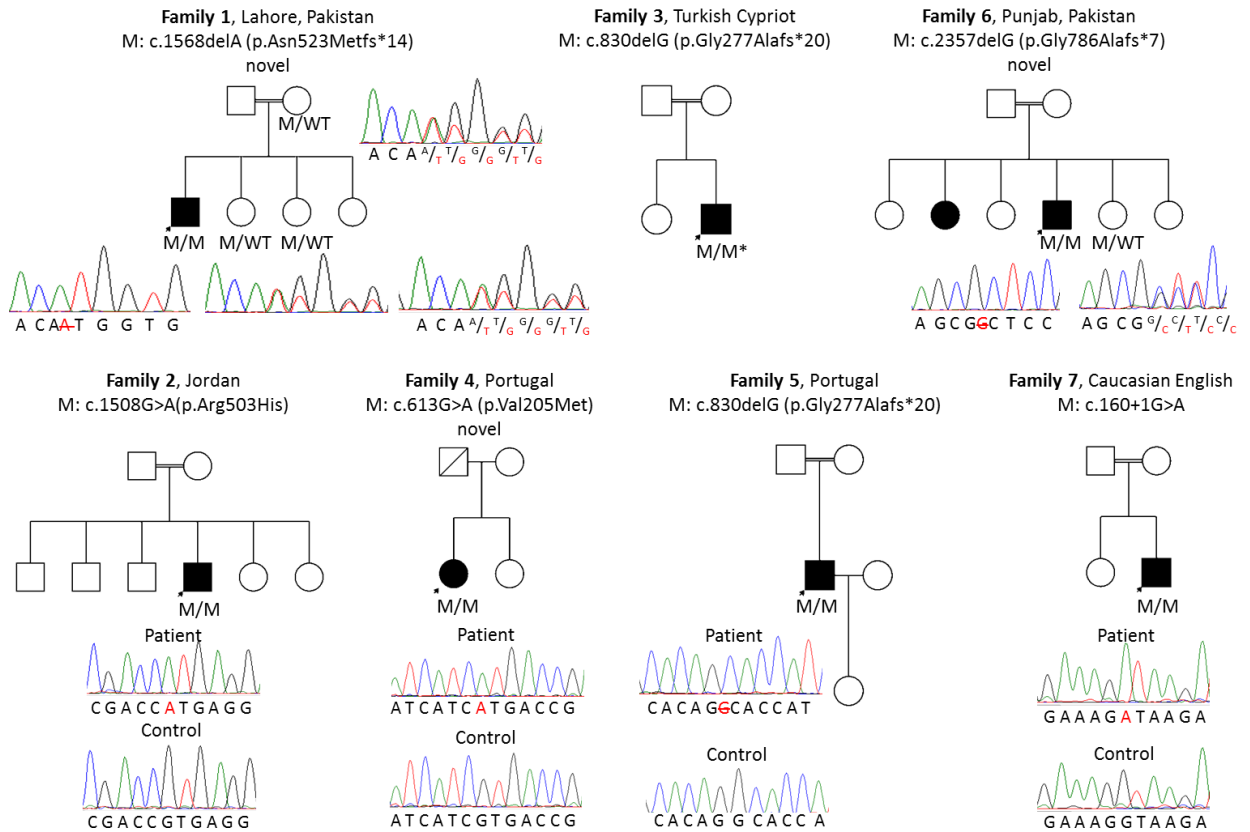


Figure 10-1: Pedigrees and chromatograms for patients with *CDH3* mutations

* mutation previously identified³⁷⁴

Vision was universally reduced at presentation. Of the 4 patients with more than one review, 3 had documented deterioration of vision, one already having severe vision loss at presentation. The mean age at last review was 30.1 years (median 25, range 18 to 57) with VA ranging from 0.18 logMAR to CF. The best VA was in patient 5 in whom VA was 0.18 logMAR each eye at age 31 years. Four patients had reported deterioration of central vision. Only patient 2 reported nyctalopia. Fundus abnormalities comprised variable degrees of atrophy of the retina, RPE and choroid in the posterior pole which extended nasal to the disc (figure 10-2). In 6 patients, the atrophy extended outside of the arcades. Patient 7 had severe chorioretinal atrophy with exposed sclera. Variable degrees of hyperpigmented spots/clumps in the macula was evident in all patients.

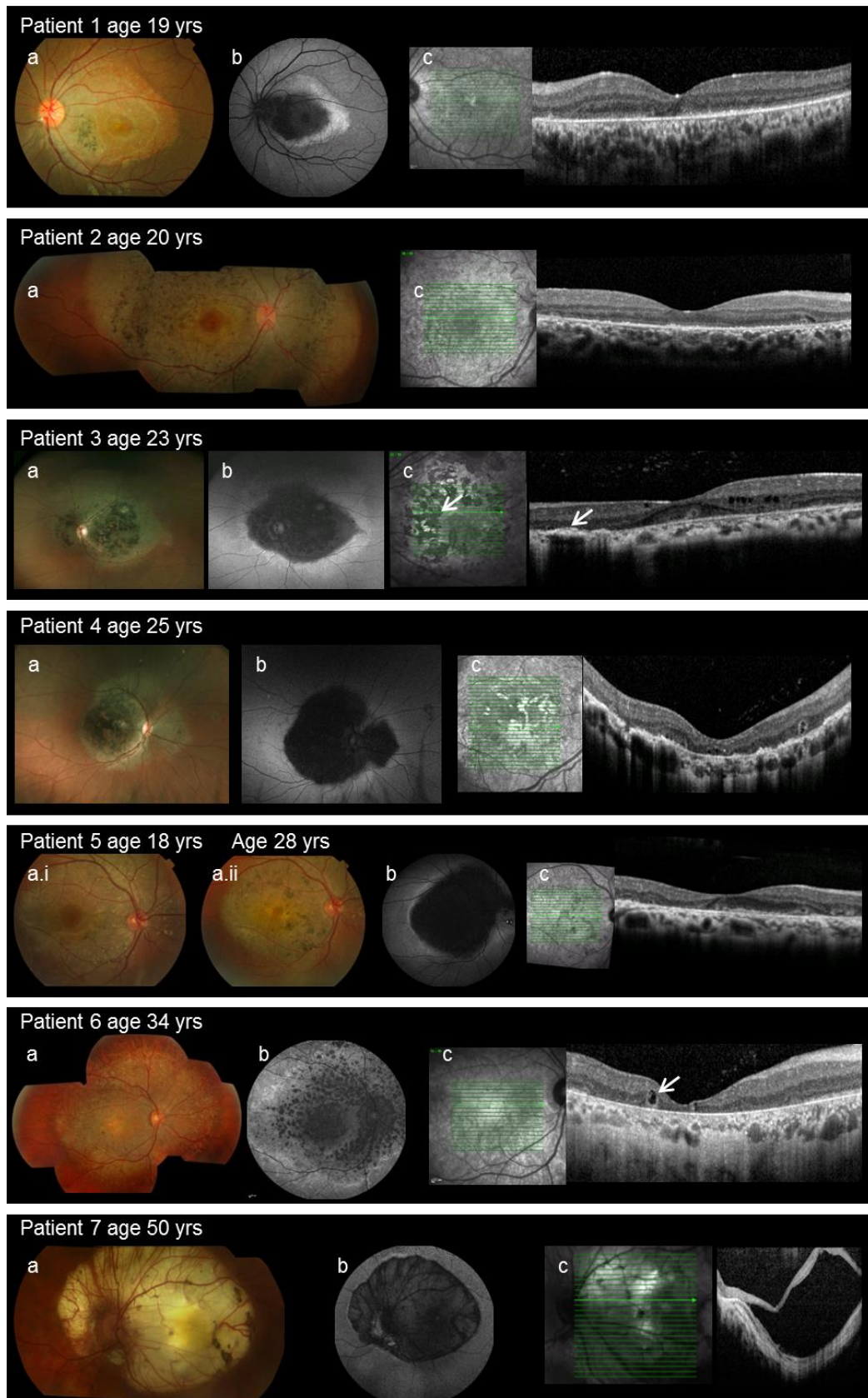


Figure 10-2: Retinal imaging in patients with HJMD

(a) Colour fundus photographs, (b) FAF, (c) OCT. Variable extent and severity of outer retinal/RPE atrophy, most severe in patient 7 with visible sclera. Pigmented lesions observed in all patients within atrophy, correspond to hypertrophy of the RPE (white arrows, patient 3). Increasing pigment demonstrated in patient 5. Loss of outer retina on OCT most severe in patient 7 who in addition has a serous detachment limited to the area of atrophy. ORTs frequently observed (white arrow, patient 6).

Serial imaging (available in 5 patients) demonstrated increasing hyperpigmentation with time in 3 patients (demonstrated in patient 5 in figure 10-2). FAF imaging demonstrated confluent hypofluorescence in areas of atrophy with a surrounding ring of relatively increased autofluorescence in 6 of 7 patients tested. In 2 patients within the area of confluent atrophy, a speckled hypofluorescence was observed. Patient 5 had small refractile deposits in both maculae, not noticed in any other patient.

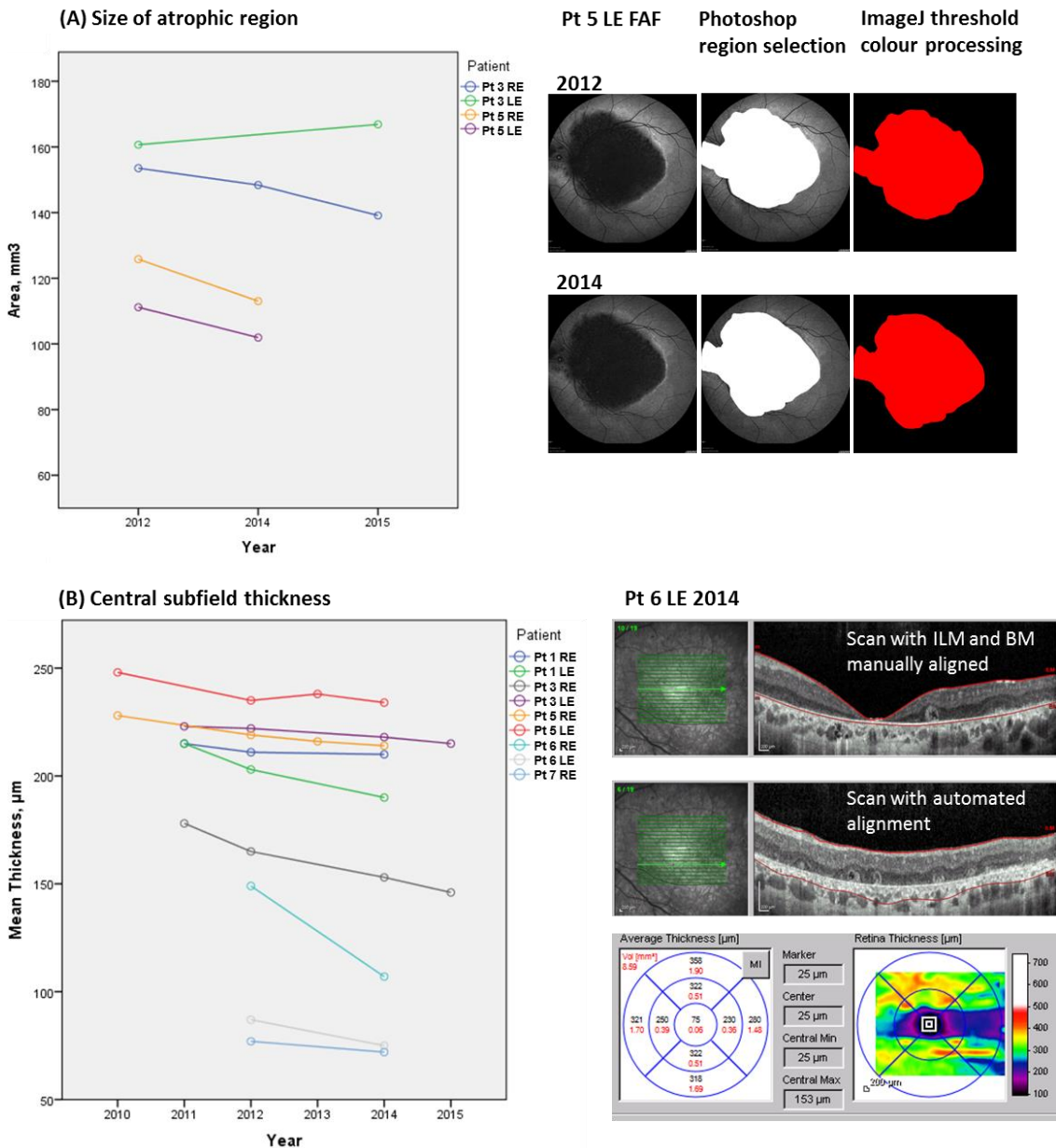


Figure 10-3: Serial imaging findings in CDH3 related HJMD
 (A) FAF imaging size of atrophic region, (B) OCT imaging central subfield thickness

OCT available in all patients, demonstrated variable degrees of atrophy. In patient 7 there was extensive atrophy of retina, RPE and choroid in addition to a serous retinal detachment over the atrophic area in the left eye (figure 10-2). In the remaining 6 patients there was outer retinal and RPE atrophy with partial preservation of the ISe band at the fovea observed in patient 5. Six patients had ORTs, patient 7 having too

extensive retinal atrophy for tubulations to be present. Five patients had serial OCT and FAF imaging over 2-10 years. The atrophic region on FAF imaging could only be accurately measured in 2 patients which demonstrated that the overall size of the atrophic region did not increase with time. However, retinal thickness within the atrophic region did decrease with time in all patients measured (figure 10-3).

Electrophysiology demonstrated undetectable PERG in 3 of the 5 patients tested, consistent with severe macular dysfunction (figure 10-4). There was a subnormal PERG P50 component in patient 3 at age 14 years in keeping with moderate macular dysfunction. In patient 5 the PERG was markedly subnormal at the age of 18 years and undetectable when examined 9 years later. Bilateral full-field ERG abnormalities were evident in patients 2 and 5, indicating mild generalised rod and cone dysfunction. There were marginal reductions in the rod-mediated ERGs in the right eye of patient 3 and rod and cone ERGs in the left eye of patient 6, but likely due to eye closure. The full-field ERGs in patient 5 showed no significant change when re-tested 9 years later.

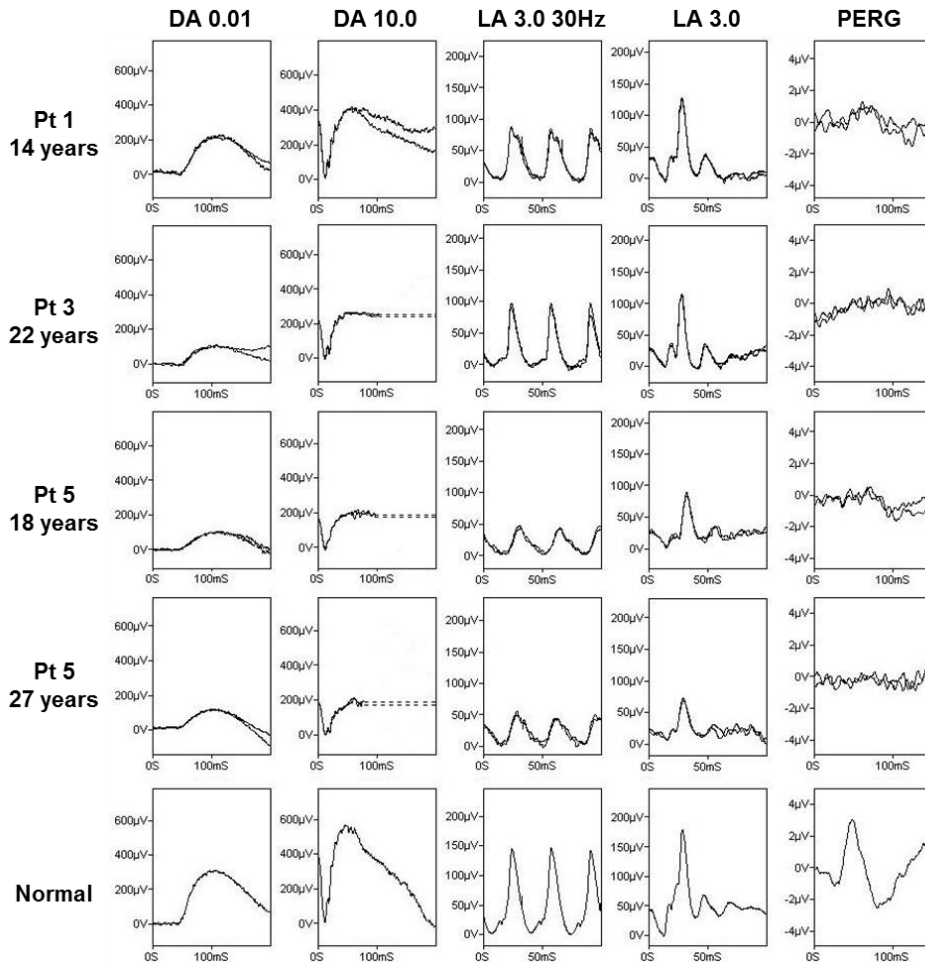


Figure 10-4: Electroretinography in CDH3 related HJMD

ERG and PERG features from one eye of patients 1, 3 and 5 and normal control. Patient 1 has normal DA ERGs and normal light-adapted LA ERGs; PERG P50 component is subnormal. Patient 3 shows mild reduction in the right eye DA ERGs and normal LA ERGs; all left eye responses were normal (not shown). Patient 5 shows mild but relatively stable abnormalities of all full-field ERGs with evidence of progressive PERG reduction over 9 years.

Systemically, all patients had thin scalp hair from at least early childhood, with normal hair elsewhere including eyebrows (figure 10-5). All patients had normal limbs.

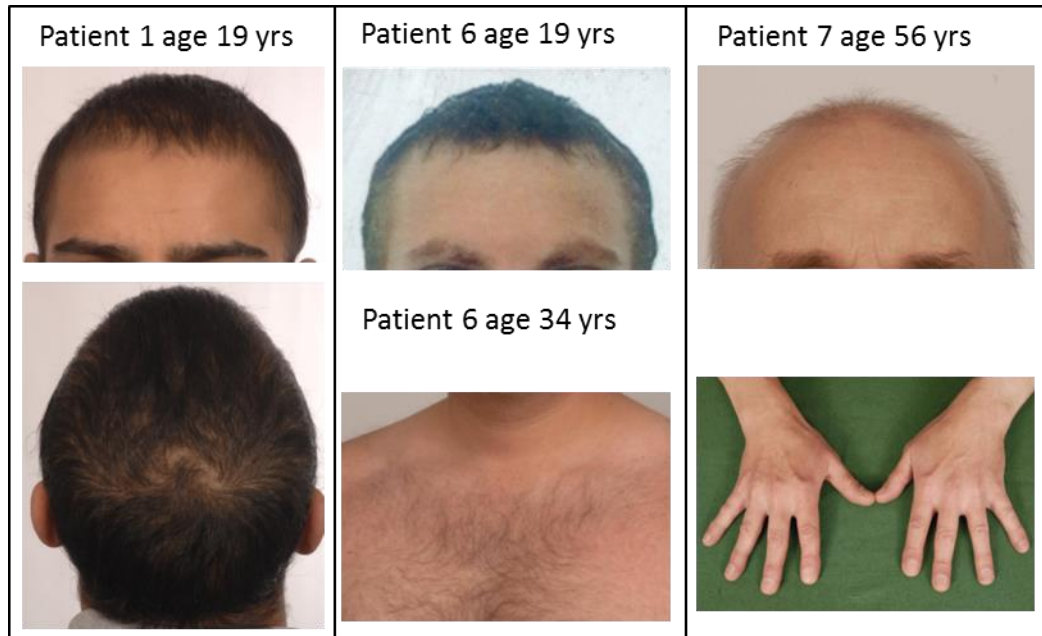


Figure 10-5: External photographs of patients 1, 6 and 7.

Head photographs demonstrate thinning of scalp hair with preservation of eyebrows and in addition in patient 6 preservation of chest hair. Hand photograph of patient 7 demonstrates normal hand morphology.

Molecular screening identified bi-allelic mutations in *CDH3* in all patients including 2 novel PTCs and 1 novel missense mutation (figure 10-1). The novel missense mutation, c.613G>A (p.Val205Met) is predicted damaging *in silico* (SIFT 0, Polyphen2 1.0). Only one other mutation was a missense change, R503H which has been previously reported in 3 affected families.^{373, 374} Both missense variants arise in codons highly conserved through the species (figure 10-6). All patients had presumed homozygote mutations.

	Val205Met	Arg503His
cod	MLIIVNVLDANDNKPVFTQD	KNGMDRES-QYVQDGKYTAL
zebrafish	MDIIVTVTDQNDNKPVFTQN	KNALDRESS-NVKDGGKYKAL
microbat	MNISIIIVTDQNDHKPKFTQD	AGVLDREDERFVRNNIYEV
rat	MNISIIIVTDQNDNKPFTQD	AGILDREDEQFVKNDIYEV
cow	MNISIIIVTDQNDHKPKFTQD	AGVLDREDEQFVRNNIYEV
squirrel	MNISIIIVTDQNDHKPNFTQA	AGILDREDERFVKNNVYEV
human	MNISIIIVTDQNDHKPKFTQD	VGTLDREDEQFVRNNIYEV
macaque	MNISIIIVTDQNDHKPKFTQD	AGTLDREDERFVRNNIYEV
chicken	MEIIVTVTDQNDNKPQFTQE	REQLDRES-PFTKNSTYVAV
flycatcher	MEIIVTVTDQNDNKPQFTQE	RDHLDRES-PFVKNSTYMAV
	* * : * * *.** ***	:***. .:: * ..

Figure 10-6: Conservation of CDH3 missense codons

10.4 Discussion

In this study of *CDH3* related retinal dystrophy, detailed phenotyping of molecularly confirmed patients has characterised the key ophthalmic and systemic features which aided diagnosis and allowed an assessment of the prognosis. The patients all presented in childhood with central visual disturbance and sparse scalp hair with a predominantly macular dystrophy. The majority of previously reported patients also presented with reduced vision in childhood except for one reported family in which the eldest child had normal visual acuity at 14 years of age although macular pigmentary change was observed.³⁷⁴

In this series, visual acuity was found to deteriorate over time except for one patient with stable and good acuity over 20 years of review and preserved foveal photoreceptors visible on OCT. Longitudinal data on visual acuity decline has not been previously reported although a trend of decreased vision with patient age has been observed.³⁸⁴ Although the majority of previously reported patients have marked macular atrophy encompassing the disc, one patient with mild atrophic changes and syndactyly of his left foot has been reported.³⁷⁶ The refractile deposits in patient 5 were much smaller than the expected size of refractile drusen and no other cause could be elucidated from the patient's past medical history.³⁸⁷ It remains unclear whether they are related to *CDH3* as it has not been observed in any other reported patient.

There has been only one previously published patient with detailed retinal imaging.³⁸⁵ This 6 year old patient had typical features of posterior pole atrophy with early loss of photoreceptors and RPE on OCT. In contrast, all patients in this study underwent detailed imaging and 5 had serial OCT investigations. All patients had marked and confluent hypofluorescence on FAF imaging which corresponded to the atrophic region. This was surrounded by an apparent ring of increased autofluorescence. OCT imaging demonstrated loss of outer retina and RPE in all patients with severe atrophy in patient 7. ORTs were frequently observed. The posterior pole appears to be atrophied from early childhood, with the degree of atrophy within that region progressing with time (based on OCT), but the overall area of atrophy (based on FAF imaging) not increasing although there were limited numbers available for analysis.

Serial ERG available in one patient demonstrated that the full field ERG abnormalities did not progress with time although the PERG worsened over the same 9-year period. Bilateral ERG abnormalities were evident in 2 of 5 cases and were relatively mild, whereas most had PERG evidence of severe macular dysfunction in keeping with the retinal imaging; the disorder appears to be largely confined to the posterior pole. Previous reports of electroretinography have largely focused on ERG and EOG findings with only one report of PERG in HJMD.³⁸¹ At age 48 years, the patient in this

report had very poor vision, an extinguished PERG and reduced cone specific ERG responses. ERG findings in previous reports have been either normal or with subnormal rod and/or cone responses.^{370, 373-376, 379, 381, 383-385} One patient was reported to have severe retinal dysfunction on ERG but no further details were given.³⁷⁷

Overall, there is evidence from visual acuities, serial retinal imaging and electrophysiology that the condition is progressive but progression is largely limited to the posterior pole. The onset of symptoms is not from birth or infancy but childhood/adolescence. There is no nystagmus in these patients. The age of onset and evidence of progression would indicate that this is a progressive dystrophy and not a developmental disorder.

The most common cause of juvenile-onset macular dystrophy is Stargardt macular dystrophy due to bi-allelic mutations in *ABCA4*.⁴⁷ This disorder may present with similar symptoms to *CDH3* related disease with central visual disturbance, macular atrophy, and either electrophysiological dysfunction confined to the macula (found in 1/3 of children with Stargardt disease) or macular and generalised retinal dysfunction usually involving cone and rod systems (found in the remainder).³⁸⁸ Not all patients with Stargardt disease have the distinctive yellow-white flecks at presentation. Patients with HJMD may initially be misdiagnosed with Stargardt disease but the 2 conditions can be distinguished most readily by examination of the scalp hair. In addition, in Stargardt disease, the peripapillary region is classically although not universally spared.³⁸⁹

CDH3 encodes P-cadherin, one of the family of cadherin transmembrane proteins that form a major component of adherens junctions important in cell to cell interactions.³⁹⁰ A total of 22 mutations in *CDH3* have been reported including those from this study, 7 missense, 2 splice site and the rest PTCs (figure 10-7, table 10-3).

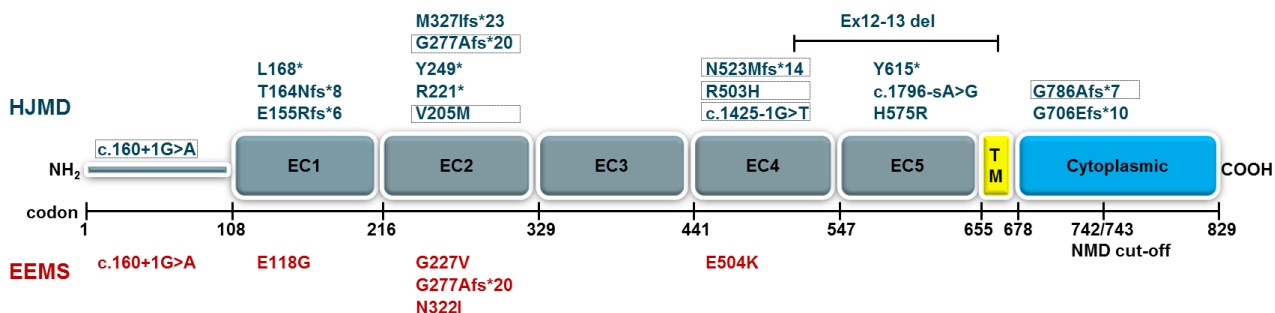


Figure 10-7: Schematic diagram of CDH3 with mutation codon location

Mutations from this study boxed. EC; extracellular, TM; transmembrane

All but one of the PTCs identified would be predicted to trigger NMD and lead to haploinsufficiency; the exception, p.G786Afs*7 arises after the predicted cut-off for NMD.²⁰⁶ Patient 6, homozygous for this variant did not have more severe disease as

may be expected if abnormal protein is produced; his onset of visual symptoms was later than all other patients in this series. Four of the 7 reported missense variants were associated with EEMS which may indicate that abnormally produced protein as opposed to a lack of protein has a particularly detrimental effect on limb development.

Nucleotide	Protein	Exon	ExAC	Phenotype	First reported
c.160+1G>A	splice	Intron 2	Not present	HJMD/EEMS	Indelman 2007
c.353A>G	p.E118G	4	Not present	EEMS	Shimomura 2008
c.462delT	p.E155Rfs*6	5	1 in 121084	HJMD	Indelman 2003
c.490dupA (reported as c.490insA)	p.T164Nfs*8	5	1 in 121396	HJMD	Shimomura 2008
c.503T>A	p.L168*	5	1 in 121404	HJMD	Indelman 2003
c.613G>A	p.V205M	6	Not present	HJMD	This study
c.661C>T	p.R221*	6	1 in 119728	HJMD	Indelman 2007
c.747C>A	p.Y249*	7	Not present	HJMD	Avitan-Hersh 2012
c.830delG (reported as c.829delG)	p.G277Afs*20	7	Not present	HJMD/EEMS	Indelman 2003
c.830G>T	p.G277V	7	Not present	EEMS	Basel-Vanagaite 2011
c.965A>T	p.N322I	8	Not present	EEMS	Kjaer 2005
c.981delG	p.M327Ifs*23	8	Not present	HJMD	Sprecher 2001
c.1425-1G>T	Splice	Intron 10	1 in 121274	HJMD	Shimomura 2008
c.1508G>A	p.R503H	11	Not present	HJMD	Indelman 2002
c.1510G>A	p.E504K	11	Not present	EEMS	Indelman 2007
c.1568delA	p.N523Mfs*14	11	Not present	HJMD	This study
Ex12-13 del	In-frame del	12-13	Not present	HJMD	Halford 2012
c.1724A>G	p.H575R	12	Not present	HJMD	Indelman 2007
c.1796-2A>G	Splice	Intron 12	3 in 121250	HJMD	Shimomura 2010
c.1845T>A	p.Y615*	13	Not present	HJMD	Indelman 2005
c.2117delG (reported as c.2112delG)	p.G706Efs*10	14	Not present	HJMD	Indelman 2003
c.2357delG	p.G786Afs*7	16	Not present	HJMD	This study

Table 10-3: All reported mutations in *CDH3*

P-cadherin regulates the development of hair, limbs and the RPE as demonstrated by upregulation of its expression in these key locations in mouse embryo studies.³⁷¹ It is not expressed in the neuroretina.^{371, 391} This would indicate that photoreceptor loss in *CDH3* related macular dystrophy is secondary to P-cadherin dysfunction in the RPE. Cadherin proteins are characterised by 5 calcium binding extracellular (EC) domains, critical to protein function. Reported mutations arise throughout the protein but all reported missense variants are found within the EC domains which may indicate that their functional impact is most significant there. The tertiary protein structure for P-cadherin has been experimentally proven using X-ray crystallography for EC1 and EC2 domains only.³⁹²

The site of disease could be primarily RPE with secondary photoreceptor loss as supported by expression studies in animal models.^{371, 391} In humans, *CDH3* mRNA has been identified in expressed sequence tags from RPE.³⁹³ From this series there is OCT evidence for concurrent loss of outer retina and RPE, not with initial photoreceptor loss as would be expected in a primary photoreceptor disorder. ORTs on OCT arise in regions of outer retinal atrophy and are typically observed in disorders in which the underlying RPE is the primary site of dysfunction such as Stargardt disease and age related macular degeneration but have also been reported as late features of photoreceptor disorders such as enhanced S-cone syndrome.¹³² It may be that rather than primary RPE dysfunction, the disorder is one of concurrent RPE and photoreceptor loss as seen in choroideraemia a condition in which ORTs are also frequently identified.³⁹⁴ It is not clear why the retina/RPE in the posterior pole is predisposed to degeneration compared to elsewhere in the fundus. The macula is the region of highest cone density and has a higher metabolic demand than the rest of the retina due to increased phototransduction.³⁹⁵ One possibility is that the increased metabolic demand in that region is sufficient to compromise the already abnormal RPE cell function. Further understanding of *CDH3* protein function in the retina/RPE is needed to ultimately define the location and mechanism of disease.

Although HJMD and EEMS are considered allelic disorders, they may be better considered as part of a phenotypic spectrum in which all patients have hypotrichosis and macular dystrophy with variable additional limb and ectodermal anomalies.³⁸³ There is no clear genotype-phenotype correlation and the same variant may be associated with a variable phenotype. For example the variant p.G277Afs*20 which has been associated with both HJMD and EEMS in the homozygous state (figure 10-7).^{374, 382} Patient 7 in this study who has no limb or ectodermal abnormalities, was found to be homozygous for c.160+1G>A. This variant has been reported once in a compound heterozygous patient in conjunction with a missense change p.E504K.³⁷⁶ The reported patient had syndactyly of his left foot suggesting an EEMS phenotype, although mild. Only 3 other variants have been reported in EEMS, all missense changes. Reported limb anomalies include severe split hand/foot malformations but may be subtle such as a single nail dysplasia, and should be specifically looked for in patients presenting with HJMD.^{371, 383}

This condition, based on symptoms, visual function, retinal imaging and electrophysiological characteristics, is centrally progressive with preserved peripheral vision. Its characteristic presentation with marked macular dysfunction in childhood with thin, sparse hair are readily recognisable features to aid diagnosis.

11 Maculopathy due to mutations in *CRB1*

11.1 Introduction

CRB1 (Crumbs homolog-1, MIM#604210) encodes a subunit of the Crumbs protein, an apical protein essential for photoreceptor morphogenesis and protection from light induced retinal degeneration.³⁹⁶ Related phenotypes are heterogeneous and include LCA, RCD and CORD with *CRB1* accounting for an estimated 11% of LCA cases.^{6, 73, 397-399} Additional associated features can include exudative telangiectasia and nanophthalmos.^{400, 401} Typical *CRB1* related disease manifests as an EORD with macular atrophy, generalised nummular pigmentation with para-arteriolar RPE sparing, and thickened, disorganised lamination on OCT although these features are variable.^{6, 397, 402} In infancy, the full phenotype may not be evident with macular atrophy and peripheral white dots early features. There have only been 4 families reported with CORD, and in one family this was associated with retinal cysts.^{6, 399} No correlation has been found between genotype and phenotype.⁴⁰³

A patient with retinal dystrophy localised to the posterior pole and encompassing the disc was investigated in this study. Initially, screening of *CDH3* was performed which was negative for any pathogenic mutation. The patient underwent WES as part of the SPEED study which identified a homozygous mutation in *CRB1*. Whilst further investigating this, a report of *CRB1* related macular dystrophy in a single family was published.⁴⁰⁴

11.2 Methods

11.2.1 Patient ascertainment

The patient was known to the retinal genetics clinic and was initially prioritised by a supervisor for *CDH3* screening. This was normal and she was subsequently recruited to the SPEED study for further investigation.

11.2.2 Clinical assessment

Full examination, imaging and EDTs were performed as part of routine care. Thickness of the ETDRS central subfield and temporal inner macula regions were measured using the automated Heidelberg Spectralis viewing module (version 6.3.4.0) with the RPE basement membrane and the ILM layers checked for accuracy in each OCT slice and manually corrected if necessary. OCT thickness over time was measured and

compared with normative data.⁴⁰⁵ Statistical analysis was not possible due to small numbers.

11.2.3 Molecular methods

WES was performed as part of the SPEED study and 2 *CRB1* variants were identified. These were confirmed by myself by Sanger sequencing with segregation performed in available relatives with specifically designed primers (table 11-1). Mutation nomenclature was assigned in accordance with GenBank Accession number NM_201253.1.

Exon	Primer forward 5' → 3'	Primer reverse 5' → 3'	Enzyme	Annealing temp (°C)	Amplicon size (bp)
2	GTTGAGGCAGCACAAAGGTCACAA AG	GTCACCTCTGCTTCTGCCACTT AG	BIOTAQ	60	740
9.1	CTCAACTTCTTCTTCCATAAAATGG GG	CCTTGCAGGCCCTTTATATT	BIOTAQ	60	659
9.2	GGCACATGGCACGAAGTGACCCT	GTATACCTTGAGGAGAGAGCTT TCC	BIOTAQ	60	776

Table 11-1: Primer pairs for sequencing of *CRB1*

11.3 Results

A patient of Bangladeshi origin developed central visual disturbance at 12 years of age. Visual acuity at presentation to Moorfields at age 19 years was R 0.5 and L 0.3 logMAR with low myopic refractive correction. There was reduced colour vision on Ishihara testing (R 5/17, L 3/17). Over 13 years of follow up, visual acuity deteriorated to R 1.3, L 1.5 logMAR. In both eyes, there was a confluent, pale chorioretinal atrophy encompassing the disc without peripapillary sparing and extending outside of the arcades with anterior retina preservation (figure 11-1). Pigmented lesions within the atrophy increased over time and on OCT imaging could be observed as localised RPE hypertrophy (figure 11-2).

FAF imaging demonstrated loss of autofluorescence in areas of atrophy which increased over time (figure 11-1). Small islands of hyperautofluorescence were observed on FAF imaging that corresponded to preserved RPE on OCT (figure 11-3). OCT generally demonstrated loss of outer retina and RPE. Disorganisation of retinal lamination was identified on peripheral OCT slices (figure 11-2).

On OCT thickness measurements, the retina was not thicker compared to published controls (table 11-2). However, these measurements were in regions of atrophy where it may be expected to be thinned. Comparison of OCT thickness over a 4 year interval did not find any notable decrease. The observed increase over time in thickness of the

central subfield particularly of the right eye may be due to epiretinal membrane formation (figure 11-1).

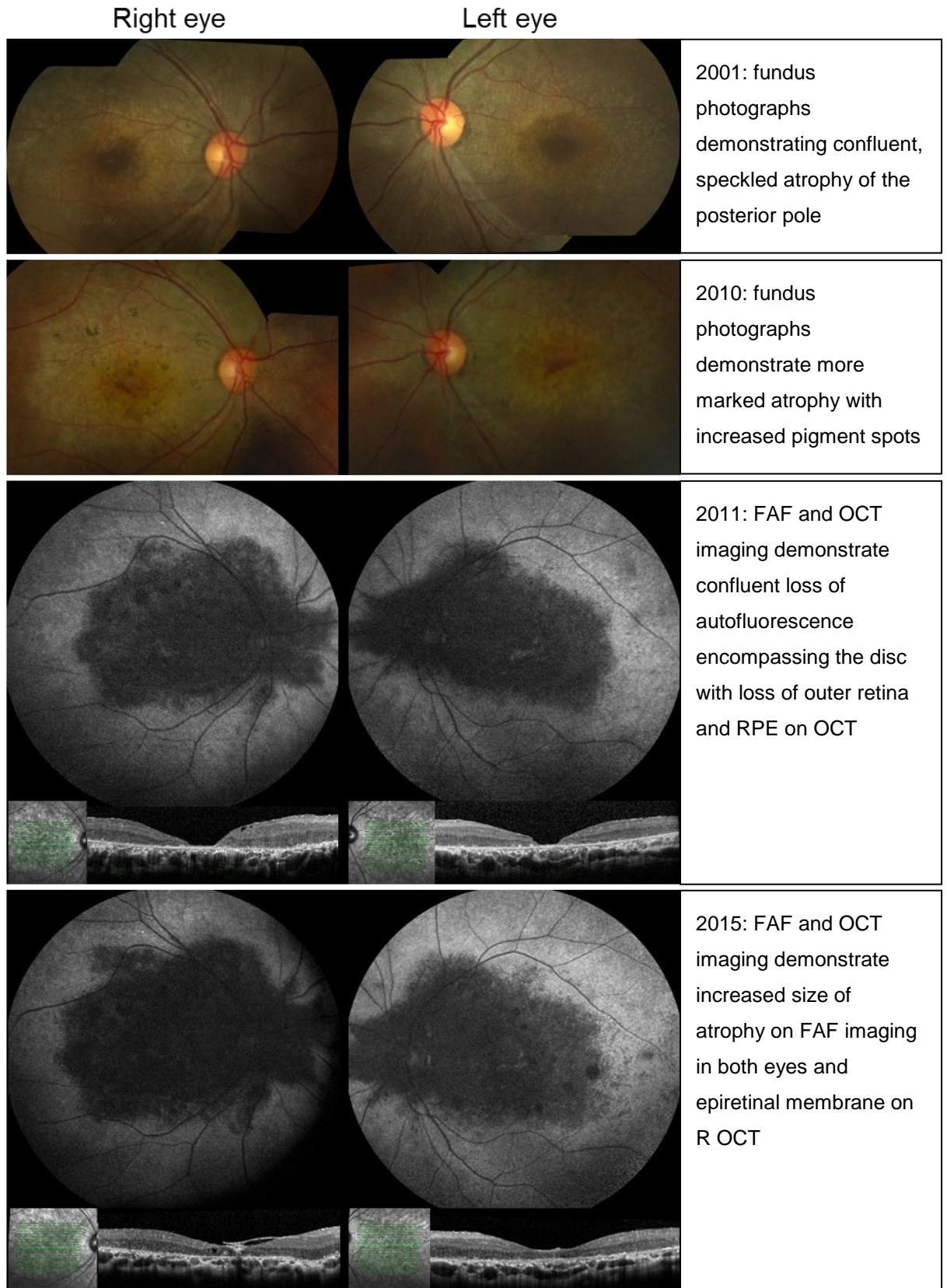


Figure 11-1: Retinal imaging in *CRB1* related maculopathy

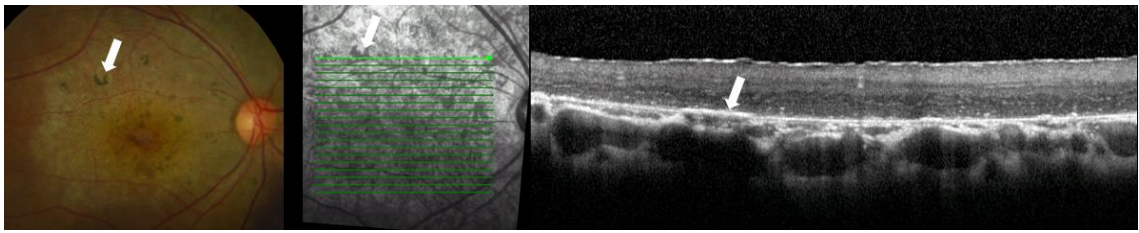


Figure 11-2: Hyperpigmented macular lesions

R fundus image and OCT with arrows at position of pigmented lesion corresponding to thickened RPE on OCT. Peripheral OCT slice also demonstrates disorganised lamination.

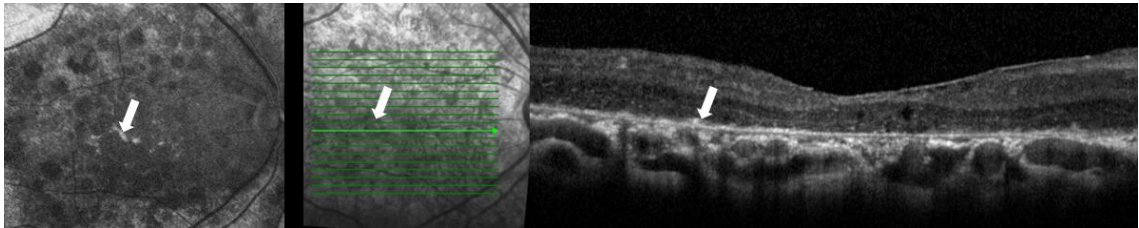


Figure 11-3: Preserved islands of RPE and photoreceptors

R 30 degree FAF imaging and OCT demonstrate small island of increased autofluorescence corresponding to preserved RPE/photoreceptors on OCT.

	Central subfield	Temporal inner macula
RE 2011	105	298
RE 2015	169	293
LE 2011	105	271
LE 2015	124	298
Controls	270	323

Table 11-2: Macula thickness in each eye compared with normative data

EDTs at age 27 years demonstrated undetectable PERG, moderately severe cone dysfunction, and milder rod dysfunction. There was mild deterioration from a previous ERG at age 20 years.

WES identified compound heterozygous mutations in *CRB1*, c.254G>A (p.Cys85Tyr), novel, not in ExAC and predicted pathogenic *in silico* (SIFT 0, Polyphen2 1.0), and c.3542dupG (p.Cys1181Trpfs*13) which has been previously reported in the homozygous state in a case of LCA.⁶ Analysis of conservation between species demonstrated that the missense variant arose within a highly conserved residue (figure 11-4). Segregation confirmed the mutations were in trans with the first variant maternally inherited and the second found in both unaffected brothers. Prior Sanger sequencing of *CDH3* identified a heterozygous variant, c.109A>T (p.Thr37Ser, rs374627741) predicted to be tolerated *in silico* (SIFT 0.49, Polyphen2 0.765).

	p.Cys85Tyr
zebrafish	CQTTVPVFPSTRCDSSSTFCQLSICQGNVTCQPTGAHPGELVCQCDSSGLLGQDCLSSAQL
turtle	CVDT-IDILEEDCNKTDDPCSSNPCLQNATCLSMAG-NLSFTCECPTGYSGTTCEFPISL
chicken	CVDMSLDTMEELCNKTSNPNPCSSNPCLQNATCLSSAG-NLNFTCECPDGYNGTTCEIAISM
flycatcher	CADASVDSVEELCNKTSNPNPCSSNPCLQNATCLGSAG-NLSFTCQCPAGYNGPTCERADSG
megabat	CA-----DKDCDNVTDPCFPNPCQGNATCVNTPG-ERSFLCECPPGYSGMTCETAIGS
mouse	CLDT-ANLNDKDCEDLKDPCFSSPCQGIATCVKIPG-EGNFLCQCPPGYSGLNCETATNS
human	CSDT-ANLNDKDCDNMKDPCFSSNPQGSATCVNTPG-ERSFLCKCPPGYSGTICETTIGS
guinea	CSDT-ANLNDKDCDNMKDPCSSNPQGIATCMNTPG-ERGFQCQCPPGYNVGTETALGS
	* . * : . * . * . ** . : * : * * * *

Figure 11-4: Conservation of novel missense residue in *CRB1*

11.4 Discussion

This study of a patient with *CRB1* related maculopathy illustrates the differences in presentation when compared with more typical *CRB1* related retinal dystrophy. The patient had central visual involvement as a presenting feature and low myopia. Patients with LCA and RCD typically have a low hyperopic refractive error and present either in infancy with severe loss of vision or in childhood with nyctalopia and mid-peripheral retinal changes.⁶ Macular atrophy is a common feature of *CRB1* related retinal dystrophy in general but is not exclusive to this molecular cause, having been reported in several other retinal dystrophies including those due to *NMNAT1*, *CRX*, *LCA5*, *RDH12*, and *PROM1*.^{6, 92, 76, 178, 205, 406} In early stages, the macular atrophy found in this series could resemble other conditions such as Stargardt disease but atrophy encompassing the disc appears indicative of either *CRB1* or *CDH3* related disease. The retinal appearance differed from other *CRB1* related retinal dystrophies by its lack of anterior retinal involvement and the large, disc-encompassing atrophy.

OCT scanning demonstrated disorganised retinal lamination in the peripheral retina and a retinal thickening greater than would be expected in a retinal dystrophy particularly within a region of atrophy. This thickening and disorganised lamination has been previously reported in *CRB1* related disease and is a useful clinical characteristic for directing molecular investigation.^{6, 249}

Four families with *CRB1* related CORD have been previously reported with central visual disturbance as presenting symptoms but without macular atrophy.^{6, 399} Only one other family has been reported with a similar maculopathy to the patient studied.⁴⁰⁴ Two siblings presented in their 20s-30s with central visual disturbance and macular atrophy that extended nasally to the disc without peripapillary sparing. The anterior retina was preserved. Retinal imaging in the sister was strikingly similar to our patient with a pale atrophic appearance to the posterior pole, marked loss of autofluorescence encompassing the disc with small islands of preserved RPE that were hyperautofluorescent and loss of outer retina and RPE structures on OCT. The brother

had less marked atrophy and crescents of hypoautofluorescence rather than the confluent autofluorescence seen in the sister. OCT was similar with the exception of oedema in one eye. At last review vision was much better in these siblings than in our patient studied, at 20/40 RE, 20/400 LE for the sister at age 45 years and 20/40 RE, 20/70 for the brother at age 41 years. This may be related to the foveal islands of preserved photoreceptors/RPE observed in both siblings. A trend towards outer macular thickening was observed although they had preserved retinal lamination.⁴⁰⁴ Marginal cone involvement was identified in the sister on ERG.

CRB1 is expressed in the retina in both the subapical region of photoreceptors adjacent to adherens junctions and in Müller cells.⁴⁰⁷ It is not expressed in the RPE with minimal expression observed in brain and testis.⁴⁰⁸ It is particularly important in retinal development for correct polarity and adhesion of retinal neuroepithelium progenitor cells.⁴⁰⁹ The CRB family of transmembrane proteins are characterised by large extracellular epidermal growth factor (EGF) and laminin-globular domains, a single transmembrane domain and a 37 amino acid intracellular domain containing specific protein-binding motifs.⁴⁰⁹ The novel missense mutation identified in this study arises within the extracellular EGF domain.

The thickening and disorganised lamination evident in *CRB1* related retinal dystrophy is thought to be developmental possibly due to the loss of normal retinal remodelling and apoptosis in retinal development.²⁴⁹ Although this has been observed at an early age it has not yet been proven to be developmental in humans. The *Crb1*^{-/-} knockout mouse develops isolated, small regions of retinal degeneration not the widespread retinal degeneration that more resembles the human disease whereas the *Crb2*^{-/-} knockout mice does have a similar phenotype.^{407, 410} CRB2 also forms part of the subapical CRB complex. In the *Crb2*^{-/-} knockout mouse, there is abnormal lamination of the neuroepithelium from embryonic day 18.5 which suggests that in humans this may also be developmental.⁴⁰⁹

12 Cone-rod dystrophy due to mutations in *ADAM9*

12.1 Introduction

ADAM9 (A disintegrin and metalloproteinase domain 9, MIM#602713) is a widely expressed integral membrane protein with multiple roles that include cell interactions with the extracellular matrix and ECM remodelling.^{411, 412} Bi-allelic loss of function mutations in *ADAM9* were identified in 4 families with CORD in 2009; all affected individuals developed reduced visual acuity in the first decade of life.⁴¹¹ A further paper detailed a consanguineous family with early onset CORD due to splice site mutations in *ADAM9*.⁴¹³ WES identified a homozygous PTC in *ADAM9* in a child with CORD with the phenotype the focus of this study.

12.2 Methods

12.2.1 Patient ascertainment

A child with CORD was known to the paediatric retinal genetic clinic and recruited for genetic investigations. No variants were identified on an APEX microarray (LCA chip). Subsequently WES was then performed.

12.2.2 Clinical assessment

I assessed and examined the proband and obtained retinal imaging. He had already undergone EDTs at 3 years of age as part of his clinical care but I arranged further EDTs at age 7 years.

12.2.3 Molecular investigations

The homozygous mutation found on WES by colleagues (AROS) was confirmed by Sanger sequencing by myself with segregation performed in available relatives with a specifically designed primer pair (table 12-1). Mutation nomenclature was assigned in accordance with GenBank Accession number NM_003816.2.

Exon	Primer forward 5' → 3'	Primer reverse 5' → 3'	Enzyme	Annealing temp (°C)	Amplicon size (bp)
10	TTGCCATTTTCCTGCCATGT	AAAGAGCTAATAAACACATAGCACA	BIOTAQ	65	401

Table 12-1: Primer pair for sequencing of *ADAM9*

12.3 Results

A male patient presented at 3 years of age. He was noted in infancy to have a right convergent squint with poor vision and eccentric fixation. There was no nystagmus. He was otherwise well with normal development. The parents were from Pakistan and were first cousins. He had one unaffected younger brother.

At first review at 3 years of age, VA was R and L 1.0 logMAR (Snellen 6/60). At last review, age 7, the vision was R 1.0 logMAR, L 0.88 logMAR (Snellen 6/48) with a hyperopic, astigmatic refractive error of R +4.00/-2.50 x 20, L +4.00/-2.00 x 180. There was a moderate left divergent squint with eccentric fixation. Early posterior sub-capsular cataract was noted.

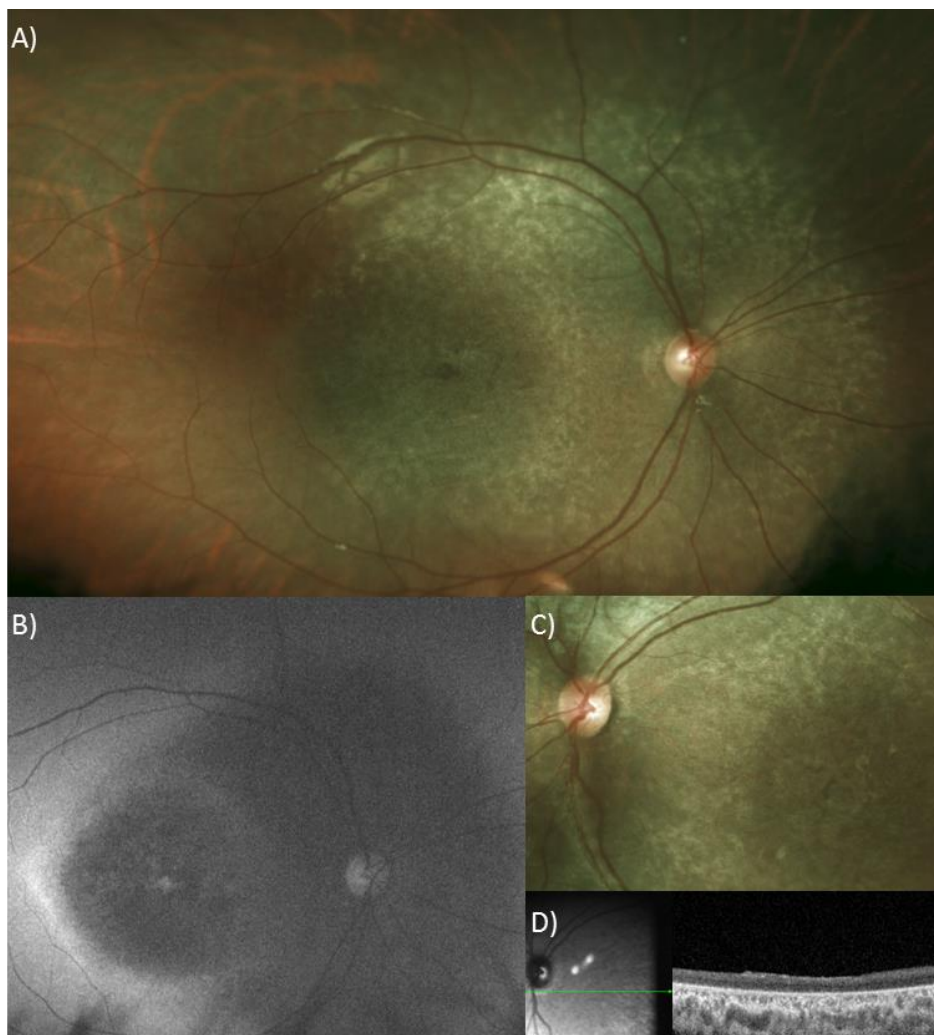


Figure 12-1: Retinal imaging in a patient with *ADAM9* related CORD

A) R Optos photograph showing a hypopigmented, atrophic region of the posterior pole, encompassing the disc with no abnormal peripheral pigment; B) R Optos FAF imaging showing reduced autofluorescence in area of atrophy with increased autofluorescence temporally at edge of atrophy; C) L Optos photograph magnified to demonstrate speckled nature of atrophy; D) L OCT showing generalised loss of outer retina

Fundus examination showed posterior pole atrophy with a white speckled appearance, which extended to the arcades and encompassed the optic disc (figure 12-1). Retinal

imaging demonstrated reduced autofluorescence in the posterior pole with atrophy of the outer retina on OCT (figure 12-1). EDTs performed at the age of 3 years using surface electrodes, revealed an undetectable PERG and borderline photopic and scotopic ERGs. At the age of 7 years the PERG and full-field ERG were performed using corneal electrodes. The PERG was undetectable in keeping with severe macular dysfunction. ERGs were mildly abnormal consistent with CORD (figure 12-2).

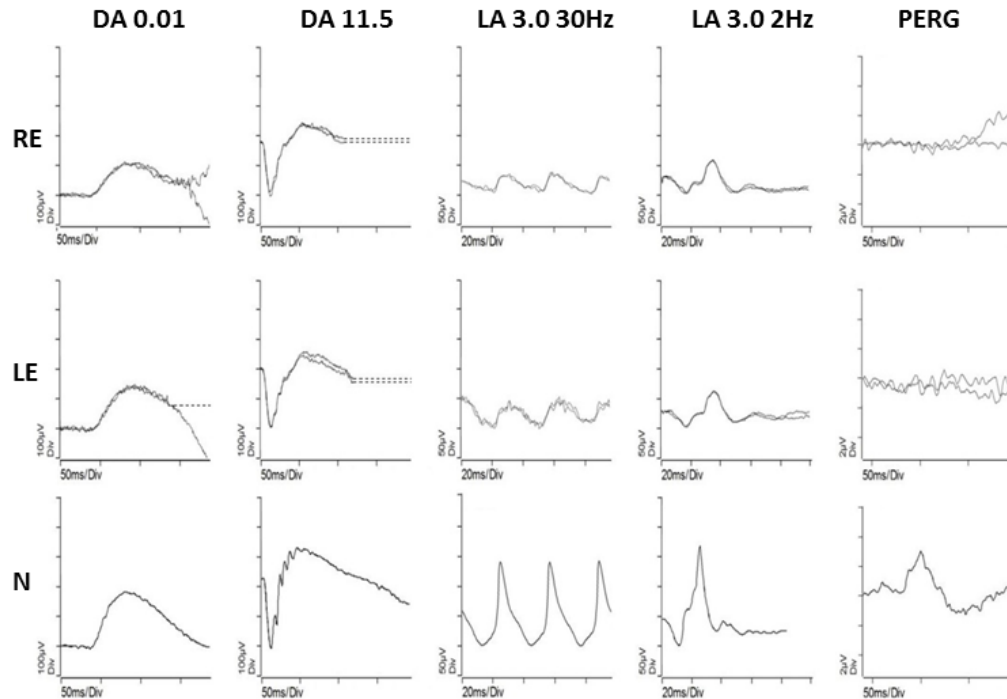


Figure 12-2: Electrophysiology in *ADAM9* related CORD

ERGs and PERG from the RE and LE of the patient compared with control N

WES identified a novel, homozygous mutation in *ADAM9*, c.967delT (p.Ser323Glnfs*33) which is not present in ExAC. On direct Sanger sequencing this was shown to segregate in the family with both parents heterozygous for this mutation (figure 12-3).

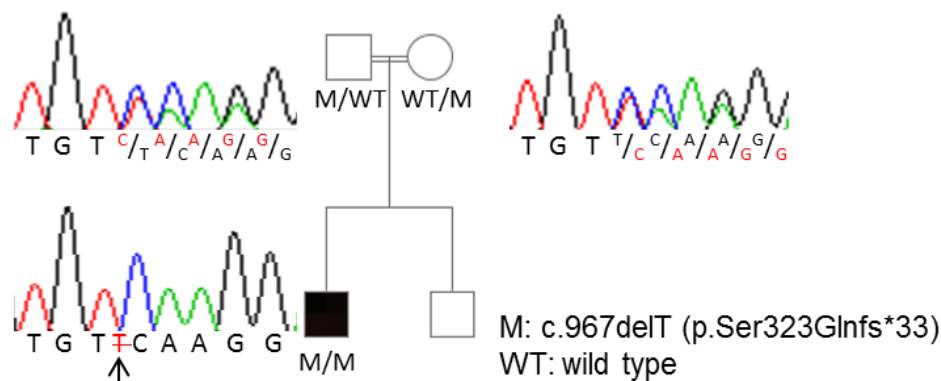


Figure 12-3: Pedigree and sequencing results

12.4 Discussion

Non-syndromic, autosomal recessive CORD is rare and usually associated with bi-allelic mutations in *ABCA4*.¹¹⁰ In the previous reports of CORD due to *ADAM9*, 5 families were identified with mutations leading to either aberrant splicing or premature truncation codons.^{411, 413} Similar to our patient, all had poor vision in their first decade of life, no nystagmus and outer retinal atrophy of the macula. Most were also noted to have discrete white patches in the posterior pole and around the disc and a peripheral pigmentary retinopathy which is not present in our patient. Retinal imaging in a previous report of the index family, demonstrated posterior pole atrophy in 2 patients in their 40's with a similar appearance to our patient.⁴¹⁴ Electrophysiology in these 2 patients demonstrated severe loss of both cone and rod function. In the recent report of a single family, the youngest patient assessed was 17 years.⁴¹³ Posterior pole atrophy was noted and in the retinal images this also encompassed the disc. No electrophysiology was available. Given the young age of our patient, we have been able to demonstrate the electrophysiological phenotype of severe loss of macular function in the early stages with relatively mild peripheral retinal dysfunction.

The ADAM family of proteins are a large group of widely expressed transmembrane and secreted proteins with multiple roles in cell adhesion, cell signalling and ectodomain proteolysis of proteins including growth factors.⁴¹⁵ Up and down regulation of a number of different ADAM proteins has been associated with cancer, cardiovascular and neurological syndromes. ADAM9 is expressed in multiple tissues in humans including stem cells, renal tubular epithelial cells, placenta, pancreas and adipose tissue. It is expressed throughout all layers of the developing retina and RPE in chickens.⁴¹⁶ There is limited available information on the expression and role of ADAM9 in the human eye.

In both a canine and mouse model, there are cone and rod photoreceptor abnormalities on electrophysiology which are not apparent in very young animals but develop with time.^{411, 417} In both models, histopathology localised the primary defect to the apical microvilli of the retinal pigment epithelium potentially mediated by failure of normal photoreceptor outer segment phagocytosis with a loss of normal contact between outer segments and the RPE. These animal models show early preservation of photoreceptor structure despite dysfunction. This together with relatively good peripheral photoreceptor function in early human disease as illustrated by this case, suggest that there is a therapeutic window for gene therapy in patients with mutations in *ADAM9*.

13 Somatic mosaic mutation of *IKBKG* in a male patient with incontinentia pigmenti

13.1 Introduction

Incontinentia pigmenti (IP, MIM#308300) is a rare, X-linked, dominant genodermatosis, normally fatal in utero in males and highly variable in females due to functional mosaicism from X-inactivation.^{418, 419} It manifests in cells of ectodermal origin with a characteristic eruption of the skin present at birth that progresses in distinct stages, and variable involvement of other systems including neurological, ocular and odontological. It arises from mutations in *IKBKG* (inhibitor of kappa light polypeptide gene enhancer in B-cells, kinase gamma, Xq28) also known as *NEMO* (nuclear factor kappaB (NFkB) essential modulator), a gene involved in the activation of NFkB, a transcription factor for inflammatory and apoptotic pathways.⁶⁷ *IKBKG* has also been shown to inhibit apoptosis in an NFkB independent manner by binding to ubiquitinated RIP1.⁴²⁰ In 72% of cases of IP, a recurrent exon 4-10 genomic rearrangement in the *IKBKG* gene is responsible with more than half of cases arising de novo.^{421, 422} In patients with a clinical diagnosis of IP, no mutation is detected in peripheral leukocytes in 13% which may be explained by functional mosaicism from X-inactivation in females and loss of mutant cells to an undetectable level in peripheral blood leukocytes, mutations in regulatory regions or in theory from mutations in other genes.^{421, 422}

In affected males there are 3 mechanisms that are associated with survival after birth; most commonly an abnormal karyotype is identified with 47, XXY (Klinefelter syndrome) and skewed X inactivation in favor of expressing wild- type *IKBKG*, secondly hypomorphic mutations that cause IP in females that are associated with a syndrome in males of ectodermal dysplasia with immunodeficiency, and finally a post-zygotic mutation leading to somatic mosaicism.⁴²³

In this study, the mechanism and significance of loss of detectable mutation in peripheral blood leukocytes of a somatic mosaic male is discussed and an alternative approach to achieving molecular diagnosis presented.

13.2 Methods

13.2.1 Patient ascertainment

The patient was known to the paediatric genetic clinic with a clinical diagnosis of IP prior to the molecular diagnosis being made. Following this, the patient was reviewed by myself and further investigations planned.

13.2.2 Clinical investigations

Full ophthalmic examination and imaging was undertaken. The patient was under the care of paediatricians and dermatology colleagues from early infancy. Systemic investigations included skin biopsy and MRI of the brain.

13.2.3 Molecular investigations

13.2.3.1 DNA extraction from multiple tissue sources

DNA extraction from blood, buccal swab and urine was performed by lab colleagues. I performed DNA extraction from the hair root following the QIAGEN protocol using 6 hairs plucked from the patient's head to ensure the hair root was included which contains the nuclear DNA. A concentration of 22.7ng/μl was obtained.

13.2.3.2 Sequencing methods

Initial molecular investigation as an infant included karyotype analysis (North West Thames regional genetics service, cytogenetics on lymphocyte culture) and screen for the common *IKBKG* deletion. Further molecular investigations were unavailable until 3 years of age when fluorescent sequence analysis (Mutation Surveyor) of *IKBKG* and its adjacent highly homologous pseudogene was performed (East Anglian Medical Genetics Service, Cambridge). Gene specific, long-range PCR of exon 3-10 of *IKBKG* (to amplify the *IKBKG* gene rather than its pseudogene) was performed followed by NGS of all coding exons and exon/intron boundaries (using Nextera XT library construction and the Illumina MiSeq[®] system, Illumina, San Diego, CA). Mosaicism of a variant was calculated based on the estimated allele frequency. Nomenclature was assigned using GenBank Accession number NM_003639. A variant was identified as novel as previously described in methods and in addition if absent from a locus specific database <http://IKBKG.lovd.nl>.

DNA from other tissues of variable embryological cell line origin were obtained at age 5-6 years including blood (mesoderm), buccal cells (ectoderm), hair roots (ectoderm) and urine (predominantly epithelial cells of urothelial and renal tubular origin hence mixed mesoderm and endoderm).⁴²⁴ Having already established the site of mutation and its location within the true gene and not the pseudogene, PCR for exon 8 only was performed (table 13-1).

Exon	Primer forward 5' → 3'	Primer reverse 5' → 3'	Enzyme	Annealing temp (°C)	Amplicon size (bp)
8	CTGCTTTGTTCTCTGTGGTGC	CATCCGTCTCCTGTGGTCAC	BIOTAQ	65	348

Table 13-1: Primer pairs for sequencing exon 8 of *IKBKG*

13.3 Results

The patient was born to parents of Czech Republic (mother) and Tanzanian Indian (father) origin at full term without complication. He presented with a neonatal seizure at 2 days old and a rash. Local dermatology assessment described the rash as initially erythematous, widespread and following Blaschko's lines. Subsequently, blisters then verrucous lesions developed with hypopigmented lines noted at 6 months and hyperpigmented streaks in the axillae and groin at 8 months (figure 13-1). He was also noted to have small peg-shaped, irregular lower incisors, eczema and dystrophic nails. Skin biopsy performed after the initial presentation identified changes consistent with IP, specifically; acanthosis of the epidermis with eosinophilic spongiosis, vesicle formation and a few necrotic keratinocytes, basal vacuolation and in the dermis, a mild, chronic inflammatory infiltrate admixed with eosinophils.

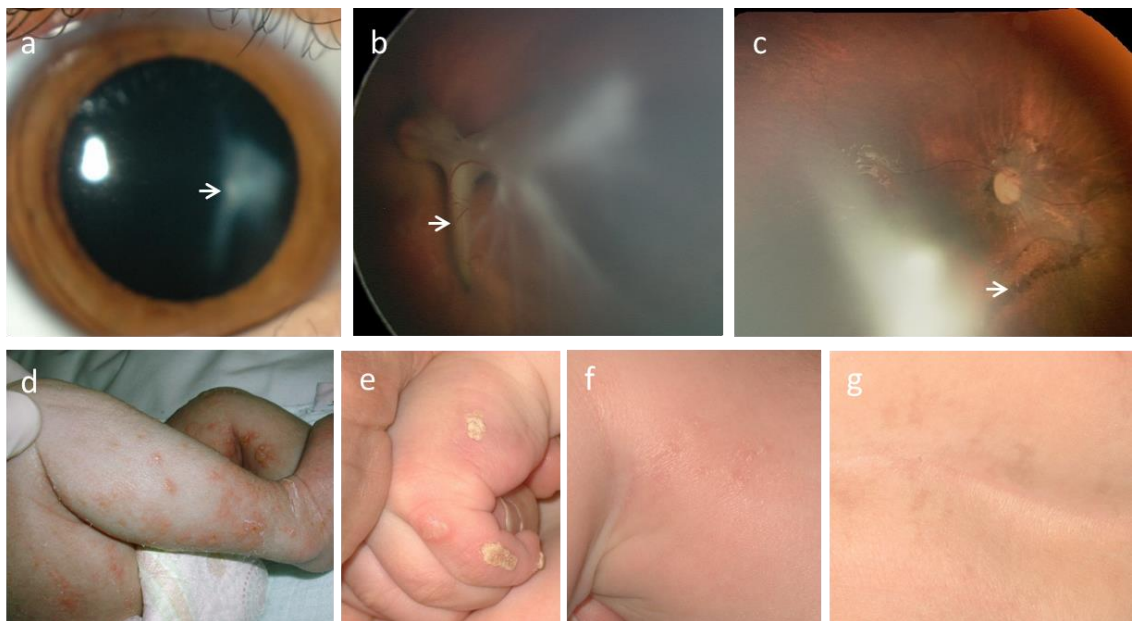


Figure 13-1: Clinical features of incontinentia pigmenti

a) Right eye anterior segment photograph age 5 years demonstrating nasal retrolental opacity visible due to persistent primary hyperplastic vitreous running from optic disc to ora serrata and posterior lens capsule; b) RetCam photograph of the right eye taken at examination under anaesthesia age 3 months, nasal view of retina demonstrating fold of retina inferonasal to disc (arrowed) with hyperplastic vitreous extending anteriorly and associated tractional retinal detachment; c) RetCam photograph age 2 years, retina is flat with a pigmented retina pigment epithelium line indicating the edge of the previous detachment (arrowed), haze inferotemporal to disc arising from the hyperplastic vitreous; d) photograph of lower limbs age 2 weeks demonstrating widespread vesicular rash e) photograph of left hand age 6 months demonstrating verrucous lesions; f) photograph of left knee age 6 months with subtle hypopigmented streaks; g) photograph of right groin age 8 months with hyperpigmented streak.

MRI performed after the seizure at 3 days of age demonstrated a subtle, low T2 signal intensity within the mesial cortex of the right frontal lobe likely to represent acute ischemia and when repeated at 5 months identified a mature infarct. Further occasional

seizures occurred always associated with fever. Development was normal except for a delay in walking (20 months).

Ophthalmological examination under anesthesia at 3 months demonstrated a total retinal detachment of the left eye with nasal funneling to a retrolental mass and subretinal hemorrhage. In the right eye there was a fovea sparing, tractional retinal detachment (figure 13-1). Persistent primary hyperplastic vitreous was noted to run from optic disc to ora serrata and the posterior aspect of the lens in the right eye. The right detachment settled spontaneously by 20 months of age and at last review at 6 years of age, vision was 0.76 logMAR (Snellen 6/38) in the right eye, NPL in the left.

Karyotype analysis was normal (46 XY). Screen for the common *IKBK*G deletion was negative. Fluorescent sequence analysis of *IKBK*G and its pseudogene detected a sequence variant in exon 8 at a low level. Gene specific, long-range PCR of exon 3-10 of *IKBK*G followed by NGS identified a novel, nonsense mutation, c.937C>T (p.Gln313*) at an approximate level of 15%.

The initial analysis which identified the mutation at a level of 15% was performed on a blood sample taken when the patient was 10 days old. A second sample from when the patient was 3 years, did not detect the mutation. Genotyping at multiple loci was performed and confirmed that the sample came from the same individual ruling out any potential sample mix-up. Analysis of maternal DNA did not identify the mutation consistent with a *de novo* event.

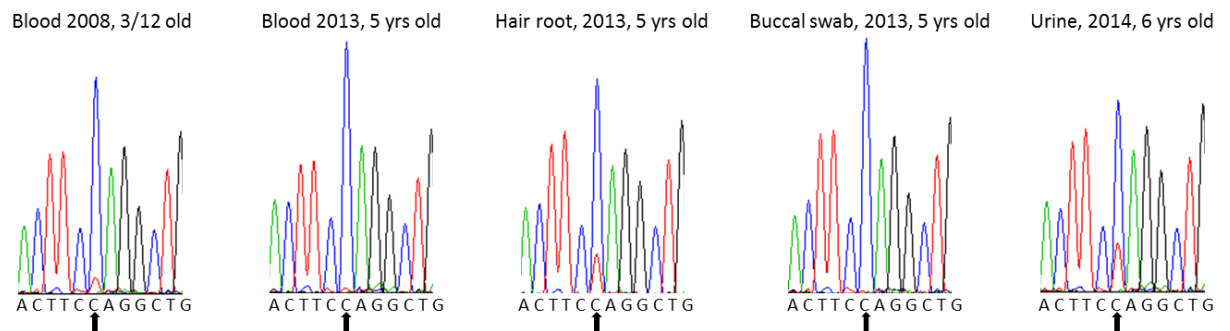


Figure 13-2: DNA chromatograms from Sanger sequencing of different tissue types

Blood 2008 and 2013, (mesoderm); hair root 2013 and buccal 2013, (ectoderm); urine 2014, (mesoderm/endoderm), arrow points to site of mutation. c.937C>T visible in blood 2008, hair root 2013 and urine 2014.

To further investigate the level of somatic mosaicism in other tissues of variable embryological cell line origin, sequencing of samples obtained at age 5-6 years was performed in addition to a blood sample from 3 months of age. This identified the mutation at low levels in the blood sample from 3 months of age, hair root from 5 years

and urine from 6 years with no detectable mutation in the blood or buccal samples obtained at 5 years of age (figure 13-2).

13.4 Discussion

In this study, the widespread clinical manifestations of IP including the classic skin eruption have been observed in a male patient. Severe ocular abnormalities were identified with bilateral retinal detachment, worse in the left eye than the right. Ocular abnormalities in IP are variable with the most frequent complication an ischaemic retinopathy leading to tractional retinal detachment, with marked asymmetry observed between eyes, similar to our patient.^{127, 425} IP is usually fatal in-utero for males but a post-zygotic mutation resulting in somatic mosaicism permitted survival. The extent of mosaicism has been investigated with detection of the mutation in cells derived from all germ layers indicating early occurrence of the mutation embryologically.⁴²⁶ Molecular diagnosis was achieved age 3 years but may have missed the mutation if DNA from infancy had not been tested. Somatic mosaicism permitting survival of males has also been described in other X-linked dominant disorders. The severe, neurodevelopmental Rett syndrome arises due to a mutation in *MECP2*, with survival in males attributed to 47, XXY karyotype or somatic mosaicism.⁴²⁷

The novel nonsense mutation c.937C>T (p.Gln313*) reported here arises in exon 8 of the *IKBKG* gene. It is predicted to lead to a truncated mRNA transcript that would undergo NMD according to the classical rules for this phenomenon.²⁰⁶ More than 70% of reported patients have the recurrent exon 4-10 rearrangement, with just under 4% a nonsense mutation.⁴²² The high rate of *de novo* aberrant recombination (approximately 2/3) is due to the *IKBKG* locus arising within a region of genomic instability, characterised by multiple micro/macro homologies, repeat sequences and tandem repeats.^{428, 429} Missense mutations are rare and can lead to a mild or severe phenotype depending on which protein pathway interactions are disrupted. For instance p.Ala323Pro is associated with a severe phenotype as it majorly disrupts NF-κB activation for all downstream pathways whereas p.Gly57Lys, associated with mild IP, disrupts interleukin-1 signalling only.⁴²² A male IP patient has not been previously reported with a nonsense mutation. However, there have been case reports of male patients with the allelic syndrome of ectodermal dysplasia and immunodeficiency in whom nonsense mutations were identified in exon 10 of *IKBKG*.^{430, 431} The resulting mRNA transcript would be predicted to avoid NMD and produce a protein that partially functions.

In a series of 18 male patients with IP, mosaic *IKBKG* deletions were identified in 3 patients with no mutations identified in the peripheral blood leukocytes of the other

15.⁴³² This finding was attributed to post-zygotic mosaicism. The lack of detectable mutation in 15 patients was thought to arise from uncontrolled apoptosis of mutant cells with evidence for this from the marked skewing of X-inactivation observed in the blood leukocytes of female carriers, indicating a major selective advantage for cells that express wild-type *IKBKG*. Further evidence for uncontrolled apoptosis was demonstrated in a male IP patient in whom the detectable levels of the common exon 4-10 rearrangement were much higher in a neonatal fibroblast sample than a blood sample age 9 years.⁴²³

In this study, the loss of detectable mutation in blood with age provides further evidence for the hypothesis that the leukocytes carrying the mutation undergo selective apoptosis. In this situation, molecular confirmation may not be possible from blood and it would be reasonable to then recommend testing of other readily accessible tissue types such as hair root or urine to enable informed genetic counselling of affected families

14 Conclusions

This thesis documents the results of the investigation of some of the rarest forms of EORD, with detailed phenotypical analysis and molecular characterisation of conditions previously unreported or with limited data. The vast molecular heterogeneity of inherited retinal disease has been demonstrated as well as the variable phenotypic expression within a specific disorder. In total, 73 patients from 52 families have been characterised in detail with an additional 66 probands molecularly screened. Thirty novel mutations in 13 genes were discovered.

Detailed phenotypic characterisation identified a number of novel features including progression of fundal changes in ESCS due to mutations in *NR2E3*; pigmentary glaucoma in Caucasian patients with Knobloch syndrome due to mutations in *COL18A1* and characterisation of the photoreceptor dysfunction as cone-rod; and evidence that *CDH3* related macular dystrophy is a centrally progressive disorder with minimal peripheral involvement.

Novel phenotype-genotype correlations included macular dystrophy due to mutations in *CRX*; non-syndromic retinal dystrophy due to mutations in *IFT140*; and the association of *LRP5* with FEVR and microcephaly. In addition a patient with retinal features resembling fundus albipunctatus due to *RPE65* mutation was characterised, this association only having been identified once in the literature before. I was able to investigate a very rare case of a male patient with IP and demonstrate an alternative approach to achieving molecular diagnosis in a mosaic patient.

Molecular diagnosis enabled accurate prognostic and inheritance risk counselling to families including a number of *CRX* families in whom recessive inheritance had been thought most likely and for families with *LRP5* and *KIF11* related disease in whom *de novo* disease could be proven giving a minimal risk for further children. In addition, a molecular diagnosis enabled appropriate targeted systemic investigations such as renal screening in patients with *IFT140* related disease, bone density scanning in *LRP5* disease and platelet function in *HPS6* related disease.

Of particular interest from this group of patients has been the occurrence of isolated ocular disease in genes thought to be associated with syndromic disease such as *IFT140* and *COL18A1* as well as the recognition of syndromic features only once a molecular diagnosis had been achieved. This occurred in *HPS6*, *CDH3* and *LRP5*. This highlights not only the variability in phenotypic expression of genes, the reason for which is largely poorly understood, but also the importance of continued systemic appraisal and suspicion of syndromic features.

There should be caution on interpreting results based on single gene screening or on assigning pathogenicity to novel mutations without functional evidence. Within this thesis, a family with FEVR and microcephaly is undergoing WGS despite a likely pathogenic variant in *LRP5* partly due to the extremely mild phenotype in the mother. WES and WGS are in theory unbiased methods of interrogating a patient's genome, assuming that the interpretation of identified variants is approached in an unbiased manner. Confirmation of variants by Sanger sequencing is important to ensure no sample/data mix-up has occurred. In addition, with novel variants of uncertain pathogenicity, segregation may not fit with disease as found in one unsolved FEVR/microcephaly patient initially found to have a heterozygous *LRP5* variant that was then found to be homozygous in her mother.

14.1 Future directions

Many questions and challenges have been raised from this work including why frequent genetic pleiotropy exists, how ubiquitously expressed proteins can cause isolated retinal disease, the exact mechanisms of disease and how WES negative patients can be molecularly solved.

Firstly, the reason for variable phenotypic expression of disease within families with *CRX*, *NR2E3* and *COL18A1* remains unclear as does the variable expression between families with no clear genotype-phenotype correlation found. *In vitro* studies of protein function can demonstrate differences such as the residual isomerase activity of hypomorphic *RPE65* mutations compared with non-hypomorphic mutations.³¹⁰ However, protein localisation studies in transiently transfected hTERT-RPE1 cells found no difference in mislocalisation between syndromic and non-syndromic *IFT140* mutations.

It is unknown why a number of ubiquitously expressed proteins including *IFT140* can cause isolated retinal disease. It may be that these mutations arise in a functional region of the protein that is critical for retinal function but is tolerated or compensated for elsewhere. These could be a retinal specific protein interaction as postulated for *IMPDH1* related RCD. *IMPDH1* encodes an ubiquitously expressed protein for guanine nucleotide synthesis but may also have a role in post-transcriptional regulation of rhodopsin mRNA.⁸⁷ In *CEP290* related disease, the common c.2991+1655A>G mutation leads to a cryptic exon insertion. Fibroblast studies have demonstrated that as much as 50% of normal protein is still expressed, which appears to be sufficient for normal ciliary function in other organs.²⁶⁸ It is still unknown why photoreceptors are specifically vulnerable. RNA-sequencing (RNA-seq) data from human retina has the potential to answer some of these questions although the interpretation of

transcriptome data is challenging. DNA and RNA analysis is typically performed on peripheral blood or skin sources with the assumption that the retinal expression will be similar. However, RNA-seq data has indicated that splicing in the retina is particularly diverse with alternate splicing events and alternate exons identified which may explain both phenotypic variability and retinal isolated disease.^{433, 434} RNA-seq has also been used to identify microexons, exons less than 51 nucleotides in length.⁴³⁵ Microexons are produced in 1% of all alternate splicing events and have a pivotal role in modulating protein interactions in neurogenesis. They may have a critical and as yet undefined role in retinal development.

Molecular mechanisms of disease have been reasonably well characterised for some retinal dystrophies including *RPE65* in which the protein function is understood and the tertiary structure has been experimentally proven.⁴³⁶ Much is still to be elucidated about the structure and function of other proteins such as *IFT140*.²³ Understanding mechanisms of disease is vital in developing novel therapies.

One of the biggest difficulties remains in interpreting whole genome data to solve patients in whom there are none or only one obvious mutation in known retinal dystrophy genes. They may have mutations in novel genes, in regulatory regions or in intronic regions critical for splicing. In WES negative patients such as 4 of the FEVR/microcephaly families studied in this thesis, interpretation of WGS data will be additionally challenging given the variable inheritance patterns possible. Sequencing multiple family members who have been clinically characterised should be helpful in this regard. The importance of intronic variants and their impact on splicing is being increasingly recognised. The common *CEP290* mutation is deeply intronic as are recently recognised deep intronic *ABCA4* variants.^{12, 437}

Whilst the cost of WGS has now become low enough to make it readily accessible as a tool for investigating patients, the challenge of interpreting the vast quantity of data remains. Approaches that utilise series of phenotypically similar patients, multiple family members and additional data such as RNA-seq are likely to have the greatest success in achieving a molecular diagnosis. For the patients and their families, an accurate molecular diagnosis, detailed phenotypic data and natural history studies are essential for providing prognostic information and counselling and for recruitment to clinical trials. Since the initial *RPE65* gene therapy trials, there are an increasing number of novel therapies being investigated and it is hoped that these will lead to a new era of treatment options for patients with these blinding disorders.^{307-309, 438-440}

15 References

1. Mitry D, Bunce C, Wormald R, et al. Causes of certifications for severe sight impairment (blind) and sight impairment (partial sight) in children in England and Wales. *Br J Ophthalmol* 2013;97:1431-1436.
2. Bertelsen M, Jensen H, Larsen M, Lorenz B, Preising MN, Rosenberg T. Prevalence and diagnostic spectrum of generalized retinal dystrophy in Danish children. *Ophthalmic Epidemiol* 2013;20:164-169.
3. Sherwin JC, Hewitt AW, Ruddle JB, Mackey DA. Genetic isolates in ophthalmic diseases. *Ophthalmic Genet* 2008;29:149-161.
4. Dryja TP, McGee TL, Reichel E, et al. A point mutation of the rhodopsin gene in one form of retinitis pigmentosa. *Nature* 1990;343:364-366.
5. Wang X, Wang H, Sun V, et al. Comprehensive molecular diagnosis of 179 Leber congenital amaurosis and juvenile retinitis pigmentosa patients by targeted next generation sequencing. *J Med Genet* 2013;50:674-688.
6. Henderson RH, Mackay DS, Li Z, et al. Phenotypic variability in patients with retinal dystrophies due to mutations in CRB1. *Br J Ophthalmol* 2011;95:811-817.
7. Hull S, Arno G, Plagnol V, et al. The phenotypic variability of retinal dystrophies associated with mutations in CRX, with report of a novel macular dystrophy phenotype. *Invest Ophthalmol Vis Sci* 2014;55:6934-6944.
8. Bowne SJ, Humphries MM, Sullivan LS, et al. A dominant mutation in RPE65 identified by whole-exome sequencing causes retinitis pigmentosa with choroidal involvement. *Eur J Hum Genet* 2011;19:1074-1081.
9. Gregory-Evans K, Kelsell RE, Gregory-Evans CY, et al. Autosomal dominant cone-rod retinal dystrophy (CORD6) from heterozygous mutation of GUCY2D, which encodes retinal guanylate cyclase. *Ophthalmology* 2000;107:55-61.
10. Wang F, Wang H, Tuan HF, et al. Next generation sequencing-based molecular diagnosis of retinitis pigmentosa: identification of a novel genotype-phenotype correlation and clinical refinements. *Hum Genet* 2014;133:331-345.
11. Estrada-Cuzcano A, Koenekoop RK, Senechal A, et al. BBS1 mutations in a wide spectrum of phenotypes ranging from nonsyndromic retinitis pigmentosa to Bardet-Biedl syndrome. *Arch Ophthalmol* 2012;130:1425-1432.
12. den Hollander AI, Koenekoop RK, Yzer S, et al. Mutations in the CEP290 (NPHP6) gene are a frequent cause of Leber congenital amaurosis. *Am J Hum Genet* 2006;79:556-561.

13. Glöckle N, Kohl S, Mohr J, et al. Panel-based next generation sequencing as a reliable and efficient technique to detect mutations in unselected patients with retinal dystrophies. *Eur J Hum Genet* 2014;22:99-104.
14. O'Sullivan J, Mullaney BG, Bhaskar SS, et al. A paradigm shift in the delivery of services for diagnosis of inherited retinal disease. *J Med Genet* 2012;49:322-326.
15. Audo I, Bujakowska KM, Léveillard T, et al. Development and application of a next-generation-sequencing (NGS) approach to detect known and novel gene defects underlying retinal diseases. *Orphanet J Rare Dis* 2012;7:8.
16. Eisenberger T, Neuhaus C, Khan AO, et al. Increasing the yield in targeted next-generation sequencing by implicating CNV analysis, non-coding exons and the overall variant load: the example of retinal dystrophies. *PLoS One* 2013;8:e78496.
17. Wang Y, Macke JP, Merbs SL, et al. A locus control region adjacent to the human red and green visual pigment genes. *Neuron* 1992;9:429-440.
18. Nishiguchi KM, Tearle RG, Liu YP, et al. Whole genome sequencing in patients with retinitis pigmentosa reveals pathogenic DNA structural changes and NEK2 as a new disease gene. *Proc Natl Acad Sci U S A* 2013;110:16139-16144.
19. Fariss RN, Li ZY, Milam AH. Abnormalities in rod photoreceptors, amacrine cells, and horizontal cells in human retinas with retinitis pigmentosa. *Am J Ophthalmol* 2000;129:215-223.
20. Busskamp V, Duebel J, Balya D, et al. Genetic reactivation of cone photoreceptors restores visual responses in retinitis pigmentosa. *Science* 2010;329:413-417.
21. Masland RH. The neuronal organization of the retina. *Neuron* 2012;76:266-280.
22. Tsujikawa M, Malicki J. Intraflagellar transport genes are essential for differentiation and survival of vertebrate sensory neurons. *Neuron* 2004;42:703-716.
23. Crouse JA, Lopes VS, Sanagustin JT, Keady BT, Williams DS, Pazour GJ. Distinct functions for IFT140 and IFT20 in opsin transport. *Cytoskeleton (Hoboken)* 2014;71:302-310.
24. Burgoyne T, Meschede IP, Burden JJ, Bailly M, Seabra MC, Futter CE. Rod disc renewal occurs by evagination of the ciliary plasma membrane that makes cadherin-based contacts with the inner segment. *Proc Natl Acad Sci U S A* 2015;112:15922-15927.
25. Mazzone F, Safa H, Finnemann SC. Understanding photoreceptor outer segment phagocytosis: use and utility of RPE cells in culture. *Exp Eye Res* 2014;126:51-60.

26. Curcio CA, Sloan KR, Kalina RE, Hendrickson AE. Human photoreceptor topography. *J Comp Neurol* 1990;292:497-523.
27. Sakurai M, Mullen KT. Cone weights for the two cone-opponent systems in peripheral vision and asymmetries of cone contrast sensitivity. *Vision Res* 2006;46:4346-4354.
28. Shirzad-Wasei N, DeGrip WJ. Heterologous Expression of Melanopsin: Present, Problems and Prospects. *Prog Retin Eye Res* 2016.
29. Lucas RJ, Lall GS, Allen AE, Brown TM. How rod, cone, and melanopsin photoreceptors come together to enlighten the mammalian circadian clock. *Prog Brain Res* 2012;199:1-18.
30. Vecino E, Rodriguez FD, Ruzafa N, Pereiro X, Sharma SC. Glia-neuron interactions in the mammalian retina. *Prog Retin Eye Res* 2015.
31. Kaylor JJ, Cook JD, Makshanoff J, Bischoff N, Yong J, Travis GH. Identification of the 11-cis-specific retinyl-ester synthase in retinal Müller cells as multifunctional O-acyltransferase (MFAT). *Proc Natl Acad Sci U S A* 2014;111:7302-7307.
32. Gariano RF, Gardner TW. Retinal angiogenesis in development and disease. *Nature* 2005;438:960-966.
33. Ohsawa R, Kageyama R. Regulation of retinal cell fate specification by multiple transcription factors. *Brain Res* 2008;1192:90-98.
34. Wallace VA. Concise review: making a retina--from the building blocks to clinical applications. *Stem Cells* 2011;29:412-417.
35. Hendrickson A. Development of Retinal Layers in Prenatal Human Retina. *Am J Ophthalmol* 2016;161:29-35.e21.
36. Vajzovic L, Hendrickson AE, O'Connell RV, et al. Maturation of the human fovea: correlation of spectral-domain optical coherence tomography findings with histology. *Am J Ophthalmol* 2012;154:779-789.e772.
37. Ye X, Wang Y, Cahill H, et al. Norrin, frizzled-4, and Lrp5 signaling in endothelial cells controls a genetic program for retinal vascularization. *Cell* 2009;139:285-298.
38. Palczewski K. Chemistry and biology of the initial steps in vision: the Friedenwald lecture. *Invest Ophthalmol Vis Sci* 2014;55:6651-6672.
39. Chen C, Thompson DA, Koutalos Y. Reduction of all-trans-retinal in vertebrate rod photoreceptors requires the combined action of RDH8 and RDH12. *J Biol Chem* 2012;287:24662-24670.
40. Jin M, Li S, Moghrabi WN, Sun H, Travis GH. Rpe65 is the retinoid isomerase in bovine retinal pigment epithelium. *Cell* 2005;122:449-459.
41. Redmond TM, Poliakov E, Yu S, Tsai JY, Lu Z, Gentleman S. Mutation of key residues of RPE65 abolishes its enzymatic role as isomerohydrolase in the visual cycle. *Proc Natl Acad Sci U S A* 2005;102:13658-13663.

42. Moiseyev G, Chen Y, Takahashi Y, Wu BX, Ma JX. RPE65 is the isomerohydrolase in the retinoid visual cycle. *Proc Natl Acad Sci U S A* 2005;102:12413-12418.
43. Marlhens F, Bareil C, Griffoin JM, et al. Mutations in RPE65 cause Leber's congenital amaurosis. *Nat Genet* 1997;17:139-141.
44. Gu SM, Thompson DA, Srikumari CR, et al. Mutations in RPE65 cause autosomal recessive childhood-onset severe retinal dystrophy. *Nat Genet* 1997;17:194-197.
45. Thompson DA, Li Y, McHenry CL, et al. Mutations in the gene encoding lecithin retinol acyltransferase are associated with early-onset severe retinal dystrophy. *Nat Genet* 2001;28:123-124.
46. den Hollander AI, McGee TL, Ziviello C, et al. A homozygous missense mutation in the IRBP gene (RBP3) associated with autosomal recessive retinitis pigmentosa. *Invest Ophthalmol Vis Sci* 2009;50:1864-1872.
47. Allikmets R. A photoreceptor cell-specific ATP-binding transporter gene (ABCR) is mutated in recessive Stargardt macular dystrophy. *Nat Genet* 1997;17:122.
48. Perrault I, Hanein S, Gerber S, et al. Retinal dehydrogenase 12 (RDH12) mutations in leber congenital amaurosis. *Am J Hum Genet* 2004;75:639-646.
49. Kohl S, Coppieters F, Meire F, et al. A nonsense mutation in PDE6H causes autosomal-recessive incomplete achromatopsia. *Am J Hum Genet* 2012;91:527-532.
50. Perrault I, Rozet JM, Calvas P, et al. Retinal-specific guanylate cyclase gene mutations in Leber's congenital amaurosis. *Nat Genet* 1996;14:461-464.
51. Little JA, Woodhouse JM, Lauritzen JS, Saunders KJ. Vernier acuity in Down syndrome. *Invest Ophthalmol Vis Sci* 2009;50:567-572.
52. Brémond-Gignac D, Copin H, Lapillonne A, Milazzo S, Development ENoSARiE. Visual development in infants: physiological and pathological mechanisms. *Curr Opin Ophthalmol* 2011;22 Suppl:S1-8.
53. Galvin JA, Fishman GA, Stone EM, Koenekoop RK. Evaluation of genotype-phenotype associations in leber congenital amaurosis. *Retina* 2005;25:919-929.
54. Forrester JV, Dick AD, McMenamin PG, Lee WR. *The Eye, Basic Sciences in Practice*. 2nd ed. Philadelphia, USA: Elsevier Limited; 2002.
55. Kay H. New method of assessing visual acuity with pictures. *Br J Ophthalmol* 1983;67:131-133.
56. Ferris FL, Kassoff A, Bresnick GH, Bailey I. New visual acuity charts for clinical research. *Am J Ophthalmol* 1982;94:91-96.

57. Thiadens AA, Hoyng CB, Polling JR, Bernaerts-Biskop R, van den Born LI, Klaver CC. Accuracy of four commonly used color vision tests in the identification of cone disorders. *Ophthalmic Epidemiol* 2013;20:114-121.
58. McCulley TJ, Golnik KC, Lam BL, Feuer WJ. The effect of decreased visual acuity on clinical color vision testing. *Am J Ophthalmol* 2006;141:194-196.
59. Gregori NZ, Feuer W, Rosenfeld PJ. Novel method for analyzing snellen visual acuity measurements. *Retina* 2010;30:1046-1050.
60. Oishi A, Ogino K, Makiyama Y, Nakagawa S, Kurimoto M, Yoshimura N. Wide-field fundus autofluorescence imaging of retinitis pigmentosa. *Ophthalmology* 2013;120:1827-1834.
61. Liew G, Moore AT, Webster AR, Michaelides M. Efficacy and prognostic factors of response to carbonic anhydrase inhibitors in management of cystoid macular edema in retinitis pigmentosa. *Invest Ophthalmol Vis Sci* 2015;56:1531-1536.
62. Anderson S, Bankier AT, Barrell BG, et al. Sequence and organization of the human mitochondrial genome. *Nature* 1981;290:457-465.
63. Consortium IHGS. Finishing the euchromatic sequence of the human genome. *Nature* 2004;431:931-945.
64. Hayden EC. Technology: The \$1,000 genome. *Nature* 2014;507:294-295.
65. Strachan T, Read A. *Human Molecular Genetics*. 4th ed. New York: Garland Science; 2011.
66. Rose AM, Bhattacharya SS. Variant haploinsufficiency and phenotypic non-penetrance in PRPF31-associated retinitis pigmentosa. *Clin Genet* 2016.
67. Smahi A, Courtois G, Vabres P, et al. Genomic rearrangement in NEMO impairs NF-kappaB activation and is a cause of incontinentia pigmenti. The International Incontinentia Pigmenti (IP) Consortium. *Nature* 2000;405:466-472.
68. Grover S, Fishman GA, Anderson RJ, Lindeman M. A longitudinal study of visual function in carriers of X-linked recessive retinitis pigmentosa. *Ophthalmology* 2000;107:386-396.
69. Taylor D, Hoyt C. *Paediatric Ophthalmology and Strabismus*: Elsevier Ltd; 2013.
70. Leber T. Ueber Retinitis pigmentosa und angeborene Amaurose. *Albrecht von Graefes Archiv für klinische und experimentelle Ophthalmologie* 1869;15:1-25.
71. Chung DC, Traboulsi EI. Leber congenital amaurosis: clinical correlations with genotypes, gene therapy trials update, and future directions. *J AAPOS* 2009;13:587-592.
72. Cremers FP, van den Hurk JA, den Hollander AI. Molecular genetics of Leber congenital amaurosis. *Hum Mol Genet* 2002;11:1169-1176.

73. Stone EM. Leber congenital amaurosis - a model for efficient genetic testing of heterogeneous disorders: LXIV Edward Jackson Memorial Lecture. *Am J Ophthalmol* 2007;144:791-811.
74. Bowne SJ, Sullivan LS, Mortimer SE, et al. Spectrum and frequency of mutations in IMPDH1 associated with autosomal dominant retinitis pigmentosa and leber congenital amaurosis. *Invest Ophthalmol Vis Sci* 2006;47:34-42.
75. Chen Y, Zhang Q, Shen T, et al. Comprehensive mutation analysis by whole-exome sequencing in 41 Chinese families with Leber congenital amaurosis. *Invest Ophthalmol Vis Sci* 2013;54:4351-4357.
76. Janecke AR, Thompson DA, Utermann G, et al. Mutations in RDH12 encoding a photoreceptor cell retinol dehydrogenase cause childhood-onset severe retinal dystrophy. *Nat Genet* 2004;36:850-854.
77. Freund CL, Wang QL, Chen S, et al. De novo mutations in the CRX homeobox gene associated with Leber congenital amaurosis. *Nat Genet* 1998;18:311-312.
78. den Hollander AI, Koenekoop RK, Mohamed MD, et al. Mutations in LCA5, encoding the ciliary protein lebercilin, cause Leber congenital amaurosis. *Nat Genet* 2007;39:889-895.
79. Dryja TP, Adams SM, Grimsby JL, et al. Null RPGRIP1 alleles in patients with Leber congenital amaurosis. *Am J Hum Genet* 2001;68:1295-1298.
80. Hagstrom SA, Watson RF, Pauer GJ, Grossman GH. Tulp1 is involved in specific photoreceptor protein transport pathways. *Adv Exp Med Biol* 2012;723:783-789.
81. Kolandaivelu S, Singh RK, Ramamurthy V. AIPL1, A protein linked to blindness, is essential for the stability of enzymes mediating cGMP metabolism in cone photoreceptor cells. *Hum Mol Genet* 2014;23:1002-1012.
82. Eblimit A, Nguyen TM, Chen Y, et al. Spata7 is a retinal ciliopathy gene critical for correct RPGRIP1 localization and protein trafficking in the retina. *Hum Mol Genet* 2015;24:1584-1601.
83. Zulliger R, Naash MI, Rajala RV, Molday RS, Azadi S. Impaired association of retinal degeneration-3 with guanylate cyclase-1 and guanylate cyclase-activating protein-1 leads to leber congenital amaurosis-1. *J Biol Chem* 2015;290:3488-3499.
84. Stone EM, Cideciyan AV, Aleman TS, et al. Variations in NPHP5 in patients with nonsyndromic leber congenital amaurosis and Senior-Loken syndrome. *Arch Ophthalmol* 2011;129:81-87.
85. Estrada-Cuzcano A, Koenekoop RK, Coppieters F, et al. IQCB1 mutations in patients with leber congenital amaurosis. *Invest Ophthalmol Vis Sci* 2011;52:834-839.

86. Sergouniotis PI, Davidson AE, Mackay DS, et al. Recessive mutations in KCNJ13, encoding an inwardly rectifying potassium channel subunit, cause leber congenital amaurosis. *Am J Hum Genet* 2011;89:183-190.
87. Mortimer SE, Xu D, McGrew D, et al. IMP dehydrogenase type 1 associates with polyribosomes translating rhodopsin mRNA. *J Biol Chem* 2008;283:36354-36360.
88. Roman AJ, Cideciyan AV, Schwartz SB, Olivares MB, Heon E, Jacobson SG. Intervisit variability of visual parameters in Leber congenital amaurosis caused by RPE65 mutations. *Invest Ophthalmol Vis Sci* 2013;54:1378-1383.
89. Wang H, den Hollander AI, Moayed Y, et al. Mutations in SPATA7 cause Leber congenital amaurosis and juvenile retinitis pigmentosa. *Am J Hum Genet* 2009;84:380-387.
90. Sohocki MM, Bowne SJ, Sullivan LS, et al. Mutations in a new photoreceptor-pineal gene on 17p cause Leber congenital amaurosis. *Nat Genet* 2000;24:79-83.
91. Lotery AJ, Jacobson SG, Fishman GA, et al. Mutations in the CRB1 gene cause Leber congenital amaurosis. *Arch Ophthalmol* 2001;119:415-420.
92. Falk MJ, Zhang Q, Nakamaru-Ogiso E, et al. NMNAT1 mutations cause Leber congenital amaurosis. *Nat Genet* 2012;44:1040-1045.
93. Perrault I, Hanein S, Zanlonghi X, et al. Mutations in NMNAT1 cause Leber congenital amaurosis with early-onset severe macular and optic atrophy. *Nat Genet* 2012;44:975-977.
94. Chiang PW, Wang J, Chen Y, et al. Exome sequencing identifies NMNAT1 mutations as a cause of Leber congenital amaurosis. *Nat Genet* 2012;44:972-974.
95. Koenekoop RK, Wang H, Majewski J, et al. Mutations in NMNAT1 cause Leber congenital amaurosis and identify a new disease pathway for retinal degeneration. *Nat Genet* 2012;44:1035-1039.
96. Friedman JS, Chang B, Kannabiran C, et al. Premature truncation of a novel protein, RD3, exhibiting subnuclear localization is associated with retinal degeneration. *Am J Hum Genet* 2006;79:1059-1070.
97. Hagstrom SA, North MA, Nishina PL, Berson EL, Dryja TP. Recessive mutations in the gene encoding the tubby-like protein TULP1 in patients with retinitis pigmentosa. *Nat Genet* 1998;18:174-176.
98. Banerjee P, Kleyn PW, Knowles JA, et al. TULP1 mutation in two extended Dominican kindreds with autosomal recessive retinitis pigmentosa. *Nat Genet* 1998;18:177-179.
99. Scholl HP, Chong NH, Robson AG, Holder GE, Moore AT, Bird AC. Fundus autofluorescence in patients with leber congenital amaurosis. *Invest Ophthalmol Vis Sci* 2004;45:2747-2752.

100. Wabbels B, Demmler A, Paunescu K, Wegscheider E, Preising MN, Lorenz B. Fundus autofluorescence in children and teenagers with hereditary retinal diseases. *Graefes Arch Clin Exp Ophthalmol* 2006;244:36-45.
101. Lorenz B, Wabbels B, Wegscheider E, Hamel CP, Drexler W, Preising MN. Lack of fundus autofluorescence to 488 nanometers from childhood on in patients with early-onset severe retinal dystrophy associated with mutations in RPE65. *Ophthalmology* 2004;111:1585-1594.
102. Traboulsi EI. The Marshall M. Parks memorial lecture: making sense of early-onset childhood retinal dystrophies--the clinical phenotype of Leber congenital amaurosis. *Br J Ophthalmol* 2010;94:1281-1287.
103. Schuil J, Meire FM, Delleman JW. Mental retardation in amaurosis congenita of Leber. *Neuropediatrics* 1998;29:294-297.
104. Petraglia AL, Chengazi HU, Chung MM, Silberstein HJ. Leber congenital amaurosis associated with Chiari I malformation: Two cases and a review of the literature. *Surg Neurol Int* 2012;3:4.
105. Marshall JD, Hinman EG, Collin GB, et al. Spectrum of ALMS1 variants and evaluation of genotype-phenotype correlations in Alström syndrome. *Hum Mutat* 2007;28:1114-1123.
106. Otto EA, Loeys B, Khanna H, et al. Nephrocystin-5, a ciliary IQ domain protein, is mutated in Senior-Loken syndrome and interacts with RPGR and calmodulin. *Nat Genet* 2005;37:282-288.
107. Hartong DT, Berson EL, Dryja TP. Retinitis pigmentosa. *Lancet* 2006;368:1795-1809.
108. Bertelsen M, Jensen H, Bregnhøj JF, Rosenberg T. Prevalence of generalized retinal dystrophy in denmark. *Ophthalmic Epidemiol* 2014;21:217-223.
109. Sandberg MA, Rosner B, Weigel-DiFranco C, Dryja TP, Berson EL. Disease course of patients with X-linked retinitis pigmentosa due to RPGR gene mutations. *Invest Ophthalmol Vis Sci* 2007;48:1298-1304.
110. Bocquet B, Lacroux A, Surget MO, et al. Relative frequencies of inherited retinal dystrophies and optic neuropathies in Southern France: assessment of 21-year data management. *Ophthalmic Epidemiol* 2013;20:13-25.
111. Rosenfeld PJ, Cowley GS, McGee TL, Sandberg MA, Berson EL, Dryja TP. A null mutation in the rhodopsin gene causes rod photoreceptor dysfunction and autosomal recessive retinitis pigmentosa. *Nat Genet* 1992;1:209-213.
112. Xu Y, Guan L, Shen T, et al. Mutations of 60 known causative genes in 157 families with retinitis pigmentosa based on exome sequencing. *Hum Genet* 2014.
113. Littink KW, van den Born LI, Koenekoop RK, et al. Mutations in the EYS gene account for approximately 5% of autosomal recessive retinitis pigmentosa

and cause a fairly homogeneous phenotype. *Ophthalmology* 2010;117:2026-2033, 2033.e2021-2027.

114. Vithana EN, Abu-Safieh L, Pelosini L, et al. Expression of PRPF31 mRNA in patients with autosomal dominant retinitis pigmentosa: a molecular clue for incomplete penetrance? *Invest Ophthalmol Vis Sci* 2003;44:4204-4209.

115. Audo I, Mohand-Saïd S, Dhaenens CM, et al. RP1 and autosomal dominant rod-cone dystrophy: novel mutations, a review of published variants, and genotype-phenotype correlation. *Hum Mutat* 2012;33:73-80.

116. Webb TR, Parfitt DA, Gardner JC, et al. Deep intronic mutation in OFD1, identified by targeted genomic next-generation sequencing, causes a severe form of X-linked retinitis pigmentosa (RP23). *Hum Mol Genet* 2012;21:3647-3654.

117. Sharon D, Sandberg MA, Rabe VW, Stillberger M, Dryja TP, Berson EL. RP2 and RPGR mutations and clinical correlations in patients with X-linked retinitis pigmentosa. *Am J Hum Genet* 2003;73:1131-1146.

118. Demirci FY, Rigatti BW, Wen G, et al. X-linked cone-rod dystrophy (locus COD1): identification of mutations in RPGR exon ORF15. *Am J Hum Genet* 2002;70:1049-1053.

119. Roosing S, Thiadens AA, Hoyng CB, Klaver CC, den Hollander AI, Cremers FP. Causes and consequences of inherited cone disorders. *Prog Retin Eye Res* 2014.

120. Thiadens AA, Phan TM, Zekveld-Vroon RC, et al. Clinical course, genetic etiology, and visual outcome in cone and cone-rod dystrophy. *Ophthalmology* 2012;119:819-826.

121. Michaelides M, Hunt DM, Moore AT. The genetics of inherited macular dystrophies. *J Med Genet* 2003;40:641-650.

122. Zahid S, Jayasundera T, Rhoades W, et al. Clinical phenotypes and prognostic full-field electroretinographic findings in Stargardt disease. *Am J Ophthalmol* 2013;155:465-473.e463.

123. Querques G, Zerbib J, Santacroce R, et al. Functional and clinical data of Best vitelliform macular dystrophy patients with mutations in the BEST1 gene. *Mol Vis* 2009;15:2960-2972.

124. Borman AD, Davidson AE, O'Sullivan J, et al. Childhood-onset autosomal recessive bestrophinopathy. *Arch Ophthalmol* 2011;129:1088-1093.

125. Salvo J, Lyubasyuk V, Xu M, et al. Next-generation sequencing and novel variant determination in a cohort of 92 familial exudative vitreoretinopathy patients. *Invest Ophthalmol Vis Sci* 2015;56:1937-1946.

126. Gilmour DF. Familial exudative vitreoretinopathy and related retinopathies. *Eye (Lond)* 2015;29:1-14.

127. O'Doherty M, Mc Creery K, Green AJ, Tuwir I, Brosnahan D. Incontinentia pigmenti--ophthalmological observation of a series of cases and review of the literature. *Br J Ophthalmol* 2011;95:11-16.
128. Dulz S, Wagenfeld L, Nickel M, et al. Novel morphological macular findings in juvenile CLN3 disease. *Br J Ophthalmol* 2015.
129. Delori F. Lipofuscin: The Origin of the Autofluorescence Signal. In: Lois N, Forrester JV (eds), *Fundus autofluorescence*. Philadelphia, USA: Wolters Kluwer; 2016.
130. Smith RT. The Normal Distribution of Fundus Autofluorescence. In: Lois N, Forrester JV (eds), *Fundus autofluorescence*. Philadelphia, USA: Wolters Kluwer; 2016.
131. Robson AG, Audo I, Webster AR. Fundus Autofluorescence in Inherited Retinal Dystrophies, Retinitis Pigmentosa. In: Lois N, Forrester JV (eds), *Fundus Autofluorescence*. Philadelphia, USA: Wolters Kluwer; 2016.
132. Goldberg NR, Greenberg JP, Laud K, Tsang S, Freund KB. Outer retinal tubulation in degenerative retinal disorders. *Retina* 2013;33:1871-1876.
133. Sujirakul T, Lin MK, Duong J, Wei Y, Lopez-Pintado S, Tsang SH. Multimodal Imaging of Central Retinal Disease Progression in a 2-Year Mean Follow-up of Retinitis Pigmentosa. *Am J Ophthalmol* 2015;160:786-798.e784.
134. Kaneko Y, Moriyama M, Hirahara S, Ogura Y, Ohno-Matsui K. Areas of nonperfusion in peripheral retina of eyes with pathologic myopia detected by ultra-widefield fluorescein angiography. *Invest Ophthalmol Vis Sci* 2014;55:1432-1439.
135. Vincent A, Robson AG, Holder GE. Pathognomonic (diagnostic) ERGs. A review and update. *Retina* 2013;33:5-12.
136. McCulloch DL, Marmor MF, Brigell MG, et al. ISCEV Standard for full-field clinical electroretinography (2015 update). *Doc Ophthalmol* 2015;130:1-12.
137. Bach M, Brigell MG, Hawlina M, et al. ISCEV standard for clinical pattern electroretinography (PERG): 2012 update. *Doc Ophthalmol* 2013;126:1-7.
138. Holder G, Robson A. *Paediatric Electrophysiology: a practical approach*. In: *Pediatric Ophthalmology, Neuro-Ophthalmology, Genetics*. Berlin: Springer; 2006.
139. Holder GE. Pattern electroretinography (PERG) and an integrated approach to visual pathway diagnosis. *Prog Retin Eye Res* 2001;20:531-561.
140. Dorey SE, Neveu MM, Burton LC, Sloper JJ, Holder GE. The clinical features of albinism and their correlation with visual evoked potentials. *Br J Ophthalmol* 2003;87:767-772.
141. Holder GE. Electrophysiological assessment of optic nerve disease. *Eye (Lond)* 2004;18:1133-1143.

142. McBain VA, Robson AG, Hogg CR, Holder GE. Assessment of patients with suspected non-organic visual loss using pattern appearance visual evoked potentials. *Graefes Arch Clin Exp Ophthalmol* 2007;245:502-510.
143. Strien J, Sanft J, Mall G. Enhancement of PCR amplification of moderate GC-containing and highly GC-rich DNA sequences. *Mol Biotechnol* 2013;54:1048-1054.
144. Flicek P, Amode MR, Barrell D, et al. Ensembl 2014. *Nucleic Acids Res* 2014;42:D749-755.
145. Sanger F, Nicklen S, Coulson AR. DNA sequencing with chain-terminating inhibitors. *Proc Natl Acad Sci U S A* 1977;74:5463-5467.
146. Lindberg P, Stjernström M, Roeraade J. Gel electrophoresis of DNA fragments in narrow-bore capillaries. *Electrophoresis* 1997;18:1973-1979.
147. Gnirke A, Melnikov A, Maguire J, et al. Solution hybrid selection with ultra-long oligonucleotides for massively parallel targeted sequencing. *Nat Biotechnol* 2009;27:182-189.
148. Meienberg J, Zerjavic K, Keller I, et al. New insights into the performance of human whole-exome capture platforms. *Nucleic Acids Res* 2015;43:e76.
149. Raczy C, Petrovski R, Saunders CT, et al. Isaac: ultra-fast whole-genome secondary analysis on Illumina sequencing platforms. *Bioinformatics* 2013;29:2041-2043.
150. Li H, Durbin R. Fast and accurate short read alignment with Burrows-Wheeler transform. *Bioinformatics* 2009;25:1754-1760.
151. McKenna A, Hanna M, Banks E, et al. The Genome Analysis Toolkit: a MapReduce framework for analyzing next-generation DNA sequencing data. *Genome Res* 2010;20:1297-1303.
152. Sund KL, Zimmerman SL, Thomas C, et al. Regions of homozygosity identified by SNP microarray analysis aid in the diagnosis of autosomal recessive disease and incidentally detect parental blood relationships. *Genet Med* 2013;15:70-78.
153. Zernant J, Külm M, Dharmaraj S, et al. Genotyping microarray (disease chip) for Leber congenital amaurosis: detection of modifier alleles. *Invest Ophthalmol Vis Sci* 2005;46:3052-3059.
154. van Huet RA, Pierrache LH, Meester-Smoor MA, et al. The efficacy of microarray screening for autosomal recessive retinitis pigmentosa in routine clinical practice. *Mol Vis* 2015;21:461-476.
155. Benson DA, Clark K, Karsch-Mizrachi I, Lipman DJ, Ostell J, Sayers EW. GenBank. *Nucleic Acids Res* 2015;43:D30-35.
156. Abecasis GR, Altshuler D, Auton A, et al. A map of human genome variation from population-scale sequencing. *Nature* 2010;467:1061-1073.

157. Kumar P, Henikoff S, Ng PC. Predicting the effects of coding non-synonymous variants on protein function using the SIFT algorithm. *Nat Protoc* 2009;4:1073-1081.
158. Adzhubei IA, Schmidt S, Peshkin L, et al. A method and server for predicting damaging missense mutations. *Nat Methods* 2010;7:248-249.
159. Reese MG, Eeckman FH, Kulp D, Haussler D. Improved splice site detection in Genie. *J Comput Biol* 1997;4:311-323.
160. Desmet FO, Hamroun D, Lalande M, Collod-Bérout G, Claustres M, Bérout C. Human Splicing Finder: an online bioinformatics tool to predict splicing signals. *Nucleic Acids Res* 2009;37:e67.
161. Sievers F, Wilm A, Dineen D, et al. Fast, scalable generation of high-quality protein multiple sequence alignments using Clustal Omega. *Mol Syst Biol* 2011;7:539.
162. Chen F, Ng PS, Faull KF, Lee RH. Cone photoreceptor betagamma-transducin: posttranslational modification and interaction with phosducin. *Invest Ophthalmol Vis Sci* 2003;44:4622-4629.
163. Berman H, Henrick K, Nakamura H. Announcing the worldwide Protein Data Bank. *Nat Struct Biol* 2003;10:980.
164. Consortium U. UniProt: a hub for protein information. *Nucleic Acids Res* 2015;43:D204-212.
165. M W. *The zebrafish book. A guide for the laboratory use of zebrafish (Danio rerio)*. 4th ed: University of Oregon Press, Eugene. ; 1993.
166. Walker MB, Kimmel CB. A two-color acid-free cartilage and bone stain for zebrafish larvae. *Biotech Histochem* 2007;82:23-28.
167. Gerety SS, Wilkinson DG. Morpholino artifacts provide pitfalls and reveal a novel role for pro-apoptotic genes in hindbrain boundary development. *Dev Biol* 2011;350:279-289.
168. Sullivan-Brown J, Bisher ME, Burdine RD. Embedding, serial sectioning and staining of zebrafish embryos using JB-4 resin. *Nat Protoc* 2011;6:46-55.
169. Parichy DM, Elizondo MR, Mills MG, Gordon TN, Engeszer RE. Normal table of postembryonic zebrafish development: staging by externally visible anatomy of the living fish. *Dev Dyn* 2009;238:2975-3015.
170. Schneider CA, Rasband WS, Eliceiri KW. NIH Image to ImageJ: 25 years of image analysis. *Nat Methods* 2012;9:671-675.
171. Freund CL, Gregory-Evans CY, Furukawa T, et al. Cone-rod dystrophy due to mutations in a novel photoreceptor-specific homeobox gene (CRX) essential for maintenance of the photoreceptor. *Cell* 1997;91:543-553.
172. Furukawa T, Morrow EM, Cepko CL. Crx, a novel otx-like homeobox gene, shows photoreceptor-specific expression and regulates photoreceptor differentiation. *Cell* 1997;91:531-541.

173. Chen S, Wang QL, Nie Z, et al. Crx, a novel Otx-like paired-homeodomain protein, binds to and transactivates photoreceptor cell-specific genes. *Neuron* 1997;19:1017-1030.
174. Peng GH, Ahmad O, Ahmad F, Liu J, Chen S. The photoreceptor-specific nuclear receptor Nr2e3 interacts with Crx and exerts opposing effects on the transcription of rod versus cone genes. *Hum Mol Genet* 2005;14:747-764.
175. Evans K, Fryer A, Inglehearn C, et al. Genetic linkage of cone-rod retinal dystrophy to chromosome 19q and evidence for segregation distortion. *Nat Genet* 1994;6:210-213.
176. Sohocki MM, Sullivan LS, Mintz-Hittner HA, et al. A range of clinical phenotypes associated with mutations in CRX, a photoreceptor transcription-factor gene. *Am J Hum Genet* 1998;63:1307-1315.
177. Kitiratschky VB, Nagy D, Zabel T, et al. Cone and cone-rod dystrophy segregating in the same pedigree due to the same novel CRX gene mutation. *Br J Ophthalmol* 2008;92:1086-1091.
178. Swain PK, Chen S, Wang QL, et al. Mutations in the cone-rod homeobox gene are associated with the cone-rod dystrophy photoreceptor degeneration. *Neuron* 1997;19:1329-1336.
179. Li L, Xiao X, Li S, et al. Detection of variants in 15 genes in 87 unrelated Chinese patients with Leber congenital amaurosis. *PLoS One* 2011;6:e19458.
180. Lotery AJ, Namperumalsamy P, Jacobson SG, et al. Mutation analysis of 3 genes in patients with Leber congenital amaurosis. *Arch Ophthalmol* 2000;118:538-543.
181. Jin ZB, Mandai M, Yokota T, et al. Identifying pathogenic genetic background of simplex or multiplex retinitis pigmentosa patients: a large scale mutation screening study. *J Med Genet* 2008;45:465-472.
182. Sankila EM, Joensuu TH, Hämäläinen RH, et al. A CRX mutation in a Finnish family with dominant cone-rod retinal dystrophy. *Hum Mutat* 2000;16:94.
183. Huang L, Xiao X, Li S, et al. CRX variants in cone-rod dystrophy and mutation overview. *Biochem Biophys Res Commun* 2012;426:498-503.
184. Nichols LL, Alur RP, Boobalan E, et al. Two novel CRX mutant proteins causing autosomal dominant Leber congenital amaurosis interact differently with NRL. *Hum Mutat* 2010;31:E1472-1483.
185. Swaroop A, Wang QL, Wu W, et al. Leber congenital amaurosis caused by a homozygous mutation (R90W) in the homeodomain of the retinal transcription factor CRX: direct evidence for the involvement of CRX in the development of photoreceptor function. *Hum Mol Genet* 1999;8:299-305.

186. Zou X, Yao F, Liang X, et al. De novo Mutations in the Cone-rod Homeobox Gene Associated with Leber Congenital Amaurosis in Chinese Patients. *Ophthalmic Genet* 2013.
187. Lines MA, Hébert M, McTaggart KE, Flynn SJ, Tennant MT, MacDonald IM. Electrophysiologic and phenotypic features of an autosomal cone-rod dystrophy caused by a novel CRX mutation. *Ophthalmology* 2002;109:1862-1870.
188. Ziviello C, Simonelli F, Testa F, et al. Molecular genetics of autosomal dominant retinitis pigmentosa (ADRP): a comprehensive study of 43 Italian families. *J Med Genet* 2005;42:e47.
189. Kohl S, Kitiratschky V, Papke M, Schaich S, Sauer A, Wissinger B. Genes and mutations in autosomal dominant cone and cone-rod dystrophy. *Adv Exp Med Biol* 2012;723:337-343.
190. Perrault I, Hanein S, Gerber S, et al. Evidence of autosomal dominant Leber congenital amaurosis (LCA) underlain by a CRX heterozygous null allele. *J Med Genet* 2003;40:e90.
191. Nakamura M, Ito S, Miyake Y. Novel de novo mutation in CRX gene in a Japanese patient with leber congenital amaurosis. *Am J Ophthalmol* 2002;134:465-467.
192. Koenekoop RK, Loyer M, Dembinska O, Beneish R. Visual improvement in Leber congenital amaurosis and the CRX genotype. *Ophthalmic Genet* 2002;23:49-59.
193. Zhang Q, Li S, Guo X, et al. Screening for CRX gene mutations in Chinese patients with Leber congenital amaurosis and mutational phenotype. *Ophthalmic Genet* 2001;22:89-96.
194. Rivolta C, Peck NE, Fulton AB, Fishman GA, Berson EL, Dryja TP. Novel frameshift mutations in CRX associated with Leber congenital amaurosis. *Hum Mutat* 2001;18:550-551.
195. Itabashi T, Wada Y, Sato H, Kawamura M, Shiono T, Tamai M. Novel 615delC mutation in the CRX gene in a Japanese family with cone-rod dystrophy. *Am J Ophthalmol* 2004;138:876-877.
196. Silva E, Yang JM, Li Y, Dharmaraj S, Sundin OH, Maumenee IH. A CRX null mutation is associated with both Leber congenital amaurosis and a normal ocular phenotype. *Invest Ophthalmol Vis Sci* 2000;41:2076-2079.
197. Paunescu K, Preising MN, Janke B, Wissinger B, Lorenz B. Genotype-phenotype correlation in a German family with a novel complex CRX mutation extending the open reading frame. *Ophthalmology* 2007;114:1348-1357.e1341.
198. Preising MN, Paunescu K, Friedburg C, Lorenz B. [Genetic and clinical heterogeneity in LCA patients. The end of uniformity]. *Ophthalmologe* 2007;104:490-498.

199. Arcot Sadagopan K, Battista R, Keep RB, Capasso JE, Levin AV. Autosomal-dominant Leber Congenital Amaurosis Caused by a Heterozygous CRX Mutation in a Father and Son. *Ophthalmic Genet* 2013.
200. Neveu MM, Dangour A, Allen E, et al. Electroretinogram measures in a septuagenarian population. *Doc Ophthalmol* 2011;123:75-81.
201. Vincent A, Robson AG, Neveu MM, et al. A phenotype-genotype correlation study of X-linked retinoschisis. *Ophthalmology* 2013;120:1454-1464.
202. Sohocki MM, Daiger SP, Bowne SJ, et al. Prevalence of mutations causing retinitis pigmentosa and other inherited retinopathies. *Hum Mutat* 2001;17:42-51.
203. Vallespin E, Cantalapiedra D, Riveiro-Alvarez R, et al. Mutation screening of 299 Spanish families with retinal dystrophies by Leber congenital amaurosis genotyping microarray. *Invest Ophthalmol Vis Sci* 2007;48:5653-5661.
204. Baker SA, Chen L, Wilkins AD, Yu P, Lichtarge O, Zoghbi HY. An AT-hook domain in MeCP2 determines the clinical course of Rett syndrome and related disorders. *Cell* 2013;152:984-996.
205. Michaelides M, Gaillard MC, Escher P, et al. The PROM1 mutation p.R373C causes an autosomal dominant bull's eye maculopathy associated with rod, rod-cone, and macular dystrophy. *Invest Ophthalmol Vis Sci* 2010;51:4771-4780.
206. Lejeune F, Maquat LE. Mechanistic links between nonsense-mediated mRNA decay and pre-mRNA splicing in mammalian cells. *Curr Opin Cell Biol* 2005;17:309-315.
207. Furukawa T, Morrow EM, Li T, Davis FC, Cepko CL. Retinopathy and attenuated circadian entrainment in Crx-deficient mice. *Nat Genet* 1999;23:466-470.
208. Roger JE, Hiriyanna A, Gotoh N, et al. OTX2 loss causes rod differentiation defect in CRX-associated congenital blindness. *J Clin Invest* 2014.
209. Tran NM, Zhang A, Zhang X, Huecker JB, Hennig AK, Chen S. Mechanistically Distinct Mouse Models for CRX-Associated Retinopathy. *PLoS Genet* 2014;10:e1004111.
210. Marmor MF, Jacobson SG, Foerster MH, Kellner U, Weleber RG. Diagnostic clinical findings of a new syndrome with night blindness, maculopathy, and enhanced S cone sensitivity. *Am J Ophthalmol* 1990;110:124-134.
211. Sohn EH, Chen FK, Rubin GS, Moore AT, Webster AR, MacLaren RE. Macular function assessed by microperimetry in patients with enhanced S-cone syndrome. *Ophthalmology* 2010;117:1199-1206.e1191.
212. Audo I, Michaelides M, Robson AG, et al. Phenotypic variation in enhanced S-cone syndrome. *Invest Ophthalmol Vis Sci* 2008;49:2082-2093.

213. Milam AH, Rose L, Cideciyan AV, et al. The nuclear receptor NR2E3 plays a role in human retinal photoreceptor differentiation and degeneration. *Proc Natl Acad Sci U S A* 2002;99:473-478.
214. Khan AO, Aldahmesh M, Meyer B. The enhanced S-cone syndrome in children. *Br J Ophthalmol* 2007;91:394-396.
215. Wang NK, Fine HF, Chang S, et al. Cellular origin of fundus autofluorescence in patients and mice with a defective NR2E3 gene. *Br J Ophthalmol* 2009;93:1234-1240.
216. Pichi F, Morara M, Veronese C, Nucci P, Ciardella AP. Multimodal imaging in hereditary retinal diseases. *J Ophthalmol* 2013;2013:634351.
217. Cheng H, Khan NW, Roger JE, Swaroop A. Excess cones in the retinal degeneration rd7 mouse, caused by the loss of function of orphan nuclear receptor Nr2e3, originate from early-born photoreceptor precursors. *Hum Mol Genet* 2011;20:4102-4115.
218. Haider NB, Jacobson SG, Cideciyan AV, et al. Mutation of a nuclear receptor gene, NR2E3, causes enhanced S cone syndrome, a disorder of retinal cell fate. *Nat Genet* 2000;24:127-131.
219. Neveling K, Collin RW, Gilissen C, et al. Next-generation genetic testing for retinitis pigmentosa. *Hum Mutat* 2012;33:963-972.
220. Khan AO, Aldahmesh MA, Al-Harhi E, Alkuraya FS. Helicoid subretinal fibrosis associated with a novel recessive NR2E3 mutation p.S44X. *Arch Ophthalmol* 2010;128:344-348.
221. Kuniyoshi K, Hayashi T, Sakuramoto H, et al. Novel mutations in enhanced S-cone syndrome. *Ophthalmology* 2013;120:431.e431-436.
222. Kannabiran C, Singh H, Sahini N, Jalali S, Mohan G. Mutations in TULP1, NR2E3, and MFRP genes in Indian families with autosomal recessive retinitis pigmentosa. *Mol Vis* 2012;18:1165-1174.
223. Coppieters F, Leroy BP, Beysen D, et al. Recurrent mutation in the first zinc finger of the orphan nuclear receptor NR2E3 causes autosomal dominant retinitis pigmentosa. *Am J Hum Genet* 2007;81:147-157.
224. Udar N, Small K, Chalukya M, Silva-Garcia R, Marmor M. Developmental or degenerative--NR2E3 gene mutations in two patients with enhanced S cone syndrome. *Mol Vis* 2011;17:519-525.
225. Park SP, Hong IH, Tsang SH, et al. Disruption of the human cone photoreceptor mosaic from a defect in NR2E3 transcription factor function in young adults. *Graefes Arch Clin Exp Ophthalmol* 2013.
226. Pachydaki SI, Klaver CC, Barbazetto IA, et al. Phenotypic features of patients with NR2E3 mutations. *Arch Ophthalmol* 2009;127:71-75.

227. Rocha-Sousa A, Hayashi T, Gomes NL, et al. A novel mutation (Cys83Tyr) in the second zinc finger of NR2E3 in enhanced S-cone syndrome. *Graefes Arch Clin Exp Ophthalmol* 2011;249:201-208.
228. Wright AF, Reddick AC, Schwartz SB, et al. Mutation analysis of NR2E3 and NRL genes in Enhanced S Cone Syndrome. *Hum Mutat* 2004;24:439.
229. Hayashi T, Gekka T, Goto-Omoto S, Takeuchi T, Kubo A, Kitahara K. Novel NR2E3 mutations (R104Q, R334G) associated with a mild form of enhanced S-cone syndrome demonstrate compound heterozygosity. *Ophthalmology* 2005;112:2115.
230. Yang Y, Zhang X, Chen LJ, et al. Association of NR2E3 but not NRL mutations with retinitis pigmentosa in the Chinese population. *Invest Ophthalmol Vis Sci* 2010;51:2229-2235.
231. Collin RW, van den Born LI, Klevering BJ, et al. High-resolution homozygosity mapping is a powerful tool to detect novel mutations causative of autosomal recessive RP in the Dutch population. *Invest Ophthalmol Vis Sci* 2011;52:2227-2239.
232. Bandah D, Merin S, Ashhab M, Banin E, Sharon D. The spectrum of retinal diseases caused by NR2E3 mutations in Israeli and Palestinian patients. *Arch Ophthalmol* 2009;127:297-302.
233. Lam BL, Goldberg JL, Hartley KL, Stone EM, Liu M. Atypical mild enhanced S-cone syndrome with novel compound heterozygosity of the NR2E3 gene. *Am J Ophthalmol* 2007;144:157-159.
234. Abu-Safieh L, Alrashed M, Anazi S, et al. Autozygome-guided exome sequencing in retinal dystrophy patients reveals pathogenetic mutations and novel candidate disease genes. *Genome Res* 2013;23:236-247.
235. Siemiatkowska AM, Arimadyo K, Moruz LM, et al. Molecular genetic analysis of retinitis pigmentosa in Indonesia using genome-wide homozygosity mapping. *Mol Vis* 2011;17:3013-3024.
236. Bernal S, Solans T, Gamundi MJ, et al. Analysis of the involvement of the NR2E3 gene in autosomal recessive retinal dystrophies. *Clin Genet* 2008;73:360-366.
237. Nakamura Y, Hayashi T, Kozaki K, et al. Enhanced S-cone syndrome in a Japanese family with a nonsense NR2E3 mutation (Q350X). *Acta Ophthalmol Scand* 2004;82:616-622.
238. Cima I, Brecej J, Sustar M, et al. Enhanced S-cone syndrome with preserved macular structure and severely depressed retinal function. *Doc Ophthalmol* 2012;125:161-168.
239. L B-T, T D, C A, F-X B, Munier FL, DF S. A heterozygous mutation in the NR2E3 Gene is associated with an autosomal dominant Retinitis Pigmentosa., *Annual Meeting of the Association for Research in Vision and Ophthalmology*. Fort Lauderdale, Florida, USA; 2006.

240. von Alpen D, Tran HV, Guex N, et al. Differential dimerization of variants linked to enhanced S-cone sensitivity syndrome (ESCS) located in the NR2E3 ligand-binding domain. *Hum Mutat* 2015;36:599-610.
241. Arden G, Wolf J, Berninger T, Hogg CR, Tzekov R, Holder GE. S-cone ERGs elicited by a simple technique in normals and in tritanopes. *Vision Res* 1999;39:641-650.
242. Koh AH, Hogg CR, Holder GE. The incidence of negative ERG in clinical practice. *Doc Ophthalmol* 2001;102:19-30.
243. Vaclavik V, Chakarova C, Bhattacharya SS, et al. Bilateral giant macular schisis in a patient with enhanced S-cone syndrome from a family showing pseudo-dominant inheritance. *Br J Ophthalmol* 2008;92:299-300.
244. Sharon D, Sandberg MA, Caruso RC, Berson EL, Dryja TP. Shared mutations in NR2E3 in enhanced S-cone syndrome, Goldmann-Favre syndrome, and many cases of clumped pigmentary retinal degeneration. *Arch Ophthalmol* 2003;121:1316-1323.
245. Yzer S, Barbazetto I, Allikmets R, et al. Expanded Clinical Spectrum of Enhanced S-Cone Syndrome. *JAMA Ophthalmol* 2013.
246. Wang NK, Lai CC, Liu CH, et al. Origin of fundus hyperautofluorescent spots and their role in retinal degeneration in a mouse model of Goldmann-Favre syndrome. *Dis Model Mech* 2013.
247. Kellner U, Zrenner E, Sadowski B, Foerster M. Enhanced S Cone Sensitivity Syndrome: Long-term Follow-up, Electrophysiological and Psychophysical Findings. *Clin Vision Sci* 1993;8:425-434.
248. Jacobson SG, Sumaroka A, Aleman TS, et al. Nuclear receptor NR2E3 gene mutations distort human retinal laminar architecture and cause an unusual degeneration. *Hum Mol Genet* 2004;13:1893-1902.
249. Jacobson SG, Cideciyan AV, Aleman TS, et al. Crumbs homolog 1 (CRB1) mutations result in a thick human retina with abnormal lamination. *Hum Mol Genet* 2003;12:1073-1078.
250. Chen J, Rattner A, Nathans J. The rod photoreceptor-specific nuclear receptor Nr2e3 represses transcription of multiple cone-specific genes. *J Neurosci* 2005;25:118-129.
251. Escher P, Gouras P, Roduit R, et al. Mutations in NR2E3 can cause dominant or recessive retinal degenerations in the same family. *Hum Mutat* 2009;30:342-351.
252. Roduit R, Escher P, Schorderet DF. Mutations in the DNA-binding domain of NR2E3 affect in vivo dimerization and interaction with CRX. *PLoS One* 2009;4:e7379.

253. Mukhopadhyay S, Wen X, Chih B, et al. TULP3 bridges the IFT-A complex and membrane phosphoinositides to promote trafficking of G protein-coupled receptors into primary cilia. *Genes Dev* 2010;24:2180-2193.
254. Wei Q, Zhang Y, Li Y, Zhang Q, Ling K, Hu J. The BBSome controls IFT assembly and turnaround in cilia. *Nat Cell Biol* 2012;14:950-957.
255. Perrault I, Saunier S, Hanein S, et al. Mainzer-Saldino syndrome is a ciliopathy caused by IFT140 mutations. *Am J Hum Genet* 2012;90:864-870.
256. Schmidts M, Frank V, Eisenberger T, et al. Combined NGS approaches identify mutations in the intraflagellar transport gene IFT140 in skeletal ciliopathies with early progressive kidney Disease. *Hum Mutat* 2013;34:714-724.
257. Khan AO, Bolz HJ, Bergmann C. Early-onset severe retinal dystrophy as the initial presentation of IFT140-related skeletal ciliopathy. *J AAPOS* 2014;18:203-205.
258. Online Mendelian Inheritance in Man. www.omim.org/entry/204000: McKusick-Nathans Institute of Genetic Medicine, Johns Hopkins University School of Medicine, under the direction of Dr. Ada Hamosh.
259. Mainzer F, Saldino RM, Ozonoff MB, Minagi H. Familial nephropathy associated with retinitis pigmentosa, cerebellar ataxia and skeletal abnormalities. *Am J Med* 1970;49:556-562.
260. Xu M, Yang L, Wang F, et al. Mutations in human IFT140 cause non-syndromic retinal degeneration. *Hum Genet* 2015.
261. Bifari IN, Elkhamary SM, Bolz HJ, Khan AO. The ophthalmic phenotype of IFT140-related ciliopathy ranges from isolated to syndromic congenital retinal dystrophy. *Br J Ophthalmol* 2015.
262. Le Quesne Stabej P, Saihan Z, Rangesh N, et al. Comprehensive sequence analysis of nine Usher syndrome genes in the UK National Collaborative Usher Study. *J Med Genet* 2012;49:27-36.
263. Beals RK, Weleber RG. Conorenal dysplasia: a syndrome of cone-shaped epiphysis, renal disease in childhood, retinitis pigmentosa and abnormality of the proximal femur. *Am J Med Genet A* 2007;143A:2444-2447.
264. Janssen S, Ramaswami G, Davis EE, et al. Mutation analysis in Bardet-Biedl syndrome by DNA pooling and massively parallel resequencing in 105 individuals. *Hum Genet* 2011;129:79-90.
265. Bachmann-Gagescu R, Dempsey JC, Phelps IG, et al. Joubert syndrome: a model for untangling recessive disorders with extreme genetic heterogeneity. *J Med Genet* 2015;52:514-522.
266. Bujakowska KM, Zhang Q, Siemiatkowska AM, et al. Mutations in IFT172 cause isolated retinal degeneration and Bardet-Biedl syndrome. *Hum Mol Genet* 2014.

267. Abu Safieh L, Aldahmesh MA, Shamseldin H, et al. Clinical and molecular characterisation of Bardet-Biedl syndrome in consanguineous populations: the power of homozygosity mapping. *J Med Genet* 2010;47:236-241.
268. Drivas TG, Wojno AP, Tucker BA, Stone EM, Bennett J. Basal exon skipping and genetic pleiotropy: A predictive model of disease pathogenesis. *Sci Transl Med* 2015;7:291ra297.
269. Jonassen JA, SanAgustin J, Baker SP, Pazour GJ. Disruption of IFT complex A causes cystic kidneys without mitotic spindle misorientation. *J Am Soc Nephrol* 2012;23:641-651.
270. Miller KA, Ah-Cann CJ, Welfare MF, et al. Cauli: a mouse strain with an Ift140 mutation that results in a skeletal ciliopathy modelling Jeune syndrome. *PLoS Genet* 2013;9:e1003746.
271. Knobloch W, Layer I. Retinal detachment and encephalocele. *J Pediatr Ophthalmol* 1971;8:181-184.
272. Czeizel AE, Göblyös P, Kustos G, Mester E, Paraicz E. The second report of Knobloch syndrome. *Am J Med Genet* 1992;42:777-779.
273. Passos-Bueno MR, Marie SK, Monteiro M, et al. Knobloch syndrome in a large Brazilian consanguineous family: confirmation of autosomal recessive inheritance. *Am J Med Genet* 1994;52:170-173.
274. Duh EJ, Yao YG, Dagli M, Goldberg MF. Persistence of fetal vasculature in a patient with Knobloch syndrome: potential role for endostatin in fetal vascular remodeling of the eye. *Ophthalmology* 2004;111:1885-1888.
275. Khan AO, Aldahmesh MA, Mohamed JY, Al-Mesfer S, Alkuraya FS. The distinct ophthalmic phenotype of Knobloch syndrome in children. *Br J Ophthalmol* 2012;96:890-895.
276. Haghghi A, Tiwari A, Piri N, et al. Homozygosity mapping and whole exome sequencing reveal a novel homozygous COL18A1 mutation causing Knobloch syndrome. *PLoS One* 2014;9:e112747.
277. Kliemann SE, Waetge RT, Suzuki OT, Passos-Bueno MR, Rosemberg S. Evidence of neuronal migration disorders in Knobloch syndrome: clinical and molecular analysis of two novel families. *Am J Med Genet A* 2003;119A:15-19.
278. Keren B, Suzuki OT, Gérard-Blanluet M, et al. CNS malformations in Knobloch syndrome with splice mutation in COL18A1 gene. *Am J Med Genet A* 2007;143A:1514-1518.
279. Paisán-Ruiz C, Scopes G, Lee P, Houlden H. Homozygosity mapping through whole genome analysis identifies a COL18A1 mutation in an Indian family presenting with an autosomal recessive neurological disorder. *Am J Med Genet B Neuropsychiatr Genet* 2009;150B:993-997.

280. Caglayan AO, Baranoski JF, Aktar F, et al. Brain malformations associated with Knobloch syndrome--review of literature, expanding clinical spectrum, and identification of novel mutations. *Pediatr Neurol* 2014;51:806-813.e808.
281. Seaver LH, Joffe L, Spark RP, Smith BL, Hoyme HE. Congenital scalp defects and vitreoretinal degeneration: redefining the Knobloch syndrome. *Am J Med Genet* 1993;46:203-208.
282. Menzel O, Bekkeheien RC, Reymond A, et al. Knobloch syndrome: novel mutations in COL18A1, evidence for genetic heterogeneity, and a functionally impaired polymorphism in endostatin. *Hum Mutat* 2004;23:77-84.
283. Williams TA, Kirkby GR, Williams D, Ainsworth JR. A phenotypic variant of Knobloch syndrome. *Ophthalmic Genet* 2008;29:85-86.
284. Suzuki OT, Sertié AL, Der Kaloustian VM, et al. Molecular analysis of collagen XVIII reveals novel mutations, presence of a third isoform, and possible genetic heterogeneity in Knobloch syndrome. *Am J Hum Genet* 2002;71:1320-1329.
285. Sertié AL, Quimby M, Moreira ES, et al. A gene which causes severe ocular alterations and occipital encephalocele (Knobloch syndrome) is mapped to 21q22.3. *Hum Mol Genet* 1996;5:843-847.
286. Sertié AL, Sossi V, Camargo AA, Zatz M, Brahe C, Passos-Bueno MR. Collagen XVIII, containing an endogenous inhibitor of angiogenesis and tumor growth, plays a critical role in the maintenance of retinal structure and in neural tube closure (Knobloch syndrome). *Hum Mol Genet* 2000;9:2051-2058.
287. Seppinen L, Pihlajaniemi T. The multiple functions of collagen XVIII in development and disease. *Matrix Biol* 2011;30:83-92.
288. Määttä M, Heljasvaara R, Pihlajaniemi T, Uusitalo M. Collagen XVIII/endostatin shows a ubiquitous distribution in human ocular tissues and endostatin-containing fragments accumulate in ocular fluid samples. *Graefes Arch Clin Exp Ophthalmol* 2007;245:74-81.
289. Francis P, Robson AG, Holder G, Moore A, Kaushal S. Inherited retinal dystrophy and asymmetric axial length. *Br J Ophthalmol* 2003;87:503-504.
290. Suzuki O, Kague E, Bagatini K, et al. Novel pathogenic mutations and skin biopsy analysis in Knobloch syndrome. *Mol Vis* 2009;15:801-809.
291. Aldahmesh MA, Khan AO, Mohamed JY, et al. No evidence for locus heterogeneity in Knobloch syndrome. *J Med Genet* 2013;50:565-566.
292. Marneros AG, Olsen BR. Age-dependent iris abnormalities in collagen XVIII/endostatin deficient mice with similarities to human pigment dispersion syndrome. *Invest Ophthalmol Vis Sci* 2003;44:2367-2372.
293. Scott A, Kotecha A, Bunce C, et al. YAG laser peripheral iridotomy for the prevention of pigment dispersion glaucoma a prospective, randomized, controlled trial. *Ophthalmology* 2011;118:468-473.

294. Chang L, Pan CW, Ohno-Matsui K, et al. Myopia-related fundus changes in Singapore adults with high myopia. *Am J Ophthalmol* 2013;155:991-999.e991.
295. Hayashi K, Ohno-Matsui K, Shimada N, et al. Long-term pattern of progression of myopic maculopathy: a natural history study. *Ophthalmology* 2010;117:1595-1611, 1611.e1591-1594.
296. Halfter W, Winzen U, Bishop PN, Eller A. Regulation of eye size by the retinal basement membrane and vitreous body. *Invest Ophthalmol Vis Sci* 2006;47:3586-3594.
297. Fukai N, Eklund L, Marneros AG, et al. Lack of collagen XVIII/endostatin results in eye abnormalities. *EMBO J* 2002;21:1535-1544.
298. Passos-Bueno MR, Suzuki OT, Armelin-Correa LM, et al. Mutations in collagen 18A1 and their relevance to the human phenotype. *An Acad Bras Cienc* 2006;78:123-131.
299. Mahajan VB, Olney AH, Garrett P, et al. Collagen XVIII mutation in Knobloch syndrome with acute lymphoblastic leukemia. *Am J Med Genet A* 2010;152A:2875-2879.
300. Aldahmesh MA, Khan AO, Mohamed JY, et al. Identification of ADAMTS18 as a gene mutated in Knobloch syndrome. *J Med Genet* 2011;48:597-601.
301. Aikio M, Hurskainen M, Brideau G, et al. Collagen XVIII short isoform is critical for retinal vascularization, and overexpression of the Tsp-1 domain affects eye growth and cataract formation. *Invest Ophthalmol Vis Sci* 2013;54:7450-7462.
302. Joyce S, Tee L, Abid A, Khaliq S, Mehdi SQ, Maher ER. Locus heterogeneity and Knobloch syndrome. *Am J Med Genet A* 2010;152A:2880-2881.
303. Thompson DA, Gyürüs P, Fleischer LL, et al. Genetics and phenotypes of RPE65 mutations in inherited retinal degeneration. *Invest Ophthalmol Vis Sci* 2000;41:4293-4299.
304. Walia S, Fishman GA, Jacobson SG, et al. Visual acuity in patients with Leber's congenital amaurosis and early childhood-onset retinitis pigmentosa. *Ophthalmology* 2010;117:1190-1198.
305. Lorenz B, Gyürüs P, Preising M, et al. Early-onset severe rod-cone dystrophy in young children with RPE65 mutations. *Invest Ophthalmol Vis Sci* 2000;41:2735-2742.
306. Weleber RG, Michaelides M, Trzuppek KM, Stover NB, Stone EM. The phenotype of Severe Early Childhood Onset Retinal Dystrophy (SECORD) from mutation of RPE65 and differentiation from Leber congenital amaurosis. *Invest Ophthalmol Vis Sci* 2011;52:292-302.

307. Cideciyan AV, Jacobson SG, Beltran WA, et al. Human retinal gene therapy for Leber congenital amaurosis shows advancing retinal degeneration despite enduring visual improvement. *Proc Natl Acad Sci U S A* 2013;110:E517-525.
308. Testa F, Maguire AM, Rossi S, et al. Three-year follow-up after unilateral subretinal delivery of adeno-associated virus in patients with Leber congenital Amaurosis type 2. *Ophthalmology* 2013;120:1283-1291.
309. Bainbridge JW, Mehat MS, Sundaram V, et al. Long-term effect of gene therapy on Leber's congenital amaurosis. *N Engl J Med* 2015;372:1887-1897.
310. Lorenz B, Poliakov E, Schambeck M, Friedburg C, Preising MN, Redmond TM. A comprehensive clinical and biochemical functional study of a novel RPE65 hypomorphic mutation. *Invest Ophthalmol Vis Sci* 2008;49:5235-5242.
311. Kondo H, Qin M, Mizota A, et al. A homozygosity-based search for mutations in patients with autosomal recessive retinitis pigmentosa, using microsatellite markers. *Invest Ophthalmol Vis Sci* 2004;45:4433-4439.
312. Marlhens F, Griffoin JM, Bareil C, Arnaud B, Claustres M, Hamel CP. Autosomal recessive retinal dystrophy associated with two novel mutations in the RPE65 gene. *Eur J Hum Genet* 1998;6:527-531.
313. Schatz P, Preising M, Lorenz B, Sander B, Larsen M, Rosenberg T. Fundus albipunctatus associated with compound heterozygous mutations in RPE65. *Ophthalmology* 2011;118:888-894.
314. Humphrey W, Dalke A, Schulten K. VMD: visual molecular dynamics. *J Mol Graph* 1996;14:33-38, 27-38.
315. Henderson RH, Waseem N, Searle R, et al. An assessment of the apex microarray technology in genotyping patients with Leber congenital amaurosis and early-onset severe retinal dystrophy. *Invest Ophthalmol Vis Sci* 2007;48:5684-5689.
316. Coppieters F, Casteels I, Meire F, et al. Genetic screening of LCA in Belgium: predominance of CEP290 and identification of potential modifier alleles in AH1 of CEP290-related phenotypes. *Hum Mutat* 2010;31:E1709-1766.
317. Jacobson SG, Cideciyan AV, Aleman TS, et al. Photoreceptor layer topography in children with leber congenital amaurosis caused by RPE65 mutations. *Invest Ophthalmol Vis Sci* 2008;49:4573-4577.
318. Jacobson SG, Aleman TS, Cideciyan AV, et al. Defining the residual vision in leber congenital amaurosis caused by RPE65 mutations. *Invest Ophthalmol Vis Sci* 2009;50:2368-2375.
319. Kiser PD, Golczak M, Lodowski DT, Chance MR, Palczewski K. Crystal structure of native RPE65, the retinoid isomerase of the visual cycle. *Proc Natl Acad Sci U S A* 2009;106:17325-17330.

320. Nikolaeva O, Takahashi Y, Moiseyev G, Ma JX. Purified RPE65 shows isomerohydrolase activity after reassociation with a phospholipid membrane. *FEBS J* 2009;276:3020-3030.
321. Nikopoulos K, Gilissen C, Hoischen A, et al. Next-generation sequencing of a 40 Mb linkage interval reveals TSPAN12 mutations in patients with familial exudative vitreoretinopathy. *Am J Hum Genet* 2010;86:240-247.
322. Poulter JA, Ali M, Gilmour DF, et al. Mutations in TSPAN12 cause autosomal-dominant familial exudative vitreoretinopathy. *Am J Hum Genet* 2010;86:248-253.
323. Poulter JA, Davidson AE, Ali M, et al. Recessive mutations in TSPAN12 cause retinal dysplasia and severe familial exudative vitreoretinopathy (FEVR). *Invest Ophthalmol Vis Sci* 2012;53:2873-2879.
324. Robitaille J, MacDonald ML, Kaykas A, et al. Mutant frizzled-4 disrupts retinal angiogenesis in familial exudative vitreoretinopathy. *Nat Genet* 2002;32:326-330.
325. Toomes C, Bottomley HM, Jackson RM, et al. Mutations in LRP5 or FZD4 underlie the common familial exudative vitreoretinopathy locus on chromosome 11q. *Am J Hum Genet* 2004;74:721-730.
326. Chen ZY, Battinelli EM, Fielder A, et al. A mutation in the Norrie disease gene (NDP) associated with X-linked familial exudative vitreoretinopathy. *Nat Genet* 1993;5:180-183.
327. Collin RW, Nikopoulos K, Dona M, et al. ZNF408 is mutated in familial exudative vitreoretinopathy and is crucial for the development of zebrafish retinal vasculature. *Proc Natl Acad Sci U S A* 2013;110:9856-9861.
328. Ke J, Harikumar KG, Erice C, et al. Structure and function of Norrin in assembly and activation of a Frizzled 4-Lrp5/6 complex. *Genes Dev* 2013;27:2305-2319.
329. Zhou Y, Wang Y, Tischfield M, et al. Canonical WNT signaling components in vascular development and barrier formation. *J Clin Invest* 2014;124:3825-3846.
330. Jarmas AL, Weaver DD, Ellis FD, Davis A. Microcephaly, microphthalmia, falciform retinal folds, and blindness. A new syndrome. *Am J Dis Child* 1981;135:930-933.
331. Young ID, Fielder AR, Simpson K. Microcephaly, microphthalmos, and retinal folds: report of a family. *J Med Genet* 1987;24:172-174.
332. Fryns JP, Smeets E, Van den Berghe H. On the nosology of the "primary true microcephaly, chorioretinal dysplasia, lymphoedema" association. *Clin Genet* 1995;48:131-133.

333. Jones GE, Ostergaard P, Moore AT, et al. Microcephaly with or without chorioretinopathy, lymphoedema, or mental retardation (MCLMR): review of phenotype associated with KIF11 mutations. *Eur J Hum Genet* 2014;22:881-887.
334. Robitaille JM, Gillett RM, LeBlanc MA, et al. Phenotypic overlap between familial exudative vitreoretinopathy and microcephaly, lymphedema, and chorioretinal dysplasia caused by KIF11 mutations. *JAMA Ophthalmol* 2014;132:1393-1399.
335. Martin CA, Ahmad I, Klingseisen A, et al. Mutations in PLK4, encoding a master regulator of centriole biogenesis, cause microcephaly, growth failure and retinopathy. *Nat Genet* 2014;46:1283-1292.
336. Passemard S, Kaindl AM, Verloes A. Microcephaly. *Handb Clin Neurol* 2013;111:129-141.
337. Wright CM, Booth IW, Buckler JM, et al. Growth reference charts for use in the United Kingdom. *Arch Dis Child* 2002;86:11-14.
338. Qin M, Hayashi H, Oshima K, Tahira T, Hayashi K, Kondo H. Complexity of the genotype-phenotype correlation in familial exudative vitreoretinopathy with mutations in the LRP5 and/or FZD4 genes. *Hum Mutat* 2005;26:104-112.
339. Liu J, Wilson S, Reh T. BMP receptor 1b is required for axon guidance and cell survival in the developing retina. *Dev Biol* 2003;256:34-48.
340. Ohkubo H, Tanino T. Electrophysiological findings in familial exudative vitreoretinopathy. *Doc Ophthalmol* 1987;65:461-469.
341. Balikova I, Robson AG, Holder GE, Ostergaard P, Mansour S, Moore AT. Ocular manifestations of microcephaly with or without chorioretinopathy, lymphedema or intellectual disability (MCLID) syndrome associated with mutations in KIF11. *Acta Ophthalmol* 2016;94:92-98.
342. Hu H, Xiao X, Li S, Jia X, Guo X, Zhang Q. KIF11 mutations are a common cause of autosomal dominant familial exudative vitreoretinopathy. *Br J Ophthalmol* 2016;100:278-283.
343. Gong Y, Slee RB, Fukai N, et al. LDL receptor-related protein 5 (LRP5) affects bone accrual and eye development. *Cell* 2001;107:513-523.
344. Boyden LM, Mao J, Belsky J, et al. High bone density due to a mutation in LDL-receptor-related protein 5. *N Engl J Med* 2002;346:1513-1521.
345. Jiao X, Ventruto V, Trese MT, Shastry BS, Hejtmancik JF. Autosomal recessive familial exudative vitreoretinopathy is associated with mutations in LRP5. *Am J Hum Genet* 2004;75:878-884.
346. Ostergaard P, Simpson MA, Mendola A, et al. Mutations in KIF11 cause autosomal-dominant microcephaly variably associated with congenital lymphedema and chorioretinopathy. *Am J Hum Genet* 2012;90:356-362.

347. Puffenberger EG, Jinks RN, Sougnez C, et al. Genetic mapping and exome sequencing identify variants associated with five novel diseases. *PLoS One* 2012;7:e28936.
348. Gargiulo A, Testa F, Rossi S, et al. Molecular and clinical characterization of albinism in a large cohort of Italian patients. *Invest Ophthalmol Vis Sci* 2011;52:1281-1289.
349. Masliah-Planchon J, Darnige L, Bellucci S. Molecular determinants of platelet delta storage pool deficiencies: an update. *Br J Haematol* 2013;160:5-11.
350. Desai N, Weisfeld-Adams JD, Brodie SE, et al. Optic neuropathy in late-onset neurodegenerative Chédiak-Higashi syndrome. *Br J Ophthalmol* 2015.
351. Oh J, Bailin T, Fukai K, et al. Positional cloning of a gene for Hermansky-Pudlak syndrome, a disorder of cytoplasmic organelles. *Nat Genet* 1996;14:300-306.
352. Anikster Y, Huizing M, White J, et al. Mutation of a new gene causes a unique form of Hermansky-Pudlak syndrome in a genetic isolate of central Puerto Rico. *Nat Genet* 2001;28:376-380.
353. Cullinane AR, Curry JA, Carmona-Rivera C, et al. A BLOC-1 mutation screen reveals that PLDN is mutated in Hermansky-Pudlak Syndrome type 9. *Am J Hum Genet* 2011;88:778-787.
354. Li K, Yang L, Zhang C, Niu Y, Li W, Liu JJ. HPS6 interacts with dynactin p150Glued to mediate retrograde trafficking and maturation of lysosomes. *J Cell Sci* 2014;127:4574-4588.
355. Zhang Q, Zhao B, Li W, et al. Ru2 and Ru encode mouse orthologs of the genes mutated in human Hermansky-Pudlak syndrome types 5 and 6. *Nat Genet* 2003;33:145-153.
356. Schreyer-Shafir N, Huizing M, Anikster Y, et al. A new genetic isolate with a unique phenotype of syndromic oculocutaneous albinism: clinical, molecular, and cellular characteristics. *Hum Mutat* 2006;27:1158.
357. Huizing M, Pederson B, Hess RA, et al. Clinical and cellular characterisation of Hermansky-Pudlak syndrome type 6. *J Med Genet* 2009;46:803-810.
358. Huizing M, Anikster Y, Fitzpatrick DL, et al. Hermansky-Pudlak syndrome type 3 in Ashkenazi Jews and other non-Puerto Rican patients with hypopigmentation and platelet storage-pool deficiency. *Am J Hum Genet* 2001;69:1022-1032.
359. Poulter JA, Al-Araimi M, Conte I, et al. Recessive mutations in SLC38A8 cause foveal hypoplasia and optic nerve misrouting without albinism. *Am J Hum Genet* 2013;93:1143-1150.

360. Charles SJ, Green JS, Grant JW, Yates JR, Moore AT. Clinical features of affected males with X linked ocular albinism. *Br J Ophthalmol* 1993;77:222-227.
361. Huizing M, Hess R, Dorward H, et al. Cellular, molecular and clinical characterization of patients with Hermansky-Pudlak syndrome type 5. *Traffic* 2004;5:711-722.
362. Tsilou ET, Rubin BI, Reed GF, et al. Milder ocular findings in Hermansky-Pudlak syndrome type 3 compared with Hermansky-Pudlak syndrome type 1. *Ophthalmology* 2004;111:1599-1603.
363. Gahl WA, Brantly M, Kaiser-Kupfer MI, et al. Genetic defects and clinical characteristics of patients with a form of oculocutaneous albinism (Hermansky-Pudlak syndrome). *N Engl J Med* 1998;338:1258-1264.
364. Gahl WA, Brantly M, Troendle J, et al. Effect of pirfenidone on the pulmonary fibrosis of Hermansky-Pudlak syndrome. *Mol Genet Metab* 2002;76:234-242.
365. Izquierdo NJ, Townsend W, Hussels IE. Ocular findings in the Hermansky-Pudlak syndrome. *Trans Am Ophthalmol Soc* 1995;93:191-200; discussion 200-192.
366. Iwata F, Reed GF, Caruso RC, Kuehl EM, Gahl WA, Kaiser-Kupfer MI. Correlation of visual acuity and ocular pigmentation with the 16-bp duplication in the HPS-1 gene of Hermansky-Pudlak syndrome, a form of albinism. *Ophthalmology* 2000;107:783-789.
367. von dem Hagen EA, Houston GC, Hoffmann MB, Morland AB. Pigmentation predicts the shift in the line of decussation in humans with albinism. *Eur J Neurosci* 2007;25:503-511.
368. Summers CG, Knobloch WH, Witkop CJ, King RA. Hermansky-Pudlak syndrome. Ophthalmic findings. *Ophthalmology* 1988;95:545-554.
369. Minkin P, Bertetti R, Lindsey S, Bovino B. Management of tooth extraction in a patient with a rare bleeding disorder associated with Hermansky-Pudlak syndrome: a case report. *J Oral Maxillofac Surg* 2015;73:219-223.
370. Sprecher E, Bergman R, Richard G, et al. Hypotrichosis with juvenile macular dystrophy is caused by a mutation in CDH3, encoding P-cadherin. *Nat Genet* 2001;29:134-136.
371. Shimomura Y, Wajid M, Shapiro L, Christiano AM. P-cadherin is a p63 target gene with a crucial role in the developing human limb bud and hair follicle. *Development* 2008;135:743-753.
372. Wagner H. Maculaaffektion, vergesellschaftet mit Haarabnormitiit von Lanugotypus, beide vielleicht angeboren bei zwei Geschwistern. *Albrecht von Graefes Archiv für Ophthalmologie* 1935;134:74-81.

373. Indelman M, Bergman R, Lurie R, et al. A missense mutation in CDH3, encoding P-cadherin, causes hypotrichosis with juvenile macular dystrophy. *J Invest Dermatol* 2002;119:1210-1213.
374. Indelman M, Hamel CP, Bergman R, et al. Phenotypic diversity and mutation spectrum in hypotrichosis with juvenile macular dystrophy. *J Invest Dermatol* 2003;121:1217-1220.
375. Indelman M, Leibur R, Jammal A, Bergman R, Sprecher E. Molecular basis of hypotrichosis with juvenile macular dystrophy in two siblings. *Br J Dermatol* 2005;153:635-638.
376. Indelman M, Eason J, Hummel M, et al. Novel CDH3 mutations in hypotrichosis with juvenile macular dystrophy. *Clin Exp Dermatol* 2007;32:191-196.
377. Jelani M, Salman Chishti M, Ahmad W. A novel splice-site mutation in the CDH3 gene in hypotrichosis with juvenile macular dystrophy. *Clin Exp Dermatol* 2009;34:68-73.
378. Shimomura Y, Wajid M, Kurban M, Christiano AM. Splice site mutations in the P-cadherin gene underlie hypotrichosis with juvenile macular dystrophy. *Dermatology* 2010;220:208-212.
379. Kamran-ul-Hassan Naqvi S, Azeem Z, Ali G, Ahmad W. A novel splice-acceptor site mutation in CDH3 gene in a consanguineous family exhibiting hypotrichosis with juvenile macular dystrophy. *Arch Dermatol Res* 2010;302:701-703.
380. Avitan-Hersh E, Indelman M, Khamaysi Z, Leibur R, Bergman R. A novel nonsense CDH3 mutation in hypotrichosis with juvenile macular dystrophy. *Int J Dermatol* 2012;51:325-327.
381. Halford S, Holt R, Németh AH, Downes SM. Homozygous deletion in CDH3 and hypotrichosis with juvenile macular dystrophy. *Arch Ophthalmol* 2012;130:1490-1492.
382. Kjaer KW, Hansen L, Schwabe GC, et al. Distinct CDH3 mutations cause ectodermal dysplasia, ectrodactyly, macular dystrophy (EEM syndrome). *J Med Genet* 2005;42:292-298.
383. Basel-Vanagaite L, Pasmanik-Chor M, Lurie R, Yeheskel A, Kjaer KW. CDH3-Related Syndromes: Report on a New Mutation and Overview of the Genotype-Phenotype Correlations. *Mol Syndromol* 2010;1:223-230.
384. Leibur R, Jermans A, Hatim G, Miller B, Sprecher E, Perlman I. Hypotrichosis with juvenile macular dystrophy: clinical and electrophysiological assessment of visual function. *Ophthalmology* 2006;113:841-847.e843.
385. Mason JO, Patel SA. A case of hypotrichosis with juvenile macular dystrophy. *Retin Cases Brief Rep* 2015;9:164-167.

386. Early Treatment Diabetic Retinopathy Study design and baseline patient characteristics. ETDRS report number 7. *Ophthalmology* 1991;98:741-756.
387. Suzuki M, Curcio CA, Mullins RF, Spaide RF. REFRACTILE DRUSEN: Clinical Imaging and Candidate Histology. *Retina* 2015;35:859-865.
388. Fujinami K, Zernant J, Chana RK, et al. Clinical and molecular characteristics of childhood-onset Stargardt disease. *Ophthalmology* 2015;122:326-334.
389. Hwang JC, Zernant J, Allikmets R, Barile GR, Chang S, Smith RT. Peripapillary atrophy in Stargardt disease. *Retina* 2009;29:181-186.
390. Gumbiner BM. Cell adhesion: the molecular basis of tissue architecture and morphogenesis. *Cell* 1996;84:345-357.
391. Xu L, Overbeek PA, Reneker LW. Systematic analysis of E-, N- and P-cadherin expression in mouse eye development. *Exp Eye Res* 2002;74:753-760.
392. Dalle Vedove A, Lucarelli AP, Nardone V, Matino A, Parisini E. The X-ray structure of human P-cadherin EC1-EC2 in a closed conformation provides insight into the type I cadherin dimerization pathway. *Acta Crystallogr F Struct Biol Commun* 2015;71:371-380.
393. Boguski MS, Lowe TM, Tolstoshev CM. dbEST--database for "expressed sequence tags". *Nat Genet* 1993;4:332-333.
394. Roosing S, Collin RW, den Hollander AI, Cremers FP, Siemiakowska AM. Prenylation defects in inherited retinal diseases. *J Med Genet* 2014;51:143-151.
395. Khandhadia S, Lotery A. Oxidation and age-related macular degeneration: insights from molecular biology. *Expert Rev Mol Med* 2010;12:e34.
396. Chartier FJ, Hardy É, Laprise P. Crumbs limits oxidase-dependent signaling to maintain epithelial integrity and prevent photoreceptor cell death. *J Cell Biol* 2012;198:991-998.
397. den Hollander AI, ten Brink JB, de Kok YJ, et al. Mutations in a human homologue of Drosophila crumbs cause retinitis pigmentosa (RP12). *Nat Genet* 1999;23:217-221.
398. den Hollander AI, Heckenlively JR, van den Born LI, et al. Leber congenital amaurosis and retinitis pigmentosa with Coats-like exudative vasculopathy are associated with mutations in the crumbs homologue 1 (CRB1) gene. *Am J Hum Genet* 2001;69:198-203.
399. Khan AO, Aldahmesh MA, Abu-Safieh L, Alkuraya FS. Childhood Cone-rod Dystrophy with Macular Cystic Degeneration from Recessive CRB1 Mutation. *Ophthalmic Genet* 2013.
400. Zenteno JC, Buentello-Volante B, Ayala-Ramirez R, Villanueva-Mendoza C. Homozygosity mapping identifies the Crumbs homologue 1 (Crb1) gene as responsible for a recessive syndrome of retinitis pigmentosa and nanophthalmos. *Am J Med Genet A* 2011;155A:1001-1006.

401. Paun CC, Pijl BJ, Siemiatkowska AM, et al. A novel crumbs homolog 1 mutation in a family with retinitis pigmentosa, nanophthalmos, and optic disc drusen. *Mol Vis* 2012;18:2447-2453.
402. Lotery AJ, Malik A, Shami SA, et al. CRB1 mutations may result in retinitis pigmentosa without para-arteriolar RPE preservation. *Ophthalmic Genet* 2001;22:163-169.
403. Bujakowska K, Audo I, Mohand-Saïd S, et al. CRB1 mutations in inherited retinal dystrophies. *Hum Mutat* 2012;33:306-315.
404. Tsang SH, Burke T, Oll M, et al. Whole Exome Sequencing Identifies CRB1 Defect in an Unusual Maculopathy Phenotype. *Ophthalmology* 2014.
405. Grover S, Murthy RK, Brar VS, Chalam KV. Normative data for macular thickness by high-definition spectral-domain optical coherence tomography (spectralis). *Am J Ophthalmol* 2009;148:266-271.
406. Mackay DS, Borman AD, Sui R, et al. Screening of a large cohort of leber congenital amaurosis and retinitis pigmentosa patients identifies novel LCA5 mutations and new genotype-phenotype correlations. *Hum Mutat* 2013;34:1537-1546.
407. Pellissier LP, Lundvig DM, Tanimoto N, et al. CRB2 acts as a modifying factor of CRB1-related retinal dystrophies in mice. *Hum Mol Genet* 2014;23:3759-3771.
408. Kantardzhieva A, Gosens I, Alexeeva S, et al. MPP5 recruits MPP4 to the CRB1 complex in photoreceptors. *Invest Ophthalmol Vis Sci* 2005;46:2192-2201.
409. Alves CH, Pellissier LP, Wijnholds J. The CRB1 and adherens junction complex proteins in retinal development and maintenance. *Prog Retin Eye Res* 2014;40:35-52.
410. van de Pavert SA, Kantardzhieva A, Malysheva A, et al. Crumbs homologue 1 is required for maintenance of photoreceptor cell polarization and adhesion during light exposure. *J Cell Sci* 2004;117:4169-4177.
411. Parry DA, Toomes C, Bida L, et al. Loss of the metalloprotease ADAM9 leads to cone-rod dystrophy in humans and retinal degeneration in mice. *Am J Hum Genet* 2009;84:683-691.
412. Mahimkar RM, Visaya O, Pollock AS, Lovett DH. The disintegrin domain of ADAM9: a ligand for multiple beta1 renal integrins. *Biochem J* 2005;385:461-468.
413. El-Haig WM, Jakobsson C, Favez T, Schorderet DF, Abouzeid H. Novel ADAM9 homozygous mutation in a consanguineous Egyptian family with severe cone-rod dystrophy and cataract. *Br J Ophthalmol* 2014.
414. Danciger M, Hendrickson J, Lyon J, et al. CORD9 a new locus for arCRD: mapping to 8p11, estimation of frequency, evaluation of a candidate gene. *Invest Ophthalmol Vis Sci* 2001;42:2458-2465.

415. Edwards DR, Handsley MM, Pennington CJ. The ADAM metalloproteinases. *Mol Aspects Med* 2008;29:258-289.
416. Yan X, Lin J, Rolfs A, Luo J. Differential expression of the ADAMs in developing chicken retina. *Dev Growth Differ* 2011;53:726-739.
417. Goldstein O, Mezey JG, Boyko AR, et al. An ADAM9 mutation in canine cone-rod dystrophy 3 establishes homology with human cone-rod dystrophy 9. *Mol Vis* 2010;16:1549-1569.
418. Landy SJ, Donnai D. Incontinentia pigmenti (Bloch-Sulzberger syndrome). *J Med Genet* 1993;30:53-59.
419. Parrish JE, Scheuerle AE, Lewis RA, Levy ML, Nelson DL. Selection against mutant alleles in blood leukocytes is a consistent feature in Incontinentia Pigmenti type 2. *Hum Mol Genet* 1996;5:1777-1783.
420. O'Donnell MA, Hase H, Legarda D, Ting AT. NEMO inhibits programmed necrosis in an NF κ B-independent manner by restraining RIP1. *PLoS One* 2012;7:e41238.
421. Fusco F, Bardaro T, Fimiani G, et al. Molecular analysis of the genetic defect in a large cohort of IP patients and identification of novel NEMO mutations interfering with NF-kappaB activation. *Hum Mol Genet* 2004;13:1763-1773.
422. Conte MI, Pescatore A, Paciolla M, et al. Insight into IKBKG/NEMO locus: report of new mutations and complex genomic rearrangements leading to incontinentia pigmenti disease. *Hum Mutat* 2014;35:165-177.
423. Kenwrick S, Woffendin H, Jakins T, et al. Survival of male patients with incontinentia pigmenti carrying a lethal mutation can be explained by somatic mosaicism or Klinefelter syndrome. *Am J Hum Genet* 2001;69:1210-1217.
424. Dörrenhaus A, Müller JI, Golka K, Jedrusik P, Schulze H, Föllmann W. Cultures of exfoliated epithelial cells from different locations of the human urinary tract and the renal tubular system. *Arch Toxicol* 2000;74:618-626.
425. Goldberg MF. The blinding mechanisms of incontinentia pigmenti. *Trans Am Ophthalmol Soc* 1994;92:167-176; discussion 176-169.
426. Roehl AC, Mussotter T, Cooper DN, et al. Tissue-specific differences in the proportion of mosaic large NF1 deletions are suggestive of a selective growth advantage of hematopoietic del(+/-) stem cells. *Hum Mutat* 2012;33:541-550.
427. Clayton-Smith J, Watson P, Ramsden S, Black GC. Somatic mutation in MECP2 as a non-fatal neurodevelopmental disorder in males. *Lancet* 2000;356:830-832.
428. Fusco F, Paciolla M, Napolitano F, et al. Genomic architecture at the Incontinentia Pigmenti locus favours de novo pathological alleles through different mechanisms. *Hum Mol Genet* 2012;21:1260-1271.

429. Aradhya S, Woffendin H, Jakins T, et al. A recurrent deletion in the ubiquitously expressed NEMO (IKK-gamma) gene accounts for the vast majority of incontinentia pigmenti mutations. *Hum Mol Genet* 2001;10:2171-2179.
430. Orange JS, Brodeur SR, Jain A, et al. Deficient natural killer cell cytotoxicity in patients with IKK-gamma/NEMO mutations. *J Clin Invest* 2002;109:1501-1509.
431. Zonana J, Elder ME, Schneider LC, et al. A novel X-linked disorder of immune deficiency and hypohidrotic ectodermal dysplasia is allelic to incontinentia pigmenti and due to mutations in IKK-gamma (NEMO). *Am J Hum Genet* 2000;67:1555-1562.
432. Fusco F, Fimiani G, Tadini G, Michele D, Ursini MV. Clinical diagnosis of incontinentia pigmenti in a cohort of male patients. *J Am Acad Dermatol* 2007;56:264-267.
433. Farkas MH, Grant GR, White JA, Sousa ME, Consugar MB, Pierce EA. Transcriptome analyses of the human retina identify unprecedented transcript diversity and 3.5 Mb of novel transcribed sequence via significant alternative splicing and novel genes. *BMC Genomics* 2013;14:486.
434. Braun TA, Mullins RF, Wagner AH, et al. Non-exonic and synonymous variants in ABCA4 are an important cause of Stargardt disease. *Hum Mol Genet* 2013;22:5136-5145.
435. Irimia M, Weatheritt RJ, Ellis JD, et al. A highly conserved program of neuronal microexons is misregulated in autistic brains. *Cell* 2014;159:1511-1523.
436. Kiser PD, Zhang J, Badiie M, et al. Catalytic mechanism of a retinoid isomerase essential for vertebrate vision. *Nat Chem Biol* 2015;11:409-415.
437. Bax NM, Sangermano R, Roosing S, et al. Heterozygous deep-intronic variants and deletions in ABCA4 in persons with retinal dystrophies and one exonic ABCA4 variant. *Hum Mutat* 2015;36:43-47.
438. Gerard X, Garanto A, Rozet JM, Collin RW. Antisense Oligonucleotide Therapy for Inherited Retinal Dystrophies. *Adv Exp Med Biol* 2016;854:517-524.
439. Schwartz SD, Regillo CD, Lam BL, et al. Human embryonic stem cell-derived retinal pigment epithelium in patients with age-related macular degeneration and Stargardt's macular dystrophy: follow-up of two open-label phase 1/2 studies. *Lancet* 2015;385:509-516.
440. Stingl K, Bartz-Schmidt KU, Besch D, et al. Subretinal Visual Implant Alpha IMS--Clinical trial interim report. *Vision Res* 2015;111:149-160.

16 Appendix: publications during research

1st author published:

Hull S, Owen N, Islam F, Tracey-White D, Plagnol V, Holder GE, Michaelides M, Carss K, Raymond FL, Rozet JM, Ramsden SC, Black GCM, Perrault I, Sarkar A, Moosajee M, Webster AR, Arno G, Moore AT. Non-syndromic retinal dystrophy due to bi-allelic mutations in the ciliary transport gene *IFT140*. *Invest Ophthalmol Vis Sci*. 2016;57(3):1053-62

Hull S, Holder GE, Robson AG, Mukherjee R, Michaelides M, Webster AR, Moore AT. Preserved visual function in retinal dystrophy due to hypomorphic *RPE65* mutations. *Br J Ophthalmol*. 2016; Feb 23. doi: 10.1136/bjophthalmol-2015-308019. [Epub ahead of print]

Hull S, Arno G, Holder GE, Plagnol V, Gomez K, Liesner R, Webster AR, Moore AT. The ophthalmic presentation of Hermansky-Pudlak syndrome 6. *Br J Ophthalmol*. 2016 Jan 28. doi:10.1136/bjophthalmol-2015-308067. [Epub ahead of print]

Hull S, Arno G, Sergouniotis PI, Tiffin P, Borman AD, Chandra A, Robson AG, Holder GE, Webster AR, Moore AT. Clinical and Molecular Characterization of Enhanced S-Cone Syndrome in Children. *JAMA Ophthalmol*. 2014;132(11):1341-9

Hull S, Arno G, Plagnol V, Chamney S, Russell-Eggitt I, Thompson D, Ramsden SC, Black GC, Robson AG, Holder GE, Moore AT, Webster AR. The phenotypic variability of retinal dystrophies associated with mutations in *CRX*, with report of a novel macular dystrophy phenotype. *Invest Ophthalmol Vis Sci*. 2014;30;55(10):6934-44

Hull S, Arno G, Thomson P, Mutch S, Webster AR, Rai H, Hill V, Moore AT. Somatic mosaicism of a novel *IKBKG* mutation in a male patient with incontinentia pigmenti. *Am J Med Genet A*. 2015 Jul;167(7):1601-4.

Hull S, Arno G, Plagnol V, Robson A, Webster A, Moore AT. Exome sequencing reveals *ADAM9* mutations in a child with cone-rod dystrophy. *Acta Ophthalmol*. 2015;93(5);e392-3

Hull S, Kalhor A, Marr J *et al*. Congenital high myopia and central macular atrophy: a report of 3 families. *Eye (Lond)*. 2015 Jul;29(7):936-42

Hull S, Moore AT. Gyrate atrophy. In Lois N, Forrester JV (eds). Fundus autofluorescence, 2nd edition, Lippincott, Williams & Wilkins, 2015

1st author in press:

Hull S*, Malik ANJ*, Arno G, Mackay DS, Plagnol V, Michaelides M, Mansour S, Albanese A, Tatton Brown K, Holder GE, Webster AR, Heath PT, Moore AT. Expanding the phenotype of *TRNT1* related immunodeficiency to include childhood cataract and inner retinal dysfunction. JAMA Ophthalmol. *joint first authors

Hull S, Webster AR. Ophthalmic Manifestations of Inherited Metabolic Disease. In Hollak CEM, Lachmann R (eds). Inherited Metabolic Disease in Adults: A Clinical Guide, Oxford University Press, 2016

Hull S, Arno G, Ku CA, Ge Z, Waseem N, Chandra A, Webster A, Robson AG, Michaelides M, Weleber RG, Davagnanam I, Chen R, Holder GE, Pennesi ME, Moore AT. Novel molecular and clinical findings in Knobloch syndrome. JAMA Ophthalmol

1st author in submission:

Hull S, Arno G, Robson AG, Broadgate S, Plagnol V, McKibbin M, Halford S, Michaelides M, Holder GE, Moore AT, Khan K, Webster AR. Detailed characterization of *CDH3* related congenital hypotrichosis with juvenile macular dystrophy, a centrally progressive disorder with limited peripheral retinal involvement. JAMA Ophthalmol

Hull S*, Mukherjee R*, Holder GE, Moore AT, Webster AR. The clinical features of retinal disease due to a dominant mutation in *RPE65*. Mol Vis. *joint first authors

Co-author published:

Scheidecker S, **Hull S**, Perdomo Y, Studer F, Pelletier V, Muller J, Stoetzel C, Schaefer E, Defoort-Dhellemmes S, Drumare I, Holder GE, Hamel CP, Webster AR, Moore AT, Puech B, Dollfus HJ. Predominantly Cone-System Dysfunction as Rare Form of Retinal Degeneration in Patients With Molecularly Confirmed Bardet-Biedl Syndrome. Am J Ophthalmol. 2015;160(2):364-372

Scheidecker S, Etard C, Haren L, Stoetzel C, **Hull S**, Arno G, Plagnol V, Drunat S, Passemard S, Toutain A, Obringer C, Koob M, Geoffroy V, Marion V, Strähle U, Ostergaard P, Verloes A, Merdes A, Moore AT, Dollfus H. Mutations in *TUBGCP4*

alter microtubule organization via the γ -tubulin ring complex in autosomal-recessive microcephaly with chorioretinopathy. *Am J Hum Genet.* 2015;96(4):666-74.

Arno G, **Hull S**, Robson AG, Holder GE, Cheetham ME, Webster AR, Plagnol V, Moore AT. Lack of Interphotoreceptor Retinoid Binding Protein Caused by Homozygous Mutation of *RBP3* Is Associated With High Myopia and Retinal Dystrophy. *Invest Ophthalmol Vis Sci.* 2015;56(4):2358-65

Hufnagel RB, Arno G, Hein ND, Hersheson J, Prasad M, Anderson Y, Krueger LA, Gregory LC, Stoetzel C, Jaworek TJ, **Hull S**, Li A, Plagnol V, Willen CM, Morgan TM, Prows CA, Hegde RS, Riazuddin S, Grabowski GA, Richardson RJ, Dieterich K, Huang T, Revesz T, Martinez-Barbera JP, Sisk RA, Jefferies C, Houlden H, Dattani MT, Fink JK, Dollfus H, Moore AT, Ahmed ZM. Neuropathy target esterase impairments cause Oliver-McFarlane and Laurence-Moon syndromes. *J Med Genet.* 2015;52(2):85-94.

Onoufriadis A, Shoemark A, Munye MM, James CT, Schmidts M, Patel M, Rosser EM, Bacchelli C, Beales PL, Scambler PJ, Hart SL, Danke-Roelse JE, Sloper JJ, **Hull S**, Hogg C, Emes RD, Pals G, Moore AT, Chung EM; UK10K, Mitchison HM. Combined exome and whole-genome sequencing identifies mutations in *ARMC4* as a cause of primary ciliary dyskinesia with defects in the outer dynein arm. *J Med Genet.* 2014;51(1):61-7.

Co-author in press:

Parfitt DA, Lane A, Ramsden CM, Carr AJF, Munro PM, Jovanovic K, Schwarz N, Kanuga N, Muthiah MN, **Hull S**, Gallo JM, da Cruz L, Moore AT, Hardcastle AJ, Coffey PJ, Cheetham ME. Patient-derived iPSC three-dimensional optic cups to test disease mechanisms and RNA therapy for inherited blindness. *Cell Stem Cell.*

Islam F, **Hull S**, Quereshi N, Mansfield DC, Moore AT, Bird A. Unusual Retinal Vascular proliferation in von Hippel-Lindau disease. *JAMA Ophthalmol.*